NOVEL INSIGHTS INTO

The Molecular Regulation of Renal and Cardiovascular Homeostasis

M.M. Brandt

Novel Insights into the Molecular Regulation of Renal and Cardiovascular Homeostasis

Maarten Matthijs Brandt

Novel Insights into the Molecular Regulation of Renal and Cardiovascular Homeostasis

Thesis Erasmus Medical Center, Rotterdam

ISBN: 978-94-6380-561-2
Printed by: ProefschriftMaken NL – www.proefschriftmaken.nl
Cover design: Jasper den Ouden

Novel Insights into the Molecular Regulation of Renal and Cardiovascular Homeostasis

Nieuwe inzichten in de moleculaire regulatie van renale en cardiovasculaire homeostase

Proefschrift

ter verkrijging van de graad van doctor aan de
Erasmus Universiteit Rotterdam
op gezag van de rector magnificus
Prof. dr. R.C.M.E. Engels
en volgens het besluit van het College voor Promoties.
De openbare verdediging zal plaatsvinden op

woensdag 11 december 2019 om 9.30 uur

Maarten Matthijs Brandt

geboren te Leeuwarden

Erasmus University Rotterdam

Promotiecommissie

Promotor
Prof. dr. D.J.G.M. Duncker

Overige leden:
Prof. dr. D. Merkus
Prof. dr. J.M. Kros
Prof. dr. M.C. Verhaar

Copromotor
Dr. C. Cheng

Financial support by the Dutch Heart Foundation for the publication of this thesis is gratefully acknowledged.

The research described in this thesis was supported by a grant of the Dutch Heart Foundation (CVON2014-11 RECONNECT).

Contents

Chapter 1

Introduction and outline of this thesis

Introduction and outline of this thesis

Historical overview on the circulatory system

Already during the Golden Age of Greece, people realized that all organisms, including humans, require nutrition and that in more complex organisms, nutrients somehow need to be distributed from the intestines throughout the body. With the discovery of the differences between arteries and veins, Praxagoras (340 BC) shaped this idea of nutrients distribution in a more conceivable concept.[1] He theorized that arteries originated in the heart and carried pneuma from the lungs to the left side of the heart, from which the breath of life was transported to the rest of the body. Veins on the other hand were supposed to begin in the liver where they carried digested food in the form of blood to the rest of the body. Building on the ideas of Praxagoras, Galen (129-216AD) experimentally demonstrated that arteries were not solely filled with pneuma, but like veins actually contained blood.[2] He postulated that blood passed from the venous side of the heart via pores in the intraventricular septum into the arteries. Via the arteries, blood was transported to all parts of the body for consumption and remaining waste was removed by the kidneys in the form of urine.[3] This refined theory lasted for fifteen centuries until William Harvey demonstrated that arteries and veins are connected in the lung- and peripheral tissues, and that blood circulates rather than that it is consumed.[1] We now know that this circulatory system is not a static entity. In fact, it is highly dynamic, capable of adapting in response to both mechanical and biochemical stimuli.

Not only has our anatomical view of the cardiovascular system evolved over time, but also our appreciation of its role in health and disease has shifted. According to the Ancient Greeks and Roman philosophers, veins contained three additional humors beside blood; yellow bile, black bile and phlegm, and until deep into the eighteenth century practically all diseases were thought to be either caused by imbalanced ratios of these four humors, or by a dysregulated blood flow pattern.[4] Nowadays however, we know that health or disease is the net result of the complex interplay between an individual's genetic background and environmental factors, and that cardiovascular homeostasis, as well as balanced dynamics in adaptation, are key components in defining the thin line between health and disease. Therefore, a thorough understanding of the mechanisms underlying or affecting this homeostasis is of major importance for development of future therapeutic strategies for cardiovascular diseases.

Vascular development

The importance of a functional circulatory system that not only allows oxygen and nutrient delivery, but for instance also facilitates efficient organism-wide immune surveillance, is

evidenced by its appearance early in development. Already in the third week of development, a primary vascular plexus is formed by vasculogenesis, a process described as *de novo* formation of blood vessels from the differentiation and association of endothelial progenitor cells.[5] In vasculogenesis, hemangioblasts differentiate from the embryonic mesoderm and eventually cluster in so called blood islands at sites of vascularization.[5] Although mechanistically not fully understood yet, Fibroblast Growth Factor (FGF) signaling has been shown to be involved in this mesodermal differentiation.[6] Progenitor cells located on the interior side of these blood islands differentiate into hematopoietic progenitor cells, which eventually give rise to blood cells. The subset of cells that surround these hematopoietic progenitor cells however, differentiates into angioblasts that will later develop into endothelial cells forming the inner lining of the mature vasculature. These angioblasts proliferate and migrate to form cellular tubes and eventually associate in a premature vascular labyrinth that provides the foundation for all major blood vessels. Genetic knockout studies in mice demonstrated that Vascular Endothelial Growth Factor A (VEGFA) signaling via its receptor Vascular Endothelial Growth Factor Receptor 2 (VEGFR2) not only stimulates hematopoiesis, but also induces cell migration and proliferation required for proper blood island formation.[7, 8]

The premature vascular labyrinth thereafter rapidly expands into a complex vascular network by a process called angiogenesis, defined as the formation of new vessels from pre-existing vessels, either via sprouting of endothelial cells, or via intussusception. In sprouting angiogenesis, capillary endothelial cells become activated upon exposure to angiogenic stimuli, including FGFs and VEGFA.[9] These factors are released in response to oxygen and nutritional stress and, amongst others, trigger enhanced transcription of several metalloproteinases (MMPs) and Angiopoietin 2 (ANGPT2).[10, 11] MMPs provide degradation of the capillary basement membrane, whereas ANGPT2 signaling via TEK Receptor Tyrosine Kinase (TIE2) results in local detachment of capillary-stabilizing pericytes.[12] To limit the number of outgrowing sprouts, only a minor proportion of the capillary endothelium transforms into angiogenic growth factor-sensitive tip cells and migrates towards the angiogenic stimulus. These tip cells are followed by stalk cells, a proliferating and lumen-forming subset of endothelial cells. Stalk cells express high levels of Vascular Endothelial Growth Factor Receptor 1 (VEGFR1/Flt1), which has a much higher affinity for VEGFA than VEGFR2, but lacks the ability to transduce its pro-angiogenic signal, rendering these stalk cells virtually irresponsive to the proangiogenic VEGFA stimulus.[13] The elongating sprouts eventually fuse with other sprouts in the expanding network via anastomosis, after which the newly formed connection gets stabilized by basement membrane deposition and pericyte

recruitment, of which the latter is highly dependent on endothelial secretion of the chemoattractant Platelet Derived Growth Factor Subunit β.[13]

Where sprouting angiogenesis contributes to expansion of the vascular network by tissue ingrowth of new vessels, intussusceptive angiogenesis concurs through division of existing vessels into multiple smaller vessels. The latter form is initiated via the formation of so called pillar core structures by opposing endothelial cells within a capillary. Pericytes and myofibroblasts invade these pillar cores and stabilize them by deposition of extracellular matrix components.[14] These tissue pillars eventually expand, resulting into splitting of the capillary. Mechanistically, there is a defined overlap with sprouting angiogenesis, although the initial stimulus for intussusceptive angiogenesis appears to come rather from biomechanical stimuli in the form of elevated flow, rather than from hypoxia.[14]

Physiological and pathological dynamics in vascular growth

The vascular system facilitates the distribution of oxygen- and nutrients throughout the body. During embryonic development a vascular network emerges, which ensures that all cells of the body are within diffusion range of oxygen and nutrients. After birth, physical growth continues and requires the vascular network to grow proportionally via a strictly regulated exposure to pro- and anti-angiogenetic stimuli. During adulthood, however, most blood vessels remain in a quiescent state, although physiological changes, including expanse of muscle mass, or cyclic development of the uterus, may still require angiogenesis-driven growth of the existing vasculature, whereas loss of adipose tissue for instance, results in vascular regression.[15]

Considering that each individual cell dependents on oxygen and nutrients, it is not surprising that dysregulation of angiogenic stimuli is involved in a great number of diseases. In diabetic patients for instance, hyperglycemia-induced pericyte detachment from the retinal capillaries results in microvascular destabilization and leakage.[16] This initial stage of capillary dysfunction is often asymptomatic, but the consecutive retinal hypoxia triggers a VEGF-dependent growth of instable capillaries into the retina and vitreous humor, eventually causing loss of sight.[16] A similar shift towards pro-angiogenic stimuli is observed in malignant cell growth. The distance over which oxygen can diffuse from capillaries to respiring tissue is typically limited from 100-200μm, and tumors rapidly grow to sizes that exceed this distance.[17] Consequently, these tumors secrete a constant and uncontrolled array of pro-angiogenic stimuli, including VEGFA, FGFs, and Interleukins, leading to ingrowth of highly disorganized immature vessels.[18] These poorly structured vessels are prone to provide an escape route for tumor cells[19], underscoring the notion that the dysregulated nature of tumor vascularization is a principal feature of disease progression.

Conversely, an imbalance in angiogenic stimuli favoring an anti-angiogenic response is also directly related to disease. In preeclampsia for instance, high circulating levels of soluble anti-angiogenic factors VEGFR1 and Endoglin are observed.[20] In addition to the VEGFA-scavenging properties of VEGFR1, Endoglin binds TGFβ, attenuating TGFβ-mediated vascular stabilization by perivascular cells, causing vascular abnormalities and hypoperfusion of the placenta, as well as glomerular endothelial dysfunction.[21]

Among the many pathways coordinating vascular growth, endothelial signaling via Frizzled (FZD) receptors has previously been shown to be of crucial importance.[22-24] The FZD receptors belong to a family of 10 transmembrane receptors (FZD1-10), which can initiate FZD/WNT canonical and non-canonical signaling upon binding with one of the 19 soluble WNT ligands. Canonical WNT signaling depends on FZD receptor and low-density lipoprotein receptor-related protein 5 or 6 co-activation, initiating Disheveled (DVL) to stabilize β-catenin, followed by β-catenin-mediated transcription.[25, 26] In contrast, non-canonical WNT signaling also involves DVL, but proceeds via WNT/Ca^{2+}-mediated activation of Nuclear factor of activated T-cells (NFAT), or Wnt/planar cell polarity-mediated activation of c-JUN N-terminal Kinase.[25] Several studies illustrated that FZD4 signaling is essential for proper retinal angiogenesis and that its inhibition causes impaired β-catenin-mediated transcription, leading to familial exudative vitreoretinopathy.[23] Murine knockout models furthermore illustrated the importance of FZD5 en FZD7 in vascular growth.[22, 24] FZD7 was shown to facilitate canonical WNT signaling, and like FZD4, to be essential for post-natal angiogenesis.[24] FZD5 silencing also induced vascular defects, but in contrast to FZD4 and FZD7, these defects appeared in the placenta and yolk sac and resulted in embryonic lethality.[22] In this thesis, we describe mechanistically how endothelial loss of FZD5 led to Protein Kinase C- (PKC) mediated upregulation of VEGFR1 and ANGPT2, which attenuated angiogenesis (**chapter 2**).

Over the last decades, studies on the mechanisms involved in angiogenesis have predominantly been focused on endothelium. Although endothelial cells play a central role in angiogenesis, capillary homeostasis relies on well-orchestrated and bidirectional cross talk between endothelium and the relatively understudied pericytes. Considering their role in maintaining vascular stability, pericytes are inseparable from neovascularization and in our attempts to get a better appreciation of this process, it is thus essential that we do not limit our scope to the endothelium. In **chapter 3** we aimed to improve our understanding of these perivascular cells, focusing particularly on how they are affected by direct microvascular endothelial interaction.

Vascular involvement in (pathological) immune regulation

Beside oxygen and nutrient delivery, the vascular network also has a profound role in immune regulation. The unique location of endothelial cells, forming the interface between tissue and inflammatory cells, enables the endothelium not only to facilitate transport of inflammatory cells, but also to specify an inflammatory response to sites of injury or infection, while protecting adjacent healthy tissue. In response to inflamed tissue-derived cytokines, such as Interleukin 1 (IL1), Tumor Necrosis Factor α (TNFα), and Interferon γ (IFNγ), vessels dilate and endothelial Nuclear Factor κB (NFκB) becomes activated.[27] This triggers the transcriptional upregulation of endothelial-leukocyte adhesion molecules, including Endothelial-Leukocyte Adhesion Molecule 1 (SELE) and Vascular Cell Adhesion Molecule 1 (VCAM1), favoring localized extravasation of leukocytes to contain and neutralize the inflammatory source.[28] The well-functioning of this inflammatory response is of major importance to maintain homeostasis in complex organisms. However, when dysregulated or chronically activated, this immune response can result in pathological events. In atherosclerosis for instance, circulating lipoprotein particles penetrate the endothelial barrier at sites of low shear stress and deposit in the subendothelial space, where they trigger the recruitment macrophages.[29] These macrophages internalize the lipoproteins and differentiate into chemokine-secreting foam cells, not only inducing proliferation and synthesis of extracellular matrix by neighboring smooth muscle cell, but also further enhancing the endothelial proinflammatory phenotype.[29] This leads to a progressive inflammatory response in the vessel wall which can eventually result in the formation of a fibrous cap, overlying a lipid-rich, highly thrombogenic necrotic core. Depending on structure and stability, these lesion can either progressively narrow the vessel lumen causing local ischemia, or rupture which could result in atherothrombotic occlusion.

Cardiac development

In line with the appearance of a vascular network, embryonic heart development occurs in an early fetal stage. In fact, the heart is the first functional organ in vertebrates, showing peristaltic contraction already at week 3 of embryonic development.[30] During subsequent development, rapid myocardial proliferation ensures appropriate cardiac growth. This process is regulated by various signaling pathways, including Neuregulin-, Insulin-Like Growth Factor- (IGF), and Bone Morphogenic Protein- (BMP) induced activation of the transcription factors GATA4, MEF2, and TBX.[31, 32] The initiation of contractility, as well as the continuous growth of the fetal heart result in the requirement of considerable amounts of energy. The low availability of lipids, in combination with a relative low fetal oxygen tension, favors the use of carbohydrates as energy substrate by cardiomyocytes, predominantly in

the form of lactate and glucose.[33] Eight weeks post conception, the heart is fully formed, after which the proliferative capacity of the myocytes slowly tapers off until birth, essentially followed by a permanent cell cycle arrest. Immediately after birth, plasma levels of fatty acids rise and the establishment of pulmonary gas exchange, providing a higher oxygen availability, enables a metabolic switch to the less oxygen efficient, but higher energy-yielding oxidative phosphorylation of fatty acids.[33] This switch in energy substrate usage is accompanied by enhanced nuclear receptor peroxisome proliferator–activated receptor alpha- (PPAR-α) and Kruppel-like factor 15- (KLF15) dependent transcription.[34] Recent evidence indicates that the metabolic substrate usage in the fetal- and neonatal heart might extend beyond energetics. It has been demonstrated that proliferating cardiomyocytes from injured zebrafish hearts show elevated expression of genes involved in glycolysis, and that inhibition of glycolysis significantly lowered cardiomyocyte proliferation[35], suggesting that the metabolic switch observed in fetal- and neonatal cardiomyocytes might serve an additional purpose in cardiomyocyte cell-cycle progression.

Physiological and pathological dynamics in cardiac adaptation

The heart needs to maintain a cardiac output commensurate with the body's demands in both normal and stressed conditions. Upon reaching adulthood, the ability of the heart to adapt to stressed conditions is limited by the low capacity of cardiomyocytes to proliferate. However, individual cardiomyocytes can undergo enlargement, a process called hypertrophy. Cardiomyocyte hypertrophy leads to increased synthesis, as well as structural reorganization of the sarcomeres, contributing to enhanced contractile mass and lower wall stress, and as a result, it enables the heart to overcome an increased workload. Depending on the initial hypertrophic stimulus, cardiac hypertrophy can either be physiological or pathological. Although both forms initially develop as an adaptive response, important phenotypical, molecular, and prognostic differences have been identified.

Physiological hypertrophy is often the result of postnatal growth, pregnancy, and exercise training, and is mainly initiated by IGF-induced activation of Phosphoinositide 3-kinase (PI3K) and Protein Kinase B (AKT).[36] It is characterized by cardiomyocyte growth in both length and width, leading to increased wall thickness and eccentric remodeling with a mild increase in ventricular volume, and preserved, or even increased contractile function.[37] In addition, physiological hypertrophy is fully reversible, develops in absence of fibrosis, cell death, and re-activation of the fetal gene program.[37] Most important, physiological hypertrophy does not progress to heart failure.

Pathological hypertrophy on the other hand leads to adverse cardiac events and often results from genetic predisposition or other cardiovascular complications, including

hypertension and myocardial infarction.[37] It mainly develops through mechanical forces and circulating factors, such as Angiotensin II (ANG II) and Endothelin 1 (ET1).[38] Stimulation of cardiomyocytes by ANG II and ET1 induces Ca^{2+}-dependent activation of NFAT, which can interact with transcriptional cofactors MEF2 and GATA4 to stimulate hypertrophy-related transcription of fetal genes, such as Skeletal Muscle α-Actin (ACTA1).[39] In addition, ANG II and ET1 induce the activation of PKC, which in cardiomyocytes is known to activate serine/threonine-protein phosphatase 1 (PP1A).[40] PP1A lowers phosphorylation of Phospholamban (PLN), leading to impaired Ca^{2+} handling caused by PLN-induced inhibition of SR Ca(2+)-ATPase 2 (SERCA2).[40] Disturbed Ca^{2+} handling, resulting in elevated cytoplasmic Ca^{2+} levels during diastole, not only lowers systolic Ca^{2+} elevations and thus contractile function[41], it also impairs actin blockade by tropomyosin during diastole, lowering the dissociation of myosin-actin cross bridges, thereby attenuating active relaxation and contributing to diastolic dysfunction.[41-43] Pathological hypertrophy is furthermore associated with elevated cell death as well as both interstitial and perivascular fibrosis. Cardiac fibrosis elevates passive stiffness of the myocardium, and consequently contributes to diastolic dysfunction. Moreover, pathological cardiac remodeling is associated with mitochondrial dysfunction, and insufficient capillary support leading to hypoxia.[44] This hypoxic state, in concert with mitochondrial dysfunction, causes a reduction of fatty acid oxidation and an increase in glycolysis and lactate metabolism.[45] These more oxygen-efficient metabolic pathways however, only produce a fraction of the ATP produced in mitochondria and cannot compensate for the loss of energy production resulting from decreased fatty acid oxidation.[37] Since both attachment of myosin heads to actin, leading to contraction, as well as detachment causing relaxation, requires ATP, a low energy availability both affects systolic and diastolic function and could contribute to development of heart failure.

Depending on the stimulus, pathological hypertrophy may either be concentric or eccentric. Concentric remodeling generally occurs in response to systolic pressure overload, whereas eccentric remodeling develops in response to volume overload-induced elevation of diastolic wall stress. These distinct compensatory responses can be explained by the Laplace law, $T=P*r/2h$, in which left ventricular wall stress (T) is directly related to left ventricular pressure (P) and radius (r), and inversely related to left ventricular wall thickness.[46] Pressure overload (↑P), for instance during chronic hypertension or aortic stenosis, causes an elevation of wall stress (↑T), which can be normalized by lowering the radius and increasing the wall thickness by the addition of new sarcomeres in parallel. This concentric remodeling initially lowers the wall stress, but in later stages progressively impairs diastolic function and contributes to the development of heart failure with preserved ejection fraction (HFpEF).[47] Volume overload (↑r) on the other hand, as observed for instance in response to mitral

regurgitation, also causes an elevation of wall stress (↑T), which can only be restored by hypertrophic remodeling of the cardiomyocytes. In contrast to concentric remodeling, volume overload causes an in-series addition of sarcomeres, thereby lengthening the cardiomyocytes.[48] This initially lowers the wall stress and enhances the stroke volume to compensate for the lost volume due to regurgitation, but proceeding elevation of the left ventricular chamber volume progressively compromises both systolic and diastolic function, eventually causing heart failure with reduced ejection fraction (HFrEF).

Vascular dynamics in cardiac remodeling

Cardiomyocyte hypertrophy, either physiological or pathological, initially serves to adapt to an increased workload. The increase in muscle mass, generated to overcome this elevated workload, results in an overall higher energy demand and an augmented supply of nutrients and oxygen is thus required. In physiologically hypertrophied hearts, local hypoxia-induced activation of Hypoxia Inducible Factor 1α (HIF1α), as well as the hypertrophic stimuli-induced activation of the transcriptional regulator GATA4, results in cardiomyocyte transcription and secretion of VEGFA[49, 50], ensuring a proportionate growth of muscle mass and microvessels. In pathological hypertrophy however, the increase in muscle mass is associated with a relative reduction in the number of capillaries, resulting in myocardial hypoxia.[51] This paradoxical reduction in capillary density might result from a Transformation-related Protein 53- (TP53) dependent inhibition of the transcriptional activity of HIF1α.[50]

A mismatch in oxygen and nutrient delivery to pathologically hypertrophied cardiomyocytes is not always the result of insufficient capillary growth. For instance, endothelial dysfunction and capillary rarefaction, as are often observed in HFpEF, also contribute to myocardial ischemia.[52] In addition to the resulting hypoxia, coronary microvascular insufficiency also results in a lower bioavailability of endothelium-derived nitric oxide (NO), leading to reduced Protein Kinase G-induced phosphorylation of the muscular spring Titin (TTN), and thus to impaired cardiac relaxation during diastole.[52] The events causing coronary microvascular dysfunction and rarefaction are still incompletely understood, though a better appreciation hereof might shed new light on the complex etiology of HFpEF.

In **chapter 4** we describe the results from an observational study in ZSF1 rats, a model for early HFpEF, in which we found that the functional cardiac impairments were associated with subendocardial development of highly proliferating endothelial clusters, showing a distinct lack of vascular morphology. These results led us to hypothesize that the hyperproliferative vascular reaction in ZSF1 heart could be part of a destructive response, that leads to replacement of functional vascular structures by fibrotic tissue with semi- and

nonfunctional microvascular clusters, which may ultimately deteriorate into large fibrotic areas that are devoid of vascular support.

Renal function and role in cardiovascular homeostasis

The primary function of the kidneys is to remove dissolved (metabolic) waste products generated by cells throughout the body. In order to do so, the kidney is composed of complex units of intertwining capillaries and renal tubules, called nephrons. These nephrons contain highly specialized structures, including the glomerulus, in which blood pressure forces fluids and dissolved solutes from the capillaries into the renal tubule. In the different segments of the renal tubule, most of the water and useful organic molecules are reclaimed, leaving a concentrated solution of waste products that enters the calyx as urine. Normal kidney function relies on adequate glomerular filtration rate (GFR), which in turn depends on glomerular blood pressure. A low GFR in response to hypovolemia results in accumulation of circulating waste products, and after prolonged presence could induce ischemic damage to the kidney.[53] Vice versa, a high GFR from the perspective of an individual nephron, for instance as an adaptive response to nephron loss, leads to glomerular hypertension and subsequent glomerulosclerosis with progressive decline in renal function.[54] Glomerular blood pressure can be regulated in multiple ways; local short-term regulation of glomerular blood pressure can be accomplished by adjusting the diameter of the pre- and post-glomerular arterioles, whereas long-term adaptation, involving adjustments of blood pressure and blood volume, is under neurohormonal control. In response to low GFR, the kidney releases renin in the circulation.[55] Renin and angiotensin converting enzyme (ACE) induces the conversion of angiotensinogen into ANG II, which stimulates vasoconstriction and secretion of antidiuretic hormone and aldosterone[55]. ANG II-induced secretion of these hormones leads to water and sodium retention, and in combination with vasoconstriction these events induce an elevation of blood pressure and GFR. When blood volume and blood pressure are too high, Natriuretic Peptide A is secreted by atrial cardiomyocytes, which opposes the effects of the renin-angiotensin system (RAS).[56]

Since kidneys for their well-functioning not only depend on normal blood pressure and blood volume, but also have a profound role in the regulation thereof, it is not surprising to find that cardiovascular and renal homeostasis are directly connected. Renal dysfunction in response to an acute or chronic decline in cardiac output (cardiorenal syndrome type I and II, respectively[57]) predominantly results from renal hypoperfusion-mediated activation of RAS.[58] Sodium and water retention induced by RAS activation causes macro- and microvascular disease, affecting both renal and cardiac homeostasis.[58] In addition to the above-described functions, ANG II also elevates renal ET1 levels, which activates NFκB- and TGFβ-induced

renal inflammation and fibrosis.[57] Moreover, low perfusion of the kidneys also causes hypoxia-induced oxidative stress, which impairs endothelial NO activity and may promote inflammation.[59] The subsequent secretion of inflammatory factors, including IL1 and TNFα, contributes to the ET1-induced renal inflammation leading to progression of renal injury and loss of kidney function. Conversely, cardiac dysfunction in response to an acute or chronic decline in renal function (renocardiac syndrome type III and IV, respectively[57]) is also highly dependent on RAS activation. As described previously, ANG II and ET1 can directly induce NFAT-dependent cardiomyocyte hypertrophy, but in addition also contribute to concentric or eccentric cardiac remodeling via the induction of hypertension and hypervolemia, respectively.[60] In addition, the secretion of proinflammatory factors in response to renal ischemia, as well as the gradual accumulation of renal toxins, also affects cardiac function by promoting endothelial dysfunction and cardiomyocyte apoptosis, and by decreasing cardiac contractility.[61]

Comorbidities in development of diastolic dysfunction

Diastolic dysfunction, often leading to HFpEF, is associated with hypertension-induced concentric cardiac remodeling. However, it has recently been shown that treatment of HFpEF with antihypertensive drugs alone does not reduce morbidity and mortality[62], implicating that the etiology of HFpEF embodies more than a relatively simple maladaptive hypertrophic response. In addition to hypertrophic remodeling, LV material from HFpEF patients also revealed presence of increased myocardial passive stiffness and incomplete relaxation, as well as oxidative stress, interstitial fibrosis and inflammation[63, 64]. Based on these findings, a new paradigm has been proposed[52], stating that HFpEF results from a comorbidity-induced systemic inflammatory state, leading to coronary microvascular dysfunction and lower NO production. The consecutive limitation in NO bioavailability impairs myocardial PKG activity, leading to cardiomyocyte hypertrophy and reduced PKG-induced phosphorylation of TTN. The prominent role of comorbidities in disease onset and progression is shared by both types of HF, however, many of these comorbidities, including obesity, diabetes, hypertension and anemia, are more prevalent in HFpEF than in HFrEF.[65] As approximately half of the HFpEF patients have five or more major comorbidities, it is hard to interpret the individual or synergistic contribution to disease development. It is for instance estimated that at least 75% of the incidence of hypertension in the human population is related to obesity, and both comorbidities thus often present together.[66] The current consensus is that metabolic- and hypertensive disease contribute to the systemic state of inflammation, and as such, potentially act synergistically in development and progression of diastolic dysfunction. However, direct evidence for such a synergistic relation is lacking.

More insight in the putative synergistic effects might provide a better understanding of the pathogenesis of HFpEF.

In **chapter 5** we tested the hypothesis that metabolic- and hypertensive disease act synergistically in development and/or progression of HFpEF. Our findings in ZSF1 rats treated with placebo or deoxycorticosterone acetate- and dietary salt-induced severe hypertension did not support this hypothesis. Instead, we found important phenotypical differences in comorbidity-induced cardiac adaptation, thus emphasizing the need for thorough and individualized phenotypical characterization of HFpEF patients.

Genetics in renal- and cardiovascular homeostasis

Health or disease appears to be the net result of the complex interplay between environmental factors and an individual's genetic background. In addition to the described comorbidities, genetic studies have also provided valuable insights in the etiology of renal- and cardiovascular disease. *In vitro* and *in vivo* verification of these genetic studies indicated that rare mutations found in genes encoding Low-Density Lipoprotein Receptor and Nephrin for instance, can initiate atherosclerotic- or renal disease, respectively.[67, 68] Besides these rare variants, genome wide association studies (GWASs) have identified multiple common variants or single nucleotide polymorphisms (SNPs) as genetic risk factors for onset and progression of renal- and cardiovascular disease.[69-72] Although strong correlations were found between these common variants and disease development, functional annotation of these loci remains an issue, as a disease-associated SNP only marks the genetic variation of its linkage disequilibrium (LD) region and does not necessarily represent the disease causing allele itself. Currently, functional annotation of GWAS data is mainly conducted by linking susceptibility loci by spatial proximity to the nearest gene coding region. However, recent epigenetic studies have also revealed that DNA is packed with regulatory elements (DREs), such as enhancers and repressors, located in both coding- and non-protein-coding DNA regions.[73] These DREs play a crucial role in transcriptional regulation in a cell type- and circumstance-specific manner. In response to a particular stimulus, activation of specific transcription factors and cofactors, in addition to increased DNA region accessibility, DREs can stimulate or repress the transcription of their targets by interacting with a target gene's transcriptional start site via the formation of 3D chromatin loops. Genetic variation co-localizing with these DREs can affect the function of these elements, potentially leading to transcriptional dysregulation. It has been reported that DREs can regulate expression levels of targets located up to thousands of kilo base pairs up- or downstream[74], which far exceeds the current standard distance for GWAS annotation. SNPs located in DRE regions could hypothetically interfere with transcriptional regulation of gene targets. If the affected DREs

regulate the expression of specific factors involved in a certain critical protective mechanism, this could contribute to onset or progression of disease.

In **chapter 6** and **chapter 7** we describe how we used circular chromosome conformation capture-sequencing (4C-seq) to identify putative candidate genes for atherosclerosis and chronic kidney disease, respectively, by examining 3D chromatin interactions of DREs colocalizing with disease-associated susceptibility loci. Cross-linking the folded and interacting DRE segments, followed by two DNA restriction-ligation steps and DNA sequencing, allowed us to identify DRE-interacting target genes that could be considered as new gene candidates for hypothesis-driven future studies.

Outline of this thesis

This thesis describes novel insights in the molecular regulation of renal and cardiovascular homeostasis in health and disease. First, in **chapter 2** we describe the mechanism by which loss of WNT receptor FZD5 attenuates the angiogenic process. Knockdown of endothelial FZD5 induced the combined transcriptional upregulation of the vascular destabilizing factor ANGPT2 and pro-angiogenic VEGFA scavenging VEGFR1. In **chapter 3** we describe a transcriptome-based analysis of the immense effect of endothelial interaction on pericyte behavior, providing us with a better appreciation of the mechanisms that contribute to pericyte-induced vascular stabilization. Moving to metabolic disease models, we present in **chapter 4** the results from a study in ZSF1 rats, in which we found that diastolic dysfunction was associated with subendocardial development of highly proliferating endothelial clusters, showing a distinct lack of vascular morphology. These results led us to hypothesize that the hyperproliferative vascular reaction in ZSF1 heart could be part of a destructive response, that induces replacement of functional vascular structures by fibrotic tissue with semi- and nonfunctional microvascular clusters, which may ultimately deteriorate into large fibrotic areas that are devoid of vascular support. In **chapter 5** we used the same ZSF1 model to test the hypothesis that metabolic- and hypertensive disease act synergistically in development of diastolic dysfunction. Our findings in ZSF1 with or without severe hypertension did not support our hypothesis and clearly indicated that obesity and hypertension induce important phenotypical differences in cardiac adaptation. Moreover, these observations emphasize the need for thorough and individualized phenotypical characterization of HFpEF patients. In **chapter 6** and **chapter 7** we describe how we used 4C-seq to identify putative candidate genes for future hypothesis-driven studies on atherosclerosis and chronic kidney disease, respectively. Examining 3D chromatin interactions of DREs that colocalize with disease-associated susceptibility loci enabled us to

identify genes that might be transcriptionally dysregulated in carriers of these variants. Finally, we interpret and discuss the results of **chapters 2-7** in **chapter 8**.

References

1. Aird, WC: Discovery of the cardiovascular system: from Galen to William Harvey. *J Thromb Haemost,* 9 Suppl 1**:** 118-129, 2011.
2. Prendergast, J: Galen's View of the Vascular System in Relation to that of Harvey. *Proc R Soc Med,* 21**:** 1839-1848, 1928.
3. Mezzogiorno, V, Mezzogiorno, A, Passiatore, C: A contribution to the history of renal structure knowledge (from Galen to Malpighi). *Ann Anat,* 175**:** 395-401, 1993.
4. Lagay, F: The legacy of humoral medicine. *Virtual Mentor,* 4, 2002.
5. Goldie, LC, Nix, MK, Hirschi, KK: Embryonic vasculogenesis and hematopoietic specification. *Organogenesis,* 4**:** 257-263, 2008.
6. Poole, TJ, Finkelstein, EB, Cox, CM: The role of FGF and VEGF in angioblast induction and migration during vascular development. *Dev Dyn,* 220**:** 1-17, 2001.
7. Shalaby, F, Rossant, J, Yamaguchi, TP, Gertsenstein, M, Wu, XF, Breitman, ML, Schuh, AC: Failure of blood-island formation and vasculogenesis in Flk-1-deficient mice. *Nature,* 376**:** 62-66, 1995.
8. Cleaver, O, Krieg, PA: VEGF mediates angioblast migration during development of the dorsal aorta in Xenopus. *Development,* 125**:** 3905-3914, 1998.
9. Cross, MJ, Claesson-Welsh, L: FGF and VEGF function in angiogenesis: signalling pathways, biological responses and therapeutic inhibition. *Trends Pharmacol Sci,* 22**:** 201-207, 2001.
10. Rodrigues, M, Xin, X, Jee, K, Babapoor-Farrokhran, S, Kashiwabuchi, F, Ma, T, Bhutto, I, Hassan, SJ, Daoud, Y, Baranano, D, Solomon, S, Lutty, G, Semenza, GL, Montaner, S, Sodhi, A: VEGF secreted by hypoxic Muller cells induces MMP-2 expression and activity in endothelial cells to promote retinal neovascularization in proliferative diabetic retinopathy. *Diabetes,* 62**:** 3863-3873, 2013.
11. Zhang, L, Yang, N, Park, JW, Katsaros, D, Fracchioli, S, Cao, G, O'Brien-Jenkins, A, Randall, TC, Rubin, SC, Coukos, G: Tumor-derived vascular endothelial growth factor up-regulates angiopoietin-2 in host endothelium and destabilizes host vasculature, supporting angiogenesis in ovarian cancer. *Cancer Res,* 63**:** 3403-3412, 2003.
12. Carmeliet, P, Jain, RK: Molecular mechanisms and clinical applications of angiogenesis. *Nature,* 473**:** 298-307, 2011.
13. Potente, M, Gerhardt, H, Carmeliet, P: Basic and therapeutic aspects of angiogenesis. *Cell,* 146**:** 873-887, 2011.
14. Mentzer, SJ, Konerding, MA: Intussusceptive angiogenesis: expansion and remodeling of microvascular networks. *Angiogenesis,* 17**:** 499-509, 2014.
15. Klagsbrun, M, D'Amore, PA: Regulators of angiogenesis. *Annu Rev Physiol,* 53**:** 217-239, 1991.
16. Ejaz, S, Chekarova, I, Ejaz, A, Sohail, A, Lim, CW: Importance of pericytes and mechanisms of pericyte loss during diabetes retinopathy. *Diabetes Obes Metab,* 10**:** 53-63, 2008.
17. Olive, PL, Vikse, C, Trotter, MJ: Measurement of oxygen diffusion distance in tumor cubes using a fluorescent hypoxia probe. *Int J Radiat Oncol Biol Phys,* 22**:** 397-402, 1992.
18. Carmeliet, P, Jain, RK: Angiogenesis in cancer and other diseases. *Nature,* 407**:** 249-257, 2000.
19. Bielenberg, DR, Zetter, BR: The Contribution of Angiogenesis to the Process of Metastasis. *Cancer J,* 21**:** 267-273, 2015.
20. J Levine, R, Maynard, S, Qian, C, Lim, K-H, England, L, Yu, K, Schisterman, E, Thadhani, R, P Sachs, B, H Epstein, F, Sibai, B, Sukhatme, V, Ananth Karumanchi, S: *Circulating Angiogenic Factors and the Risk of Preeclampsia*, 2004.
21. Venkatesha, S, Toporsian, M, Lam, C, Hanai, J, Mammoto, T, Kim, YM, Bdolah, Y, Lim, KH, Yuan, HT, Libermann, TA, Stillman, IE, Roberts, D, D'Amore, PA, Epstein, FH, Sellke, FW, Romero, R, Sukhatme, VP, Letarte, M, Karumanchi, SA: Soluble endoglin contributes to the pathogenesis of preeclampsia*. Nat Med,* 12**:** 642-649, 2006.
22. Ishikawa, T, Tamai, Y, Zorn, AM, Yoshida, H, Seldin, MF, Nishikawa, S, Taketo, MM: Mouse Wnt receptor gene Fzd5 is essential for yolk sac and placental angiogenesis. *Development,* 128**:** 25-33, 2001.
23. Paes, KT, Wang, E, Henze, K, Vogel, P, Read, R, Suwanichkul, A, Kirkpatrick, LL, Potter, D, Newhouse, MM, Rice, DS: Frizzled 4 is required for retinal angiogenesis and maintenance of the blood-retina barrier. *Invest Ophthalmol Vis Sci,* 52**:** 6452-6461, 2011.
24. Peghaire, C, Bats, ML, Sewduth, R, Jeanningros, S, Jaspard, B, Couffinhal, T, Duplaa, C, Dufourcq, P: Fzd7 (Frizzled-7) Expressed by Endothelial Cells Controls Blood Vessel Formation Through Wnt/beta-Catenin Canonical Signaling. *Arterioscler Thromb Vasc Biol,* 36**:** 2369-2380, 2016.
25. Niehrs, C: The complex world of WNT receptor signalling. *Nat Rev Mol Cell Biol,* 13**:** 767-779, 2012.

26. MacDonald, BT, Tamai, K, He, X: Wnt/beta-catenin signaling: components, mechanisms, and diseases. *Dev Cell,* 17**:** 9-26, 2009.
27. Lawrence, T: The nuclear factor NF-kappaB pathway in inflammation. *Cold Spring Harb Perspect Biol,* 1**:** a001651, 2009.
28. Brown, JD, Lin, CY, Duan, Q, Griffin, G, Federation, A, Paranal, RM, Bair, S, Newton, G, Lichtman, A, Kung, A, Yang, T, Wang, H, Luscinskas, FW, Croce, K, Bradner, JE, Plutzky, J: NF-kappaB directs dynamic super enhancer formation in inflammation and atherogenesis. *Mol Cell,* 56**:** 219-231, 2014.
29. Ross, R, Agius, L: The process of atherogenesis--cellular and molecular interaction: from experimental animal models to humans. *Diabetologia,* 35 Suppl 2**:** S34-40, 1992.
30. Gittenberger-de Groot, AC, Bartelings, MM, Deruiter, MC, Poelmann, RE: Basics of cardiac development for the understanding of congenital heart malformations. *Pediatr Res,* 57**:** 169-176, 2005.
31. Rupert, CE, Coulombe, KLK: IGF1 and NRG1 Enhance Proliferation, Metabolic Maturity, and the Force-Frequency Response in hESC-Derived Engineered Cardiac Tissues. *Stem Cells Int,* 2017**:** 7648409, 2017.
32. Schleich, JM, Abdulla, T, Summers, R, Houyel, L: An overview of cardiac morphogenesis. *Arch Cardiovasc Dis,* 106**:** 612-623, 2013.
33. Piquereau, J, Ventura-Clapier, R: Maturation of Cardiac Energy Metabolism During Perinatal Development. *Front Physiol,* 9**:** 959, 2018.
34. Prosdocimo, DA, John, JE, Zhang, L, Efraim, ES, Zhang, R, Liao, X, Jain, MK: KLF15 and PPARalpha Cooperate to Regulate Cardiomyocyte Lipid Gene Expression and Oxidation. *PPAR Res,* 2015**:** 201625, 2015.
35. Honkoop, H, de Bakker, D, Aharonov, A, Kruse, F, Shakked, A, Nguyen, P, de Heus, C, Garric, L, Muraro, M, Shoffner, A, Tessadori, F, Peterson, J, Noort, W, Posthuma, G, Grün, D, van der laarse, W, Klumperman, J, Jaspers, R, Poss, K, Bakkers, J: *A metabolic switch from OXPHOS to glycolysis is essential for cardiomyocyte proliferation in the regenerating heart*, 2018.
36. McMullen, JR, Shioi, T, Huang, WY, Zhang, L, Tarnavski, O, Bisping, E, Schinke, M, Kong, S, Sherwood, MC, Brown, J, Riggi, L, Kang, PM, Izumo, S: The insulin-like growth factor 1 receptor induces physiological heart growth via the phosphoinositide 3-kinase(p110alpha) pathway. *J Biol Chem,* 279**:** 4782-4793, 2004.
37. Nakamura, M, Sadoshima, J: Mechanisms of physiological and pathological cardiac hypertrophy. *Nat Rev Cardiol,* 15**:** 387-407, 2018.
38. Archer, CR, Robinson, EL, Drawnel, FM, Roderick, HL: Endothelin-1 promotes hypertrophic remodelling of cardiac myocytes by activating sustained signalling and transcription downstream of endothelin type A receptors. *Cell Signal,* 36**:** 240-254, 2017.
39. Molkentin, JD, Lu, JR, Antos, CL, Markham, B, Richardson, J, Robbins, J, Grant, SR, Olson, EN: A calcineurin-dependent transcriptional pathway for cardiac hypertrophy. *Cell,* 93**:** 215-228, 1998.
40. Braz, JC, Gregory, K, Pathak, A, Zhao, W, Sahin, B, Klevitsky, R, Kimball, TF, Lorenz, JN, Nairn, AC, Liggett, SB, Bodi, I, Wang, S, Schwartz, A, Lakatta, EG, DePaoli-Roach, AA, Robbins, J, Hewett, TE, Bibb, JA, Westfall, MV, Kranias, EG, Molkentin, JD: PKC-alpha regulates cardiac contractility and propensity toward heart failure. *Nat Med,* 10**:** 248-254, 2004.
41. Fearnley, CJ, Roderick, HL, Bootman, MD: Calcium signaling in cardiac myocytes. *Cold Spring Harb Perspect Biol,* 3**:** a004242, 2011.
42. Asp, ML, Martindale, JJ, Heinis, FI, Wang, W, Metzger, JM: Calcium mishandling in diastolic dysfunction: mechanisms and potential therapies. *Biochim Biophys Acta,* 1833**:** 895-900, 2013.
43. Pouleur, H: Diastolic dysfunction and myocardial energetics. *Eur Heart J,* 11 Suppl C**:** 30-34, 1990.
44. Schirone, L, Forte, M, Palmerio, S, Yee, D, Nocella, C, Angelini, F, Pagano, F, Schiavon, S, Bordin, A, Carrizzo, A, Vecchione, C, Valenti, V, Chimenti, I, De Falco, E, Sciarretta, S, Frati, G: A Review of the Molecular Mechanisms Underlying the Development and Progression of Cardiac Remodeling. *Oxid Med Cell Longev,* 2017**:** 3920195, 2017.
45. van Bilsen, M, van Nieuwenhoven, FA, van der Vusse, GJ: Metabolic remodelling of the failing heart: beneficial or detrimental? *Cardiovasc Res,* 81**:** 420-428, 2009.
46. Frohlich, ED, Susic, D: Pressure overload. *Heart Fail Clin,* 8**:** 21-32, 2012.
47. Heinzel, FR, Hohendanner, F, Jin, G, Sedej, S, Edelmann, F: Myocardial hypertrophy and its role in heart failure with preserved ejection fraction. *J Appl Physiol (1985),* 119**:** 1233-1242, 2015.
48. Rossi, MA, Carillo, SV: Cardiac hypertrophy due to pressure and volume overload: distinctly different biological phenomena? *Int J Cardiol,* 31**:** 133-141, 1991.

49. Heineke, J, Auger-Messier, M, Xu, J, Oka, T, Sargent, MA, York, A, Klevitsky, R, Vaikunth, S, Duncan, SA, Aronow, BJ, Robbins, J, Crombleholme, TM, Molkentin, JD: Cardiomyocyte GATA4 functions as a stress-responsive regulator of angiogenesis in the murine heart. *J Clin Invest,* 117**:** 3198-3210, 2007.
50. Sano, M, Minamino, T, Toko, H, Miyauchi, H, Orimo, M, Qin, Y, Akazawa, H, Tateno, K, Kayama, Y, Harada, M, Shimizu, I, Asahara, T, Hamada, H, Tomita, S, Molkentin, JD, Zou, Y, Komuro, I: p53-induced inhibition of Hif-1 causes cardiac dysfunction during pressure overload. *Nature,* 446**:** 444-448, 2007.
51. Oka, T, Akazawa, H, Naito, AT, Komuro, I: Angiogenesis and cardiac hypertrophy: maintenance of cardiac function and causative roles in heart failure. *Circ Res,* 114**:** 565-571, 2014.
52. Paulus, WJ, Tschope, C: A novel paradigm for heart failure with preserved ejection fraction: comorbidities drive myocardial dysfunction and remodeling through coronary microvascular endothelial inflammation. *J Am Coll Cardiol,* 62**:** 263-271, 2013.
53. Basile, DP, Anderson, MD, Sutton, TA: Pathophysiology of acute kidney injury. *Compr Physiol,* 2**:** 1303-1353, 2012.
54. Helal, I, Fick-Brosnahan, GM, Reed-Gitomer, B, Schrier, RW: Glomerular hyperfiltration: definitions, mechanisms and clinical implications. *Nat Rev Nephrol,* 8**:** 293-300, 2012.
55. Lavoie, JL, Sigmund, CD: Minireview: overview of the renin-angiotensin system--an endocrine and paracrine system. *Endocrinology,* 144**:** 2179-2183, 2003.
56. de Bold, AJ: Atrial natriuretic factor: a hormone produced by the heart. *Science,* 230**:** 767-770, 1985.
57. Shamseddin, MK, Parfrey, PS: Mechanisms of the cardiorenal syndromes. *Nat Rev Nephrol,* 5**:** 641-649, 2009.
58. Rea, ME, Dunlap, ME: Renal hemodynamics in heart failure: implications for treatment. *Curr Opin Nephrol Hypertens,* 17**:** 87-92, 2008.
59. Bongartz, LG, Cramer, MJ, Doevendans, PA, Joles, JA, Braam, B: The severe cardiorenal syndrome: 'Guyton revisited'. *Eur Heart J,* 26**:** 11-17, 2005.
60. Amann, K, Rychlik, I, Miltenberger-Milteny, G, Ritz, E: Left ventricular hypertrophy in renal failure. *Kidney Int Suppl,* 68**:** S78-85, 1998.
61. Lekawanvijit, S: Cardiotoxicity of Uremic Toxins: A Driver of Cardiorenal Syndrome. *Toxins (Basel),* 10, 2018.
62. Tsioufis, C, Georgiopoulos, G, Oikonomou, D, Thomopoulos, C, Katsiki, N, Kasiakogias, A, Chrysochoou, C, Konstantinidis, D, Kalos, T, Tousoulis, D: Hypertension and Heart Failure with Preserved Ejection Fraction: Connecting the Dots. *Curr Vasc Pharmacol,* 16**:** 15-22, 2017.
63. Westermann, D, Lindner, D, Kasner, M, Zietsch, C, Savvatis, K, Escher, F, von Schlippenbach, J, Skurk, C, Steendijk, P, Riad, A, Poller, W, Schultheiss, HP, Tschope, C: Cardiac inflammation contributes to changes in the extracellular matrix in patients with heart failure and normal ejection fraction. *Circ Heart Fail,* 4**:** 44-52, 2011.
64. van Heerebeek, L, Borbely, A, Niessen, HW, Bronzwaer, JG, van der Velden, J, Stienen, GJ, Linke, WA, Laarman, GJ, Paulus, WJ: Myocardial structure and function differ in systolic and diastolic heart failure. *Circulation,* 113**:** 1966-1973, 2006.
65. Mentz, RJ, Kelly, JP, von Lueder, TG, Voors, AA, Lam, CS, Cowie, MR, Kjeldsen, K, Jankowska, EA, Atar, D, Butler, J, Fiuzat, M, Zannad, F, Pitt, B, O'Connor, CM: Noncardiac comorbidities in heart failure with reduced versus preserved ejection fraction. *J Am Coll Cardiol,* 64**:** 2281-2293, 2014.
66. Leggio, M, Lombardi, M, Caldarone, E, Severi, P, D'Emidio, S, Armeni, M, Bravi, V, Bendini, MG, Mazza, A: The relationship between obesity and hypertension: an updated comprehensive overview on vicious twins. *Hypertens Res,* 40**:** 947-963, 2017.
67. Rader, DJ, Cohen, J, Hobbs, HH: Monogenic hypercholesterolemia: new insights in pathogenesis and treatment. *J Clin Invest,* 111**:** 1795-1803, 2003.
68. Ovunc, B, Ashraf, S, Vega-Warner, V, Bockenhauer, D, Elshakhs, NA, Joseph, M, Hildebrandt, F, Gesellschaft fur Padiatrische Nephrologie Study, G: Mutation analysis of NPHS1 in a worldwide cohort of congenital nephrotic syndrome patients. *Nephron Clin Pract,* 120**:** c139-146, 2012.
69. Kottgen, A, Pattaro, C, Boger, CA, Fuchsberger, C, Olden, M, Glazer, NL, Parsa, A, Gao, X, Yang, Q, Smith, AV, O'Connell, JR, Li, M, Schmidt, H, Tanaka, T, Isaacs, A, Ketkar, S, Hwang, SJ, Johnson, AD, Dehghan, A, Teumer, A, Pare, G, Atkinson, EJ, Zeller, T, Lohman, K, Cornelis, MC, Probst-Hensch, NM, Kronenberg, F, Tonjes, A, Hayward, C, Aspelund, T, Eiriksdottir, G, Launer, LJ, Harris, TB, Rampersaud, E, Mitchell, BD, Arking, DE, Boerwinkle, E, Struchalin, M, Cavalieri, M, Singleton, A, Giallauria, F, Metter, J, de Boer, IH, Haritunians, T, Lumley, T,

Siscovick, D, Psaty, BM, Zillikens, MC, Oostra, BA, Feitosa, M, Province, M, de Andrade, M, Turner, ST, Schillert, A, Ziegler, A, Wild, PS, Schnabel, RB, Wilde, S, Munzel, TF, Leak, TS, Illig, T, Klopp, N, Meisinger, C, Wichmann, HE, Koenig, W, Zgaga, L, Zemunik, T, Kolcic, I, Minelli, C, Hu, FB, Johansson, A, Igl, W, Zaboli, G, Wild, SH, Wright, AF, Campbell, H, Ellinghaus, D, Schreiber, S, Aulchenko, YS, Felix, JF, Rivadeneira, F, Uitterlinden, AG, Hofman, A, Imboden, M, Nitsch, D, Brandstatter, A, Kollerits, B, Kedenko, L, Magi, R, Stumvoll, M, Kovacs, P, Boban, M, Campbell, S, Endlich, K, Volzke, H, Kroemer, HK, Nauck, M, Volker, U, Polasek, O, Vitart, V, Badola, S, Parker, AN, Ridker, PM, Kardia, SL, Blankenberg, S, Liu, Y, Curhan, GC, Franke, A, Rochat, T, Paulweber, B, Prokopenko, I, Wang, W, Gudnason, V, Shuldiner, AR, Coresh, J, Schmidt, R, Ferrucci, L, Shlipak, MG, van Duijn, CM, Borecki, I, Kramer, BK, Rudan, I, Gyllensten, U, Wilson, JF, Witteman, JC, Pramstaller, PP, Rettig, R, Hastie, N, Chasman, DI, Kao, WH, Heid, IM, Fox, CS: New loci associated with kidney function and chronic kidney disease. *Nat Genet,* 42**:** 376-384, 2010.

70. Okada, Y, Sim, X, Go, MJ, Wu, JY, Gu, D, Takeuchi, F, Takahashi, A, Maeda, S, Tsunoda, T, Chen, P, Lim, SC, Wong, TY, Liu, J, Young, TL, Aung, T, Seielstad, M, Teo, YY, Kim, YJ, Lee, JY, Han, BG, Kang, D, Chen, CH, Tsai, FJ, Chang, LC, Fann, SJ, Mei, H, Rao, DC, Hixson, JE, Chen, S, Katsuya, T, Isono, M, Ogihara, T, Chambers, JC, Zhang, W, Kooner, JS, KidneyGen, C, Consortium, CK, Albrecht, E, consortium, G, Yamamoto, K, Kubo, M, Nakamura, Y, Kamatani, N, Kato, N, He, J, Chen, YT, Cho, YS, Tai, ES, Tanaka, T: Meta-analysis identifies multiple loci associated with kidney function-related traits in east Asian populations. *Nat Genet,* 44**:** 904-909, 2012.
71. Consortium, CAD, Deloukas, P, Kanoni, S, Willenborg, C, Farrall, M, Assimes, TL, Thompson, JR, Ingelsson, E, Saleheen, D, Erdmann, J, Goldstein, BA, Stirrups, K, Konig, IR, Cazier, JB, Johansson, A, Hall, AS, Lee, JY, Willer, CJ, Chambers, JC, Esko, T, Folkersen, L, Goel, A, Grundberg, E, Havulinna, AS, Ho, WK, Hopewell, JC, Eriksson, N, Kleber, ME, Kristiansson, K, Lundmark, P, Lyytikainen, LP, Rafelt, S, Shungin, D, Strawbridge, RJ, Thorleifsson, G, Tikkanen, E, Van Zuydam, N, Voight, BF, Waite, LL, Zhang, W, Ziegler, A, Absher, D, Altshuler, D, Balmforth, AJ, Barroso, I, Braund, PS, Burgdorf, C, Claudi-Boehm, S, Cox, D, Dimitriou, M, Do, R, Consortium, D, Consortium, C, Doney, AS, El Mokhtari, N, Eriksson, P, Fischer, K, Fontanillas, P, Franco-Cereceda, A, Gigante, B, Groop, L, Gustafsson, S, Hager, J, Hallmans, G, Han, BG, Hunt, SE, Kang, HM, Illig, T, Kessler, T, Knowles, JW, Kolovou, G, Kuusisto, J, Langenberg, C, Langford, C, Leander, K, Lokki, ML, Lundmark, A, McCarthy, MI, Meisinger, C, Melander, O, Mihailov, E, Maouche, S, Morris, AD, Muller-Nurasyid, M, Mu, TC, Nikus, K, Peden, JF, Rayner, NW, Rasheed, A, Rosinger, S, Rubin, D, Rumpf, MP, Schafer, A, Sivananthan, M, Song, C, Stewart, AF, Tan, ST, Thorgeirsson, G, van der Schoot, CE, Wagner, PJ, Wellcome Trust Case Control, C, Wells, GA, Wild, PS, Yang, TP, Amouyel, P, Arveiler, D, Basart, H, Boehnke, M, Boerwinkle, E, Brambilla, P, Cambien, F, Cupples, AL, de Faire, U, Dehghan, A, Diemert, P, Epstein, SE, Evans, A, Ferrario, MM, Ferrieres, J, Gauguier, D, Go, AS, Goodall, AH, Gudnason, V, Hazen, SL, Holm, H, Iribarren, C, Jang, Y, Kahonen, M, Kee, F, Kim, HS, Klopp, N, Koenig, W, Kratzer, W, Kuulasmaa, K, Laakso, M, Laaksonen, R, Lee, JY, Lind, L, Ouwehand, WH, Parish, S, Park, JE, Pedersen, NL, Peters, A, Quertermous, T, Rader, DJ, Salomaa, V, Schadt, E, Shah, SH, Sinisalo, J, Stark, K, Stefansson, K, Tregouet, DA, Virtamo, J, Wallentin, L, Wareham, N, Zimmermann, ME, Nieminen, MS, Hengstenberg, C, Sandhu, MS, Pastinen, T, Syvanen, AC, Hovingh, GK, Dedoussis, G, Franks, PW, Lehtimaki, T, Metspalu, A, Zalloua, PA, Siegbahn, A, Schreiber, S, Ripatti, S, Blankenberg, SS, Perola, M, Clarke, R, Boehm, BO, O'Donnell, C, Reilly, MP, Marz, W, Collins, R, Kathiresan, S, Hamsten, A, Kooner, JS, Thorsteinsdottir, U, Danesh, J, Palmer, CN, Roberts, R, Watkins, H, Schunkert, H, Samani, NJ: Large-scale association analysis identifies new risk loci for coronary artery disease. *Nat Genet,* 45**:** 25-33, 2013.
72. Traylor, M, Farrall, M, Holliday, EG, Sudlow, C, Hopewell, JC, Cheng, YC, Fornage, M, Ikram, MA, Malik, R, Bevan, S, Thorsteinsdottir, U, Nalls, MA, Longstreth, W, Wiggins, KL, Yadav, S, Parati, EA, Destefano, AL, Worrall, BB, Kittner, SJ, Khan, MS, Reiner, AP, Helgadottir, A, Achterberg, S, Fernandez-Cadenas, I, Abboud, S, Schmidt, R, Walters, M, Chen, WM, Ringelstein, EB, O'Donnell, M, Ho, WK, Pera, J, Lemmens, R, Norrving, B, Higgins, P, Benn, M, Sale, M, Kuhlenbaumer, G, Doney, AS, Vicente, AM, Delavaran, H, Algra, A, Davies, G, Oliveira, SA, Palmer, CN, Deary, I, Schmidt, H, Pandolfo, M, Montaner, J, Carty, C, de Bakker, PI, Kostulas, K, Ferro, JM, van Zuydam, NR, Valdimarsson, E, Nordestgaard, BG, Lindgren, A, Thijs, V, Slowik, A, Saleheen, D, Pare, G, Berger, K, Thorleifsson, G, Australian Stroke Genetics Collaborative, WTCCC, Hofman, A, Mosley, TH, Mitchell, BD, Furie, K, Clarke, R, Levi, C, Seshadri, S, Gschwendtner, A, Boncoraglio, GB, Sharma, P, Bis, JC, Gretarsdottir, S, Psaty, BM, Rothwell, PM, Rosand, J, Meschia, JF, Stefansson, K, Dichgans,

M, Markus, HS, International Stroke Genetics, C: Genetic risk factors for ischaemic stroke and its subtypes (the METASTROKE collaboration): a meta-analysis of genome-wide association studies. *Lancet Neurol,* 11**:** 951-962, 2012.

73. Maurano, MT, Humbert, R, Rynes, E, Thurman, RE, Haugen, E, Wang, H, Reynolds, AP, Sandstrom, R, Qu, H, Brody, J, Shafer, A, Neri, F, Lee, K, Kutyavin, T, Stehling-Sun, S, Johnson, AK, Canfield, TK, Giste, E, Diegel, M, Bates, D, Hansen, RS, Neph, S, Sabo, PJ, Heimfeld, S, Raubitschek, A, Ziegler, S, Cotsapas, C, Sotoodehnia, N, Glass, I, Sunyaev, SR, Kaul, R, Stamatoyannopoulos, JA: Systematic localization of common disease-associated variation in regulatory DNA. *Science,* 337**:** 1190-1195, 2012.
74. Williamson, I, Hill, RE, Bickmore, WA: Enhancers: from developmental genetics to the genetics of common human disease. *Dev Cell,* 21**:** 17-19, 2011.

Chapter 2

Endothelial loss of FZD5 stimulates PKC/Ets1-mediated transcription of ANGPT2 and VEGFR1

Maarten M. Brandt, Christian G.M. van Dijk, Ihsan Chrifi, Heleen M. Kool, Petra Burgisser, Laura Louzao-Martinez, Jiayi Pei, Robbert J. Rottier, Marianne C. Verhaar, Dirk J. Duncker, Caroline Cheng.

Angiogenesis, 2018; PMID: 2984551

Abstract

Formation of a functional vascular system is essential and its formation is a highly regulated process initiated during embryogenesis, which continues to play important roles throughout life in both health and disease. In previous studies, FZD5 was shown to be critically involved in this process and here we investigated the molecular mechanism by which endothelial loss of this receptor attenuates angiogenesis.

Using short interference RNA mediated loss of function assays, the function and mechanism of signaling via FZD5 was studied in human endothelial cells (ECs). Our findings indicate that FZD5 signaling promotes neovessel formation *in vitro* in a collagen matrix based 3D co-culture of primary vascular cells. Silencing of FZD5 reduced EC proliferation, as a result of G_0/G_1 cell cycle arrest, and decreased cell migration. Furthermore, FZD5 knockdown resulted in enhanced expression of the factors ANGPT2 and VEGFR1, which are mainly known for their destabilizing effects on the vasculature. In FZD5 silenced ECs, ANGPT2 and VEGFR1 upregulation was induced by enhanced PKC signaling, without the involvement of canonical WNT signaling, non-canonical WNT/Ca^{2+} mediated activation of NFAT, and non-canonical WNT/PCP mediated activation of JNK. We demonstrated that PKC induced transcription of ANGPT2 and VEGFR1 involved the transcription factor Ets1.

The current study demonstrates a pro-angiogenic role of FZD5, which was shown to be involved in endothelial tubule formation, cell cycle progression and migration, and partly does so by repression of PKC/Ets1 mediated transcription of VEGFR1 and ANGPT2.

Introduction

New formation of blood vessels from pre-existing vessels, a process called angiogenesis, is a critical step in embryogenesis and continues to play important roles throughout life in both health and disease.[1] It is a dynamic process that is tightly regulated by a diverse range of signal transduction cascades and imbalances in these pathways can be a causative or a progressive factor in many diseases.[2]

Multiple studies suggest an important role for endothelial signal transduction via Frizzled (FZD) receptors in angiogenesis.[3-5] The FZD receptors belong to a family of 10 transmembrane receptors (FZD1-10), which can initiate FZD/WNT canonical and non-canonical signaling upon binding with one of the 19 soluble WNT ligands. Canonical WNT signaling depends on FZD receptor and LRP 5/6 co-activation, initiating Disheveled (DVL) to stabilize β-catenin, followed by β-catenin-mediated transcriptional regulation.[6-8] In contrast, non-canonical WNT signaling also involves DVL, but proceeds via WNT/Ca^{2+} mediated-activation of Nuclear factor of activated T-cells (NFAT) or WNT/Planar Cell Polarity (PCP) mediated activation of c-JUN N-terminal Kinase (JNK).[6] A potential link between FZD5 and angiogenesis was previously demonstrated in FZD5 full knockout mice.[5] FZD5 silencing induced *in utero* death at approximately E10.5, which was associated with vascular defects in the placenta and yolk sac. Furthermore, isolated endothelial cells (ECs) from FZD5 deficient mice showed a reduction in cell proliferation, which is crucial for neo vessel formation. These findings suggest that FZD5 can be an important regulator of angiogenesis. However, the exact type of endothelial FZD5/WNT signaling and the downstream molecular mechanism causal to the poor vascular phenotype in absence of this receptor requires further in depth evaluation.

Here we studied the angiogenic potential of FZD5 and investigated the signaling pathways that are mediated by FZD5/WNT signaling in human ECs. Our findings indicate that WNT5a, which is endogenously expressed in ECs, binds and signals via FZD5, but in absence of this receptor triggers a poor angiogenic phenotype via an alternative signaling route. We demonstrated that FZD5 is essential for neovessel formation *in vitro* in a collagen matrix based 3D co-culture of primary human vascular cells. Silencing of FZD5 reduced EC proliferation as a result of G_0/G_1 cell cycle arrest and decreased cell migration capacity. Furthermore, FZD5 knockdown resulted in enhanced expression of the factors Angiopoietin 2 (ANGPT2) and Fms Related Tyrosine Kinase 1 (VEGFR1), which are mainly known for their destabilizing effects on the vasculature.[9-11] In FZD5 silenced ECs, ANGPT2 and VEGFR1 upregulation was induced by enhanced Protein Kinase C (PKC) signaling, without the involvement of canonical WNT signaling, non-canonical WNT/Ca^{2+} mediated activation of NFAT, and non-canonical WNT/PCP mediated activation of JNK. Further downstream,

PKC induced transcription of ANGPT2 and VEGFR1 involved the transcription factor Protein C-Ets-1 (Ets1), as knockdown of both FZD5 and Ets1 resulted in a marked repression of ANGPT2 and VEGFR1 expression levels. In addition, silencing of Ets1 partially restored the impaired endothelial tubule formation capacity of FZD5 silenced ECs.

Methods

Cell culture

Human Umbilical Vein Endothelial Cells (HUVECs; Lonza) and Human Brain Vascular Pericytes (Sciencell) were cultured on gelatin coated plates in EGM2 medium (EBM2 medium supplemented with EGM2 bullet kit; Lonza, and 100U/ml penicillin/streptomycin; Lonza) and DMEM (supplemented with 100U/ml penicillin/streptomycin; Lonza, and 10% FCS; Lonza) respectively, in 5% CO_2 at 37 ˚C. The experiments were performed with cells at passage 3-5. Lentivirus green fluorescent protein (GFP) transduced HUVECs and lentivirus discosoma sp. red fluorescent protein (dsRED) transduced pericytes were used at passage 5-7. HUVECs and GFP-labeled HUVECs were used from 6 different batches derived from pooled donors. Pericytes and dsRED-labeled pericytes were used from 8 different batches derived from single donors. FZD5, Ets1, and WNT5a knockdown in HUVECs was achieved by cell transfection of a pool containing 4 targeting short interference RNA (siRNA) sequences, whereas PKC isoforms where knocked down with individual siRNA strands (Dharmacon), all in a final concentration of 100nM. Control cells were either untreated or transfected with a pool of 4 non-targeting siRNA sequences (Dharmacon) in a final concentration of 100nM. Target sequences are listed in table 1. Inhibition of GSK3β, NFAT, JNK, and PKC activation was achieved with 20μM LiCl (Sigma), 1μM Cyclosporine A (CsA; Sigma), 20μM SP600125 (Sigma), and 5, 10 and 20nM staurosporine (CST) respectively. Phosphatase activity was inhibited with 50nM Calyculin A. Free Ca^{2+} induced activation of NFAT-mediated transcription was achieved with 10μM A23187. In experiments involving a serum starvation step, the cells were cultured for 24 hours in EBM2.

Quantitative PCR and Western blot analysis

Total RNA was isolated using RNA mini kit (Bioline) and reversed transcribed into cDNA using iScript cDNA synthesis kit (Bioline). Gene expression was assessed by qPCR using SensiFast SYBR & Fluorecein kit (Bioline) and primers as listed in table 2. Expression levels are relative to the housekeeping gene β-actin. For assessment of protein levels, cells were lysed in cold NP-40 lysis buffer (150mM NaCl, 1.0% NP-40, 50 mM Tris, pH 8.0)

Table 1: siRNA sequences used in cell culture.

Target gene	*Target sequence*
Non-targeting	UGGUUUACAUGUCGACUAA
	UGGUUUACAUGUUGUGUGA
	UGGUUUACAUGUUUUCUGA
	UGGUUUACAUGUUUUCCUA
FZD5	GCAUUGUGGUGGCCUGCUA
	GCACAUGCCCAACCAGUUC
	AAAUCACGGUGCCCAUGUG
	GAUCCGCAUCGGCAUCUUC
Ets1	AUAGAGAGCUACGAUAGUU
	GAAAUGAUGUCUCAAGCAU
	GUGAAACCAUAUCAAGUUA
	CAGAAUGACUACUUUGCUA
WNT5a	GCCAAGGGCUCCUACGAGA
	GUUCAGAUGUCAGAAGUAU
	CAUCAAAGAAUGCCAGUAU
	GAAACUGUGCCACUUGUAU
PKCα	UAAGGAACCACAAGCAGUA
PKCδ	CCAUGUAUCCUGAGUGGAA
PKCε	GUGGAGACCUCAUGUUUCA
PKCη	GCACCUGUGUCGUCCAUAA

supplemented with 1mM β-glycerolphosphate, 1mM PMSF, 10mM NaF, 1mM NaOV, and protease inhibitor cocktail (Roche). Total protein concentration was quantified by Pierce® BCA Protein Assay Kit (Thermo Scientific) as a loading control. Lysates were denaturated in Laemmli buffer (60mM Tris pH 6.8, 2% SDS, 10% glycerol, 5% β-mercaptoethanol, 0.01% bromophenol blue) at 90°C for 5 min followed by electrophoresis on a 10% SDS-page gel (Biorad). Subsequently, proteins were transferred to a nitrocellulose membrane (Pierce) and incubated for 1 hour in PBS with 5% non-fat milk, followed by incubation with rabbit anti-FZD5 (Milipore), goat anti-β-actin (Abcam), rabbit anti-β-catenin, anti-non-phospho β-catenin and phospho-β-catenin (CST, validated in Supplemental Figure 3A), rabbit anti-ANGPT2 (Abcam), rabbit anti-JNK and phospho-JNK (CST, validated in Supplemental Figure 4C), rabbit anti-JUN and phospho-JUN (CST, validated in Supplemental Figure 4C), rabbit anti-WNT5a (CST) rabbit anti-DVL2 (CST) according to manufacturer's description. Protein bands were visualized with the Li-Cor detection system (Westburg). Levels of secreted VEGFR1 in cultured medium were assessed 72 hours post transfection using a VEGFR1 ELISA kit (R&D systems).

Table 2: Primer sequences used for (q)PCR.

Gene	*Sense primer sequence*	*Antisense primer sequence*
FZD1	GCCCTCCTACCTCAACTACCA	ACTGACCAAATGCCAATCCA
FZD2	GCTTCCACCTTCTTCACTGTC	GCAGCCCTCCTTCTTGGT
FZD3	CTTCCCTGTCGTAGGCTGTGT	GGGCTCCTTCAGTTGGTTCT
FZD4	ATGAACTGACTGGCTTGTGCT	TGTCTTTGTCCCATCCTTTTG
FZD5	TACCCAGCCTGTCGCTAAAC	AAAACCGTCCAAAGATAAACTGC
FZD6	GCGGAGTGAAGGAAGGATTAG	TGAACAAGCAGAGATGTGGAA
FZD7	CGCCTCTGTTCGTCTACCTCT	CTTGGTGCCGTCGTGTTT
FZD8	GCCTATGGTGAGCGTGTCC	CTGGCTGAAAAAGGGGTTGT
FZD9	CTGGTGCTGGGCAGTAGTTT	GCCAGAAGTCCATGTTGAGG
FZD10	CCTTCATCCTCTCGGGCTTC	AGGCGTTCGTAAAAGTAGCAG
WNT1	CAACAGCAGTGGCCGATGGTGG	CGGCCTGCCTCGTTGTTGTGAAG
WNT2	GTCATGAACCAGGATGGCACA	TGTGTGCACATCCAGAGCTTC
WNT2b	AAGATGGTGCCAACTTCACCG	CTGCCTTCTTGGGGGCTTTGC
WNT3	GAGAGCCTCCCCGTCCACAG	CTGCCAGGAGTGTATTCGCATC
WNT3a	CAGGAACTACGTGGAGATCATG	CCATCCCACCAAACTCGATGTC
WNT4	GCTCTGACAACATCGCCTAC	CTTCTCTCCCGCACATCC
WNT5a	GACCTGGTCTACATCGACCCC	GCAGCACCAGTGGAACTTGCA
WNT5b	TGAAGGAGAAGTACGACAGC	CTCTTGAACTGGTTGTAGCC
WNT6	TTATGGACCCTACCAGCAT	ATGTCCTGTTGCAGGATG
WNT7a	GCCGTTCACGTGGAGCCTGTGCGTGC	AGCATCCTGCCAGGGAGCCCGCAGCT
WNT7b	GATTCGGCCGCTGGAACTGCTC	TGGCCCACCTCGCGGAACTTAG
WNT8a	CTGGTCAGTGAACAATTTCC	GTAGCACTTCTCAGCCTGTT
WNT8b	GTCTTTTCACCTGTGTCCTC	AGGCTGCAGTTTCTAGTCAG
WNT10a	CTGTTCTTCCTACTGCTGCT	ACACACACCTCCATCTGC
WNT10b	GCACCACAGCGCCATCCTCAAG	GGGGTCTCGCTCACAGAAGTCAGGA
WNT11	CACTGAACCAGACGCAACAC	CCTCTCTCCAGGTCAAGCAAA
WNT14	ACAAGTATGAGACGGCACTC	AGAAGCTAGGCGAGTCATC
WNT15	TGAAACTGCGCTATGACTC	GTGAGTCCTCCATGTACACC
WNT16	GAGAGATGGAACTGCATGAT	GATGGGGAAATCTAGGAACT
AXIN2	TTGAATGAAGAAGAGGAGTGGA	TCGGGAAATGAGGTAGAGACA
CCND1	GTCCATGCGGAAGATCGTCG	TCTCCTTCATCTTAGAGGCCACG
C-MYC	CACAGCAAACCTCCTCACAG	CGCCTCTTGACATTCTCCTC
ANGPT1	GCTGAACGGTCACACAGAGA	CTTTCCCCCTCAAAGAAAGC
ANGPT2	TTATCACAGCACCAGCAAGC	TTCGCGAGAACAAATGTGAG
VEGFA	AAGGAGGAGGGCAGAATCAT	ATCTGCATGGTGATGTTGGA

VEGFR2	AGCGATGGCCTCTTCTGTAA	ACACGACTCCATGTTGGTCA
VEGFR1	TGTCAATGTGAAACCCCAGA	GTCACACCTTGCTCCGGAAT
DSCR1	GAGGACGCATTCCAAATCAT	AGTCCCAAATGTCCTTGTGC
TF	TACTTGGCACGGGTCTTCTC	TGTCCGAGGTTTGTCTCCA
Ets1	GGAGCAGCCAGTCATCTTTC	GGTCCCGCACATAGTCCTT
PKCα	CGACTGGGAAAAACTGGAGA	ACTGGGGGTTGACATACGAG
PKCδ	ATTGCCGACTTTGGGATGT	TGAAGAAGGGGTGGATTTTG
PKCε	AAGCCACCCTTCAAACCAC	GGCATCAGGTCTTCACCAAA
PKCη	TCCCACACAAGTTCAGCATC	CCCAATCCCATTTCCTTCTT
MMP1	GATTCGGGGAGAAGTGATGTT	CGGGTAGAAGGGATTTGTG
B-actin	TCCCTGGAGAAGAGCTACGA	AGCACTGTGTTGGCGTACAG

3D analysis of endothelial tubule formation

Twenty-four hours post siRNA transfection, GFP-labeled HUVECs were harvested and suspended with non-transfected dsRED labeled pericytes in collagen as previously described by Stratman.[12] In summary, HUVECs and pericytes were mixed in a 5:1 ratio in EBM2 supplemented with Ascorbic Acid, Fibroblast Growth Factor, and 2% FCS from the EGM2 bullet kit. Additionally, C-X-C motif chemokine 12, Interleukin 3, and Stem Cell Factor were added in a concentration of 800ng/ml (R&D systems). The cell mixture was suspended in bovine collagen (Gibco) with a final concentration of 2mg/ml and pipetted in a 96 wells plate. One hour of incubation in 5% CO_2 at 37 ˚C was followed by the addition of 100µl of the adjusted EBM2 medium on the collagen gels. The addition of recombinant human ANGPT2 and VEGFR1 (R&D systems) was done 24 hours post seeding in the collagen matrix, both in a final concentration of 1000ng/ml. Forty-eight hours and 120 hours post seeding, these co-cultures were imaged by fluorescence microscopy, followed by analysis of the number of junctions, the number of tubules, and the tubule length using AngioSys. At least 3 technical replicates were averaged per condition per independent replicate.

Migration assay

Twenty-four hours post siRNA transfection, HUVECs were plated at a density of 0.5 x 10^5 cells/well in an Oris™ Universal Cell migration Assembly Kit (Platypus Technologies) derived 96 well plate with cell seeding stoppers. Twenty-four hours post sub culturing, the cell stoppers were removed and cells were allowed to migrate into the cell free region for 16 hours in 5% CO_2 at 37 ˚C. Subsequently, the cells were washed in PBS and stained by Calcein-AM followed by visualization using fluorescence microscopy. Wells in which cell seeding stoppers were not removed were used as a negative control. Results were analyzed

by Clemex. At least 3 technical replicates were averaged per condition per independent replicate.

Intracellular immunofluorescent staining

Forty-eight hours post siRNA transfection, HUVECs were seeded on gelatin coated glass coverslips in 12 wells plates at a density of 0.5 x 10^5 cells/well (sub-confluent) and 3.5 x 10^5 cells/well (confluent). Subsequently, cells adhered for 24 hours followed by fixation for 15 min in 4% paraformaldehyde and blocking for 60 min in PBS with 5% bovine serum albumin (Sigma) and 0.3% Triton X-100 (Sigma). After blocking, coverslips were placed on droplets PBS with 1% BSA and 0.3% Triton X-100 containing rabbit anti-β-catenin antibody (CST) for 16 hours in a humidified environment at 4°C. Thereafter, coverslips were incubated on PBS with 1% BSA and 0.3% Triton X-100 containing an Alexa Fluor 594-labeled secondary antibody (Invitrogen) and phalloidin-rhodamin (Invitrogen) for 1 hour at room temperature, finally followed by mounting the stained coverslips on vectashield with DAPI (Brunschwig). Coverslips were imaged by confocal microscopy.

Proliferation, cell cycle assay and apoptosis

Twenty-four hours post siRNA transfection, HUVECs were seeded in 6 wells plates at a density of 0.5 x 10^5 cells/well. To study the effect of FZD5 knockdown on proliferation, HUVECs were harvested 24 hours, 48 hours, and 72 hours post sub culturing and counted by flow cytometry. For analysis of cell cycle progression, cells were harvested 48h post sub culturing and fixated in 70% ethanol for 60 minutes on ice. Subsequently, cells were stained with PI and treated with RNAse (Sigma) for 30 minutes at 37 ˚C and analyzed by flow cytometry. Apoptosis was studied 72 hours after transfection using an *in situ* cell death detection kit (Roche) as described by manufacturer on 4% PFA fixated cells.

WNT5a adenovirus preparation, transduction and stimulation

Recombinant adenoviruses were produced using the Gateway pAd/CMV/V5DEST vector and ViraPowerTM Adenoviral Expression System (Invitrogen), according to manufacturer's instructions. Briefly, the WNT5a expression cassette was cloned from the pENTR^{TM} 221 WNT5a entry vector (Invitrogen) into pAd/CMV/V5-DEST expression vector (Invitrogen) via the LR-reaction II (invitrogen). After verification by DNA sequencing, the pAd/CMV plasmids were linearized by Pac1 restriction and subsequently transfected with Lipofectamine 2000 (Invitrogen) in 293A cells. Infected cells were harvested by the time 80% of the cells detached from plates followed by isolation of viral particles from crude viral lysate. HeLa cells were used to produce WNT5a (or dsRED, referred to as adSHAM) by transduction with

a calculated 5 viral particles per cell. Forty-eight hours post transduction, HeLa cells were cultured for 24 hours on EBM2, which eventually was used to stimulate serum-starved endothelium for 3 hours.

Statistical analysis

For each experiment, N represents the number of independent replicates. Statistical analysis was performed by GraphPad Prism using one-way ANOVA followed by post hoc Tukey's test, unless stated otherwise. Results are expressed as mean ± SEM. Significance was assigned when $P<0.05$ (two-tailed).

Results

FZD5 siRNA induces a specific knockdown of endothelial FZD5

The function of FZD5 was studied *in vitro* using siRNA mediated silencing in HUVECs, which were shown to express all FZD receptors other than FZD10 (Supplemental Figure 1A), and WNT2b, 3, 4, 5a, and 11 (Supplemental Figure 1B). Both qPCR and Western blot analysis confirmed a significant loss of FZD5 expression in cells treated with an siRNA pool specific for FZD5, compared to untreated control cells and cells treated with a pool of non-targeting siRNA, referred to as siSHAM (Supplemental Figure 1C-D). Although FZD receptors share highly similar domains, knockdown of FZD5 was specific. None of the other FZD receptors were differentially expressed after treatment with FZD5 siRNA, other than FZD5 (Supplemental Figure 1C).

WNT5a signals via endothelial FZD5

Previous studies listed WNT5a and Secreted Frizzled-Related Protein 2 (SFRP2) as most likely candidates to activate FZD5-mediated signaling in ECs.[13-15] In contrast to SFRP2[16], WNT5a is endogenously expressed by HUVECs (Supplemental Figure 1B). To address the potential signal capacities of this endogenously expressed WNT5a as ligand for FZD5, HeLa cells were transduced with an adenoviral overexpression plasmid for WNT5a to produce cultured medium containing high levels of this WNT ligand. HeLa cells were selected for this purpose over HUVECs as these cells were shown to have a more refined machinery to produce and secrete functional WNT5a than HUVECs, as illustrated by enhanced mRNA expression of WNTless (WLS) and Porcupine (PORCN) (data not shown). Transduction with this overexpression vector (adWNT5a) led to a significant upregulation of WNT5a compared to dsRED control transduced cells (adSHAM) (Figure 1A). To assess whether FZD5 was involved in transducing the signal of WNT5a, cultured medium from transduced HeLa cells

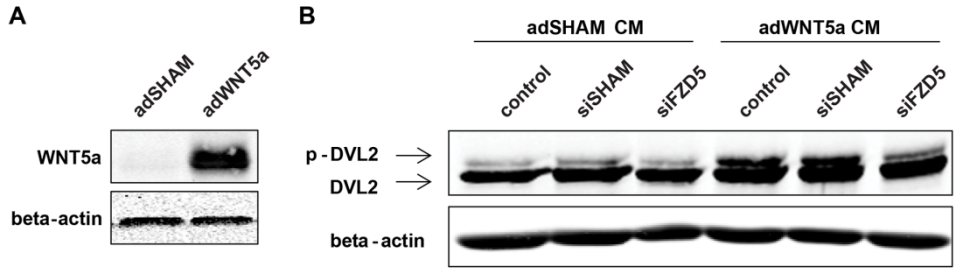

Figure 1: WNT5a induced FZD5-mediated DVL activation in HUVECs. (A) Representative Westernblot of adenoviral-based WNT5a overexpression in HeLa cells, 72 hours post transduction. N=4. **(B)** Representative Western blot of DVL and phosphorylated DVL in HUVECs after 3 hours stimulation with cultured medium (CM) from HeLa cells overexpressing dsRED or WNT5a, 72 hours post siRNA transfection in HUVECs. N=6

was applied to serum starved HUVECs after which DVL activation was monitored. Western blot analysis showed that WNT5a strongly induced DVL phosphorylation in untreated or non-targeting siRNA treated HUVECs, however this effect was blocked in absence of FZD5 (Figure 1B), confirming the importance of endothelial FZD5 in transducing WNT5a signaling.

FZD5 expression is essential for endothelial proliferation, migration, and tubule formation

The angiogenic capacities of these FZD5 silenced HUVECs were evaluated in a well-validated *in vitro* 3D angiogenesis assay developed for studying formation of micro-capillary structures.[12] In this assay, HUVECs with Green Fluorescent Protein (GFP) marker expression and dsRED labelled pericytes directly interact in a collagen type I matrix environment, resulting in EC sprouting, tubule formation, and neovessel stabilization as a result of perivascular recruitment of pericytes. At day 5 post-seeding, well-defined, micro-capillaries with pericyte coverage can be observed. Imaging and quantification of the vascular structures was conducted at day 2 and 5. Endothelial knockdown of FZD5 strongly impaired endothelial tubule formation (Figure 2A). Quantification revealed a significant reduction in the total tubule length, the number of endothelial junctions, and the number of endothelial tubules, both after 2 and 5 days (Figure 2B).

To get a better insight in the causative factor for this poor vascular phenotype, the migration and proliferation capacities of FZD5 silenced ECs were studied. A plug-in migration assay was performed to analyze the effects of FZD5 knockdown on endothelial mobility. Knockdown of FZD5 significantly inhibited the migration of ECs towards the open cell-devoid area compared to untreated and non-targeting siRNA treated ECs (Figure 3A-B). In addition, knockdown of FZD5 significantly reduced cell numbers compared to control and siSHAM condition (Figure 3C). To clarify whether this was a result of impaired cell proliferation or

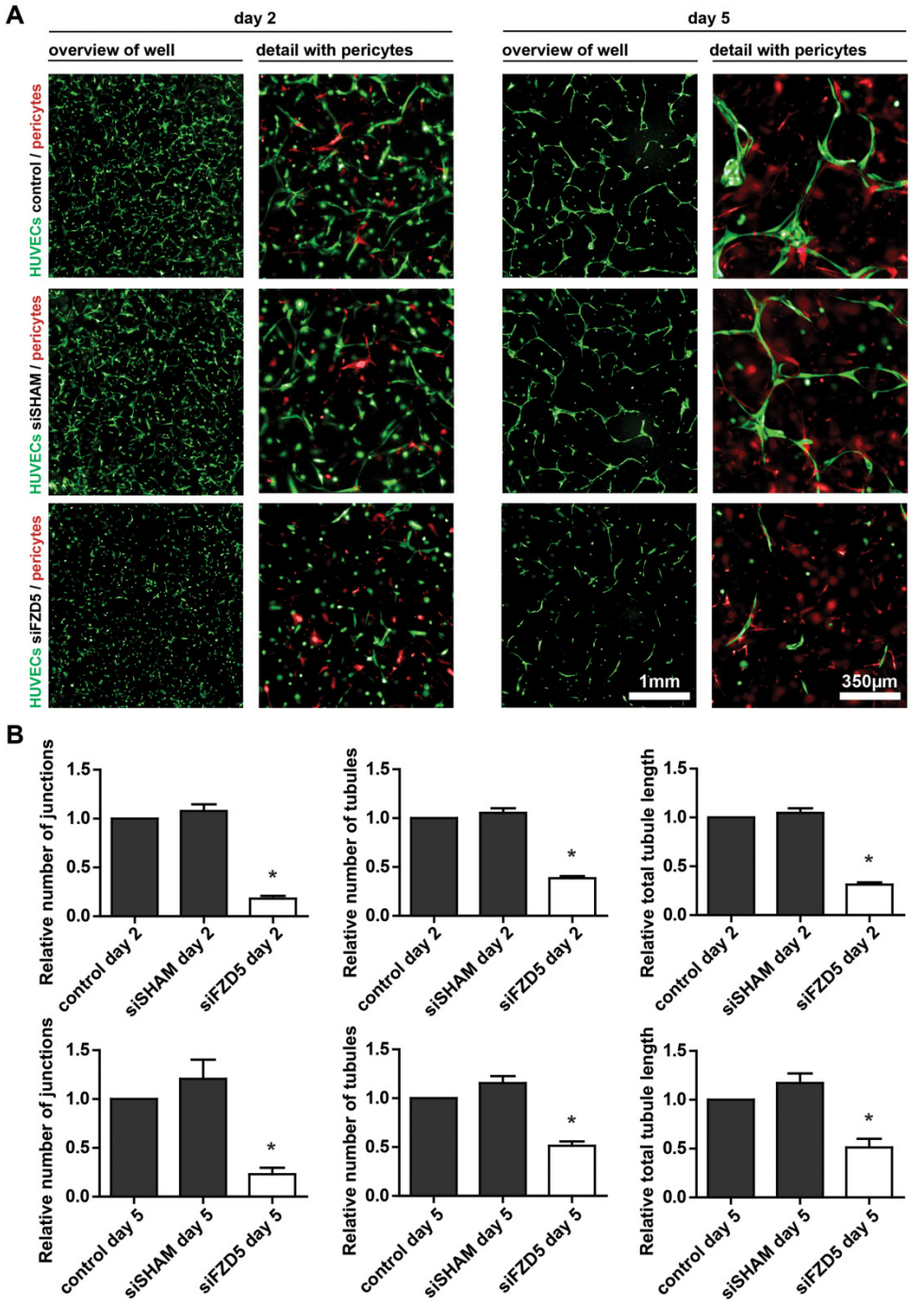

Figure 2: FZD5 expression is crucial for vascular formation *in vitro*. (A) Representative fluorescent microscope images of GFP labelled HUVECs (green) in coculture with dsRED labelled pericytes (red) in a 3D collagen matrix during vascular formation. Shown are the results at day 2 and 5 of non-transfected

◄control, siSHAM, and siFZD5 conditions. Scale bar in the left columns represents 1mm. Scale bar in the right columns represents 350µm. **(B)** Bar graphs show the quantified results of the coculture assay. Shown are the total tubule length, and the number of endothelial junctions and tubules relative to the control conditions, both after 2 days and 5 days. N=4, *P<0.05 compared to control and siSHAM condition.

increased apoptosis, cell cycle progression was analyzed in a cell-cycle assay in which total DNA was stained with PI, followed by flow cytometry. A strong increase of cells in the G_0/G_1 phase of the cell-cycle was observed after knockdown of FZD5, indicative of a cell cycle arrest (Figure 3D-E). For apoptosis analysis, a terminal deoxynucleotidyl transferase dUTP nick end labeling (TUNEL) based detection staining was used. Although seeded in similar densities, FZD5 knockdown led to a significant reduction of nuclei per image field.

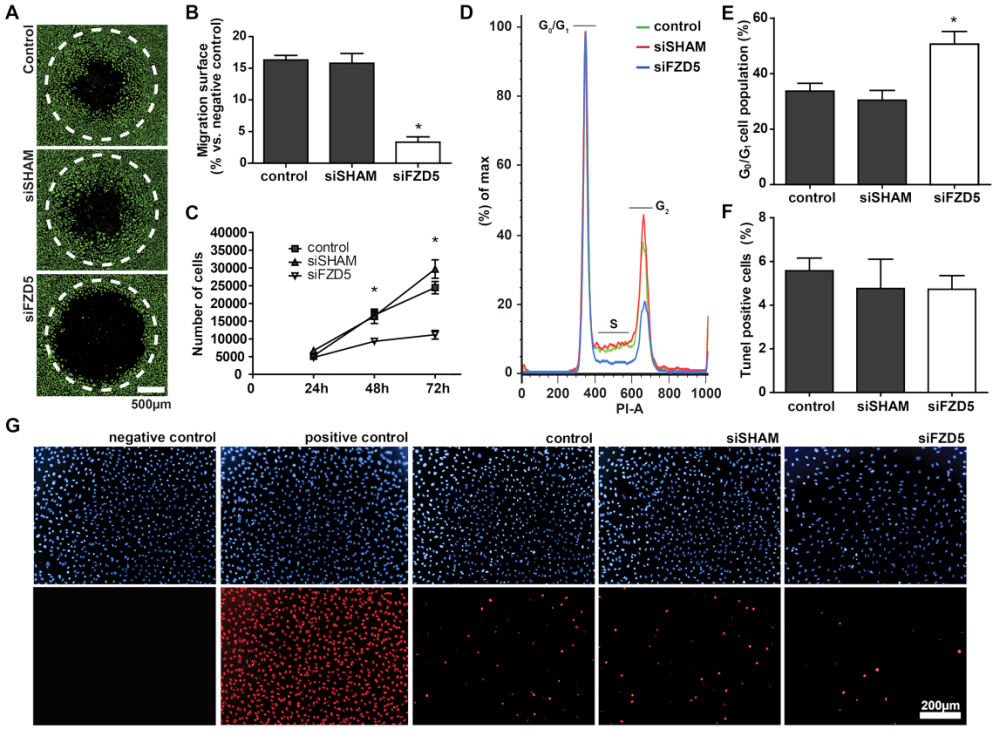

Figure 3: Endothelial knockdown of FZD5 significantly inhibited EC migration and proliferation, but had no effect on apoptosis. (A) Representative fluorescent microscope images of Calcein-AM labelled HUVECs (green) in a plug-stopper based migration assay. Shown are the results of 16 hours of migration of non-transfected control, siSHAM, and siFZD5 conditions. Scale bar represents 500µm. Open migration areas produced by the plug-stopper before initiation of the assay are indicated by dotted lines. **(B)** Bar graph shows the quantified results of migration assay. Shown are the percentages of

◄surface area within the dotted circle covered by HUVECs after 16 hours of migration. N=4, *P<0.05 compared to control and siSHAM condition. **(C)** ECs expansion at 24 hours, 48 hours, and 72 hours post seeding in similar densities, as quantified by flow cytometry. N=3, *P<0.05 compared to control and siSHAM condition (two-way ANOVA followed by Bonferroni post hoc test). **(D)** Representative histogram of flow cytometric analysis of PI based DNA staining showing the distribution of cells over the cell-cycle in the different groups at 48 hours post transfection. **(E)** Quantified results of cell-cycle analysis. Percentage of cells in G_0/G_1 phase is shown. N=3, *P<0.05 compared to control and siSHAM condition. **(F)** Quantified results of TUNEL staining. Percentage TUNEL positive cells of total number of cell is shown, 72 hours post-transfection of control, siSHAM, and siFZD5 conditions. N=3, no significance. **(G)** Representative fluorescent microscope images of DAPI bases nuclei staining in HUVECs (blue, upper row) and TUNEL staining of the same cells (red, lower row). Positive control was treated with DNAse solution. Scale bar represents 200μm.

However, the relative number of TUNEL positive nuclei in the FZD5 knockdown condition was similar when compared to control and siSHAM condition, showing that the reduction of ECs in the FZD5 knockdown condition is not related to increased apoptosis (Figure 3F-G).

Loss of FZD5 does not interfere with endogenous canonical WNT signaling

To further dissect the molecular mechanism of endothelial FZD5 signaling in angiogenesis, known FZD/WNT signaling pathways were studied. Downstream FZD signaling occurs via the canonical WNT signaling pathway, also known as the WNT/β-catenin pathway, or by the less well described non-canonical WNT signaling pathways. Activation of canonical WNT signaling is characterized by an accumulation of cytoplasmic β-catenin, eventually resulting in nuclear translocation and subsequent expression of β-catenin dependent target genes. To evaluate the effect of FZD5 knockdown on the canonical WNT signaling pathway, total levels of β-catenin, as well as phospho-β-catenin (ser33/37/thr41) and non phospho-β-catenin (active) were examined 24h, 48h and 72h post transfection by Western blot. Ser33/37/thr41 phosphorylation is induced by GSK3β and primes β-catenin for subsequent degradation, and could be indicative for a reduced activity of canonical WNT signaling. Total β-catenin, as well as non phospho-β-catenin (active) levels were unaffected by FZD5 silencing, and no phospho-β-catenin (ser33/37/thr41) was observed in all conditions (Figure 4A-B), even though the antibody was capable of detecting GSK3β-induced β-catenin phosphorylation (Figure 4C). Furthermore, expression levels of previously described endothelial target genes of β-catenin were studied using qPCR, but no differences were observed in the expression of AXIN2, CCND1 and C-MYC after knockdown of FZD5 (Figure 4D). An immunofluorescent staining, validated to detect cellular distribution of β-catenin (Supplemental Figure 3B), was also performed on transfected ECs, as stable total levels of β-catenin found by Western blot did not deviate between cytoplasmic- or nuclear localized β-

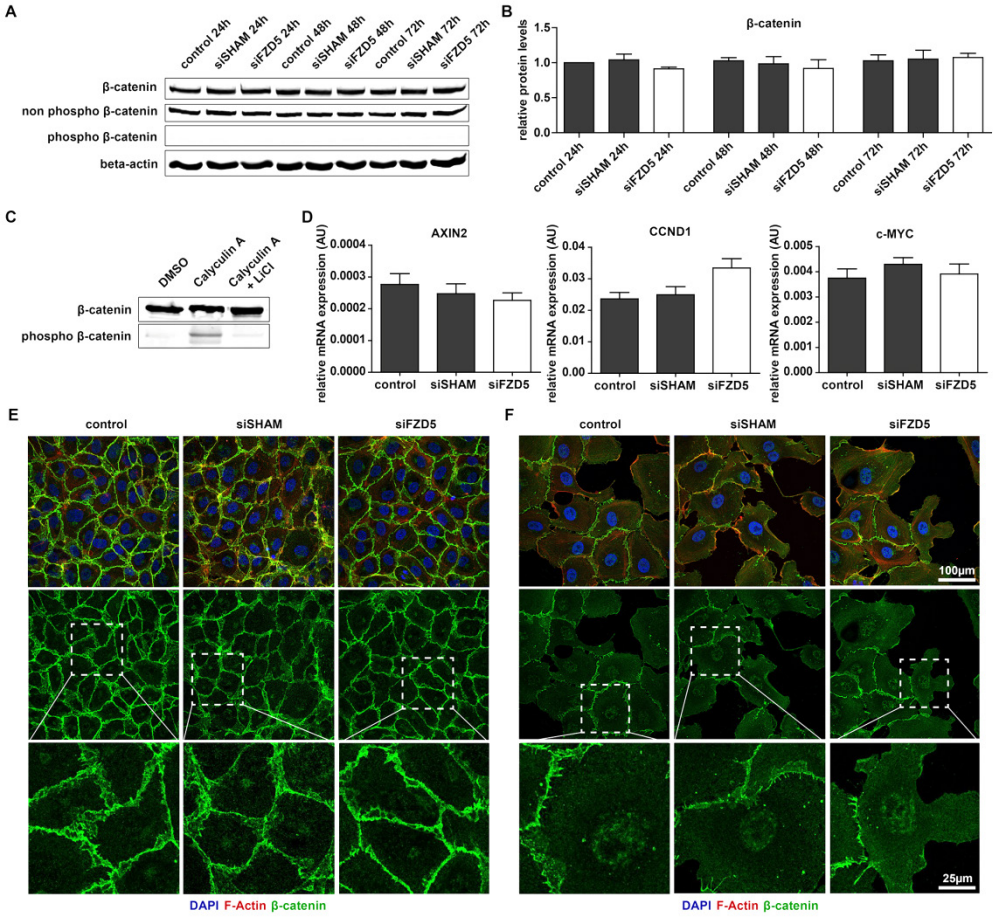

Figure 4: FZD5 knockdown did not affect the canonical WNT signaling pathway in ECs. (A) Representative Western blot result of total levels of β-catenin, non phospho-β-catenin, phospho-β-catenin (ser33/37/thr41), and β-actin loading control, at different time points post-transfection. **(B)** Quantified results of β-catenin Western blot. Shown are β-catenin levels relative to β-actin loading control. N=3, no significance. **(C)** Western blot result of total levels of β-catenin and phospho-β-catenin in response to treatment with the phosphatase inhibitor Calyculin A (50nM) with and without a 30 minute pretreatment of the GSK3β inhibitor LiCl (20mM). **(D)** QPCR analysis of the mRNA expression levels of β-catenin target genes AXIN2, Cyclin D1 (CCND1) and C-MYC in the different conditions 72 hours post transfection. N=4, no significance. **(E)** Immunofluorescent staining β-catenin (green), F-actin (red), and DAPI (blue) in confluent and sub-confluent **(F)** HUVECs after knockdown of FZD5. N=3.

catenin. In line with the other experiments focusing on β-catenin-mediated signaling, no differences in β-catenin localization were observed after knockdown of FZD5, both in confluent and sub confluent cells (Figure 4E and 4F, respectively).

FZD5 knockdown induces the expression of several (anti-) angiogenic factors

To further elucidate the anti-angiogenic phenotype observed after FZD5 knockdown, expression levels of several important regulators of angiogenesis were analyzed. In contrast to what was previously reported[17], our findings in HUVECs indicate that expression of

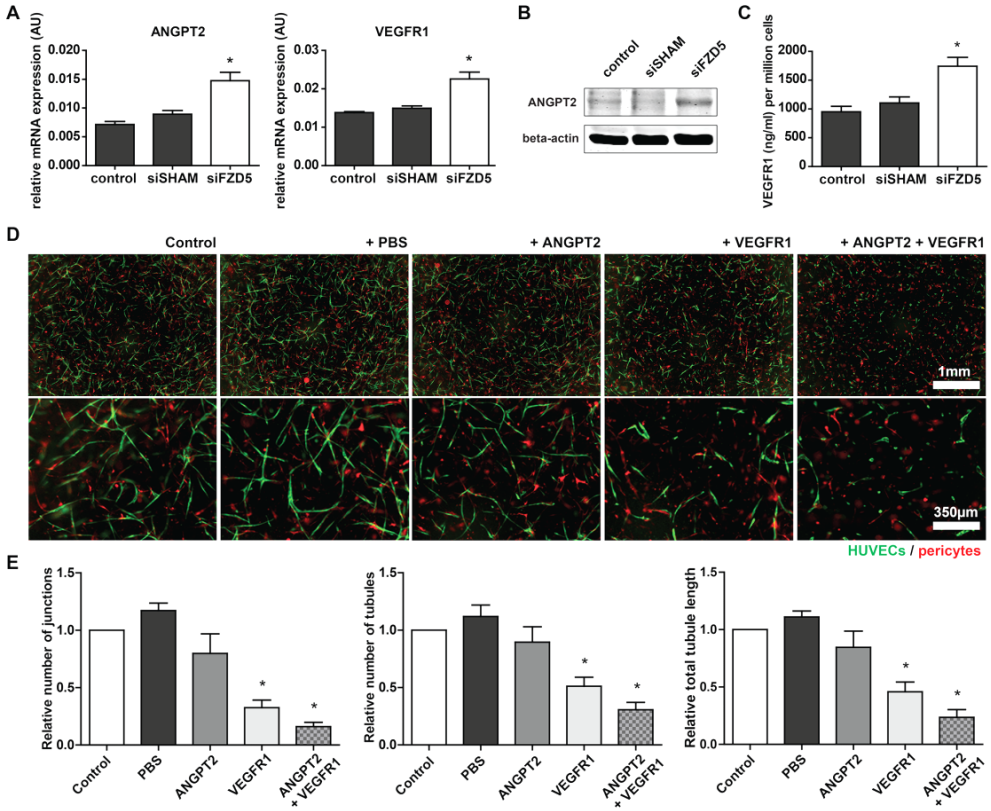

Figure 5: FZD5 knockdown led to increased expression of vascular regression associated genes VEGFR1 and ANGPT2. (A) QPCR results of expression levels of ANGPT2 and VEGFR1 in the different conditions 72 hours post transfection. N=11, *P<0.05 compared to control and siSHAM condition. **(B)** Representative Western blot results of ANGPT2 expression levels in the different conditions 72 hours post transfection. N=3. **(C)** Enzyme-linked immuno sorbent assay based quantification of secreted VEGFR1 levels in cultured endothelial medium 72h post transfection. N=8, *P<0.05 compared to control and siSHAM condition. **(D)** Representative fluorescent microscope images of GFP labelled HUVECs (green) in coculture with dsRED labelled pericytes (red) in a 3D collagen matrix during vascular formation. Shown are the results at day 5 of an untreated control, and after stimulation with PBS, ANGPT2 (1000ng/ml), VEGFR1 (1000ng/ml), and ANGPT2 + VEGFR1 (1000ng/ml both). Scale bar in the upper row represent 1mm, in the bottom row 350µm. **(E)** Bar graphs show the quantified results of the coculture assay. Shown are the total tubule length, and the number of endothelial junctions and tubules after 5 days. N=4, *P<0.05 compared to control and siSHAM condition.

Tissue Factor (TF) is not positively regulated by FZD5 signaling, as FZD5 knockdown did not attenuate TF expression. In fact, TF was slightly upregulated in FZD5 silenced HUVECs compared to untreated control cells, yet was statistically equal to non-targeting siRNA treated HUVECs (Supplemental Figure 2). Interestingly, Vascular Endothelial Growth Factor A (VEGFA) decoy receptor VEGFR1, and the vascular destabilizing factor ANGPT2 were significantly upregulated at both mRNA and protein level in HUVECs treated with FZD5 siRNA when compared to untreated or non-targeting siRNA treated HUVECs (Figure 5A-C). Expression levels of VEGF receptor 2, VEGFA, as well as ANGPT1 remained unaffected in absence of FZD5 (Supplemental Figure 2). In line with previous findings of Lobov *et al.*, combined addition of VEGFR1 and ANGPT2 in the 3D coculture system completely attenuated endothelial tubule formation (Figure 5D-E).[9]

Knockdown of a FZD receptor could not only attenuate signal transduction, but due to impaired inhibitory crosstalk between the individual pathways, or via alternative receptor binding by the WNT ligand could also have a stimulatory effect.[18, 19] Since FZD5 knockdown had no effect on the canonical WNT signaling pathway, the described non-canonical WNT/Ca^{2+} and PCP pathways were studied for their potential role in the upregulation of ANGPT2 and VEGFR1. Activation of the WNT/Ca^{2+} pathway could induce VEGFR1 and ANGPT2 transcription, as stimulation of the WNT/Ca^{2+} pathway leads to free Ca^{2+}-induced activation of Calcineurin, which in turn could promote NFAT-mediated transcription by dephosphorylating NFAT.[6] The mRNA expression level of Down Syndrome Critical Region 1 (DSCR1) was evaluated to assess the potential link between FZD5 knockdown and NFAT activation, as DSCR1 is a profound target gene of NFAT, involved in a feedback loop to fine-tune NFAT-mediated transcription.[20, 21] However, no correlation between endothelial knockdown of FZD5 and DSCR1 upregulation was observed (Figure 6A). The involvement of NFAT-mediated transcription was also evaluated by pharmacological inhibition of the WNT/Ca^{2+} signaling cascade using the Calcineurin inhibitor Cyclosporine A (CsA). The effectiveness of CsA (1μM) was confirmed by its ability to inhibit calcium ionophore (A23187) induced transcription of DSCR1 as a result of free Ca^{2+}-mediated NFAT activation in ECs (Figure 6A). In line with the absence of DSCR1 upregulation in the FZD5 knockdown condition, the upregulation of VEGFR1 and ANGPT2 could not be linked to an increase of NFAT-mediated transcription in the FZD5 knockdown condition, as CsA stimulation failed to reduce ANGPT2 and VEGFR1 upregulation in FZD5 silenced cells (Figure 6B).

Besides activation of the WNT/Ca^{2+} pathway, the PCP pathway could also stimulate the expression of VEGFR1 and ANGPT2 via activation of the WNT/PCP signaling cascade linked to downstream JNK-induced transcriptional activation of c-JUN.[22, 23] Activation of JNK/c-JUN-mediated transcription involves phosphorylation of JNK, which was slightly

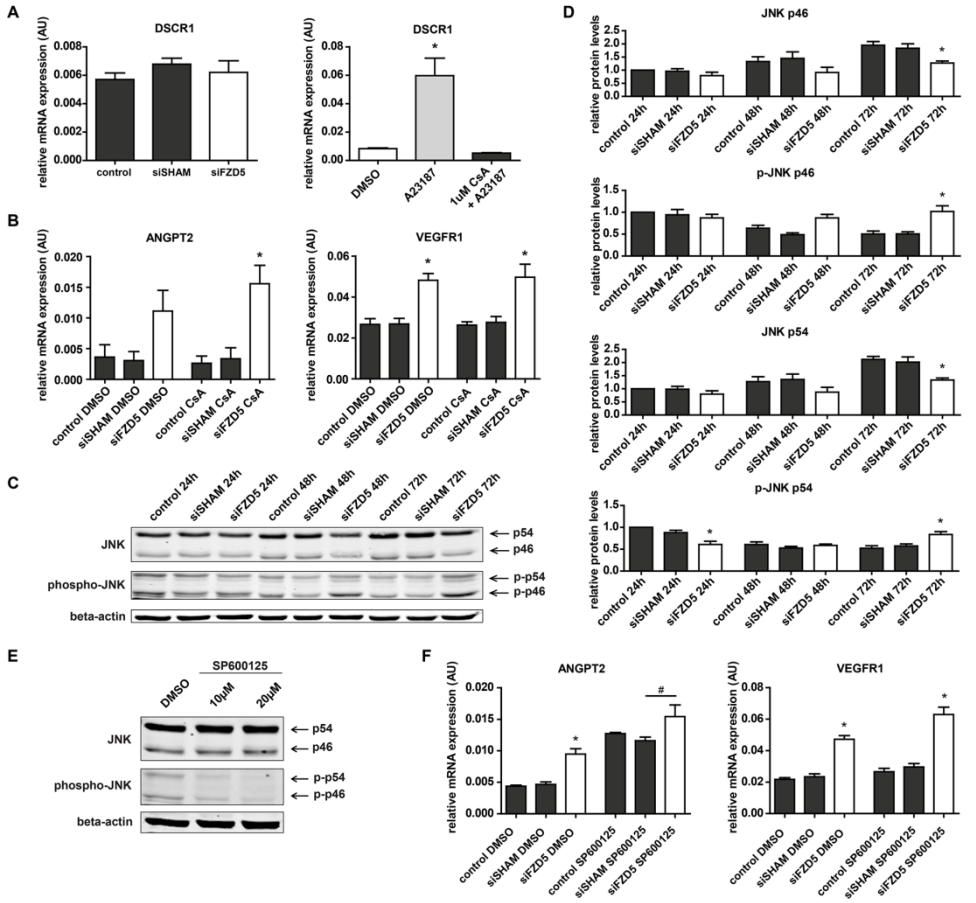

Figure 6: FZD5 knockdown led to increased expression of vascular regression associated genes VEGFR1 and ANGPT2, independent of the non-canonical WNT/Ca^{2+} and PCP pathways. (A) QPCR results of NFAT target gene Dscr1 in the different conditions 72 hours post transfection and in response to ionophore A23187 (10μM) induced Ca^{2+} flux, with and without NFAT inhibitor Cyclosporin A (CsA) (1μM). N=5, *P<0.05 compared to control and siSHAM condition, and DMSO treated and CsA + A23187 treated ECs respectively. **(B)** ANGPT2 and VEGFR1 mRNA expression levels in HUVECs in response to CsA, supplemented 48 hours post transfection. N=4, *P<0.05 compared to control and siSHAM condition (two-way ANOVA followed by Bonferroni post hoc test). **(C)** Representative Western blot of total JNK, phospho-JNK, and β-actin levels at different time points post-transfection. **(D)** Quantified results of JNK and phospho-JNK Western blot. Shown are individual (phospho) JNK isoform (p46 and p54) levels relative to β-actin loading control. N=6, *P<0.05 compared to control and siSHAM condition within 1 time comparison (24, 48 or 72 hours). **(E)** Western blot of total JNK, phospho-JNK, and β-actin levels in response to different concentrations of JNK inhibitor SP600125 after 1 hour. **(F)** QPCR analysis showing the effect of SP600125, supplemented 48 hours post transfection, on VEGFR1 and ANGPT2 mRNA levels in the different conditions. N=4, *P<0.05 compared to control and siSHAM condition, #P<0.05 as indicated in graph (two-way ANOVA followed by Bonferroni post hoc test).

increased both 48h and 72h post transfection (Figure 6C-D). JNK-mediated phosphorylation of c-JUN however was not observed (supplemental Figure 4A-B). Since JNK is a kinase with a broad spectrum of downstream substrates[24], the JNK inhibitor SP600125 was used to block activation of JNK to define whether the enhanced phosphorylation of JNK played a role in the upregulation of VEGFR1 and ANGPT2. The effectiveness of SP600125 (20μM) was confirmed by its ability to inhibit JNK phosphorylation in ECs (Figure 6E). Treatment of HUVECs with SP600125 did not diminish FZD5 silencing-induced upregulation of VEGFR1 and ANGPT2 (Figure 6F). In contrast, SP600125 treatment rather induced a general upregulation of ANGPT2, indicating that activation of JNK was not causally related to the FZD5 knockdown-mediated upregulation of both genes.

ANGPT2 and VEGFR1 upregulation is mediated via PKC and Ets1

Previously it was demonstrated that WNT signal transduction could also involve PKC.[25-27] PKCs are part of a kinase family with a diverse range of potential downstream targets. To verify whether FZD5 knockdown-induced upregulation of VEGFR1 and ANGPT2 depended on activation of PKC, HUVECs were treated with the PKC inhibitor Staurosporine in the concentration range of 5nM to 20nM, as not all different PKC family members are equally inhibited at similar concentrations. Interestingly, both ANGPT2 and VEGFR1 overexpression induced by FZD5 knockdown was dose dependently reduced by PKC inhibition compared to control and siSHAM condition (Supplemental Figure 5A). Since HUVECs express multiple PKC isoforms[28, 29], PKC expression was knocked down by siRNA to interrogate which isoform mediated the observed upregulation of ANGPT2 and VEGFR1. Individual PKC isoform knockdown only had a minor effect on the FZD5 knockdown-induced overexpression of the anti-angiogenic factors, whereas combined knockdown of the novel PKCs (nPKCs) completely attenuated the upregulation of ANGPT2 and VEGFR1 (Figure 7A, Supplemental Figure 5B).

PKC signaling can induce elevated synthesis of the transcription factor Ets1[30, 31], which has binding sites in the promoter regions of both ANGPT2 and VEGFR1.[32, 33] Ets1 was significantly upregulated in absence of FZD5, which was orchestrated by PKC (Supplemental Figure 5C). Involvement of Ets1 in transcriptional regulation of ANGPT2 and VEGFR1 was evaluated in the FZD5 knockdown condition using a double knockdown of both FZD5 and Ets1. Knockdown of Ets1 alone had no effect on the expression of VEGFR1 and ANGPT2 compared to control and siSHAM condition, indicating no active transcription regulation of these two genes by Ets1 in control conditions. However, knockdown of Ets1 in FZD5-silenced HUVECs fully inhibited upregulation of ANGPT2 and partially inhibited the upregulation of VEGFR1 when compared to FZD5-silenced controls (Figure 7B). The

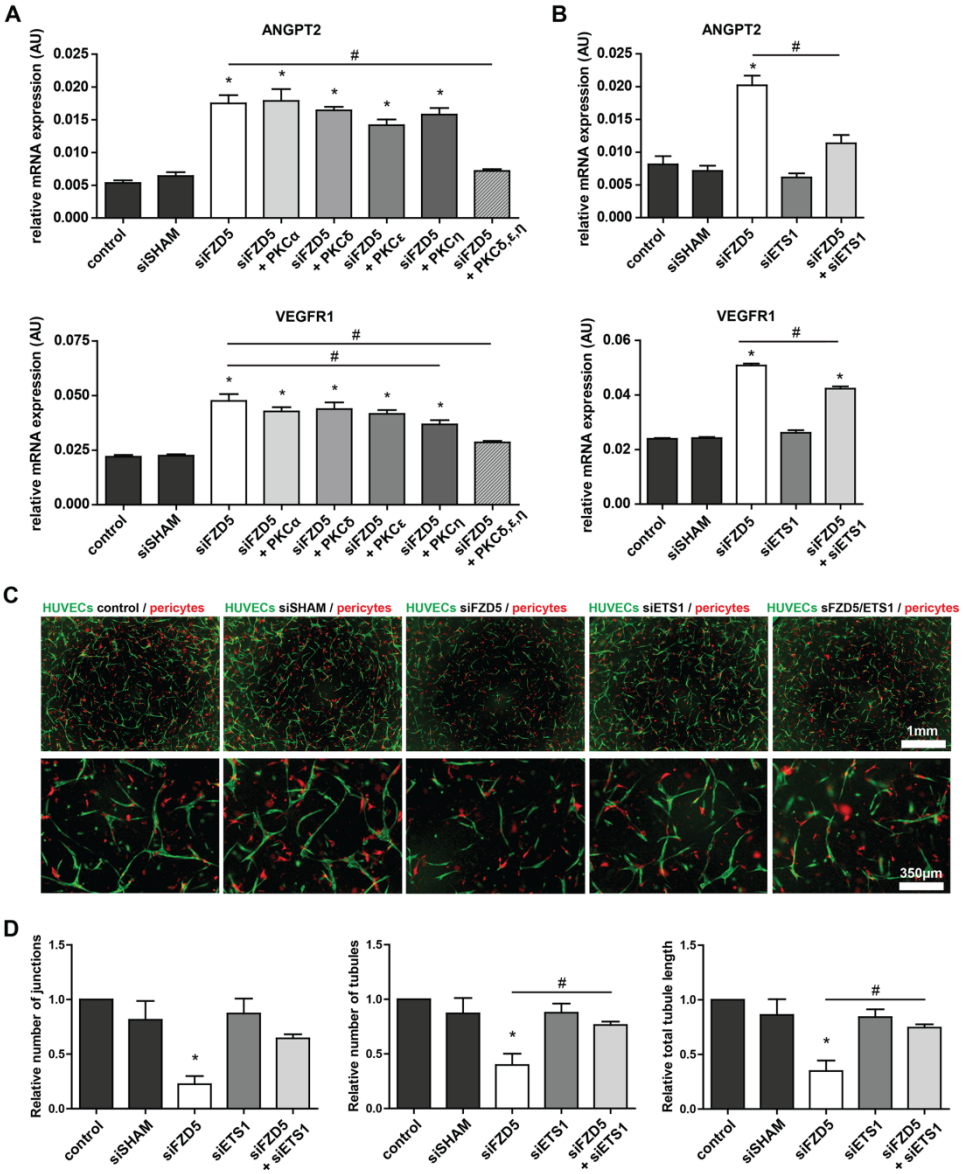

Figure 7: FZD5 knockdown induced upregulation of ANGPT2 and VEGFR1 expression is mediated via enhanced PKC and Ets1 signaling. (A) QPCR results showing expression levels of ANGPT2 and VEGFR1 in HUVECs after knockdown of FZD5 alone, in combination with different PKC isoforms, and in combination with all novel PKC isoforms (PKCδ,ε,η), 48 hours post transfection. N=4, *P<0.05 compared to control and siSHAM condition, #P<0.05 as indicated in graph. **(B)** QPCR results of ANGPT2 and VEGFR1 expression in HUVECs, 72 hours post transfection, with and without knockdown of transcription factor Ets1, a downstream target of PKC. N=4, *P<0.05 compared to control and siSHAM condition, #P<0.05 as indicated in graph. **(C)** Representative fluorescent microscope images of GFP labelled HUVECs (green) in coculture with dsRED labelled pericytes (red) in a 3D collagen matrix

◄ during vascular formation. Shown are the results at day 5 of non-transfected control, siSHAM, siFZD5, siEts1 and the combined knockdown of FZD5 and Ets1. Scale bar in the upper row represent 1mm, in the bottom row 350µm. **(D)** Bar graphs show the quantified results of the coculture assay. Shown are the total tubule length, and the number of endothelial junctions and tubules after 5 days. N=6, *P<0.05 compared to control and siSHAM condition, #P<0.05 as indicated in graph.

involvement of Ets1-induced transcription was further substantiated by a similar Ets1 dependent upregulation of Matrix metalloproteinase 1 (MMP1), a verified endothelial target gene of Ets1 (Supplemental Figure 6A-B).[34] To evaluate if the anti-angiogenic phenotype of FZD5 silencing observed in the 3D angiogenesis coculture assay was mediated via this pathway, Ets1 was silenced in GFP-labeled HUVECs. Analysis of the 3D coculture results demonstrated that inhibition of Ets1 in the FZD5 knockdown condition partly rescued the FZD5 knockdown mediated reduction of endothelial tubule formation (Figure 7C-D).

Discussion

The main findings of the current study are: (1) Endothelial FZD5 expression is essential for vascular formation, as shown in a 3D coculture assay. (2) FZD5 silencing inhibits EC proliferation and migration. (3) Endothelial loss of FZD5 expression does not interfere with endogenous canonical WNT signaling. (4) FZD5 knockdown leads to increased expression of vascular regression associated factors VEGFR1 and ANGPT2, independent of both the non-canonical WNT/Ca^{2+}-mediated activation of NFAT and PCP-mediated activation JNK. (5) Inhibition of nPKC signaling, as well as knockdown of the PKC target Ets1 suppressed the upregulation of VEGFR1 and ANGPT2 in absence of FZD5. The Ets1 knockdown intervention also partially rescued the FZD5 knockdown-induced inhibitory effect on new vessel formation.

Previously it was reported that FZD5 is indispensable for murine embryogenesis.[5] FZD5 knockout embryos died *in utero* from severe defects in yolk sac and placenta vascularization. Using trophoblast specific FZD5 knockout mice, Lu and co-workers reported that the observed phenotype in the FZD5 full knockout placenta was partly initiated by a defect in chorionic branching morphogenesis.[35] As defective branching morphogenesis of the chorion of these mice resulted in a smaller placental labyrinth layer compared to wild-type littermates, it remained difficult to distinguish whether the placental defects observed in the FZD5 full knockout mice were indeed vascular related, or the outcome of proportional growth limitations resulting from the reduced villous volume. In our study, we demonstrated that endothelial knockdown of FZD5 *in vitro* leads to a severe reduction in vascular tubule

formation in a 3D coculture model, thereby providing evidence for the direct role of FZD5 in new vessel growth.

The most detailed described FZD/WNT signaling cascade is the canonical or ß-catenin dependent pathway. Without stimulation of the canonical pathway, ß-catenin is degraded by a destruction complex consisting of Axin, Glycogen Synthase Kinase 3ß, Adenomatous Polyposis Coli, and Casein Kinase 1α. Upon binding of WNT ligands to a FZD receptor in the presence of the co-receptor Lrp5 or Lrp6, a conformation change in Lrp extracts Axin away from the destruction complex, leading to an increase in intracellular ß-catenin levels. When translocated into the nucleus, ß-catenin binds to the TCF/Lef complex and promotes the expression of ß-catenin target genes.[6-8] Knockdown of a FZD receptor could both have an inhibiting effect on this pathway, due to a reduction in receptors capable of transducing a signal for downstream signaling cascade activation, and an activating effect, either due to impaired inhibitory crosstalk between the individual pathways or via alternative receptor binding by the WNT ligand.[18, 19] Involvement of FZD5 in this canonical pathway appears to be tissue dependent. Steinhart *et al.* recently demonstrated that canonical WNT signaling via FZD5 was involved in pancreatic tumor growth and Caricasole *et al.* reported enhanced ß-catenin mediated signaling upon WNT7a interaction with both FZD5 and Lrp6 in the rat pheochromocytoma cell line PC12.[36, 37] In the mouse optic vesicle however, no evidence suggest that FZD5 activates or suppresses canonical WNT signaling.[38, 39] Our analysis of endogenous canonical FZD/WNT signaling suggests that FZD5 is not involved in WNT ß-catenin signaling in ECs.

In contrast to the ß-catenin target genes, expression levels of ANGPT2 and VEGFR1 were significantly upregulated in HUVECs with suppressed FZD5 expression. ANGPT2 on itself is known to have a positive effect on neovessel formation, as it is involved in pericyte detachment and destabilization of the endothelium to potentiate the actions of pro-angiogenic factors.[40, 41] However, in absence of VEGFA, or in the presence of an increased expression of VEGFR1, a decoy receptor for VEGFA, ANGPT2 is known to induce vascular regression.[9-11] Both ANGPT2 and VEGFR1 are potential downstream target genes of the non-canonical FZD/WNT signaling pathways. Upon stimulation of the FZD/WNT/Ca^{2+} pathway, activation of phospholipase C leads to cleavage of the membrane component PIP2 into DAG and IP3. When IP3 binds its receptor on the endoplasmic reticulum, Ca^{2+} is released in the cytosol, activating the transcription factor NFAT via Calcineurin.[6] In recent studies, VEGFR1 and ANGPT2 were shown to be transcriptional targets of NFAT.[42, 43] Like ANGPT2 and VEGFR1, the endogenous NFAT inhibitor DSCR1 is also a verified target of

the transcription factor NFAT[20, 21], yet our data showed that the expression level of DSCR1 remained stable after knockdown of FZD5. More important, our experiments demonstrated that inhibition of NFAT activation with CsA after endothelial knockdown of FZD5 did not inhibit the upregulation of ANGPT2 and VEGFR1, suggesting that it was unlikely that the enhanced transcription of these anti-angiogenic factors was mediated by enhanced activity of NFAT. Alternatively, stimulation of the FZD/WNT/PCP pathway could also induce the transcription of VEGFR1 and ANGPT2 via GTPase mediated activation of JNK, which eventually activates c-JUN based transcription.[6] Multiple studies provided evidence for transcriptional regulation of VEGFR1 and ANGPT2 either by c-JUN alone, or by the transcription complex AP-1 involving c-JUN.[22, 23] Our data indicated that FZD5 knockdown led to an increase in JNK phosphorylation, but no increase in c-JUN phosphorylation was observed. In addition, inhibition of JNK activity with SP600125 ruled out the involvement of the PCP-JNK signal transduction axis as causal factor for the enhanced expression of vascular regression associated factors ANGPT2 and VEGFR1 in ECs with FZD5 knockdown, as upregulation of these factors remained evident. In future studies however, it remains of interest to further dissect the relevance of this altered JNK signaling in absence of FZD5.

Multiple reports have previously suggested a role for PKC involvement in FZD/WNT signaling.[25-27] Staurosporine, as well as siRNA-mediated knockdown of nPKCs inhibited the upregulation of ANGPT2 and VEGFR1 in HUVECs with suppressed expression of FZD5, indicating the involvement of PKC signaling in the transcriptional regulation of these genes in FZD5 silenced ECs. The promoter regions of both ANGPT2 and VEGFR1 contain binding sites of the transcription factor Ets1[32, 33], which was shown by our data to be PKC dependently upregulated in absence of FZD5. Our results demonstrate the involvement of enhanced Ets1 mediated transcription of these two genes in FZD5 silenced ECs, as Ets1 knockdown resulted in a marked repression of ANGPT2 and VEGFR1 expression levels. Another validated endothelial target of PKC/Ets1-mediated transcription MMP1, which like ANGPT2 and VEGFR1 was previously shown to be involved in vascular regression[34], was also upregulated via Ets1 in absence of FZD5. The involvement of Ets1 was further validated using the 3D coculture model, in which Ets1 knockdown in FZD5 silenced ECs partially rescued the inhibitory effect on new vessel formation that was observed in FZD5 silenced conditions. These results indicate a repressing function on PKC/Ets1 signaling by FZD5 in ECs, leading to reduced expression of vascular regression associated factors ANGPT2 and VEGFR1.

In this study the effect of FZD5 knockdown on the different FZD/WNT signaling routes was studied without the addition of exogenous WNT factors. HUVECs secrete WNT factors themselves, amongst which the typical canonical factor WNT3 and non-canonical factor WNT5a. Knockdown of endothelial FZD5 led to functional defects, as well as differential expression of important genes in the angiogenic process, indicating that lack of FZD5 interferes with endogenous FZD/WNT signaling. The nature of this endogenous signaling in absence of FZD5 was shaped by the finding that combined knockdown of FZD5 and endogenous WNT5a significantly suppressed ANGPT2 and VEGFR1 upregulation (Supplemental Figure 7). It was previously demonstrated that WNT factors induce signaling

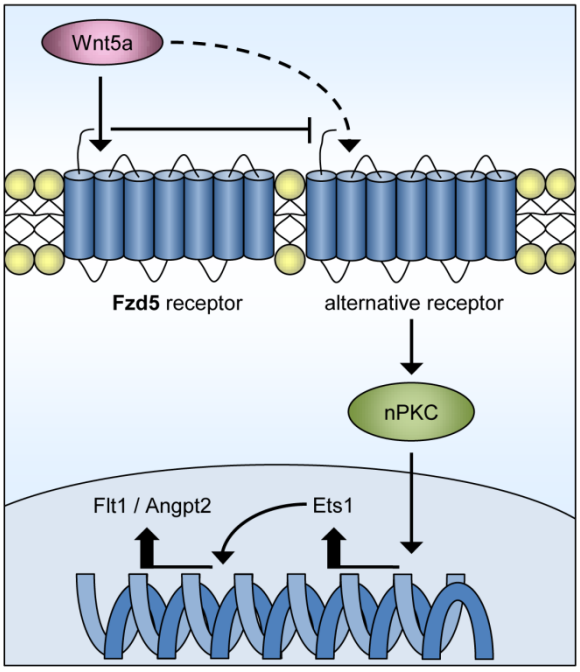

Figure 8: Schematic representation of the proposed model of signaling via FZD5 in ECs. Our data provide evidence for a new proposed model of signaling in ECs in absence of FZD5 in which knockdown of this receptor provokes its ligand WNT5a to signal via an alternative receptor, thereby triggering the activation of nPKC/Ets1-mediated transcription of vascular regression associated factors, amongst which VEGFR1 and ANGPT2.

via a variety of FZD and non-FZD receptors, and that binding selectivity is receptor context dependent.[13, 44] As suppression of endogenous WNT5a signaling partially rescued the FZD5 knockdown induced upregulation of ANGPT2 and VEGFR1, our data suggest that endothelial knockdown of FZD5 provokes its ligand WNT5a to signal via an alternative receptor, thereby triggering the activation of the observed PKC/Ets1-mediated transcription (Figure 8). Although our experiments demonstrate that this alternative signaling route via PKC and Ets1 plays an important role in the poor angiogenic phenotype in absence of FZD5, the relative contribution of suppressed FZD5 signaling itself to this phenomenon is

yet to be determined. Future studies should also aim to identify the unknown alternative WNT5a receptor.

The aim of this study was to explore the involvement of FZD5 in vascular and perivascular biology, which might eventually serve as a foundation for future therapeutic strategies, e.g. in modulating tumor vasculature. A recent genome-wide CRISPR-Cas9 study demonstrated that FZD5 is a potential druggable target in specific subtypes of pancreatic tumors.[36] Signaling via FZD5 in these tumor cells was shown to be crucial in β-catenin mediated proliferation and treatment of these pancreatic adenocarcinoma cells with FZD5 antibodies led to inhibited cell growth, both *in vitro* and in xenograft models *in vivo*. Although these pancreatic adenocarcinoma tumors are not excessively vascularized, they were previously shown to depend on angiogenesis for growth.[45, 46] Our data demonstrate the importance of FZD5 in ECs during angiogenesis and might imply that targeting the FZD5 in these types of tumors not only affects the pancreatic adenocarcinoma cells, but could in addition potentially result in beneficial suppression of tumor vascularization.

In summary, the current study provides evidence for an important role of endothelial FZD5 in angiogenesis, thereby providing novel insights in the molecular mechanism causal to the poor angiogenic phenotype in absence of this receptor.

References

1. Potente, M, Gerhardt, H, Carmeliet, P: Basic and therapeutic aspects of angiogenesis. *Cell,* 146**:** 873-887, 2011.
2. Carmeliet, P: Angiogenesis in health and disease. *Nat Med,* 9**:** 653-660, 2003.
3. Paes, KT, Wang, E, Henze, K, Vogel, P, Read, R, Suwanichkul, A, Kirkpatrick, LL, Potter, D, Newhouse, MM, Rice, DS: Frizzled 4 is required for retinal angiogenesis and maintenance of the blood-retina barrier. *Invest Ophthalmol Vis Sci,* 52**:** 6452-6461, 2011.
4. Peghaire, C, Bats, ML, Sewduth, R, Jeanningros, S, Jaspard, B, Couffinhal, T, Duplaa, C, Dufourcq, P: FZD7 (Frizzled-7) Expressed by Endothelial Cells Controls Blood Vessel Formation Through WNT/beta-Catenin Canonical Signaling. *Arterioscler Thromb Vasc Biol,* 36**:** 2369-2380, 2016.
5. Ishikawa, T, Tamai, Y, Zorn, AM, Yoshida, H, Seldin, MF, Nishikawa, S, Taketo, MM: Mouse WNT receptor gene FZD5 is essential for yolk sac and placental angiogenesis. *Development,* 128**:** 25-33, 2001.
6. Niehrs, C: The complex world of WNT receptor signalling. *Nat Rev Mol Cell Biol,* 13**:** 767-779, 2012.
7. MacDonald, BT, Tamai, K, He, X: WNT/beta-catenin signaling: components, mechanisms, and diseases. *Dev Cell,* 17**:** 9-26, 2009.
8. Clevers, H: WNT/beta-catenin signaling in development and disease. *Cell,* 127**:** 469-480, 2006.
9. Lobov, IB, Brooks, PC, Lang, RA: Angiopoietin-2 displays VEGF-dependent modulation of capillary structure and endothelial cell survival in vivo. *Proc Natl Acad Sci U S A,* 99**:** 11205-11210, 2002.
10. Zygmunt, T, Gay, CM, Blondelle, J, Singh, MK, Flaherty, KM, Means, PC, Herwig, L, Krudewig, A, Belting, HG, Affolter, M, Epstein, JA, Torres-Vazquez, J: Semaphorin-PlexinD1 signaling limits angiogenic potential via the VEGF decoy receptor sVEGFR1. *Dev Cell,* 21**:** 301-314, 2011.
11. Hanahan, D: Signaling vascular morphogenesis and maintenance. *Science,* 277**:** 48-50, 1997.
12. Stratman, AN, Malotte, KM, Mahan, RD, Davis, MJ, Davis, GE: Pericyte recruitment during vasculogenic tube assembly stimulates endothelial basement membrane matrix formation. *Blood,* 114**:** 5091-5101, 2009.
13. Dijksterhuis, JP, Baljinnyam, B, Stanger, K, Sercan, HO, Ji, Y, Andres, O, Rubin, JS, Hannoush, RN, Schulte, G: Systematic mapping of WNT-FZD protein interactions reveals functional selectivity by distinct WNT-FZD pairs. *J Biol Chem,* 290**:** 6789-6798, 2015.
14. He, X, Saint-Jeannet, JP, Wang, Y, Nathans, J, Dawid, I, Varmus, H: A member of the Frizzled protein family mediating axis induction by WNT-5A. *Science,* 275**:** 1652-1654, 1997.
15. Peterson, YK, Nasarre, P, Bonilla, IV, Hilliard, E, Samples, J, Morinelli, TA, Hill, EG, Klauber-DeMore, N: Frizzled-5: a high affinity receptor for secreted frizzled-related protein-2 activation of nuclear factor of activated T-cells c3 signaling to promote angiogenesis. *Angiogenesis,* 20**:** 615-628, 2017.
16. Goodwin, AM, Sullivan, KM, D'Amore, PA: Cultured endothelial cells display endogenous activation of the canonical WNT signaling pathway and express multiple ligands, receptors, and secreted modulators of WNT signaling. *Dev Dyn,* 235**:** 3110-3120, 2006.
17. Arderiu, G, Espinosa, S, Pena, E, Aledo, R, Badimon, L: Monocyte-secreted WNT5a interacts with FZD5 in microvascular endothelial cells and induces angiogenesis through tissue factor signaling. *J Mol Cell Biol,* 6**:** 380-393, 2014.
18. Topol, L, Jiang, X, Choi, H, Garrett-Beal, L, Carolan, PJ, Yang, Y: WNT-5a inhibits the canonical WNT pathway by promoting GSK-3-independent beta-catenin degradation. *J Cell Biol,* 162**:** 899-908, 2003.
19. Flentke, GR, Garic, A, Hernandez, M, Smith, SM: CaMKII represses transcriptionally active beta-catenin to mediate acute ethanol neurodegeneration and can phosphorylate beta-catenin. *J Neurochem,* 128**:** 523-535, 2014.
20. Minami, T, Horiuchi, K, Miura, M, Abid, MR, Takabe, W, Noguchi, N, Kohro, T, Ge, X, Aburatani, H, Hamakubo, T, Kodama, T, Aird, WC: Vascular endothelial growth factor- and thrombin-induced termination factor, Down syndrome critical region-1, attenuates endothelial cell proliferation and angiogenesis. *J Biol Chem,* 279**:** 50537-50554, 2004.
21. Lange, AW, Molkentin, JD, Yutzey, KE: DSCR1 gene expression is dependent on NFATc1 during cardiac valve formation and colocalizes with anomalous organ development in trisomy 16 mice. *Dev Biol,* 266**:** 346-360, 2004.
22. Ye, FC, Blackbourn, DJ, Mengel, M, Xie, JP, Qian, LW, Greene, W, Yeh, IT, Graham, D, Gao, SJ: Kaposi's sarcoma-associated herpesvirus promotes angiogenesis by inducing angiopoietin-2 expression via AP-1 and Ets1. *J Virol,* 81**:** 3980-3991, 2007.

23. Salomonsson, L, Svensson, L, Pettersson, S, Wiklund, O, Ohlsson, BG: Oxidised LDL decreases VEGFR-1 expression in human monocyte-derived macrophages. *Atherosclerosis,* 169**:** 259-267, 2003.
24. Bogoyevitch, MA, Kobe, B: Uses for JNK: the many and varied substrates of the c-Jun N-terminal kinases. *Microbiol Mol Biol Rev,* 70**:** 1061-1095, 2006.
25. Liu, A, Chen, S, Cai, S, Dong, L, Liu, L, Yang, Y, Guo, F, Lu, X, He, H, Chen, Q, Hu, S, Qiu, H: WNT5a through noncanonical WNT/JNK or WNT/PKC signaling contributes to the differentiation of mesenchymal stem cells into type II alveolar epithelial cells in vitro. *PLoS One,* 9**:** e90229, 2014.
26. Sheldahl, LC, Park, M, Malbon, CC, Moon, RT: Protein kinase C is differentially stimulated by WNT and Frizzled homologs in a G-protein-dependent manner. *Curr Biol,* 9**:** 695-698, 1999.
27. Kinoshita, N, Iioka, H, Miyakoshi, A, Ueno, N: PKC delta is essential for Dishevelled function in a noncanonical WNT pathway that regulates Xenopus convergent extension movements. *Genes Dev,* 17**:** 1663-1676, 2003.
28. Lorenzi, O, Frieden, M, Villemin, P, Fournier, M, Foti, M, Vischer, UM: Protein kinase C-delta mediates von Willebrand factor secretion from endothelial cells in response to vascular endothelial growth factor (VEGF) but not histamine. *J Thromb Haemost,* 6**:** 1962-1969, 2008.
29. Gliki, G, Abu-Ghazaleh, R, Jezequel, S, Wheeler-Jones, C, Zachary, I: Vascular endothelial growth factor-induced prostacyclin production is mediated by a protein kinase C (PKC)-dependent activation of extracellular signal-regulated protein kinases 1 and 2 involving PKC-delta and by mobilization of intracellular Ca2+. *Biochem J,* 353**:** 503-512, 2001.
30. Naito, S, Shimizu, S, Maeda, S, Wang, J, Paul, R, Fagin, JA: Ets-1 is an early response gene activated by ET-1 and PDGF-BB in vascular smooth muscle cells. *Am J Physiol,* 274**:** C472-480, 1998.
31. Lindemann, RK, Ballschmieter, P, Nordheim, A, Dittmer, J: Transforming growth factor beta regulates parathyroid hormone-related protein expression in MDA-MB-231 breast cancer cells through a novel Smad/Ets synergism. *J Biol Chem,* 276**:** 46661-46670, 2001.
32. Wakiya, K, Begue, A, Stehelin, D, Shibuya, M: A cAMP response element and an Ets motif are involved in the transcriptional regulation of flt-1 tyrosine kinase (vascular endothelial growth factor receptor 1) gene. *J Biol Chem,* 271**:** 30823-30828, 1996.
33. Hegen, A, Koidl, S, Weindel, K, Marme, D, Augustin, HG, Fiedler, U: Expression of angiopoietin-2 in endothelial cells is controlled by positive and negative regulatory promoter elements. *Arterioscler Thromb Vasc Biol,* 24**:** 1803-1809, 2004.
34. Naito, S, Shimizu, S, Matsuu, M, Nakashima, M, Nakayama, T, Yamashita, S, Sekine, I: Ets-1 upregulates matrix metalloproteinase-1 expression through extracellular matrix adhesion in vascular endothelial cells. *Biochem Biophys Res Commun,* 291**:** 130-138, 2002.
35. Lu, J, Zhang, S, Nakano, H, Simmons, DG, Wang, S, Kong, S, Wang, Q, Shen, L, Tu, Z, Wang, W, Wang, B, Wang, H, Wang, Y, van Es, JH, Clevers, H, Leone, G, Cross, JC, Wang, H: A positive feedback loop involving Gcm1 and FZD5 directs chorionic branching morphogenesis in the placenta. *PLoS Biol,* 11**:** e1001536, 2013.
36. Steinhart, Z, Pavlovic, Z, Chandrashekhar, M, Hart, T, Wang, X, Zhang, X, Robitaille, M, Brown, KR, Jaksani, S, Overmeer, R, Boj, SF, Adams, J, Pan, J, Clevers, H, Sidhu, S, Moffat, J, Angers, S: Genome-wide CRISPR screens reveal a WNT-FZD5 signaling circuit as a druggable vulnerability of RNF43-mutant pancreatic tumors. *Nat Med*, 2016.
37. Caricasole, A, Ferraro, T, Iacovelli, L, Barletta, E, Caruso, A, Melchiorri, D, Terstappen, GC, Nicoletti, F: Functional characterization of WNT7A signaling in PC12 cells: interaction with A FZD5 x LRP6 receptor complex and modulation by Dickkopf proteins. *J Biol Chem,* 278**:** 37024-37031, 2003.
38. Burns, CJ, Zhang, J, Brown, EC, Van Bibber, AM, Van Es, J, Clevers, H, Ishikawa, TO, Taketo, MM, Vetter, ML, Fuhrmann, S: Investigation of Frizzled-5 during embryonic neural development in mouse. *Dev Dyn,* 237**:** 1614-1626, 2008.
39. Maretto, S, Cordenonsi, M, Dupont, S, Braghetta, P, Broccoli, V, Hassan, AB, Volpin, D, Bressan, GM, Piccolo, S: Mapping WNT/beta-catenin signaling during mouse development and in colorectal tumors. *Proc Natl Acad Sci U S A,* 100**:** 3299-3304, 2003.
40. Rennel, ES, Regula, JT, Harper, SJ, Thomas, M, Klein, C, Bates, DO: A human neutralizing antibody specific to Ang-2 inhibits ocular angiogenesis. *Microcirculation,* 18**:** 598-607, 2011.
41. White, RR, Shan, S, Rusconi, CP, Shetty, G, Dewhirst, MW, Kontos, CD, Sullenger, BA: Inhibition of rat corneal angiogenesis by a nuclease-resistant RNA aptamer specific for angiopoietin-2. *Proc Natl Acad Sci U S A,* 100**:** 5028-5033, 2003.
42. Stefater, JA, 3rd, Lewkowich, I, Rao, S, Mariggi, G, Carpenter, AC, Burr, AR, Fan, J, Ajima, R, Molkentin, JD, Williams, BO, Wills-Karp, M, Pollard, JW, Yamaguchi, T, Ferrara, N, Gerhardt,

H, Lang, RA: Regulation of angiogenesis by a non-canonical WNT-VEGFR1 pathway in myeloid cells. *Nature,* 474**:** 511-515, 2011.

43. Minami, T, Jiang, S, Schadler, K, Suehiro, J, Osawa, T, Oike, Y, Miura, M, Naito, M, Kodama, T, Ryeom, S: The calcineurin-NFAT-angiopoietin-2 signaling axis in lung endothelium is critical for the establishment of lung metastases. *Cell Rep,* 4**:** 709-723, 2013.
44. van Amerongen, R, Mikels, A, Nusse, R: Alternative WNT signaling is initiated by distinct receptors. *Sci Signal,* 1**:** re9, 2008.
45. Hotz, HG, Gill, PS, Masood, R, Hotz, B, Buhr, HJ, Foitzik, T, Hines, OJ, Reber, HA: Specific targeting of tumor vasculature by diphtheria toxin-vascular endothelial growth factor fusion protein reduces angiogenesis and growth of pancreatic cancer. *J Gastrointest Surg,* 6**:** 159-166; discussion 166, 2002.
46. Hotz, HG, Reber, HA, Hotz, B, Sanghavi, PC, Yu, T, Foitzik, T, Buhr, HJ, Hines, OJ: Angiogenesis inhibitor TNP-470 reduces human pancreatic cancer growth. *J Gastrointest Surg,* 5**:** 131-138, 2001.

Supplemental data

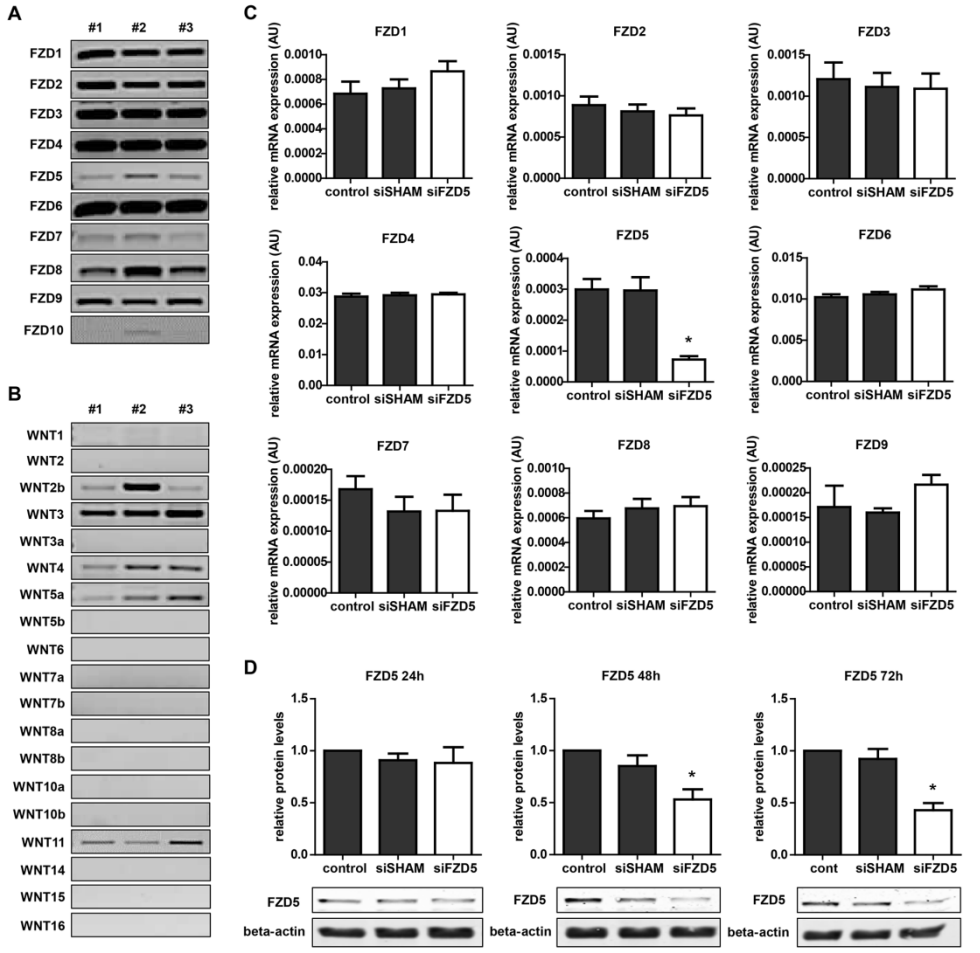

Supplemental Figure 1: FZD5 siRNA induced a significant and specific knockdown of FZD5. (A) PCR results showing expression levels of FZD receptors in HUVECs. N=3 (#1-3 indicate these replicates). **(B)** PCR results showing expression levels of WNT ligands in HUVECs. N=3 (#1-3 indicate these replicates). **(C)** QPCR results of expression levels of all FZD receptors expressed in HUVECs (FZD1-9) in the different conditions 20 hours post transfection. N=7, *P<0.05 compared to control and siSHAM condition. **(D)** Representative Western blot of FZD5 and β-actin levels 72 hours post transfection. N=5.

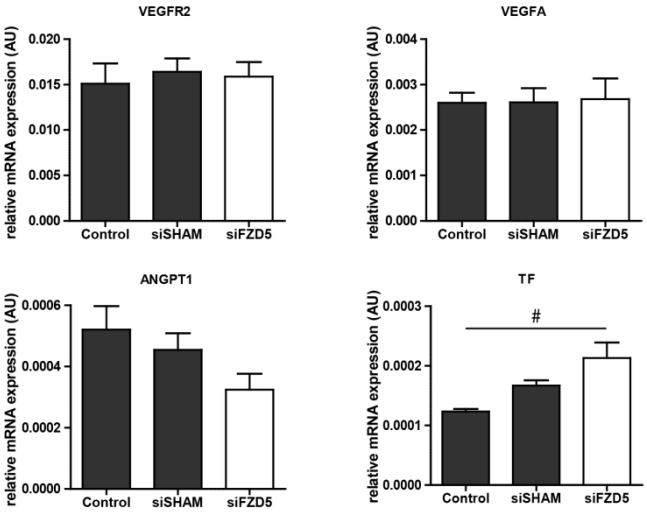

Supplemental Figure 2: Effect of FZD5 knockdown on important angiogenic regulators. qPCR results showing expression levels of VEGFR2, VEGFA, ANGPT1 and TF in the different conditions 72 hours post transfection. N=5, #P<0.05 compared to untreated control condition.

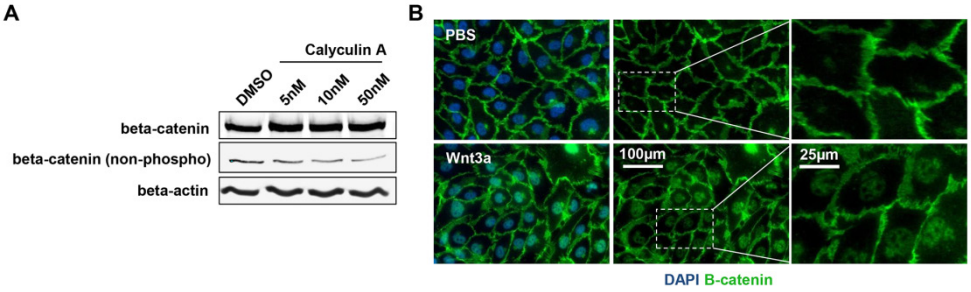

Supplemental Figure 3: Positive control experiments for β-catenin Western blot and immunofluorescent staining. (A) Representative Western blot of total β-catenin, non-phospho β-catenin, and β-actin levels in HUVECs after 30 min stimulation with DMSO or different concentrations of the phosphatase inhibitor Calyculin A (positive control for verification of phosphorylation status). **(B)** Representative immunofluorescent staining of β-catenin (green) in HUVECs after stimulation with PBS or recombinant WNT3a. Scale bars represent 100µm and 25µm.

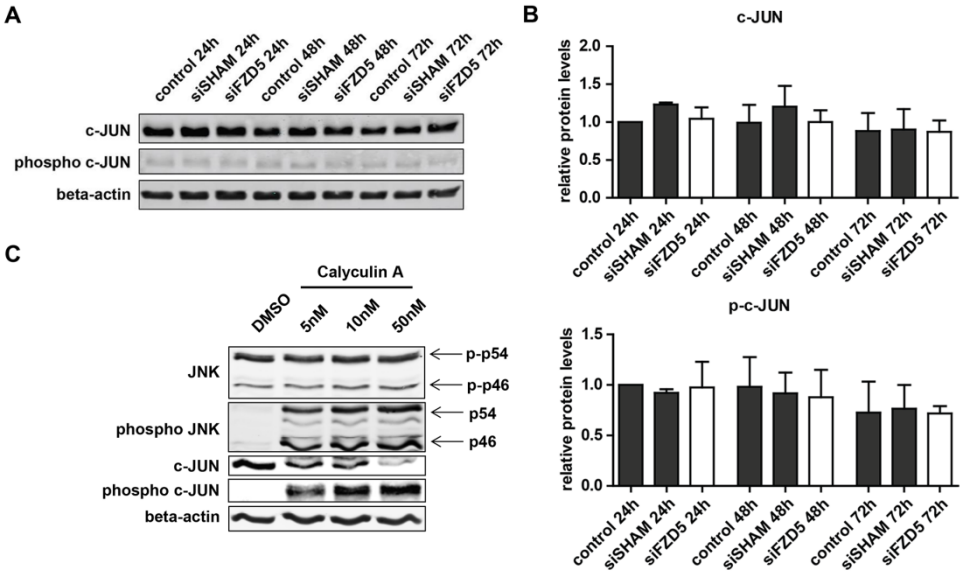

Supplemental Figure 4: FZD5 knockdown did not affect c-JUN phosphorylation. (A) Representative Western blot of total c-JUN, phospho c-JUN and β-actin levels at different time points post-transfection. **(B)** Quantified results of c-JUN and phospho c-JUN Western blot. Shown are (phospho) c-JUN levels relative to β-actin loading control. N=3, no significance. **(C)** Representative Western blot of total JNK, phospho JNK, total c-JUN, phospho c-JUN and β-actin levels in HUVECs after 30 min stimulation with DMSO or different concentrations of the phosphatase inhibitor Calyculin A (positive control for verification of phosphorylation status).

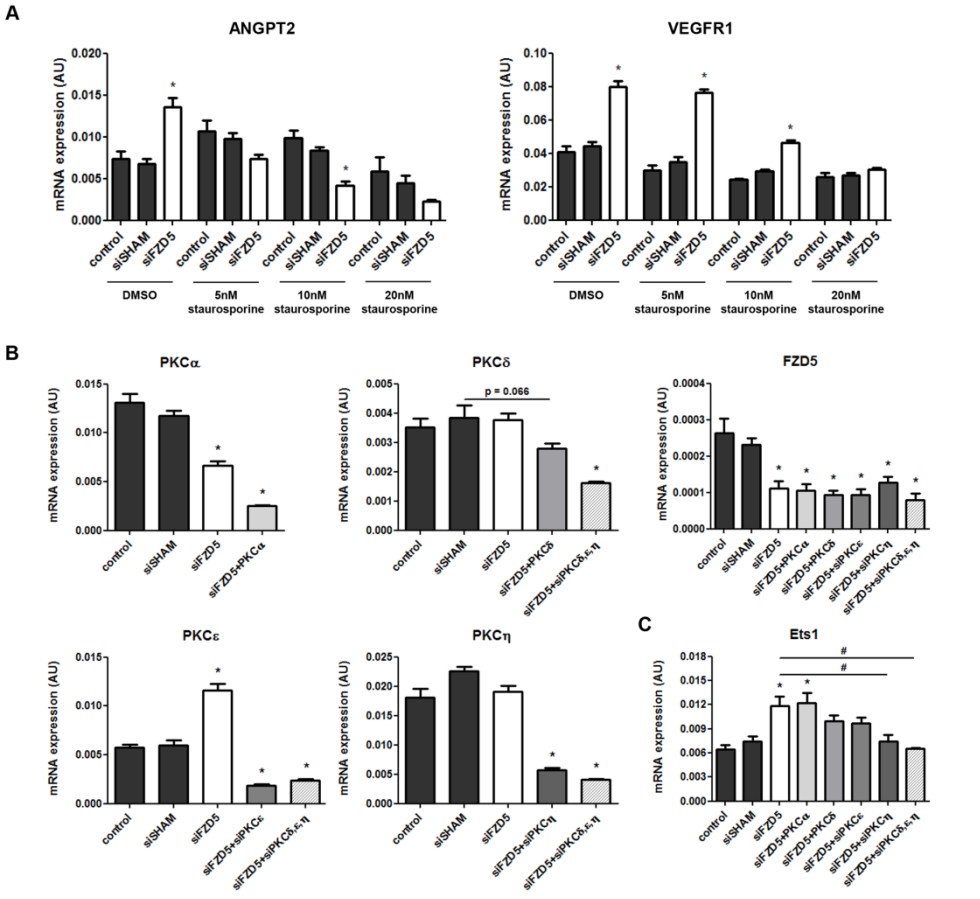

Supplemental Figure 5: Upregulation of ANGPT2 and VEGFR1 in HUVECs with suppressed FZD5 expression via novel PKC signaling. (A) QPCR results of ANGPT2 and VEGFR1 in response to treatment to PKC inhibitor staurosporine (0-20nM), supplemented 48 hours post transfection to the different conditions. N=4, *P<0.05 compared to control and siSHAM condition within comparable conditions (two-way ANOVA followed by Bonferroni post hoc test). **(B)** QPCR results showing expression levels of conventional PKC isoform PKCα, novel PKC isoforms PKCδ, PKCε, and PKCη, FZD5, and transcription factor Ets1 **(C)** in HUVECs after knockdown of FZD5 alone, in combination with different PKC isoforms, and in combination with all novel PKC isoforms (PKCδ,ε,η), 48 hours post transfection. N=4, *P<0.05 compared to control and siSHAM condition, #P<0.05 as indicated in graph.

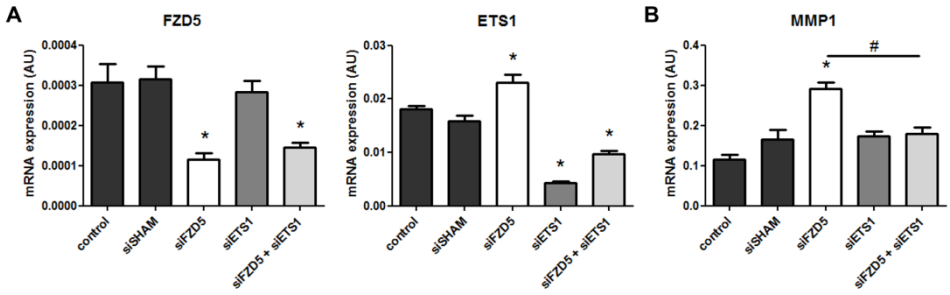

Supplemental Figure 6: FZD5 and Ets1 knockdown validation and Ets1 dependent MMP1 expression in absence of FZD5. qPCR results showing expression levels of FZD5 and Ets1 **(A)**, and Ets1 target gene MMP1 **(B)** in HUVECs after knockdown of FZD5, Ets1, and in a combined knockdown of FZD5 and Ets1, 72 hours post transfection. N=4, *P<0.05 compared to control and siSHAM condition, #P<0.05 as indicated in graph.

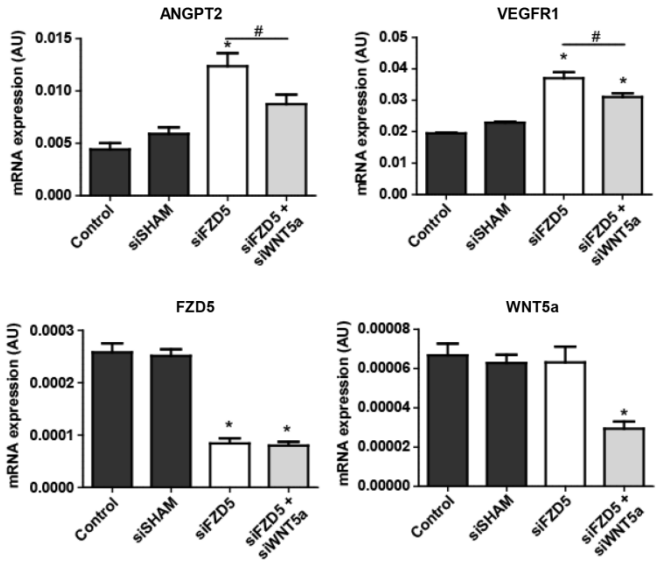

Supplemental Figure 7: Endogenous endothelial WNT5a expression triggers ANGPT2 and VEGFR1 upregulation in absence of FZD5. qPCR results showing expression levels of ANGPT2, VEGFR1, FZD5 and WNT5a in HUVECs after knockdown of FZD5 alone or in combination with Wnt5a, 72 hours post transfection. N=11, *P<0.05 compared to control and siSHAM condition, #P<0.05 as indicated in graph.

Chapter 3

Transcriptome analysis reveals microvascular endothelial cell-dependent pericyte differentiation

Maarten M. Brandt, Christian G.M. van Dijk, Ranganath Maringanti, Ihsan Chrifi, Rafael Kramann, Marianne C. Verhaar, Dirk J. Duncker, Michal Mokry, Caroline Cheng.

Scientific Reports, 2019 (in press)

Abstract

Microvascular homeostasis is strictly regulated, requiring close interaction between endothelial cells and pericytes. Here, we aimed to improve our understanding of how microvascular crosstalk affects pericytes. Human-derived pericytes, cultured in absence, or presence of human endothelial cells, were studied by RNA sequencing. Compared with mono-cultured pericytes, a total of 6704 genes were differentially expressed in co-cultured pericytes. Direct endothelial contact induced transcriptome profiles associated with pericyte maturation, suppression of extracellular matrix production, proliferation, and morphological adaptation. In vitro studies confirmed enhanced pericyte proliferation mediated by endothelial-derived PDGFβ and pericyte-derived HB-EGF and FGF2. Endothelial-induced PLXNA2 and ACTR3 upregulation also triggered pericyte morphological adaptation. Pathway analysis predicted a key role for TGFβ signaling in endothelial-induced pericyte differentiation, whereas the effect of signaling via gap- and adherens junctions was limited. We demonstrate that endothelial cells have a major impact on the transcriptional profile of pericytes, regulating endothelial-induced maturation, proliferation, and suppression of ECM production.

Introduction

Complex organisms such as vertebrates rely on a well-functioning circulatory system to meet the body's oxygen and nutrient demand, and to remove waste products. The circulatory system is composed of blood vessels, lined by a single layer of endothelial cells (ECs) on the luminal side. These ECs are surrounded by a basement membrane which they share with mural cells. In the microvasculature, these mural cells consist of pericytes.[1]

Maintaining microvascular homeostasis is a strictly regulated process, which requires close interplay between ECs and pericytes. Dysregulation of this comprehensive interaction is associated with the onset and progression of a variety of diseases.[2] Lack of pericytes compromises vascular integrity and causes leaky unstable vessels (e.g. in rapidly growing tumors)[3], as well as highly proliferative endothelium (e.g. in diabetic retinopathy).[4] Moreover, pericytes have previously been linked to pathological organ fibrosis[5], though whether injury-induced stimulation, or loss of endothelial interaction drives this differentiation is poorly understood. Former studies on microvascular cross-talk provided valuable insights into the mechanisms involved in regulating vascular homeostasis. For instance, Platelet Derived Growth Factor β (PDGFβ) secretion by ECs was shown to modulate pericyte proliferation and migration towards the endothelium[4], whereas pericyte-derived Vascular Endothelial Growth Factor A (VEGFA) and Angiopoietin 1 (ANGPT1) secretion were reported to promote endothelial survival and maturation.[6, 7] In addition to these paracrine interactions, ECs and pericytes also connect physically. At distinct places, the basement membrane separating the two cell types is interrupted, allowing the formation of direct connection sites called peg and socket contacts.[8] These contacts are highly enriched in gap- and adherens junctions, which provide a direct signaling route for ions, nutrients, metabolites, and secondary messengers.[9] Over the years, numerous studies have focused on the different aspects of signaling between these closely associated microvascular cells. However, since most emphasis was put on how pericytes affect endothelial behavior, only little is known about the consequence of this cross-talk for pericytes.

To gain a deeper understanding of the impact of vascular crosstalk on these critical, yet relatively underexposed, contributors of microvascular homeostasis, an RNA sequence-(RNAseq) based analysis was performed to compare the mRNA expression profiles of single cultured pericytes, with those of pericytes cultured in direct contact with endothelial cells. The results demonstrate that ECs have a major impact on the transcriptional profile of pericytes and provide functional evidence for endothelium-induced pericyte maturation, proliferation, and suppression of ECM expression.

Methods

Cell culture

HMVECs (Lonza) and human brain-derived pericytes (Sciencell) were cultured on 0.1% gelatin coated plates in EGM-2MV medium (EBM2 medium supplemented with EGM-2MV bullet kit; Lonza) and DMEM (supplemented with 10% fetal calf serum (FCS); Lonza), respectively, in 5% CO_2 at 37 ˚C. HMVECs were transduced with a lentiviral GFP construct and pericytes with a lentiviral dsRED construct. Experiments were performed with cells at passage 4-6. CDH2, CX43, HB-EGF, FGF2 and VEGFA, PLXN2A, ACTR3 knockdown in pericytes, and PDGFβ knockdown in HMVECs was achieved by cell transfection with a pool containing 4 targeting siRNA sequences (Dharmacon) in a final concentration of 100nM. Control cells were transfected with a pool of 4 non-targeting siRNA sequences (Dharmacon) in a final concentration of 100nM. Target sequences are listed in Table 1.

Table 1: siRNA sequences used for knockdown experiments

Target gene	Target sequence	
Non-targeting	UGGUUUACAUGUCGACUAA	UGGUUUACAUGUUUUCUGA
	UGGUUUACAUGUUGUGUGA	UGGUUUACAUGUUUUCCUA
CDH2	GUGCAACAGUAUACGUUAA	CAUAGUAGCUAAUCUAACU
	GGACCCAGAUCGAUAUAUG	GACAGCCUCUUCUCAAUGU
CX43	CAGUCUGCCUUUCGUUGUA	GUACAUCUAUGGAUUCAGC
	UGACAAGGUUCAAGCCUAC	GAACCUACAUCAUCAGUAU
PDGFβ	CCGAGGAGCUUUAUGAGAU	GCAAGCACCGGAAAUUCAA
	GAAGAAGGAGCCUGGGUUC	GGGCCGAGUUGGACCUGAA
HB-EGF	GAAAAUCGCUUAUAUACCU	GGACCCAUGUCUUCGGAAA
	UGAAGUUGGGCAUGACUAA	GGAGAAUGCAAAUAUGUGA
FGF2	CUAAAUGUGUUACGGAUGA	GCUAAGAGCUGAUUUUAAU
	UCAAAGGAGUGUGUGCUAA	GAUGGAAGAUUACUGGCUU
VEGFA	GCAGAAUCAUCACGAAGUG	GGAGUACCCUGAUGAGAUC
	CAACAAAUGUGAAUGCAGA	GAUCAAACCUCACCAAGGC
PLXNA2	GGUCAAUGAGUGAGAUCGU	CCAGCCAAGUUUCGUCAUA
	CUGGGAACCUAAUCGAUUU	ACUAUGAGCUACACAGCGA
ACTR3	GCAGUAAAGGAGCGCUAUA	GGAAUUGAGUGGUGGUAGA
	GUGAUUGGCAGCUGUAUUA	GCCAAAACCUAUUGAUGUA

Fluorescence-activated cell sorting

GFP-labeled HMVECs and dsRED-labeled pericytes were seeded in a confluent layer (4 million cells) on 10cm dishes, either in co-culture at a 5:1 (HMVECs:pericytes) ratio, or in single culture (Figure 1A). Both single cultures and co-cultures were cultured on EBM supplemented with 5% FCS for 6h, followed by 20h on EBM supplemented with 0.5% FCS. For fluorescence activated cell sorting (FACS), cells were trypsinized, washed once in cold PBS and suspended in cold sterile filtered PBS containing 2% bovine serum albumin. GFP-labeled HMVECs and dsRED-labeled pericytes were separately sorted in cold FCS based on their fluorescent signal. Subsequently, cells were washed once in cold PBS, lysed in RNA lysis buffer and stored at -80 ˚C (Figure 1B).

RNA sequencing

RNA sequencing was done as previously described.[10] Briefly, sequencing libraries were made from poly-adenylated RNA using the Rapid Directional RNA-Seq Kit (NEXTflex) and sequenced on Illumina NextSeq500 to produce single-end 75 base long reads (Utrecht Sequencing Facility). Reads were aligned to the human reference genome GRCh37 using STAR version2.4.2a. Read groups were added to the BAM files with Picard's AddOrReplaceReadGroups (v1.98). The BAM files were sorted with Sambamba v0.4.5, and transcript abundances were quantified with HTSeq-count version 0.6.1p117 using the union mode. Subsequently, reads per kilobase of transcript per million reads sequenced were calculated with edgeR's rpkm() function. Differentially expressed genes in the transcriptome data were identified using the DESeq2 package with standard settings.[11]

Quantitative PCR and Western blot analysis

RNA was reverse transcribed into cDNA using iScript cDNA synthesis kit (Bioline). Gene expression was assessed by qPCR using SensiFast SYBR & Fluorecein kit (Bioline) and primers as listed in Table 2. Expression levels are relative to the housekeeping gene Ribosomal Phosphoprotein P0 (RPLP0) and RNA Polymerase II Subunit L (POLR2L). For assessment of protein levels, cells were lysed in cold NP-40 lysis buffer (150mM NaCl, 1.0% NP-40, 50 mM Tris, pH 8.0) supplemented with 1mM β-glycerolphosphate, 1mM PMSF, 10mM NaF, 1mM NaOV, and protease inhibitor cocktail (Roche). Total protein concentration was quantified by Pierce® BCA Protein Assay Kit (Thermo Scientific) as a loading control. Lysates were denaturated in Laemmli buffer at 90°C for 5 min followed by electrophoresis on a 10% SDS-PAGE gel (Biorad). Subsequently, proteins were transferred to a nitrocellulose membrane (Pierce) and incubated for 1 hour in PBS with 5% non-fat milk,

followed by incubation with rabbit anti-CX43 and rabbit anti-N-cadherin (CST) according to manufacturer's description. Protein bands were visualized with the Li-Cor detection system (Westburg).

Table 2: Primer sequences used for (q)PCR

Gene	Sense primer sequence	Antisense primer sequence
RPLP0	CAGATTGGCTACCCAACTGTT	GGAAGGTGTAATCCGTCTCCAC
POLR2L	TCACTTGTGGCAAGATCGTCG	GGGTGCATAATTGAGCAGCTTC
GLI1	TCCTACCAGAGTCCCAAGTTTC	GCCCTATGTGAAGCCCTATTT
NG2	ACCTTCAACTACAGGGCACAAG	AGGACATTGGTGAGGACAGG
ACTA2	ACTGAGCGTGGCTATTCCTTC	CAGGCAACTCGTAACTCTTCTC
CD146	CTGCTGAGTGAACCACAGGA	CACCTGGCCTGTCTCTTCTC
NES	CCTGGGAAAGGGAGAGTACC	GATTCAGCTCTGCCTCATCC
PDGFRβ	GAGGAATCCCTCACCCTCTC	GGGTATATGGCCTTGCTTCA
BBC3	GACCTCAACGCACAGTACGAG	AGGAGTCCCATGATGAGATTGT
T53INP1	TTCCTCCAACCAAGAACCAG	GATGCCGGTAAACAGGAAAA
GDF15	CTCCAGATTCCGAGAGTTGC	AGAGATACGCAGGTGCAGGT
CDK1	CTGGGGTCAGCTCGTTACTC	AGGCTTCCTGGTTTCCATTT
RBL1	ATACGACTTGGCGAATCAGG	GAGCGCTTCTTGGTGTAAGG
MYC	CTCCTGGCAAAAGGTCAGAG	TCGGTTGTTGCTGATCTGTC
MCM2	ATTTCGTCCTGGGTCCTTTCT	CTGGTTTCACCTCCTGGTTCT
CCND1	GTCCATGCGGAAGATCGTCG	TCTCCTTCATCTTAGAGGCCACG
PDGFβ	CCCCACACTCCACTCTGATT	GCCCTGGCCTCTAGTCTTCT
FGF2	AGAGCGACCCTCACATCAAG	TCGTTTCAGTGCCACATACC
HB-EGF	GGTGGTGCTGAAGCTCTTTC	GCTTGTGGCTTGGAGGATAA
VEGFA	CATCCAATCGAGACCCTGG	ATGTGCTGGCCTTGGTGAG
PLXNA2	AAAGGAAGAGGACCCCAGAA	GACAGCAAGCACAGAAGCAC
ACTR3	CTGGGTTGCGGAAGTGATAG	TGTATACCCCGTGCCACAGT
CTGF	CCGTACTCCCAAAATCTCCA	GTAATGGCAGGCACAGGTCT
TAGLN	AAGAATGATGGGCACTACCG	ACTGATGATCTGCCGAGGTC
SERPINE1	TCTTTGGTGAAGGGTCTGCT	TTGAATCTGCTGCTGGGTTT
CX43	TGGATTCAGCTTGAGTGCTG	GGTCGCTCTTTCCCTTAACC
CDH2	GACAATGCCCCTCAAGTGTT	CCATTAAGCCGAGTGATGGT

Immunofluorescent staining

Pericytes labeled with dsRED were seeded in a confluent layer (50.000 cells) on 96 wells plates in a 1:5 ratio, either with unlabeled HMVECs, or with unlabeled pericytes. After seeding, the cells were cultured on EBM supplemented with 5% FCS for 6h, followed by 20h on EBM supplemented with 0.5% FCS. After 20h in culture, cells were fixed for 20min in 2% paraformaldehyde and blocked for 60min in PBS containing 5% bovine serum albumin (Sigma) and 0.3% Triton X-100 (Sigma). Hereafter, 100µl PBS containing 1% BSA, 0.3% Triton X-100, and 1:400 rabbit anti-Ki67 antibody (CST) was added per well, followed by a 16h incubation at 4°C. After incubation with the primary antibody, Ki67 was stained with an Alexa Fluor 594-labeled secondary antibody (Invitrogen), dissolved (1:200) in PBS containing 1% BSA and 0.3% Triton X-100 for 2h at room temperature. Vectashield with DAPI (Brunschwig) was applied to the fixed cell cultures, followed by imaging using fluorescence microscopy. Analysis of Ki67 positive pericyte nuclei was averaged per individual experiment from at least 5 random image fields in ImageJ using the Cell Counter plugin.

Pathway analysis

RNAseq results were analyzed using IPA. IPA was used to study upstream regulators (growth factors and transcriptional regulators) of differentially expressed genes. P-values were calculated based on a right-tailed Fisher Exact Test, calculated by IPA.

Statistics

Data are presented as means ± SEM. Groups were compared by students t-test (two-tailed) or 1-way ANOVA followed by Tukey post hoc test when appropriate. Statistical significance was accepted when $p<0.05$.

Results

Endothelial cells markedly affect pericyte phenotype

To evaluate the impact of endothelial-pericyte interaction on pericyte behavior, discosoma sp. red- (dsRED) labeled pericytes were cultured in a confluent layer either alone, or in the presence of green fluorescent protein- (GFP) labeled human dermal microvascular endothelial cells (HMVECs), enabling direct contact between the two different cell types fluorescent signal, after which RNA was isolated and processed for RNA sequencing (Figure 1B). A comparison of the transcription profile of single cultured pericytes and co-cultured pericytes in a principal component analysis (PCA) clearly illustrated the major effect

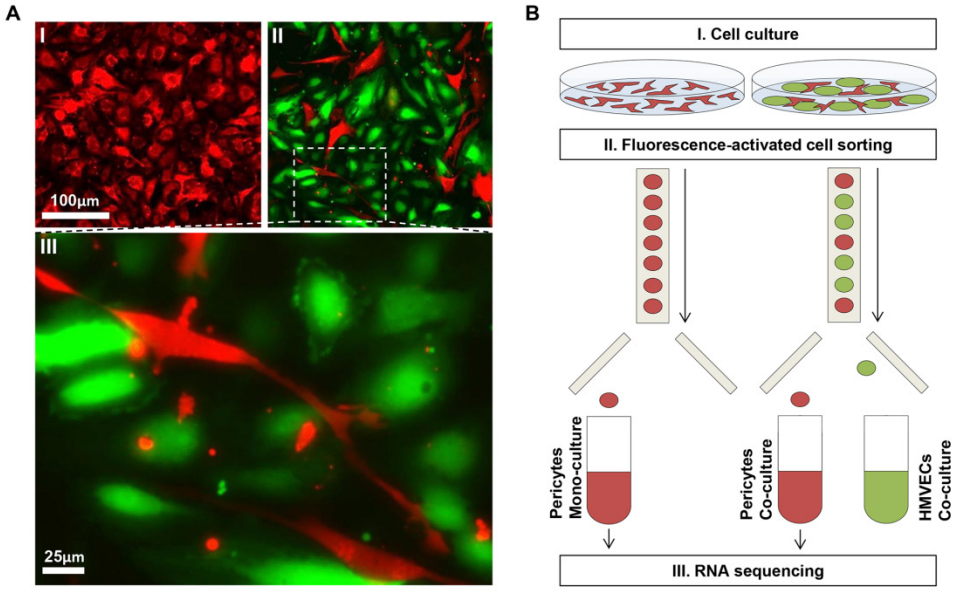

Figure 1: Expression profiles were generated from mono- and co-cultured pericytes via RNA sequencing. (A) Pericytes labeled with dsRED (red) were either cultured alone (I), or in direct contact with GFP-labeled HMVECs (green) (II). Magnified view of co-cultured cells clearly shows the elongated pericytes that appear to be in contact with multiple ECs (III). **(B)** Schematic overview of the experiments: Pericytes labeled with dsRED were cultured in a confluent layer, either alone, or in direct contact with GFP-labeled HMVECs for the duration of 20 hours (I). Hereafter, cells were trypsinized and sorted based on fluorescent signal (II), after which RNA was isolated from the pericytes for RNA sequencing (III).

of endothelial-pericyte crosstalk on pericytes (Figure 2A). In total, 6704 genes were differentially expressed (P adjusted <0.05; Figure 2B). Of these 6704 differentially expressed genes, 6081 were protein coding genes (almost one third of the estimated 19000 protein coding genes in the human genome)[12], suggesting that direct contact with ECs dramatically affects pericyte's transcriptomes.

Direct contact with endothelium stimulates pericyte maturation

A newly formed endothelial network is initially unstable and requires support from recruited pericytes. These pericytes either migrate from adjacent vessels or differentiate from local mesenchymal stem cells.[13] Comparing expression profiles from single cultured pericytes with pericytes co-cultured with ECs clearly illustrated the importance of interaction with ECs in this differentiation process. Expression of Glioma-associated oncogene 1 (GLI1), a zinc

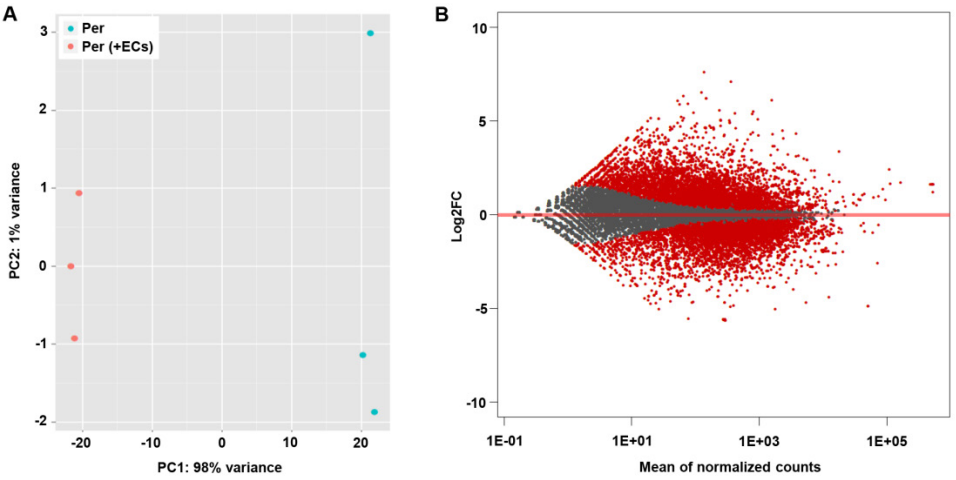

Figure 2: Endothelial cells have a major impact on the expression profile of pericytes. (A) PCA plot of expression profiles in single cultured pericytes (blue) and co-cultured pericytes (red). **(B)** Graphic display of differential gene expression (MA plot) in which log2FC is plotted against the mean of normalized counts. Red dots represent the 6704 differentially expressed genes (P adjusted <0.05), gray dots represent non-differentially expressed genes.

finger type transcription factor and downstream effector of the Hedgehog signaling pathway that has been reported to be expressed in pericyte-like progenitors[14], was significantly reduced in co-cultured pericytes (Figure 3A). In contrast, well-validated pericyte markers, including Chondroitin Sulfate Proteoglycan 4 (CSPG4/NG2), Alpha Smooth Muscle Actin 2 (ACTA2), Melanoma Cell Adhesion Molecule (CD146), and Nestin (NES), were highly upregulated after direct interaction with ECs (Figure 3B). Interestingly, Platelet Derived Growth Factor Receptor B (PDGFRβ), one of the most frequently used pericyte- and mesenchyme markers, was significantly downregulated in co-cultured pericytes (Figure 3B).

Endothelial signaling stimulates pericyte proliferation and survival

Prior studies showed that pericyte-endothelial interaction had a profound positive effect on endothelial survival and maturation.[15] Interestingly, studying the upstream transcription factors of the differentially expressed genes using QIAGEN's Ingenuity Pathway Analysis (IPA) led to the suggestion that direct interaction with ECs also stimulated pericyte proliferation and survival (Figure 4A), which corresponds with functional findings reported previously.[16] Expression levels of 330 Tumor Protein 53- (TP53) dependent target genes in co-cultured pericytes, including BCL2 Binding Component 3 (BBC3), Tumor Protein P53 Inducible Nuclear Protein 1 (TP53INP1), and Growth Differentiation Factor 15 (GDF15),

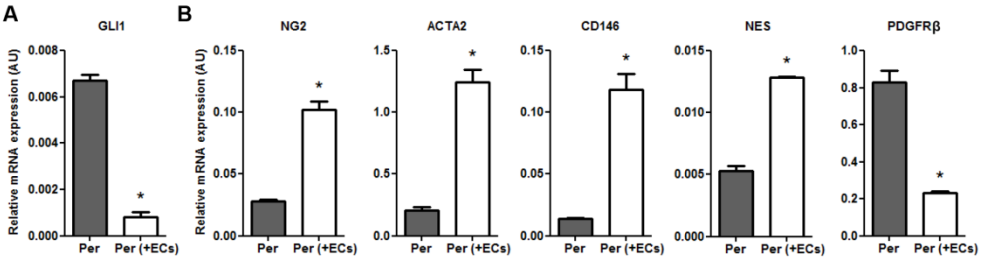

Figure 3: Direct contact with endothelium stimulates pericyte maturation. (A) QPCR results showing expression levels of mesenchymal transcription factor GLI1, and **(B)** pericyte markers NG2, ACTA2, CD146, NES, and PDGFRβ relative to RPLP0 and POLR2L in pericytes in monoculture (Per), and after 20h in co-culture with HMVECs (Per+ECs). N=3, *P<0.05 compared to pericytes in monoculture.

suggested suppressed activity of this pro-apoptotic and cell cycle inhibiting factor (Figure 4B). Vice versa, the activity of proliferation-stimulating transcription factors E2F1 and E2F3 appeared to be enhanced in co-cultured pericytes. Expression of 139 E2F target genes, including Cyclin Dependent Kinase 1 (CDK1), Retinoblastoma Transcriptional Corepressor Like 1 (RBL1), Proto-Oncogene C-Myc (MYC), Minichromosome Maintenance Complex Component 2 (MCM2), and Cyclin D1 (CCND1), was significantly enhanced after direct interaction with ECs (Figure 4C). To functionally validate the impact of endothelial contact on pericyte proliferation, we performed immunostaining for the proliferation (G1/S/G2M) marker Ki67 in dsRED-labeled pericytes, cultured in a confluent layer either with unlabeled HMVECs, or with unlabeled pericytes (Figure 4D). In line with the observed transcriptional adaptations in co-cultured pericytes, quantification of the percentage of Ki67-positive nuclei in dsRED labeled pericytes clearly illustrated a significantly increased pericyte proliferation during co-culture with endothelium as compared with mono-cultured pericytes (Figure 4E). It was previously reported that pericyte proliferation could be stimulated by VEGFA[17], potentially via an autocrine signaling loop resulting from endothelium-induced upregulation of VEGFA expression in pericytes. In the present study however, a significant downregulation of VEGFA was observed in co-cultured pericytes, though expression was still higher than in co-cultured ECs (Figure 4F). To evaluate the involvement of pericyte-derived VEGFA in pericyte proliferation, as well as that of potent growth factors Heparin-binding EGF-like growth factor (HB-EGF) and fibroblast growth factor 2 (FGF2), which in contrast to VEGFA were upregulated in co-cultured pericytes, short interference RNA-(siRNA) mediated knockdown was performed in dsRED-labeled pericytes followed by coculture with ECs and Ki-67 immunostaining (Supplemental Figure 1A and 1C).

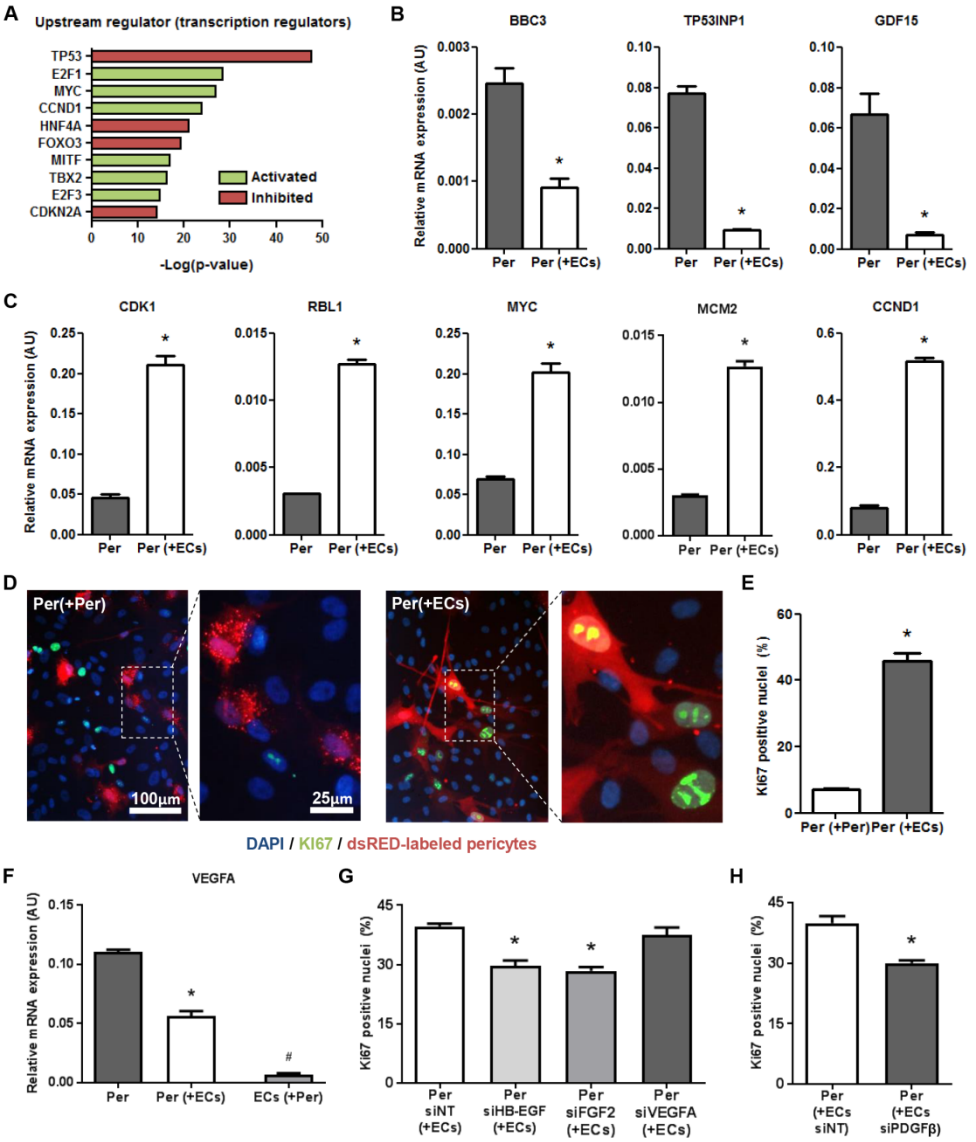

Figure 4: Endothelial signaling stimulates pericyte proliferation and survival. (A) IPA-derived prediction of activated or repressed transcription regulators in co-cultured pericytes compared with single cultured pericytes. Plotted is the –log(p-value) of overlap, in which green indicates predicted activation in co-culture versus predicted inhibition in red. **(B)** QPCR results showing expression levels of TP53 target genes BBC3, TP53INP1, and GDF15, as well as **(C)** E2F target genes CDK1, RBL1, MYC, MCM2 and CCND1 relative to RPLP0 and POLR2L in pericytes in monoculture (Per), and after 20h in co-culture with HMVECs (Per+ECs). N=3, *P<0.05 compared to pericytes in monoculture. **(D)** Immunofluorescent Ki67 (green), and DAPI (blue) staining in dsRED-labeled pericytes, either cultured with unlabeled HMVECs (left) or with unlabeled pericytes (right). **(E)** Bar graph shows the quantified

◄ results of the Ki67 staining. Shown are the percentages of dsRED-labeled pericyte nuclei positive for the proliferation marker Ki67. N=3, *P<0.05 compared to dsRED-labeled pericytes in culture with unlabeled pericytes. **(F)** QPCR results showing expression levels of VEGFA in pericytes in monoculture (Per), and after 20h in co-culture in both pericytes (Per+ECs) and HMVECs (ECs+Per). N=3, *P<0.05 compared to pericytes in monoculture and ECs in co-culture, #P<0.05 compared to pericytes in mono- and co-culture. **(G)** Bar graph showing the percentage of Ki67 positive nuclei in dsRED-labeled pericytes after knockdown of HB-EGF, FGF2, and VEGFA in pericytes, and **(H)** PDGFβ in ECs. N=4, *P<0.05 compared to siNT-treated condition.

Quantification of the percentage of Ki67-positive nuclei in dsRED labeled pericytes revealed that knockdown of VEGFA had no effect on pericyte proliferation, whereas knockdown of HB-EGF and FGF2 significantly reduced the proliferative response of pericytes in co-culture with pericytes (Figure 4G). Similarly, endothelial knockdown of PDGFβ, a well-known pericyte mitogen that was upregulated in co-cultured ECs (Supplemental Figure 1B and 1D), significantly reduced proliferation of pericytes in co-culture with ECs (Figure 4H).

Direct endothelial contact triggers outgrowth of pericyte projections

Mature pericytes have a highly specialized morphology that is distinctly different from other microvascular cells. They align their nuclei with the endothelium and extend thin processes along and around the capillaries. These elongated projections allow individual pericytes to contact and communicate with multiple ECs and were recently shown to have an active role in maintaining normal cerebral microvascular lumen diameter.[18] These thin processes show morphological similarities with axons growing from neurons. Growing axons have a highly dynamic structure at the peripheral tip, called the growth cone, which senses the environment for attracting or repelling guiding cues. Following these cues, actin remodeling at the leading edge guides the growth cone, followed by a polymerizing and elongating bundle of microtubules.[19] Interestingly, an exceptionally high number of genes involved in this process was differentially expressed in co-cultured pericytes, as identified by IPA. Among these differentially expressed genes was a variety of different growth cone-guiding molecules, including Semaphorins (SEMA), Ephrins (EFN), Netrins (NTN), and their respective receptors (Figure 5A). Many Alpha and Beta Tubulins (TUBA and TUBB, respectively), composing the core of the growing projections, were upregulated in co-cultured pericytes (Figure 5B). Similarly, enhanced expression was observed for Cofilins (CFL) and all but one Actin Related Protein 2/3 Complex subunits (ARPC), which regulate actin polymerization required for growth cone dynamics (Figure 5B).[20] To verify whether these transcriptional adaptations were associated with morphological changes that resemble outgrowth of pericyte projections, dsRED-labeled pericytes were again cultured in a

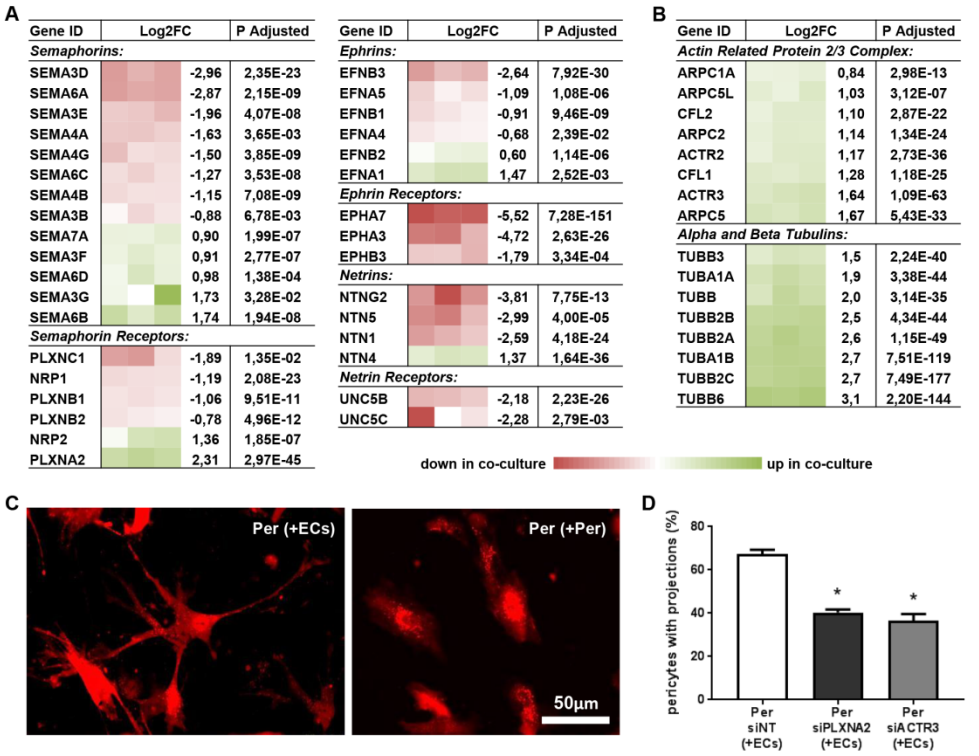

Figure 5: Direct endothelial contact triggers outgrowth of pericyte projections. (A) schematic presentation of RNAseq data for differentially expressed Semaphorins, Ephrins, Netrins, and their respective receptors, as well as **(B)** subunits of the Actin Related Protein 2/3 Complex and Tubulins, which were all listed by IPA in a group of 200 differentially expressed genes involved in projection outgrowth. Shown is a color-based representation of the log2FC in each of the 3 individual experiments (red is downregulated in co-culture, green is upregulated in co-culture), followed by the average log2FC and the adjusted p-value. **(C)** Representative fluorescence microscopy images of dsRED-labeled pericytes in co-culture with unlabeled HMVECs (left), or with unlabeled pericytes (right). **(D)** Bar graph showing the percentage of dsRED-labeled pericytes with outgrowth of projections after knockdown of PLXNA2 and ACTR3 in pericytes. N=4, *P<0.05 compared to siNT-treated condition.

confluent layer for the duration of 20 hours, either in combination with unlabeled HMVECs, or with unlabeled pericytes followed by fluorescent microscopy imaging. Interestingly, pericytes in direct contact with ECs had a completely different morphology, indeed forming extensive projections (Figure 5C). To study whether the differentially expressed growth cone-guiding molecules could in fact be involved in the observed morphological adaptation in pericytes, a proof-of-principle approach was used in which Plexin A2 (PLXNA2) and Actin Related Protein 3 (ACTR3), both well expressed and highly upregulated in co-cultured pericytes (Supplemental Figure 2A), were knocked down (Supplemental Figure 2B). After

culturing these siRNA-transfected pericytes in a confluent layer with HMVECs for the duration of 20 hours, the percentage of protrusion-forming pericytes was quantified using fluorescence microscopy. Knockdown of both PLXNA2 and ACTR3 significantly reduced the relative number of pericytes with projections (Figure 5D), substantiating the idea that direct interaction with ECs triggered a transcriptional response in pericytes necessary for morphological maturation.

Endothelial interaction suppresses overall ECM production in pericytes

Recent studies showed that pericytes, detaching from the capillaries, not only leave the microvascular endothelium in a vulnerable position, but at the same time might undergo differentiation into ECM-producing cells themselves.[5, 21] Whether this differentiation is a consequence of disrupted mutual cross-talk, or involves other extravascular signaling routes is not fully understood. Interestingly, expression of 24 Collagen subtypes was significantly suppressed in pericytes co-cultured with endothelial cells, compared with mono-cultured pericytes (Figure 6A). Moreover, a variety of other ECM components, including Fibronectin 1 (FN1), and Alpha- and Beta Laminins (LAMA and LAMB, respectively) was transcriptionally downregulated in co-cultured pericytes (Figure 6A). This suppressed ECM expression in co-cultured pericytes might argue that differentiation into a fibrotic phenotype is indeed inhibited by direct interaction with ECs. Several studies have suggested that pericyte differentiation towards ECM producing cells depends on enhanced Transforming Growth Factor B (TGFβ) signaling.[22, 23] However, in line with findings from many other studies (reviewed by Gaengel *et al.*[24]), our findings indicated that pericytes in contact with ECs have much higher activation of TGFβ signaling than pericytes lacking interaction with ECs. In fact, based on 315 differentially expressed genes, IPA considered TGFβ1 (overlap p-value 3.56E-34) as the most active upstream growth factor in co-cultured pericytes (Figure 6B). Other upregulated genes in co-cultured pericytes beside ACTA2, included Connective Tissue Growth Factor (CTGF), Smooth Muscle Protein 22 Alpha (TAGLN), and Plasminogen Activator Inhibitor 1 (SERPINE1), all of which are well-known TGFβ target genes (Figure 6C). These findings illustrate that, even in the presence of activated TGFβ signaling, ECM excretion by pericytes is suppressed when in contact with endothelium.

Destabilizing key gap- and adherens junctions has no effect on transcriptional adaptation

In the mature microvasculature, pericytes and ECs are embedded in a shared basement membrane. At distinct places this basement membrane is interrupted, enabling pericytes and ECs to form direct connections called peg and socket interactions. These sites are

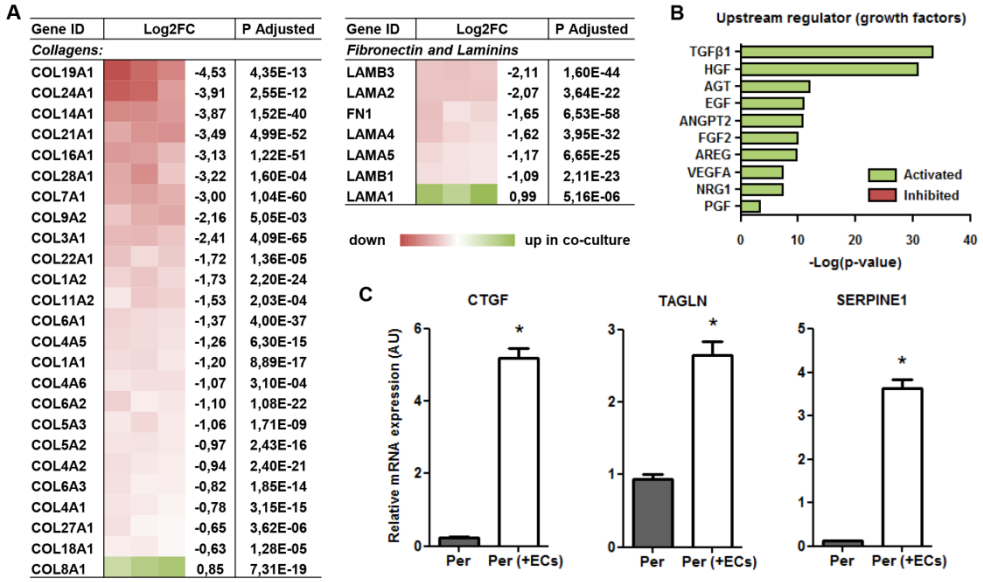

Gene ID	Log2FC	P Adjusted
Collagens:		
COL19A1	-4,53	4,35E-13
COL24A1	-3,91	2,55E-12
COL14A1	-3,87	1,52E-40
COL21A1	-3,49	4,99E-52
COL16A1	-3,13	1,22E-51
COL28A1	-3,22	1,60E-04
COL7A1	-3,00	1,04E-60
COL9A2	-2,16	5,05E-03
COL3A1	-2,41	4,09E-65
COL22A1	-1,72	1,36E-05
COL1A2	-1,73	2,20E-24
COL11A2	-1,53	2,03E-04
COL6A1	-1,37	4,00E-37
COL4A5	-1,26	6,30E-15
COL1A1	-1,20	8,89E-17
COL4A6	-1,07	3,10E-04
COL6A2	-1,10	1,08E-22
COL5A3	-1,06	1,71E-09
COL5A2	-0,97	2,43E-16
COL4A2	-0,94	2,40E-21
COL6A3	-0,82	1,85E-14
COL4A1	-0,78	3,15E-15
COL27A1	-0,65	3,62E-06
COL18A1	-0,63	1,28E-05
COL8A1	0,85	7,31E-19

Gene ID	Log2FC	P Adjusted
Fibronectin and Laminins		
LAMB3	-2,11	1,60E-44
LAMA2	-2,07	3,64E-22
FN1	-1,65	6,53E-58
LAMA4	-1,62	3,95E-32
LAMA5	-1,17	6,65E-25
LAMB1	-1,09	2,11E-23
LAMA1	0,99	5,16E-06

Figure 6: Endothelial interaction suppresses overall ECM production in pericytes. (A) Schematic presentation of RNAseq data for differentially expressed Collagens, Laminins, and Fibronectin. Shown is a color-based representation of the log2FC in each of the 3 individual experiments (red is downregulated in co-culture, green is upregulated in co-culture), followed by the average log2FC and the adjusted p-value. **(B)** IPA-derived prediction of the most activated or repressed growth factors in co-cultured pericytes compared with single cultured pericytes. Plotted is the –log(p-value) of overlap, in which green indicates predicted activation in co-culture versus predicted inhibition in red. **(C)** QPCR results showing expression levels of TGFβ target genes CTGF, TAGLN, and SERPINE1 relative to RPLP0 and POLR2L in pericytes in monoculture (Per), and after 20h in co-culture with HMVECs (Per+ECs). N=3, *P<0.05 compared to pericytes in monoculture.

enriched in CDH2 adherens junctions and CX43 gap junctions, which provide a direct signaling route for ions, nutrients, metabolites, and secondary messengers, and which is complementary to paracrine signaling routes (Figure 7A). This direct signaling was previously reported to play a key role in a particular aspect of endothelium-induced mural cell differentiation.[25] Interestingly in the present study, both CDH2 and CX43 were significantly upregulated in co-cultured pericytes, as validated by qPCR, suggesting enhanced requirement and thus signaling via these direct contacts in co-cultured pericytes (Figure 7B). This raised the question to what extent this signaling was mandatory for pericyte differentiation. To address this questions, we took a similar approach as listed in Figure 1, but pericytes were now treated with non-targeting (NT) siRNA, CHD2-targeting siRNA, or CX43-targeting siRNA, to disrupt the main gap- and adherens junctions, followed

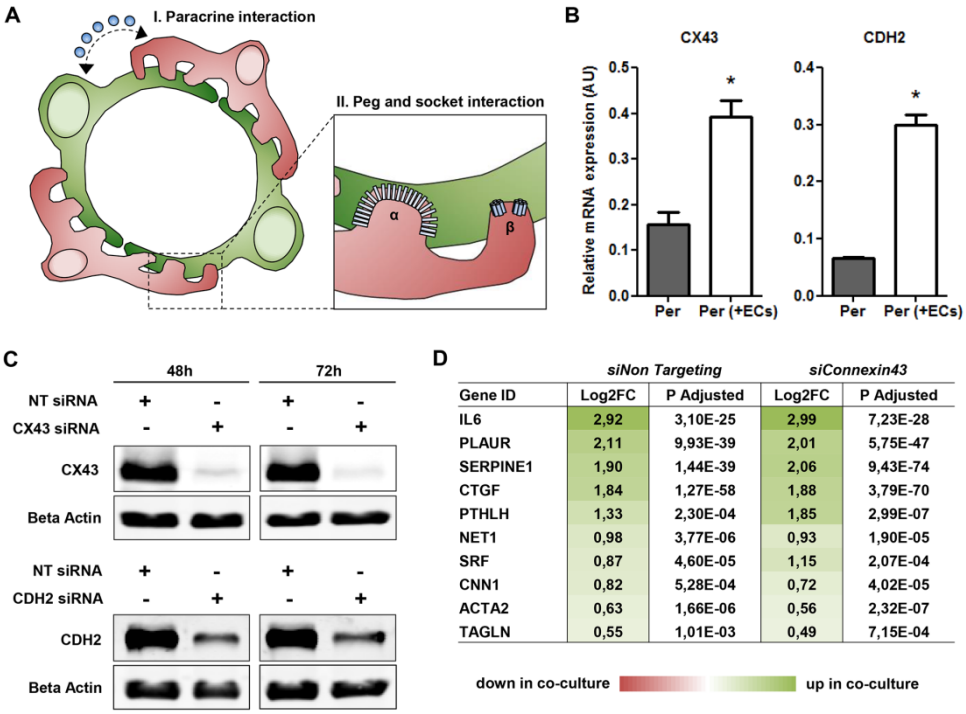

Gene ID	Log2FC	P Adjusted	Log2FC	P Adjusted
IL6	2,92	3,10E-25	2,99	7,23E-28
PLAUR	2,11	9,93E-39	2,01	5,75E-47
SERPINE1	1,90	1,44E-39	2,06	9,43E-74
CTGF	1,84	1,27E-58	1,88	3,79E-70
PTHLH	1,33	2,30E-04	1,85	2,99E-07
NET1	0,98	3,77E-06	0,93	1,90E-05
SRF	0,87	4,60E-05	1,15	2,07E-04
CNN1	0,82	5,28E-04	0,72	4,02E-05
ACTA2	0,63	1,66E-06	0,56	2,32E-07
TAGLN	0,55	1,01E-03	0,49	7,15E-04

Figure 7: Destabilizing key gap- and adherens junctions does not affect transcriptional adaptation (A) Pericytes (red) and ECs (green) can either interact via paracrine interaction (I) or via direct interaction at peg and socket contacts (II). These contacts are enriched in adherens junction protein CDH (α) and gap junction protein CX43 (β). **(B)** QPCR results showing expression levels of CX43 and CDH2 relative to RPLP0 and POLR2L in pericytes in monoculture (Per), and after 20h in co-culture with HMVECs (Per+ECs). N=3, *P<0.05 compared to pericytes in monoculture. **(C)** Representative Western blots of CX43, CDH2, and β-actin levels in pericyte lysates at 48h and 72h post-transfection. N=4. **(D)** Schematic presentation of RNAseq data for differentially expressed TGFβ target genes. Shown is a color-based representation of the log2FC (red is downregulated in co-culture, green is upregulated in co-culture), followed by the adjusted p-value. N=3.

by RNA sequencing. Knockdown efficiency was validated by Western blot for both CDH2 and CX43 (Figure 7C). Expression profiles of co-cultured pericytes treated with NT siRNA were compared with that of co-cultured pericytes with either CDH2- or CX43 knockdown. It was observed that, beside siRNA-mediated downregulation of CDH2 and CX43, only KRT8 was differentially expressed in co-cultured pericytes with suppressed CX43 expression compared with co-cultured pericytes treated with NT siRNA (Log2FC: 0.54, adjusted p-value: 2.43E-02). KRT8 however was also upregulated in single cultured pericytes after CX43 knockdown (Log2FC: -0.52, adjusted p-value: 1.28E-02), indicating this was not

related to destabilized interaction among ECs and pericytes. This also implicates that, in contrast to what has previously been reported, lack of CX43 expression thus did not block TGFβ-induced mural cell maturation. In co-cultured pericytes treated with CX43-targeting siRNA, an evident upregulation was still observed for known TGFβ target genes CTGF, ACTA2, TAGLN, and SERPINE1 (Figure 7D).

Discussion

The main findings of the current study are: (1) Interaction with ECs drives pericyte differentiation and maturation. (2) ECs stimulate pericyte proliferation and survival. (3) Direct endothelial contact stimulates the outgrowth of pericyte projections, and (4) represses overall ECM production in these perivascular cells. (5) Key gap- and adherens junctions genes CX43 and CDH2 do not appear to be involved in endothelium-induced differentiation of pericytes.

Pericytes have previously been described to be multipotent cells.[26, 27] Thus, Crisan *et al.* reported that pericytes from multiple human organs, isolated using a combination of surface markers (including NG2, CD146, and PDGFRβ), were myogenic, osteogenic, chondrogenic, and adipogenic.[28] In light of these findings, it is not unexpected that direct interaction with ECs, resembling the physiological microvascular situation, triggers a defined adaptation in gene expression in these highly plastic cells when compared with single cultured pericytes. At the same time, these findings also align with studies showing that disease-induced loss of EC-pericyte interaction has a major impact on pericyte behavior. Among the differentially expressed genes in co-cultured pericytes there was a variety of well-known pericyte markers. The enhanced transcription of these markers was consistent with previous findings showing that endothelial contact with pericytes or mesenchymal progenitor cells plays a major role in their differentiation towards mature pericytes.[14, 29] Remarkably, beside all upregulated pericyte markers, one of the most frequently used pericyte markers, PDGFRβ, was downregulated in pericytes after direct contact with ECs. PDGFRβ is a membrane-bound receptor with high affinity for Platelet Derived Growth Factor β and δ (PDGFβ and δ, respectively).[30] PDGFβ is abundantly expressed in ECs, and during vascular development endothelial-derived PDGFβ triggers pericyte proliferation and migration towards a newly formed vessel to effectuate pericyte-induced vascular stabilization.[31] Noteworthy, PDGFRβ expression is highly dependent on cell cycle activation, in a way that actively dividing cells have suppressed expression of the receptor.[32] The transcription factor MYC, actively involved in cell cycle progression, was identified as a key repressor of the PDGFRβ

promoter.[33, 34] Co-cultured pericytes were validated by Ki67 immunostaining to be actively proliferating, and not only was their expression of MYC upregulated almost threefold, analysis using IPA also suggested active transcriptional modulation by MYC in co-cultured pericytes (overlap p-value 1.03E-27). It is therefore likely that, among all the upregulated pericyte markers, the observed proliferative response in pericytes after direct contact with ECs triggers the – perhaps somewhat counterintuitive – suppression of PDGFRβ.

The enhanced proliferation in pericytes after contact with ECs supports the work of Tarallo *et al.*[16] Using cell culture inserts, on which pericytes and ECs were cultured on either side, they found that ECs enhanced the number of pericytes, albeit after a relative long incubation of 8 days. Taking into consideration that TGFβ was confirmed by IPA to be the most active upstream growth factor inducing the observed transcriptional response, the increased proliferation was remarkable as TGFβ has been reported in multiple different studies to have an inhibiting effect on this process.[35, 36] This implies that other mitogenic factors must have compensated for the TGFβ-induced proliferation stop. VEGFA was previously found to directly induce proliferation in pericytes[17]. However, in contrast to the findings of Darland *et al.*, who demonstrated that ECs induced VEGFA expression in pericytes[37], a significant downregulation of VEGFA was found in co-cultured pericytes in the present study. In combination with the significantly lower expression of VEGFA in ECs, it therefore seemed unlikely that the enhanced proliferation in co-cultured pericytes was VEGFA-dependent. Moreover, several other mitogens, that were either highly expressed in ECs or showed elevated transcription in pericytes after interaction with ECs, have been reported for pericytes, including the aforementioned PDGFβ, FGF2 and HB-EGF.[38-40] Both FGF2 and HB-EGF were significantly upregulated in pericytes co-cultured with ECs, and based on the observed transcriptional response IPA also listed these factors among the most active upstream growth factors (overlap p-values 9.53E-11 and 1.02E-11, respectively). Interestingly, siRNA-mediated knockdown of HB-EGF and FGF2 in pericytes, as well as PDGFβ in HMVECs, significantly reduced Ki67 positivity of co-cultured pericytes, whereas levels of Ki67 were not affected in VEGFA siRNA-treated pericytes. These findings substantiate that, beside paracrine stimulation with the well-documented endothelial-derived PDGFβ, direct contact with ECs triggers the transcription of these particular growth factors that could stimulate pericyte proliferation in an autocrine fashion.

The endothelium-induced differentiation also involved morphological adaptations. Pericytes cultured in the absence of ECs had a somewhat bipolar elongated shape, whereas pericytes cultured in the presence of ECs were characterized by long and thin projections, a morphology that resembles the physiological shape of mature pericytes, which project finger-like extension around the capillary wall. The observed morphological differences were

accompanied by transcriptional adaption of particular genes. Individually, these genes can be involved in various cellular processes. Upregulation of tubulin isoforms for instance, is also observed during distinct phases of the cell cycle and migration.[41] The ARP2/3 complex, in concert with CFLs, has been shown to be involved in the dynamics of lamellipodia growth[42], whereas many growth cone-guiding molecules have also been shown to be involved in vascular patterning, mostly affecting endothelial tip cell behavior. For example, signaling via the NRP receptor stimulates growth cone-collapse in the nervous systems in response to SEMAs[43], yet they appear to induce endothelial tip-cell extension and vessel sprouting in the vascular system in response to VEGF.[44] Similarly, signaling of NTNs via UNC-5 Netrin Receptors (UNC5), downregulated in co-cultured pericytes, was shown to have a repulsive effect on endothelial branching[45, 46], and Eph receptors and EFNs were reported to be involved in segregation of ECs with distinct arterial- or venous fates.[47] However, the fact that in co-cultured pericytes developing long cellular protrusions, 200 genes (overlap p-value 6.78E-13) associated with axonal guidance were differentially expressed, suggested that these signaling molecules may also have a profound effect on pericyte behavior. The hypothesized activation of growth cone-guiding in pericytes upon endothelial interaction was substantiated by the finding that siRNA-mediated downregulation of PLXNA2 and ACTR3, both upregulated in co-cultured pericytes, significantly reduced the relative number of pericytes with projections. The reduction of projection outgrowth after knockdown of ACTR3 was not unexpected considering its role in onset of actin filament formation.[48] However, PLXNs generally transduce the inhibitory effect of SEMAs on axon outgrowth[49], and consequently, loss of PLXNA2 was expected to actually stimulate outgrowth of pericyte projections. In ECs and U87MG glioblastoma cells, however, it was demonstrated that stimulation with SEMA3B and SEMA6A only in presence of PLXNA2 induced localized disassembly of the actin cytoskeleton and focal adhesion points, followed by cell contraction and the appearance of thin projections that remain attached to the substrate around the contracted cell[50], yielding a morphological resemblance with the co-cultured pericytes. To date, little is known about the growth cone-guiding signaling pathways in pericytes, yet the associated morphological changes may be of great importance for vascular integrity, as was recently shown in the adult mouse brain, where local ablation of pericytes provoked resident pericytes to extend the tips of their projections to cover the endothelium and to restore local vascular function.[18]

The present study further provides evidence for an endothelium-induced suppression of overall ECM production in pericytes. This finding partially contrasts with the study of Stratman *et al.*, in which basement membrane ECM expression was investigated in single-cultured and co-cultured human umbilical vein ECs and bovine pericytes in a collagen

matrix.[51] Similar to our findings, they observed a defined downregulation of FN1 in pericytes cultured in the presence of ECs, yet a variety of other ECM molecules, including COL4A1 and COL4A2, demonstrated increased transcription levels in co-cultured pericytes. These apparent inconsistencies in transcriptional response are likely the result of differences in experimental approach, however, since we found that Glyceraldehyde-3-Phosphate Dehydrogenase, used by Stratman *et al.* as reference gene, was differentially expressed in co-cultured pericytes, it is difficult to draw definite conclusions. The findings on ECM expression do however appear to be in line with the many studies demonstrating that, upon organ injury, pericytes detach and migrate from the endothelium and differentiate into ECM-producing cells.[5, 14, 21, 52] The observed suppression of ECM production in co-cultured pericytes, however, went paradoxically along with enhanced TGFβ signaling. This enhanced TGFβ signaling itself is not unexpected, as several studies demonstrated that direct contact of pericytes with ECs triggers the activation of latent TGFβ, thereby inducing a swift activation of TGFβ-mediated signaling.[53] The paradox lies in the fact that TGFβ is well known for its role in transforming pericytes into ECM-producing fibroblasts.[54] These findings thus illustrate that, even in the presence of activated TGFβ signaling, ECM production by pericytes is suppressed when in contact with endothelium, implying that either the actual level of TGFβ determines healthy or pathological pericyte differentiation, or that a thus far unknown endothelial-derived cue must be counteracting TGFβ-induced differentiation of pericytes into fibrotic cells.

Beside secreted signaling molecules, such as VEGFA and PDGFβ, ECs and pericytes also interact in a more direct physical manner. At distinct places, the basement membrane separating the two cell types is interrupted, allowing the formation of direct contacts called peg and socket contacts.[8] These contacts are highly enriched in gap- and adherens junctions CX43 and CDH2, respectively.[9] In the present study, the expression of these molecules was suppressed in pericytes to assess if, and which, transcriptional adaptations in pericytes upon co-culture with ECs were regulated via these direct contacts. Unexpectedly, transcriptional comparison of co-cultured pericytes treated with NT siRNA and co-cultured pericytes with suppressed CX43 or CDH2 expression did not reveal significant differences. Hirschi *et al.* demonstrated that CX43 deficient mesenchymal cells lost their ability to activate latent TGFβ, and as a result were unable to differentiate into mature mural cells.[25] This is in contrast to our study where we did not observe any effect on TGFβ-mediated transcription in pericytes with suppressed CX43 expression. Our results suggest that endothelium-induced pericyte differentiation is not mediated by key gap- and adherens junctions CX43 and CDH2.

In conclusion, the present study provides important evidence for pericyte differentiation upon interaction with ECs, by showing endothelium-induced pericyte maturation and proliferation, and suppression of ECM expression. However, functional gap- and adherens junctions do not appear to be involved in this process.

References

1. Armulik, A, Genove, G, Betsholtz, C: Pericytes: developmental, physiological, and pathological perspectives, problems, and promises. *Dev Cell,* 21**:** 193-215, 2011.
2. Carmeliet, P: Angiogenesis in health and disease. *Nat Med,* 9**:** 653-660, 2003.
3. Morikawa, S, Baluk, P, Kaidoh, T, Haskell, A, Jain, RK, McDonald, DM: Abnormalities in pericytes on blood vessels and endothelial sprouts in tumors. *Am J Pathol,* 160**:** 985-1000, 2002.
4. Hellstrom, M, Gerhardt, H, Kalen, M, Li, X, Eriksson, U, Wolburg, H, Betsholtz, C: Lack of pericytes leads to endothelial hyperplasia and abnormal vascular morphogenesis. *J Cell Biol,* 153**:** 543-553, 2001.
5. Humphreys, BD, Lin, SL, Kobayashi, A, Hudson, TE, Nowlin, BT, Bonventre, JV, Valerius, MT, McMahon, AP, Duffield, JS: Fate tracing reveals the pericyte and not epithelial origin of myofibroblasts in kidney fibrosis. *Am J Pathol,* 176**:** 85-97, 2010.
6. Augustin, HG, Koh, GY, Thurston, G, Alitalo, K: Control of vascular morphogenesis and homeostasis through the angiopoietin-Tie system. *Nat Rev Mol Cell Biol,* 10**:** 165-177, 2009.
7. Carmeliet, P, Jain, RK: Molecular mechanisms and clinical applications of angiogenesis. *Nature,* 473**:** 298-307, 2011.
8. Allsopp, G, Gamble, HJ: An electron microscopic study of the pericytes of the developing capillaries in human fetal brain and muscle. *J Anat,* 128**:** 155-168, 1979.
9. Winkler, EA, Bell, RD, Zlokovic, BV: Central nervous system pericytes in health and disease. *Nat Neurosci,* 14**:** 1398-1405, 2011.
10. Brandt, MM, Meddens, CA, Louzao-Martinez, L, van den Dungen, NAM, Lansu, NR, Nieuwenhuis, EES, Duncker, DJ, Verhaar, MC, Joles, JA, Mokry, M, Cheng, C: Chromatin Conformation Links Distal Target Genes to CKD Loci. *J Am Soc Nephrol,* 29**:** 462-476, 2018.
11. Love, MI, Huber, W, Anders, S: Moderated estimation of fold change and dispersion for RNA-seq data with DESeq2. *Genome Biol,* 15**:** 550, 2014.
12. Ezkurdia, I, Juan, D, Rodriguez, JM, Frankish, A, Diekhans, M, Harrow, J, Vazquez, J, Valencia, A, Tress, ML: Multiple evidence strands suggest that there may be as few as 19,000 human protein-coding genes. *Hum Mol Genet,* 23**:** 5866-5878, 2014.
13. van Dijk, CG, Nieuweboer, FE, Pei, JY, Xu, YJ, Burgisser, P, van Mulligen, E, el Azzouzi, H, Duncker, DJ, Verhaar, MC, Cheng, C: The complex mural cell: pericyte function in health and disease. *Int J Cardiol,* 190**:** 75-89, 2015.
14. Kramann, R, Schneider, RK, DiRocco, DP, Machado, F, Fleig, S, Bondzie, PA, Henderson, JM, Ebert, BL, Humphreys, BD: Perivascular Gli1+ progenitors are key contributors to injury-induced organ fibrosis. *Cell Stem Cell,* 16**:** 51-66, 2015.
15. Franco, M, Roswall, P, Cortez, E, Hanahan, D, Pietras, K: Pericytes promote endothelial cell survival through induction of autocrine VEGF-A signaling and Bcl-w expression. *Blood,* 118**:** 2906-2917, 2011.
16. Tarallo, S, Beltramo, E, Berrone, E, Porta, M: Human pericyte-endothelial cell interactions in co-culture models mimicking the diabetic retinal microvascular environment. *Acta Diabetol,* 49 Suppl 1**:** S141-151, 2012.
17. Yamagishi, S, Yonekura, H, Yamamoto, Y, Fujimori, H, Sakurai, S, Tanaka, N, Yamamoto, H: Vascular endothelial growth factor acts as a pericyte mitogen under hypoxic conditions. *Lab Invest,* 79**:** 501-509, 1999.
18. Berthiaume, AA, Grant, RI, McDowell, KP, Underly, RG, Hartmann, DA, Levy, M, Bhat, NR, Shih, AY: Dynamic Remodeling of Pericytes In Vivo Maintains Capillary Coverage in the Adult Mouse Brain. *Cell Rep,* 22**:** 8-16, 2018.
19. Seiradake, E, Jones, EY, Klein, R: Structural Perspectives on Axon Guidance. *Annu Rev Cell Dev Biol,* 32**:** 577-608, 2016.
20. Marsick, BM, Flynn, KC, Santiago-Medina, M, Bamburg, JR, Letourneau, PC: Activation of ADF/cofilin mediates attractive growth cone turning toward nerve growth factor and netrin-1. *Dev Neurobiol,* 70**:** 565-588, 2010.
21. Lin, SL, Kisseleva, T, Brenner, DA, Duffield, JS: Pericytes and perivascular fibroblasts are the primary source of collagen-producing cells in obstructive fibrosis of the kidney. *Am J Pathol,* 173**:** 1617-1627, 2008.
22. Chen, YT, Chang, FC, Wu, CF, Chou, YH, Hsu, HL, Chiang, WC, Shen, J, Chen, YM, Wu, KD, Tsai, TJ, Duffield, JS, Lin, SL: Platelet-derived growth factor receptor signaling activates pericyte-myofibroblast transition in obstructive and post-ischemic kidney fibrosis. *Kidney Int,* 80**:** 1170-1181, 2011.

23. Sava, P, Ramanathan, A, Dobronyi, A, Peng, X, Sun, H, Ledesma-Mendoza, A, Herzog, EL, Gonzalez, AL: Human pericytes adopt myofibroblast properties in the microenvironment of the IPF lung. *JCI Insight,* 2, 2017.
24. Gaengel, K, Genove, G, Armulik, A, Betsholtz, C: Endothelial-mural cell signaling in vascular development and angiogenesis. *Arterioscler Thromb Vasc Biol,* 29**:** 630-638, 2009.
25. Hirschi, KK, Burt, JM, Hirschi, KD, Dai, C: Gap junction communication mediates transforming growth factor-beta activation and endothelial-induced mural cell differentiation. *Circ Res,* 93**:** 429-437, 2003.
26. Brighton, CT, Lorich, DG, Kupcha, R, Reilly, TM, Jones, AR, Woodbury, RA, 2nd: The pericyte as a possible osteoblast progenitor cell. *Clin Orthop Relat Res***:** 287-299, 1992.
27. Farrington-Rock, C, Crofts, NJ, Doherty, MJ, Ashton, BA, Griffin-Jones, C, Canfield, AE: Chondrogenic and adipogenic potential of microvascular pericytes. *Circulation,* 110**:** 2226-2232, 2004.
28. Crisan, M, Yap, S, Casteilla, L, Chen, CW, Corselli, M, Park, TS, Andriolo, G, Sun, B, Zheng, B, Zhang, L, Norotte, C, Teng, PN, Traas, J, Schugar, R, Deasy, BM, Badylak, S, Buhring, HJ, Giacobino, JP, Lazzari, L, Huard, J, Peault, B: A perivascular origin for mesenchymal stem cells in multiple human organs. *Cell Stem Cell,* 3**:** 301-313, 2008.
29. Song, S, Ewald, AJ, Stallcup, W, Werb, Z, Bergers, G: PDGFRbeta+ perivascular progenitor cells in tumours regulate pericyte differentiation and vascular survival. *Nat Cell Biol,* 7**:** 870-879, 2005.
30. Betsholtz, C: Biology of platelet-derived growth factors in development. *Birth Defects Res C Embryo Today,* 69**:** 272-285, 2003.
31. Lindahl, P, Johansson, BR, Leveen, P, Betsholtz, C: Pericyte loss and microaneurysm formation in PDGF-B-deficient mice. *Science,* 277**:** 242-245, 1997.
32. Vaziri, C, Faller, DV: Repression of platelet-derived growth factor beta-receptor expression by mitogenic growth factors and transforming oncogenes in murine 3T3 fibroblasts. *Mol Cell Biol,* 15**:** 1244-1253, 1995.
33. Izumi, H, Molander, C, Penn, LZ, Ishisaki, A, Kohno, K, Funa, K: Mechanism for the transcriptional repression by c-Myc on PDGF beta-receptor. *J Cell Sci,* 114**:** 1533-1544, 2001.
34. Mao, DY, Barsyte-Lovejoy, D, Ho, CS, Watson, JD, Stojanova, A, Penn, LZ: Promoter-binding and repression of PDGFRB by c-Myc are separable activities. *Nucleic Acids Res,* 32**:** 3462-3468, 2004.
35. Sieczkiewicz, GJ, Herman, IM: TGF-beta 1 signaling controls retinal pericyte contractile protein expression. *Microvasc Res,* 66**:** 190-196, 2003.
36. Rustenhoven, J, Aalderink, M, Scotter, EL, Oldfield, RL, Bergin, PS, Mee, EW, Graham, ES, Faull, RL, Curtis, MA, Park, TI, Dragunow, M: TGF-beta1 regulates human brain pericyte inflammatory processes involved in neurovasculature function. *J Neuroinflammation,* 13**:** 37, 2016.
37. Darland, DC, Massingham, LJ, Smith, SR, Piek, E, Saint-Geniez, M, D'Amore, PA: Pericyte production of cell-associated VEGF is differentiation-dependent and is associated with endothelial survival. *Dev Biol,* 264**:** 275-288, 2003.
38. Papetti, M, Shujath, J, Riley, KN, Herman, IM: FGF-2 antagonizes the TGF-beta1-mediated induction of pericyte alpha-smooth muscle actin expression: a role for myf-5 and Smad-mediated signaling pathways. *Invest Ophthalmol Vis Sci,* 44**:** 4994-5005, 2003.
39. Hosaka, K, Yang, Y, Nakamura, M, Andersson, P, Yang, X, Zhang, Y, Seki, T, Scherzer, M, Dubey, O, Wang, X, Cao, Y: Dual roles of endothelial FGF-2-FGFR1-PDGF-BB and perivascular FGF-2-FGFR2-PDGFRbeta signaling pathways in tumor vascular remodeling. *Cell Discov,* 4**:** 3, 2018.
40. Yu, X, Radulescu, A, Chen, CL, James, IO, Besner, GE: Heparin-binding EGF-like growth factor protects pericytes from injury. *J Surg Res,* 172**:** 165-176, 2012.
41. Parker, AL, Kavallaris, M, McCarroll, JA: Microtubules and their role in cellular stress in cancer. *Front Oncol,* 4**:** 153, 2014.
42. Wu, C, Asokan, SB, Berginski, ME, Haynes, EM, Sharpless, NE, Griffith, JD, Gomez, SM, Bear, JE: Arp2/3 is critical for lamellipodia and response to extracellular matrix cues but is dispensable for chemotaxis. *Cell,* 148**:** 973-987, 2012.
43. Chen, H, Bagri, A, Zupicich, JA, Zou, Y, Stoeckli, E, Pleasure, SJ, Lowenstein, DH, Skarnes, WC, Chedotal, A, Tessier-Lavigne, M: Neuropilin-2 regulates the development of selective cranial and sensory nerves and hippocampal mossy fiber projections. *Neuron,* 25**:** 43-56, 2000.
44. Gerhardt, H, Ruhrberg, C, Abramsson, A, Fujisawa, H, Shima, D, Betsholtz, C: Neuropilin-1 is required for endothelial tip cell guidance in the developing central nervous system. *Dev Dyn,* 231**:** 503-509, 2004.

45. Leonardo, ED, Hinck, L, Masu, M, Keino-Masu, K, Ackerman, SL, Tessier-Lavigne, M: Vertebrate homologues of C. elegans UNC-5 are candidate netrin receptors. *Nature,* 386**:** 833-838, 1997.
46. Lu, X, Le Noble, F, Yuan, L, Jiang, Q, De Lafarge, B, Sugiyama, D, Breant, C, Claes, F, De Smet, F, Thomas, JL, Autiero, M, Carmeliet, P, Tessier-Lavigne, M, Eichmann, A: The netrin receptor UNC5B mediates guidance events controlling morphogenesis of the vascular system. *Nature,* 432**:** 179-186, 2004.
47. Herbert, SP, Huisken, J, Kim, TN, Feldman, ME, Houseman, BT, Wang, RA, Shokat, KM, Stainier, DY: Arterial-venous segregation by selective cell sprouting: an alternative mode of blood vessel formation. *Science,* 326**:** 294-298, 2009.
48. Pollard, TD: Regulation of actin filament assembly by Arp2/3 complex and formins. *Annu Rev Biophys Biomol Struct,* 36**:** 451-477, 2007.
49. Kong, Y, Janssen, BJ, Malinauskas, T, Vangoor, VR, Coles, CH, Kaufmann, R, Ni, T, Gilbert, RJ, Padilla-Parra, S, Pasterkamp, RJ, Jones, EY: Structural Basis for Plexin Activation and Regulation. *Neuron,* 91**:** 548-560, 2016.
50. Sabag, AD, Smolkin, T, Mumblat, Y, Ueffing, M, Kessler, O, Gloeckner, CJ, Neufeld, G: The role of the plexin-A2 receptor in Sema3A and Sema3B signal transduction. *J Cell Sci,* 127**:** 5240-5252, 2014.
51. Stratman, AN, Malotte, KM, Mahan, RD, Davis, MJ, Davis, GE: Pericyte recruitment during vasculogenic tube assembly stimulates endothelial basement membrane matrix formation. *Blood,* 114**:** 5091-5101, 2009.
52. Kramann, R, Wongboonsin, J, Chang-Panesso, M, Machado, FG, Humphreys, BD: Gli1(+) Pericyte Loss Induces Capillary Rarefaction and Proximal Tubular Injury. *J Am Soc Nephrol,* 28**:** 776-784, 2017.
53. Sato, Y, Tsuboi, R, Lyons, R, Moses, H, Rifkin, DB: Characterization of the activation of latent TGF-beta by co-cultures of endothelial cells and pericytes or smooth muscle cells: a self-regulating system. *J Cell Biol,* 111**:** 757-763, 1990.
54. Wu, CF, Chiang, WC, Lai, CF, Chang, FC, Chen, YT, Chou, YH, Wu, TH, Linn, GR, Ling, H, Wu, KD, Tsai, TJ, Chen, YM, Duffield, JS, Lin, SL: Transforming growth factor beta-1 stimulates profibrotic epithelial signaling to activate pericyte-myofibroblast transition in obstructive kidney fibrosis. *Am J Pathol,* 182**:** 118-131, 2013.

Supplemental data

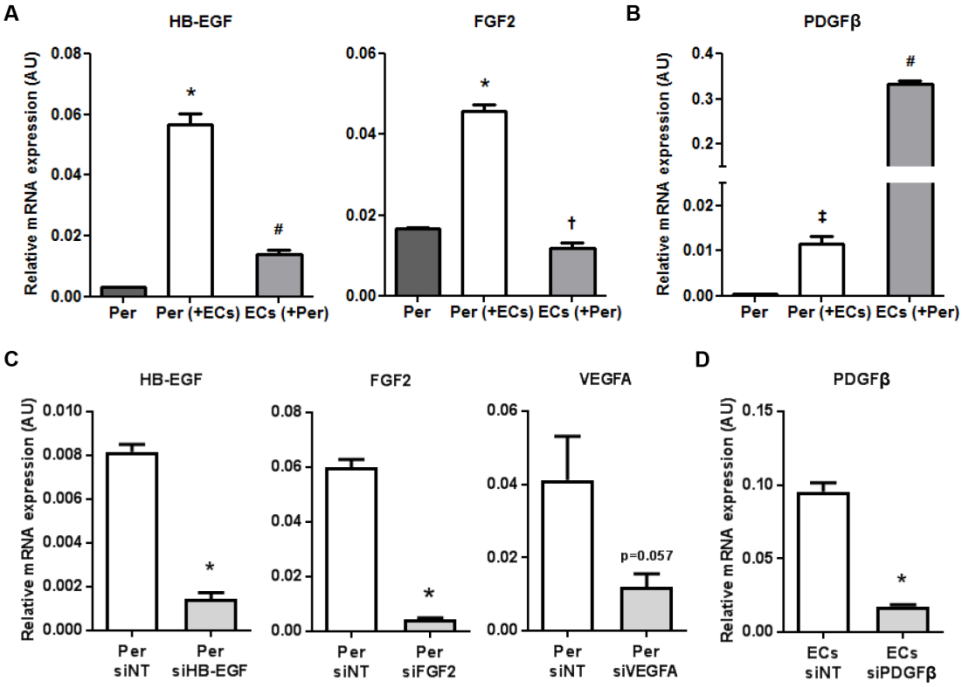

Supplemental Figure 1: Endothelial PDGFβ, and pericyte HB-EGF and FGF2, are upregulated in co-cultured cells and were, like VEGFA, downregulated by siRNA. (A) QPCR results showing expression levels of HB-EGF, FGF2, and PDGFβ relative to RPLP0 and POLR2L in mono- and co-cultured pericytes and co-cultured ECs. N=3, * P<0.05 compared to pericytes in monoculture and ECs in co-culture, # P<0.05 compared to pericytes in mono- and co-culture, ‡ P<0.05 compared to ECs in co-culture, † P<0.05 compared to pericytes in co-culture. **(C)** QPCR results showing expression levels of HB-EGF, FGF2 and VEGFA in pericytes, as well as **(D)** PDGFβ in ECs relative to RPLP0 and POLR2L. N=3-4, * P<0.05 compared to siNT-treated control.

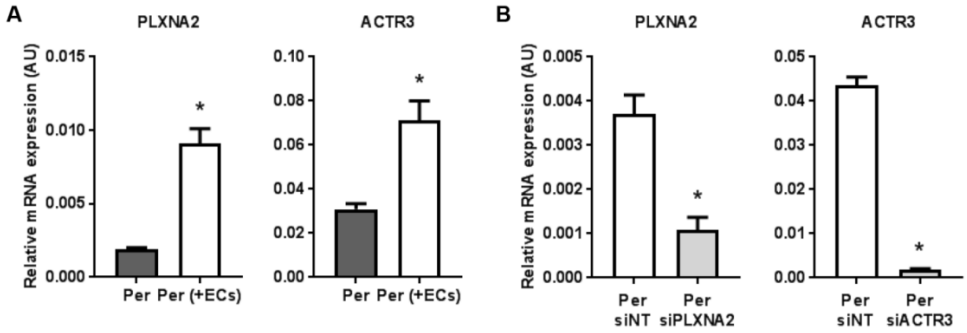

Supplemental Figure 2: PLXNA2 and ACTR3 are upregulated in co-cultured pericytes and were downregulated by siRNA. (A) QPCR results showing expression levels of PLXNA2 and ACTR3 relative to RPLP0 and POLR2L in mono- and co-cultured pericytes. N=3, * P<0.05 compared to pericytes in monoculture. **(B)** QPCR results showing expression levels of PLXNA2 and ACTR3 relative to RPLP0 and POLR2L in siRNA treated pericytes. N=3-4, * P<0.05 compared to siNT-treated control.

Chapter 4

Distinct cardiac- and renal microvascular responses characterize HFpEF progression in obese ZSF1 rats

Christian G.M. van Dijk*, Nynke R. Oosterhuis*, Yan Juan Xu*, Maarten M. Brandt, Walter J. Paulus, Loek van Heerebeek, Dirk J. Duncker, Marianne C. Verhaar, Dulce Fontoura, André P. Lourenço, Adelino F. Leite-Moreira, Inês Falcão-Pires, Jaap A. Joles, Caroline Cheng. (* Authors contributed equally)

Circulation: Heart Failure, 2016; PMID: 27056881

Abstract

The combination of cardiac and renal disease driven by metabolic risk factors, referred to as cardiorenal metabolic syndrome (CRMS), is increasingly recognized as a critical pathological entity. The contribution of (micro)vascular injury to CRMS is considered to be substantial. However, mechanistic studies are hampered by lack of *in vivo* models that mimic the natural onset of the disease. Here, we evaluated the coronary and renal microvasculature during CRMS development in obese diabetic Zucker fatty/Spontaneously hypertensive heart failure F1 hybrid (ZSF1) rats. Echocardiographic, urine, and blood evaluations were conducted in 3 groups (Wistar-Kyoto, lean ZSF1, and obese ZSF1) at 20 and 25 weeks of age. Immunohistological evaluation of renal and cardiac tissues was conducted at both time points. At 20 and 25 weeks, obese ZSF1 rats showed higher body weight, significant left ventricular hypertrophy, and impaired diastolic function compared with all other groups. Indices of systolic function did not differ between groups. Obese ZSF1 rats developed hyperproliferative vascular foci in the subendocardium, which lacked microvascular organization and were predilection sites of inflammation and fibrosis. In the kidney, obese ZSF1 animals showed regression of the peritubular and glomerular microvasculature, accompanied by tubulointerstitial damage, glomerulosclerosis, and proteinuria. The obese ZSF1 rat strain is a suitable *in vivo* model for CRMS, sharing characteristics with the human syndrome during the earliest onset of disease. In these rats, CRMS induces microvascular fibrotic responses in heart and kidneys, associated with functional impairment of both organs.

Introduction

Cardiorenal syndrome (CRS) represents the interdependent relation between the heart and kidneys during disease onset and progression. This important link between cardiac and renal pathophysiology is demonstrated by the high prevalence of chronic kidney disease (CKD) in patients with heart failure and vice versa, whereas dysfunction in both organs is strongly associated with increased morbidity and mortality.[1] Recent findings have also highlighted the connection between CRS and metabolic risk factors: metabolic syndrome is a multitude of risk factors that includes high blood pressure, hyperglycemia, obesity, and dyslipidemia from which at least 3 occur together, thereby functioning as a synergistic complex that drastically increases the risk of cardiovascular disease.[2] This syndrome is growing ever more prevalent, affecting approximately 20% of adults in the aging Western population.[3] A significant amount of evidence clearly shows a strong relation between metabolic syndrome and onset and progression of cardiovascular disease.[4, 5] In regard to renal disease, a clear association between metabolic syndrome and renal dysfunction has also been described.[4, 6] Thus, metabolic risk factors seem to be the driving force behind cardiovascular and CKD disease, and hence CRS. Similarly, the association between all individual components of metabolic syndrome and CRS development is now well established and is increasingly recognized as a separate disease-entity termed cardiorenal metabolic syndrome (CRMS).[1, 6, 7] At present, rodent CRS models typically involve renal ablation and coronary ligation, either alone or in combination to directly induce diastolic and systolic dysfunction.[8] An *in vivo* model that uses metabolic triggers may be more relevant for studies that focus on onset and early progression of CRS. Here we propose the obese diabetic Zucker fatty/Spontaneously hypertensive heart failure F1 hybrid (ZSF1) rat strain as a model for CRMS.[9] Recently, we have reported that obese ZSF1 rats develop heart failure with preserved ejection fraction (HFpEF) between weeks 10 and 20 of natural aging.[9] The ZSF1 strain also autonomously develops renal disease, making it suitable for studying CKD in relation to metabolic triggers.[10, 11] HFpEF development in obese ZSF1 rats was characterized by progressive left ventricle (LV) diastolic dysfunction, concentric LV remodeling, and hypertrophy.[12] This was preceded by insulin resistance, glycosuria, and proteinuria.[9] This phenotype is consistent with CRMS in humans, which is defined by the presence of metabolic syndrome in addition to insulin resistance, microalbuminurina, and reduced renal function.[13] Therefore, these data indicate that the obese ZSF1 strain may be used as an *in vivo* model of CRS early progression against a well-defined background of metabolic injury, thus providing a model to study CRMS. Obese ZSF1 rats also experienced increased vascular stiffness and lack of NO response, consistent with endothelial dysfunction.[14] Persistent nitrosative/oxidative stress and inflammation have been observed

in the coronary microvascular bed of patients with HFpEF.[15, 16] Vascular oxidative stress leading to endothelial dysfunction and inflammation has been proposed as one of the key pathways in HFpEF and CRS[17-20], and it is strongly linked to metabolic risk factors.[19, 21] However, details of the cardiac and renal microvasculature response in CRMS remain to be investigated. Consequently, we studied the microvascular changes in the heart and kidney during progression of HFpEF and renal dysfunction in obese ZSF1 rats.

Methods

Ethics

All animal studies were carried out in accordance with the Council of Europe Convention (Directive [2010/63/EU]) for the protection of vertebrate animals used for experimental and other scientific purposes with the approval of the National and Local Animal Care Committee of Faculty of Medicine of Porto. Animal experiments were performed according to ARRIVE (Animal Research: Reporting of *In Vivo* Experiments) guidelines.

Animal Model

Nine-week-old male Wistar Kyoto (WKY, n=12), ZSF1 Lean (ZSF1 Ln, n=10), and ZSF1 Obese rats (ZSF1 Ob, n=12) were obtained from Charles River (Barcelona, Spain) and housed in a light, temperature, and humidity controlled environment after a 12-hour light–dark cycle with free access to water and standard diet (Purina diet no. 5008). Phenotypic evaluation was conducted after 1 week of acclimatization, consisting of metabolic and echocardiographic studies. Weight gain was monitored every third day. In weeks 18 and 24, phenotypic evaluation was repeated. Cardiac hemodynamic measurements followed by euthanasia were performed at 20th and 25th week. Heart and kidneys were excised, weighed, fixed in formaldehyde, and embedded in paraffin for further analysis.

Echocardiography Evaluation

Rats were anesthetized by inhalation of sevoflurane (8 and 2.5%–3% for induction and maintenance, respectively; Penlon Sigma Delta), mechanically ventilated while homeostasis was maintained by anesthetic monitoring. After applying echocardiography gel, a linear 15MHz probe (Sequoia 15L8W) was positioned on the thorax. Systolic and diastolic wall thickness and cavity dimensions were recorded in M-mode and 2-dimensional (2D) echocardiography, at the level just above the papillary muscles in the parasternal short-axis view. The long-axis diastolic dimensions of the LV and transverse aortic root diameter were recorded by 2D and M-mode echocardiography, respectively, in the parasternal long-axis

view. Aortic flow velocity was recorded by pulsed-wave Doppler above the aortic valve. Mitral flow velocity tracings were obtained with pulsed-wave Doppler above the mitral leaflets, peak systolic tissue velocity, and e′ were measured with tissue Doppler at the medial mitral annulus and lateral mitral annulus, respectively, and left atrial dimensions were measured at their maximum, by 2D echocardiography in the 4-chamber view. Acquisitions were conducted while suspending mechanical ventilation and recordings were averaged from 3 consecutive heartbeats (Siemens Acuson Sequoia C512). LV mass and volumes were calculated by the 2D area-length method and M-mode. For evaluation of diastolic function, peak velocity of early (E), and late (A) mitral inflow and the ratio of E over e′ were measured as an indicator of LV filling pressure. Myocardial performance index was retrieved from the mitral flow pattern. Volumes and masses were indexed for body surface area as defined by 9.1*body weight $(BW)^{2/3}$.

Measurement of biochemical variables

Plasma samples were treated with chloroform to remove lipids which interfere with plasma analysis. Chloroform and plasma (1:1) were centrifuged at 1000 x g for 30 minutes. Supernatant was transferred to a new tube and centrifuged at 10000 x g for 45 minutes. Supernatant was transferred to a new tube and used for creatinine and urea analysis. Plasma and urine creatinine were enzymatically measured (DiaSys PAP FS; DiaSys Diagnostic Systems, Holzheim, Germany). Plasma urea was enzymatically measured (DiaSys Urea CT FS; DiaSys Diagnostic Systmes, Holzheim, Germany). Total protein excretion was measured using Bradford method (BioRad Laboratories, Veenendaal, Netherlands). Thiobarbituric Acid Reactive Substances (TBARS) as indicators for the level of systemic oxidative stress were measured colorimetrically (Cayman Chemical, Ann Arbor, MI).

Hemodynamic evaluation

Animals were sedated with 100 µg.kg-1 and 5 mg.kg-1 intraperitoneal fentanyl and midazolam, respectively), followed by anesthesia (8 and 2.5–3% sevoflurane for induction and maintenance, respectively; Penlon Sigma Delta), endotracheal intubation, and mechanical ventilation (TOPO, Kent scientific). Fluid replacement with warm Ringer's lactate at 32 mL.kg-1.h-1 (NE-1000, New Era Pump Systems) was administered through a peripheral dorsal foot vein catheter (24G) and animals were maintained at 38°C on a heating pad. A flowmeter probe was transiently placed in the ascending aorta for cardiac output (CO) calibration (2.5PS, Transonic). A pressure-volume catheter (SPR-847 Millar Instruments) was inserted in the LV apex and placed along the LV long axis. Silk threads

were placed around the inferior vena cava to enable transient occlusions. Parallel conductance was determined by 40μL 10% hypertonic saline injection and slope factor α was derived by simultaneous measurement of CO by a flowmeter placed around ascending aorta (TS420, Transonic). After a stabilization period of 30 minutes, recordings were obtained at suspended end-expiration. Transient 5-7 cycle occlusions of the inferior vena cava occlusions were performed to obtain load independent indexes of LV chamber stiffness by fitting an exponential function to the end-diastolic pressure-volume relationship (EDPVR) as previously described.[9] Single beat occlusions of the ascending aorta were performed to assess diastolic response to isovolumic afterload as reported.[22] Three separate acquisitions were obtained and averaged in each animal. Data with arrhythmia, heart rate changes higher than 2% or evidence of incomplete afterload elevations were excluded. Resting periods were allowed between each intervention. Signals were continuously acquired (MPVS 300, Millar Instruments), recorded at 1000Hz (ML880 PowerLab 16/30, ADinstruments), and analyzed (PVAN 3.5, Millar Instruments). To account for large differences in body weight between groups, volumes were indexed for body surface area as estimated by 9.1*body weight in grams¾. Upon completion of experiments, blood (4mL) wascollected for volume calibration (910–1048, Millar instruments) and storage. Finally the anesthetized animals were euthanized by exsanguination. Right ventricle (RV), LV and interventricular septum (IVS) were weighed after dissection, and tibia length (TL) was measured. Samples were snap-frozen and stored at -80ºC or processed for histology. Weights were normalized to TL.

Renal and cardiac immunohistochemistry

Three to five μm sections were sliced from formaldehyde-fixed, paraffin-embedded kidneys and hearts. For the analysis of the kidneys, tubulointerstitial (TI) damage and glomerulosclerosis (GS) were scored on Periodic-acid Schiff (PAS) stained sections in a blinded manner. TI damage was scored on a scale of 1-5 in at least 10 different non-overlapping fields per animal. Scored variables include the amount of peritubular inflammatory infiltrate, interstitial fibrosis, tubular atrophy and tubular dilatation. GS was scored on at least 30 separate glomeruli by quadrants, on a scale of 0 to 4, with 0 meaning no quadrant affected and 4 meaning that the whole glomerulus was affected. Scored variables for GS were matrix expansion, sclerosis, adhesion of Bowman's capsule and dilation. For both TI and GS a total damage score was calculated. Peritubular and glomerular endothelium was stained with a primary antibody for JG12 (mouse anti-JG12, BMS1104, 1:200, Bender Medsystems GmbH, Vienne, Austria). Deparaffinized sections were subjected to heat-induced antigen retrieval by incubation with citrate/HCl buffer (pH

6.0) at 100°C for 20 minutes. As a secondary antibody brightvision-HRP (ImmunoLogic, Duiven, Netherlands) was used. Positive cells were visualized with Vector Nova Red (Vector Laboratories, Burlingame, CA) and counterstained with hematoxylin. Sections were scanned using an Aperio ScanScope XT (Aperio Technologies, Vista, CA) and analyzed using Adobe Photoshop (Adobe Systems, San Jose, CA) and ImageJ software. Ten tubular fields and 30 glomeruli were selected and the percentage of JG12+ area was calculated, to correct JG12+ area for glomerular size. For the analysis of the heart, deparaffinized cardiac sections were subjected to heatinduced antigen retrieval with antigen retriever 2100 (Aptum Biologics Ltd, UK) with citrate/HCl buffer (pH 6.0) for 20 minutes. After a brief wash with PBS, sections were blocked with superblock (Life Technologies, Netherlands) for 1 hour before overnight incubation at 4˚C with the following primary antibodies; rabbit anti-NG2 (1:100, Abcam ab5320), rabbit anti-PDGFRβ (1:100, Abcam ab32570), biotin labelled anti-Lectin (1:200, Sigma-Aldrich L-3759), mouse anti-JG12 (1:100, eBioscience BMS1104), rabbit anti-Ki67 (1:100, Thermo Scientific RM-9106), goat anti-Collagen IV (1:50, Millipore AB769), rabbit antiFibronectin (1:100, Sigma Aldrich F3648), mouse anti-CD68 (1:100, Abcam ab31630), and mouse anti-CD3 (1:100, Dako M7254). Appropriate secondary antibodies (Invitrogen, Netherlands) were used for visualization under fluorescent microscope. Nuclei were counterstained with DAPI (1 µg/ml, Sigma-Aldrich). Images were taken by Olympus BX53 microscope. The numbers of NG2+ or PDGFRβ+ foci were counted for the whole heart section by microscope examination. For quantification of Lectin staining, pictures from the left ventricle were randomly obtained from lectin stained heart sections (4 in the endocardium, 4 near the epicardium). Images were analysed using ImageJ (v1.49) by quantification of the percentage of the lectin+ area per image area.

Immunofluorescence cell staining

Human umbilical vein endothelial cells (HUVECs), pericytes and vascular smooth muscle cells (VSMCs) were seeded on sterile glass cover slips and cultured in EGM-2 (Lonza), DMEM (Gibco, #41965), and SmGM-2 (Lonza) medium respectively for four days at 37˚C. Cells were first washed with PBS and then fixed with cold methanol for 10 minutes. Cells were blocked with Super blot (ScyTek Laboratories #AAA125) for 1 hour at room temperature. After that, cells were incubated with rabbit anti-NG2 (1:100, Abcam ab5320) or rabbit anti-PDGFRβ (1:100, Abcam ab32570) antibodies overnight at 4˚C. After washing with PBS, this was followed by incubation with Alex Flour 488-conjugated goat anti rabbit antibody for 1 hour at room temperature. Nuclei were counterstained with DAPI. Images were taken with the same setting by Olympus BX53 microscope with 20x objective.

QPCR analysis

Total RNA of HUVECs, pericytes, VSMCs and fibroblasts was isolated using RNAeasy kit (Qiagen) and treated with DNAse to remove genomic DNA contamination. cDNA was generated using iScript cDNA synthesis kit (Bio-Rad) according to manufacturer's instructions. Quantitative PCR was performed on the BioRad CFX96 RT system using SYBR Green, and mRNA expression levels were normalized to the housekeeping gene B-actin. The PCR primers used are listed in table 1.

Table 1: Primer sequences used for (q)PCR.

Gene	***Sense primer sequence***	***Antisense primer sequence***
COL4A1	ACGGGGGAAAACATAAGACC	TGGCGCACTTCTAAACTCCT
COL4A2	TTATGCACTGCCTAAAGAGGAGC	CCCTTAACTCCGTAGAAACCAAG
B-actin	TCCCTGGAGAAGAGCTACGA	AGCACTGTGTTGGCGTACAG

Statistics

Groups were compared by 2-way ANOVA for repeated measurements, followed by Student–Newman–Keuls post hoc test using SigmaPlot 12.3 (Systat Software Inc, San Jose, CA). Data are presented as mean±SD. $P<0.05$ was considered significant. Alternatively, 1-way ANOVA Kruskal–Wallis test was used, followed by Dunn multiple comparison test.

Results

HFpEF Progression in obese ZSF1 rats

Obese ZSF1 rats had LV hypertrophy, as shown by increased echocardiographic indices of LV mass and LV posterior wall thickness at end diastole versus WKY and lean ZSF1 rats at 25 weeks of age, and increased LV+IVS weight/tibial length compared to WKY and lean ZSF1 rats at 20 and 25 weeks of age (Tables 2 and 3). Echocardiographic data showed preserved systolic function in all groups as assessed by ejection fraction, fractional shortening, and cardiac index at 20 or 25 weeks of age (Table 3). In contrast, obese ZSF1 rats presented with increased ratio of E to early diastolic tissue Doppler mitral annulus velocity (e′), significantly increased E/e′/end-diastolic volume ratios, and increased left atrial area (Table 3), indicative of impaired diastolic function. Hemodynamic evaluation showed significant increase in Tau, end-diastolic pressure, and end-diastolic pressure volume relationship β1 in obese ZSF1 rats at 25 weeks of age compared with WKY and lean ZSF1 rats at 20 and 25 weeks (Supplemental Table 1). Furthermore, right ventricular weight/tibial length and lung weight/tibial length were increased in obese ZSF1 rats at 25 weeks

compared to WKY and lean ZSF1 rats at 20 and 25 weeks of age (Table 2). Systolic, diastolic, and mean blood pressure levels were increased in the obese ZSF1 rats at 25 weeks compared to WKY and lean ZSF1 rats (Supplemental Table 2).

Table 2: Morphometrics of WKY, lean and obese ZSF1 Rats

	WKY 20wks	ZSF1 ln 20wks	ZSF1 ob 20wks	WKY 25wks	ZSF1 ln 25wks	ZSF1 ob 25wks
body weight (g)	360 ± 31	410 ± 26	595 ± 31*	368 ± 24	469 ± 23†‡	633 ± 36*†
TL (mm)	39.4 ± 0.8	41.9 ± 0.9§	40.1 ± 1.3	38.8 ± 0.5	40.9 ± 0.8§	39.2 ± 1.0
LV+IVS weight/TL (mg/mm)	30.1 ± 3.9	28.2 ± 1.0	36.4 ± 2.5*	32.6 ± 4.0	35.0 ± 3.3†	37.4 ± 2.2‡
RV weight/TL (mg/mm)	3.4 ± 1.1	2.7 ± 0.4	4.1 ± 0.6#	3.1 ± 0.8	3.6 ± 0.5	4.8 ± 1.2*
lung weight/TL (mg/mm)	34.9 ± 5.3	40.6 ± 7.8	55.1 ± 5.2*	45.4 ± 6.1†	48.8 ± 3.3†	64.7 ± 3.0*†

Two-way ANOVA with Student–Newman–Keuls post hoc test. n=5-6 animals per group. Values are mean±SD. IVS indicates interventricular septum; LV, left ventricle; RV, right ventricle; TL, tibial length; and WKY, Wistar Kyoto. *P<0.05 vs. WKY and ZSF1 Ln 20 or 25; †P<0.05 vs. week 20; ‡P<0.05 vs. WKY 20 or 25; §P<0.05 vs. WKY and ZSF1 Ob 20 or 25; #P<0.05 vs. ZSF1 Ln.

Table 3: Echocardiographic data for WKY, lean and obese ZSF1 rats

	WKY 20wks	ZSF1 ln 20wks	ZSF1 ob 20wks	WKY 25wks	ZSF1 ln 25wks	ZSF1 ob 25wks
Heart rate (bpm)	299 ± 18	337 ± 5	309 ± 24	298 ± 55	301 ± 33	282 ± 24
dLVPW (mm)	1.40 ± 0.00	1.45 ± 0.07	1.47 ± 0.11	1.11± 0.05*	1.25 ± 0.15‡	1.46 ± 0.11‡
LV mass (mg)	483 ± 93	628 ± 14	797 ± 35†	386 ± 81	604 ± 142†	976 ± 201*‡
FS (%)	35.4 ± 3.7	41.2 ± 4.4	37.9 ± 1.8	36.2 ± 7.4	34.8 ± 6.1	35.4 ± 5.3
EF (%)	70.8 ± 4.8	77.3 ± 4.7	73.3 ± 2.1	71.0 ± 9.0	69.2 ± 7.9	69.7 ± 6.6
S (mm/s)	45 ± 3	59 ± 6†	58 ± 4†	48 ± 7	54 ± 4	52 ± 4
CI (µl/min/cm^2)	212 ± 30	187 ± 50	215 ± 19	172 ± 32	178 ± 11	220 ± 40
MPI (Tei)	0.60 ± 0.01	0.59 ± 0.01	0.62 ± 0.02	0.64 ± 0.03	0.62 ± 0.05	0.60 ± 0.04
E/A	1.79 ± 0.42	1.40 ± 0.08	1.33 ± 0.15‡	1.68 ± 0.24	1.56 ± 0.13	1.30 ± 0.19‡
E/e'	12.7 ± 0.05	11.9 ± 2.3	16.7 ± 0.9‡	12.2 ± 1.6	11.9 ± 2.1	14.3 ± 1.4*
E/e'/EDV (log^2)	22.9 ± 4.7	13.2 ± 1.6	11.4 ± 0.6†	21.4 ± 9.9	12.5 ± 5.0†	9.0 ± 2.5†
LAA (mm^2)	2.48 ± 0.08	2.81 ± 0.30	3.51 ± 0.06‡	2.25 ± 0.14	2.70 ± 0.30†	3.71 ± 0.13‡
EDVI (µl/cm^2)	1.30 ± 0.17	1.87 ± 0.17	2.35 ± 0.22	1.37 ± 0.41	1.87 ± 0.46	2.45 ± 0.49

Two-way ANOVA with Student–Newman–Keuls post hoc test. n=2 to 4 animals per group at 20 weeks; n=5 to 6 animals per group at 25 weeks. Values are mean±SD. CI indicates cardiac index; dLVPW, left ventricular posterior wall measured in diastole; E/A, ratio between peak E and A waves of pulsed-wave Doppler mitral flow velocity; EDVI, end-diastolic volume indexed for body surface area; E/e′, ratio between peak E-wave velocity of pulsed-wave Doppler mitral flow and peak e′-wave velocity of tissue Doppler at the lateral mitral annulus; EF, ejection fraction; EVD; end-diastolic volume; FS, fractional shortening; HR, heart rate; LAA, left atrial area; MPI, myocardial performance or Tei index; S, peak systolic tissue Doppler velocity at the mitral annulus; and WKY, Wistar Kyoto. *P<0.05 vs week 20; †P<0.05 vs WKY 20 or 25; ‡P<0.05 vs WKY and ZSF1 Ln 20 or 25.

Obese ZSF1 rats develop multiple subendocardial microstructures enriched in ECs

Hematoxylin/eosin examination of heart cross-sections revealed no major differences in tissue morphology between WKY and lean ZSF1 rats at 20 or 25 weeks of age. However, multiple areas with high cell density were observed at subendocardial locations of obese ZSF1 rats at both time points, which were absent in WKY and lean ZSF1 rats (Figure 1A-B). High magnification assessment identified these ZSF1 Ob-specific areas as irregular star-shaped foci composed of >50 mononuclear cells, located in the interstitial space between the cardiomyocytes (Figure 1C-G). Erythrocytes were detected in the extravascular space (Figure 1D and 1F), or in the lumen of capillary-like arrangements (Figure 1D, 1F and 1H), suggesting that these foci may contain vascular cells.

Lectin+ ECs were organized in a well-structured capillary network in both WKY and lean ZSF1 rats at 20 and 25 weeks of age (Figure 2A-B). Similarly, a well-organized capillary network was observed in obese ZSF1 rats at both 20 and 25 weeks of age in the areas outside the foci (Figure 2A-B). Quantification of lectin staining showed a significant increase in capillary area in obese ZSF1 rats at 20 weeks of age compared with WKY and lean ZSF1 rats (9.3±1.0 versus 4.7±1.1 and 5.8±1.0, respectively; $P<0.01$), whereas at 25 weeks, capillary areas normalized between groups, mainly because of the increase in WKY and lean ZSF1 rats (Figure 2C). The subendocardial foci in obese ZSF1 rats also stained positive for lectin, indicating that most of the accumulated cells were endothelial cells (Figure 2D-E). In contrast to the coherent lectin+ capillary structures that were found outside the foci, the bulk of lectin+ ECs inside these foci showed a distinct lack of vascular morphology with only limited luminal and monolayer organization (Figure 2D-E, inserts).

Subendocardial foci are enriched in NG2+ and PDGFRβ+ pericytes

Pericytes are vascular mural cells that are typically found in the capillary bed. They are vital for microvascular survival and regulation of blood flow.[23] Immunostaining experiments using cultured human vascular cells demonstrate that NG2 and PDGFRβ are suitable markers for mural cells, predominantly pericytes, being minimally expressed by endothelial cells (Supplemental Figure 1A). Immunostaining for NG2 identified vascular pericytes located in the subendocardial foci, further validating their vascular identity. In WKY and lean ZSF1 rats, NG2+ pericytes were detected at their characteristic peri-EC localization, as shown by lectin double staining (Figure 3A). In contrast, in obese ZSF1 rats, the number of NG2+ pericytes was markedly increased in the regions outside the foci (Figure 3A). In the subendocardial foci, NG2+ pericytes were also observed in close distance to lectin+ ECs (Figure 3A-B). Although some coverage of vascular structures could be recognized, the majority of the

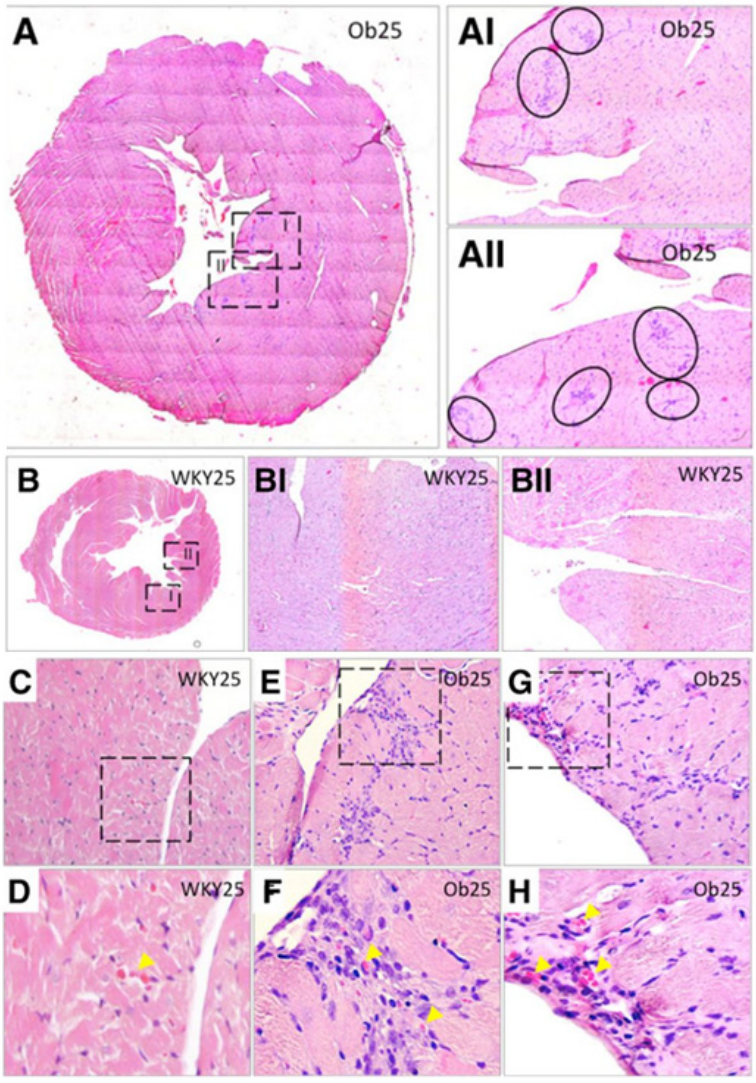

Figure 1: High cell density subendocardial foci develop specifically in the left ventricles of obese ZSF1 rats, but not in lean ZSF1 rats and WKY rats. Representative hematoxylin /eosin-stained LV cross-sections obese ZSF1 rats and WKY rats at 25 weeks of age. **(A)** Low magnification micrograph of the whole heart section of obese ZSF1 rats. **(AI-AII)** Higher magnification micrographs, high cell density subendocardial foci marked by black circles. **(B)** Low magnification figure of heart section of WKY. **(BI-BII)** Higher magnification figures showing the absence of high cell density subendocardial foci. **(C)** High magnification figure showing typical morphology at the LV subendocardial location in WKY rats. **(D)** High magnification detail. Erythrocytes in the capillary bed are indicated by arrowhead. **(E-G)**, High magnification examples showing foci morphology in obese ZSF1 rats. **(F-H)** High magnification details with erythrocytes indicated by arrowheads.

NG2+ pericytes formed atypical multilayered clusters mixed with lectin+ ECs (Figure 3B). To further validate the vascular content of the foci in obese ZSF1 rats, pericytes were stained with a second vascular mural cell marker, PDGFRβ, in combination with a second EC

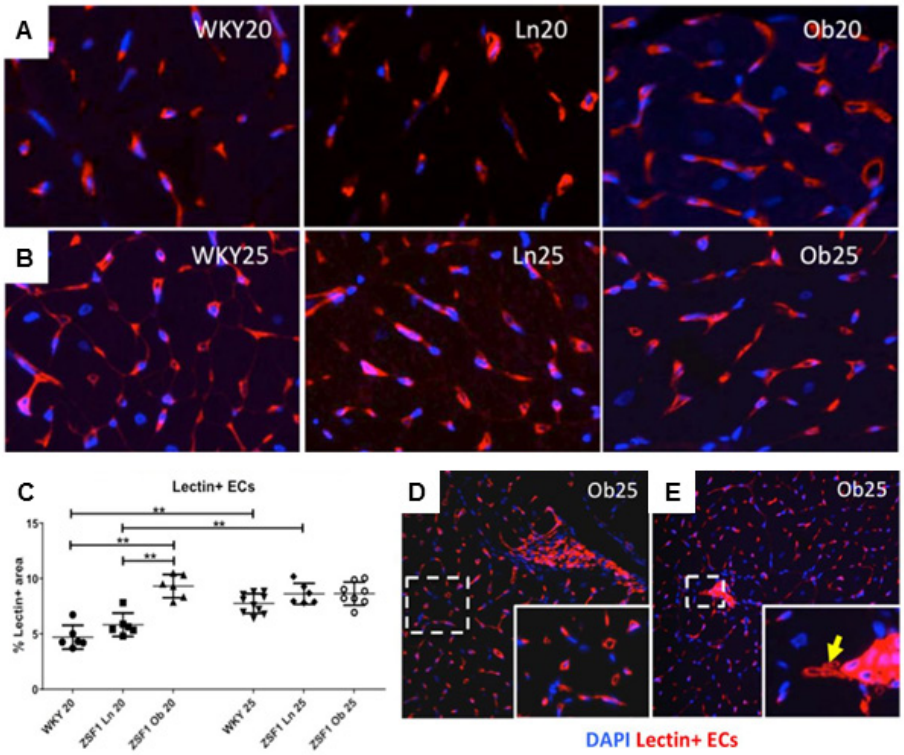

Figure 2: Subendocardial foci in obese ZSF1 rats are enriched with lectin+ EC. Representative LV cross-sections from WKY, lean and obese ZSF1 rats at **(A)** 20 and **(B)** 25 weeks of age, stained for lectin+ endothelium (red signal). Cell nuclei are stained with DAPI (blue signal). **(C)** Quantification of lectin+ endothelial area (%) in WKY, lean and obese ZSF1 rats at 20 and 25 weeks of age. Mean±SD, **P<0.01. High magnification detail panels showing the microcapillary structures in obese ZSF1 rats **(D)** outside and **(E)** inside the subendocardial foci. Arrow indicates vascular structures with open lumen.

marker, JG12. PDGFRβ+ pericytes were detected in WKY and lean ZSF1 rats at peri-EC localization (Figure 3C). In the obese ZSF1 rats, PDGFRβ+ pericytes accumulated in the foci and were atypically organized with limited perivascular coverage (Figure 3C-D). In the capillary network directly surrounding these foci, an increase in PDGFRβ+ pericytes was observed when compared with the capillary network in WKY and lean ZSF1 rats (Figure 3E-F). The number of vascular foci increased by 9- and 20-fold in obese ZSF1 rats versus WKY rats and by 4- and 27-fold compared with lean ZSF1 rats, at 20 and 25 weeks, respectively, when quantified using the NG2+ signal (P<0.001; Figure 3G). Similarly, quantification of foci using the PDGFRβ+ signal showed increases of 7- and 25-fold in obese ZSF1 rats versus WKY and of 4- and 29-fold in obese versus lean ZSF1 rats at 20 and 25 weeks, respectively

(P<0.001; Figure 3G, right graph). Based on both the NG2 and the PDGFRβ method of quantification, the number of foci also increased in obese ZSF1 rats over time (P<0.001; Figure 3G). Combined, these data identify the subendocardial structures as vascular cells enriched foci that specifically develop in obese ZSF1 rats.

Increased proliferation, fibrosis and AGTR1 expression in vascular foci of obese ZSF1 rats

The large number of vascular cells in the foci point toward increased endothelial cell proliferation. We used a combination of lectin and Ki67 staining to assess the number of proliferating endothelial cells. In the foci of obese ZSF1 rats, lectin+ ECs were enriched in nuclear Ki67 signals when compared with the surrounding tissue that displayed a regular organization of microvascular network (Figure 4A and 4C). These results were verified using a second JG12/Ki67 staining combination, which demonstrated a similar preferential signal of Ki67 in JG12+ ECs located in the foci (Figure 4B and 4D).

Fibrogenic activity in these foci was investigated by histological PAS examination, a staining method that is often used to detect extracellular deposition of (vascular) basal membrane glycoproteins. Extracellular fibril-like Periodic acid-Schiff+ structures were detected in between vascular cells located in the foci, pointing toward active glycoprotein deposition (cross-section of WKY rats compared with obese ZSF1 foci at 25 weeks; Figure 5A–5F). Double staining for lectin+ ECs and fibronectin showed limited deposition of these early fibrosis-associated extra cellular matrix components in the regular capillary network of WKY and lean ZSF1 rats (Figure 5G). In contrast, fibronectin deposition was increased in the subendocardial foci of obese ZSF1 rats, and in the vascular network surrounding these foci (Figure 5G and 5H). Double staining for PDGFRβ+ pericytes and collagen IV, a vascular basal membrane component predominantly produced by vascular cells, showed robust collagen IV deposition in the regular capillary network of WKY and lean ZSF1 rats (Figure 5I). Similarly, collagen IV was detected in the PDGFRβ+ foci and direct surrounding capillaries of obese ZSF1 rats (Figure 5I and 5J).

Activation of the renin–angiotensin–aldosterone system (RAAS) may contribute to CRMS and HFpEF development in the obese ZSF1 animals. Immunostaining for AGTR1, the angiotensin II receptor most associated with cardiac hypertrophy, VSMC hyperproliferation, and vascular constriction, showed increased expression of AGTR1 by cardiomyocytes and interstitial perivascular cells in obese ZSF1 rats versus WKY and lean ZSF1 control rats in areas outside the vascular foci (Figure 5K and 5L). AGTR1 was highly expressed by both lectin+ ECs and perivascular cells in the obese ZSF1-specific vascular foci (Figure 5M).

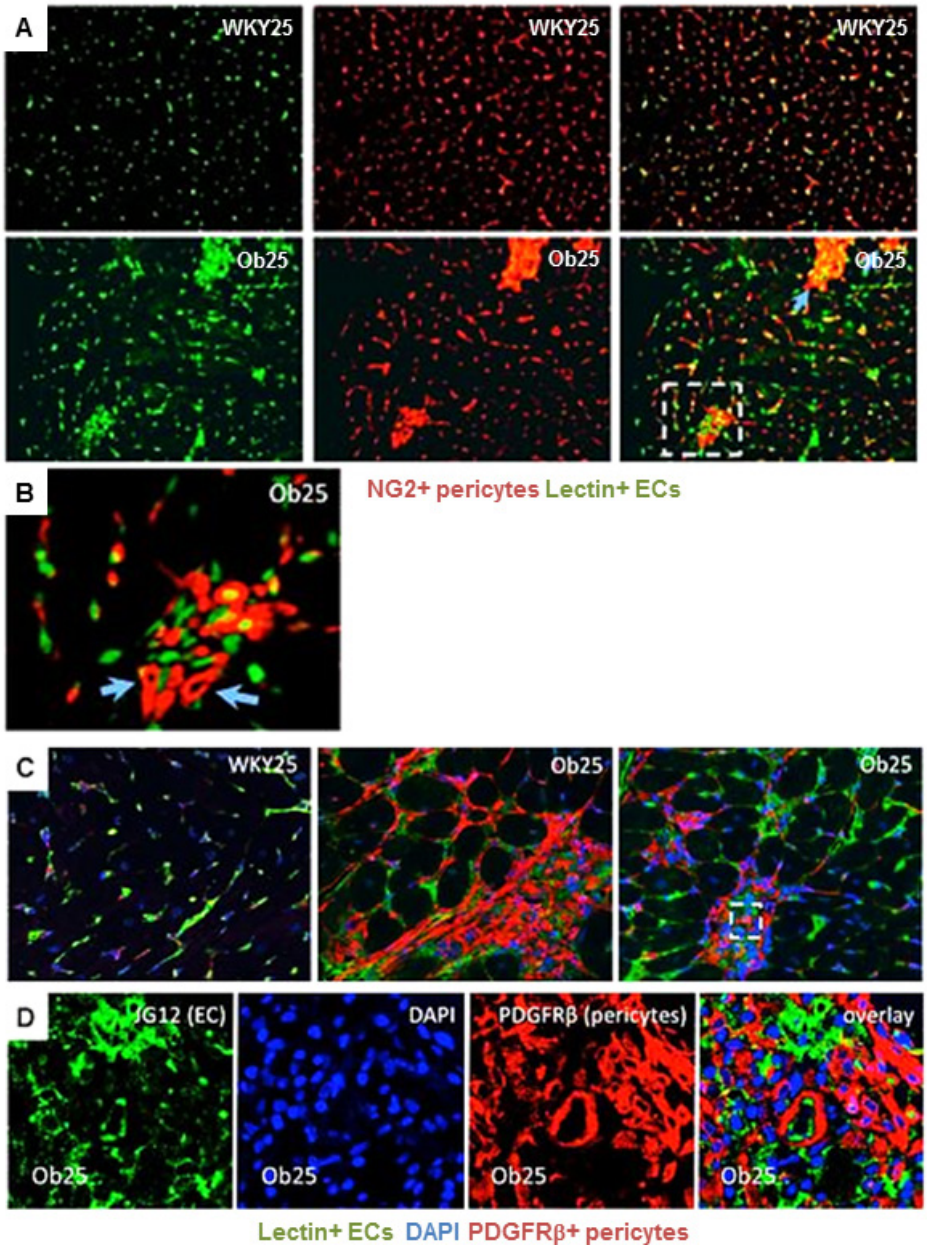

Figure 3: Subendocardial foci in obese ZSF1 rats are enriched with NG2+ and PDGFRβ+ pericytes. (A) Representative LV cross-sections of WKY and obese ZSF1 rats at 25 weeks of age, stained for NG2+ pericytes (green signal) and lectin+ endothelium (red signal). **(B)** High magnification detail showing disorganized clusters of lectin+ ECs and NG2+ pericytes in the subendocardial foci of obese ZSF1 rats. Arrows indicate lectin+ vascular structures with open lumens. **(C)** Representative LV cross-sections of WKY and obese ZSF1 rats at 25 weeks of age, stained for JG12+ endothelium (green

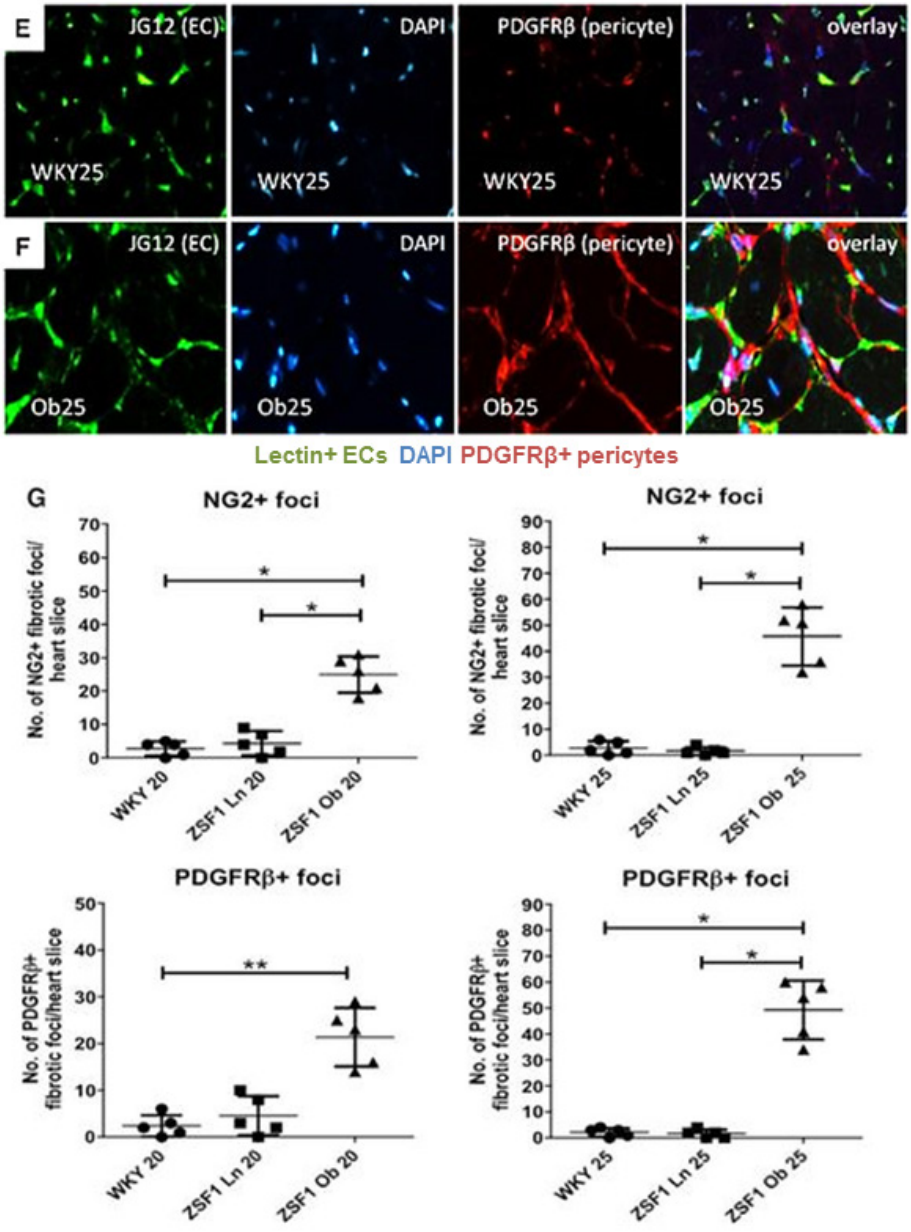

◄ signal), and PDGFRβ+ pericytes (red signal). Cell nuclei are stained with DAPI (blue signal). High magnification detail panels showing **(D)** clusters of disorganized JG12+ ECs and PDGFRβ+ pericytes in subendocardial foci of obese ZSF1 rats, **(E)** typical organization of the microcapillary bed at the subendocardial location of WKY rats, **(F)** increase of PDGFRβ+ pericyte coverage of the JG12+ microcapillary bed directly surrounding the subendocardial foci of obese ZSF1 rats. **(G)** Quantification of the number of subendocardial foci per heart cross-section, determined by NG2 and PDGFRβ+ staining in WKY, lean and obese ZSF1 rats at 20 and 25 weeks of age. Mean±SD. *P<0.05, **P<0.01.

Vascular foci of obese ZSF1 rats are enriched for circulating immune cells

To assess whether inflammatory cells contribute to the fibrogenic process, double staining for lectin+ ECs and CD3+ T cells was conducted. Perivascular CD3+ T cells were absent in the microvascular bed of WKY and lean ZSF1 rats (Figure 6A). In contrast, perivascular CD3+ T cells were detected in limited numbers in obese ZSF1 rats in the vascular foci, whereas the remaining capillary network showed no CD3+ T-cell recruitment. Similarly, double staining for lectin+ ECs and ED1+ macrophages showed an absence of perivascular macrophages in capillary networks of WKY and lean ZSF1 rats, whereas in obese ZSF1 rats, ED1+ macrophages accumulated in the subendocardial foci, indicating active recruitment of circulating immune cells at these sites (Figure 6B).

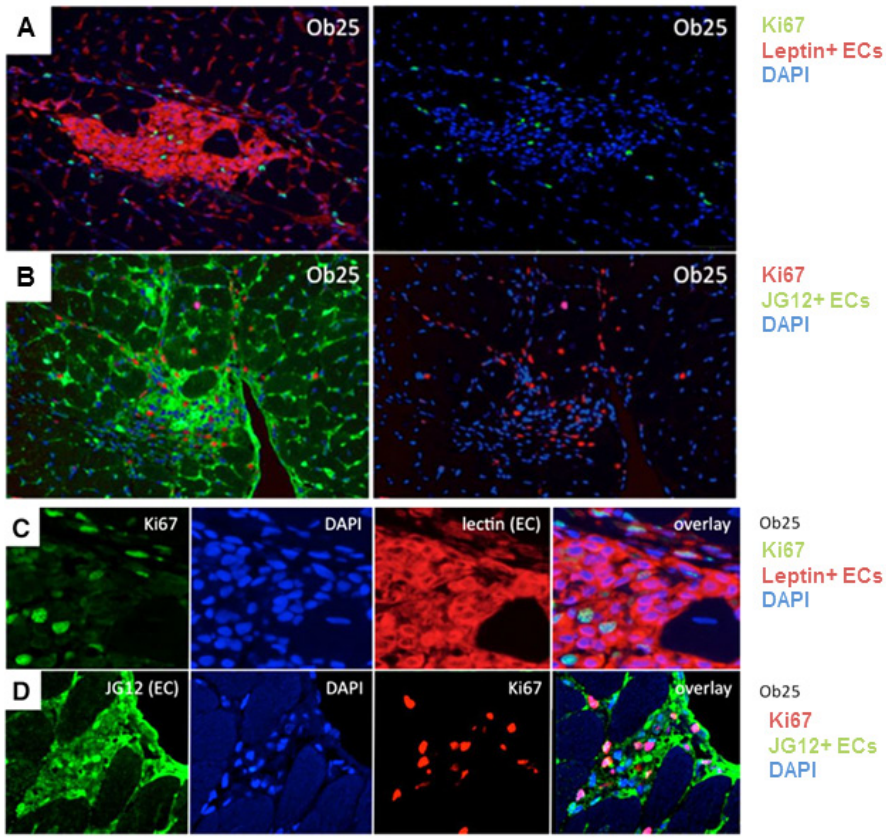

Figure 4: Subendocardial foci in obese ZSF1 rats are sites of increased endothelial cell proliferation. Representative images of subendocardial foci of obese ZSF1 rats at 25 weeks of age, stained for **(A)** lectin+ endothelium (red signal) and Ki67 cell proliferation marker (green signal), and **(B)** JG12+ endothelium (green signal), and Ki67 (red signal). Cell nuclei are stained with DAPI (blue signal). High magnification detail panels showing **(C)** lectin-Ki67 staining and **(D)** JG12-Ki67 staining.

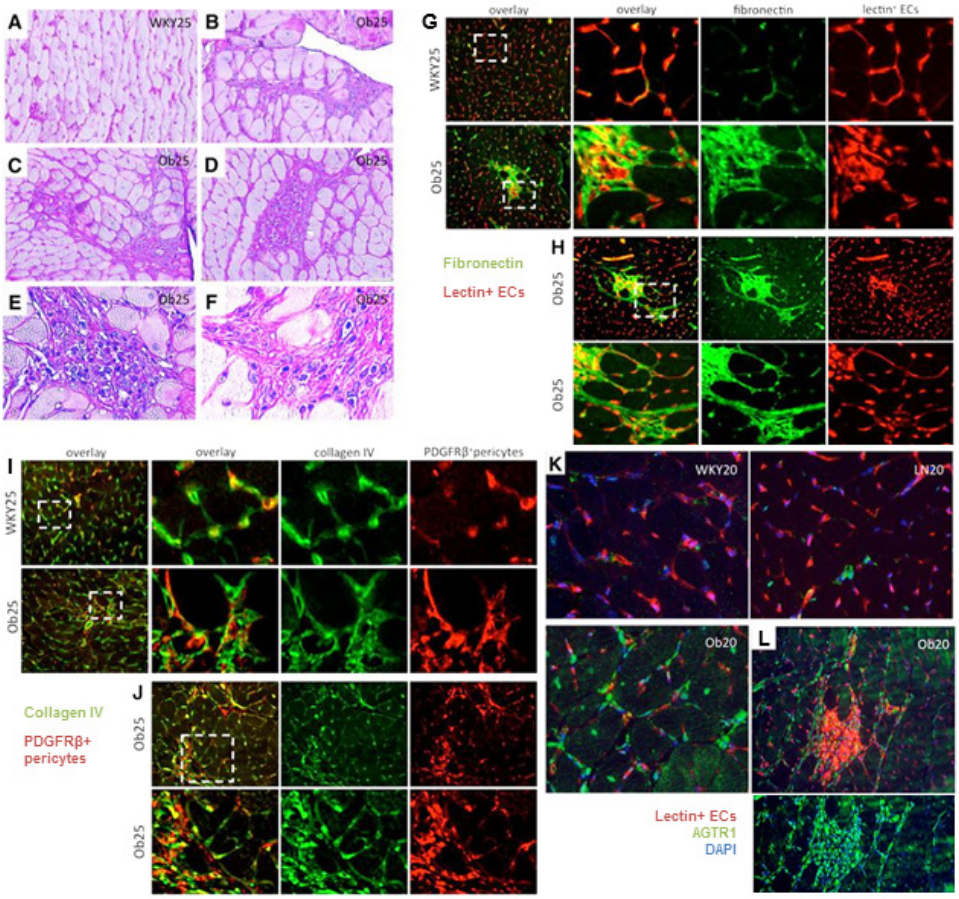

Figure 5: Onset of fibrosis at the subendocardial foci of obese ZSF1 rats. Representative PAS–stained LV cross-sections of WKY and obese ZSF1 rats at 25 weeks of age. **(A)** Extra cellular matrix (ECM) glycoprotein deposition in the interstitial space between cardiomyocytes in WKY. (**B-D**) Accumulation of ECM glycoprotein in subendocardial foci of obese ZSF1 rats. **(E-F)** High magnification detail showing PAS signal distribution in subendocardial foci of obese ZSF1 rats. **(G)** Representative LV cross-sections of WKY and obese ZSF1 rats at 25 weeks of age, stained for ECM fibronectin (green signal) and lectin+ endothelium (red signal) at low magnification (left panel in each row) and at high magnification (remaining panels). **(H)** Representative example of overlap between fibronectin and lectin+ endothelial distribution in subendocardial foci of obese ZSF1 rats at low (top) and high magnification (bottom). **(I)** Cross-sections of the LVs of WKY and obese ZSF1 rats at 25 weeks, stained for vascular basal membrane collagen IV (green signal) and PDGFRß+ pericytes/mural cells (red signal) at low magnification (left panel in each row) and at high magnification (remaining panels). **(J)** Representative example of overlap between fibronectin and lectin+ endothelial distribution in subendocardial foci of obese ZSF1 rats at low (top) and high magnification (bottom). Increased expression of AGTR1 by cardiomyocytes and subendothelial foci of obese ZSF1 rats. **(K)** Representative LV stainings of WKY, lean and obese ZSF1 rats at 20 weeks of age, double stained for

◄ lectin+ endothelium (red signal), and AGTR1+ cells (green signal). Cell nuclei are stained with DAPI (blue signal). **(L)** Quantified results depicting the AGTR1+ areas in WKY, lean and obese ZSF1 rats at 20 weeks of age. Mean±SD. *P<0.05. **(M)** Representative example of overlap between AGTR1 (green signal) and lectin+ endothelial (red signal) distribution in subendocardial foci of obese ZSF1 rats. Cell nuclei are stained with DAPI (blue signal).

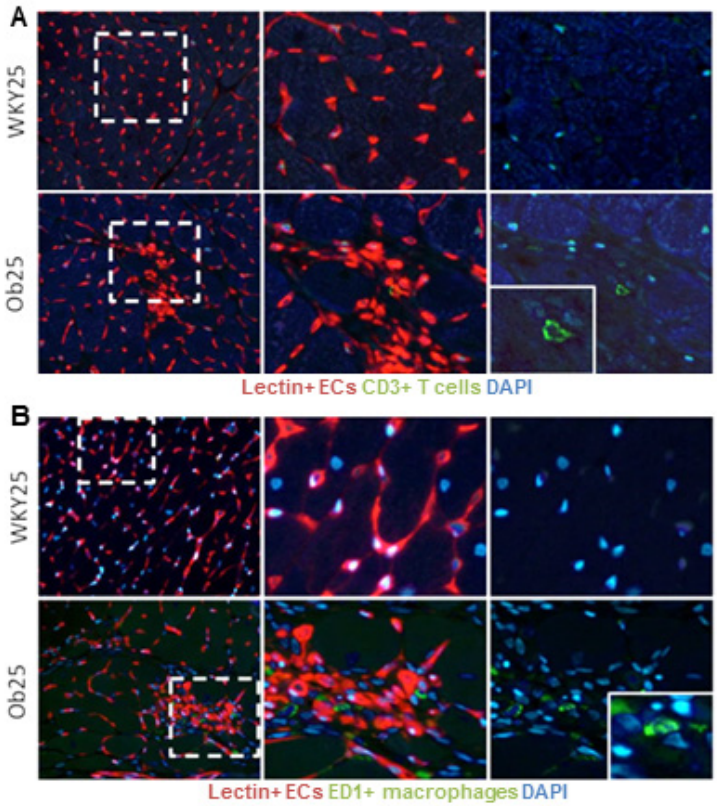

Figure 6: Recruitment of circulatory immune cells at subendocardial foci of obese ZSF1 rats. Representative LV stainings of WKY and obese ZSF1 rats at 25 weeks of age, double stained for **(A)** lectin+ endothelium (red signal) and CD3+ T cells (green signal), and **(B)** lectin+ endothelium (red signal) and ED1+ macrophages (green signal) at low magnification (left panel in each row) and at higher magnification (remaining panels). Cell nuclei are stained with DAPI (blue signal).

Decline of renal function in obese ZSF1 rats

Compared with WKY rats, plasma creatinine was not elevated in lean and obese ZSF1 rats at 20 and 25 weeks, whereas plasma urea levels were only slightly increased at 20 weeks. At 20 and 25 weeks, a 9- and 38-fold increase in protein/creatinine ratio was observed, respectively, in obese ZSF1 rats compared with WKY rats (P<0.001; Table 4). Similarly, at 20 and 25 weeks, a 6- and 37-fold increase in protein/creatinine ratio was observed in obese ZSF1 rats compared with lean ZSF1 rats (P<0.001; Table 4). Oxidative stress, measured by TBARS, was increased in obese ZSF1 rats compared with WKY and lean ZSF1 rats at both time points (P<0.001; Table 4). No differences in protein/creatinine and TBARS/creatinine ratio were observed between WKY and lean ZSF1 rats.

Tabel 4: Biochemical variables for WKY, lean and obese ZSF1 rats

	WKY 20wks	ZSF1 ln 20wks	ZSF1 ob 20wks	WKY 25wks	ZSF1 ln 25wks	ZSF1 ob 25wks
Plasma						
Creatinine (µmol/L)	36.1 ± 1.9	28.3 ± 8.9	21.1 ± 5.5*	34.2 ± 8.7	36.0 ± 8.5	22.4 ± 7.6†
Urea (mmol/L)	4.1 ± 0.2	5.3 ± 0.7*	6.3 ± 1.0*	7.3 ± 1.1‡	6.7 ± 0.5‡	5.9 ± 0.7*
Urine						
Protein/creatinine ratio	119 ± 17	181 ± 9	1086 ± 871†	126 ± 8	130 ± 5	4774 ± 239†
TBARS/creatinine ratio	4.1 ± 0.2	3.8 ± 0.6	19.3 ± 15.1‡	3.0 ± 0.1	2.3 ± 0.1	49.7 ± 8.5†

Two-way ANOVA with Student–Newman–Keuls post hoc test. Plasma sample size; n=3 to 6 animals per group at 20 weeks. n=5 to 6 animals per group at 25 weeks. Urine plasma size; n=2 to 4 animals per group at 20 weeks. n=4 animals per group at 25 weeks. Values are mean±SD. TBARS indicates thiobarbituric acid reactive substance; and WKY, Wistar Kyoto. ‡P<0.05 vs week 20; *P<0.05 vs WKY 20 or 25; †P<0.05 vs WKY and ZSF1 Ln 20 or 25.

Degradation of renal endothelium and progressive glomerulosclerosis in obese ZSF1 rats

The highest chronic TI damage and glomerulosclerosis scores were measured in obese ZSF1 rats compared with WKY and lean ZSF1 rats at 20 and 25 weeks of age (Figure 7A and 7B). Compared with WKY rats, glomerulosclerosis was increased in lean ZSF1 rats (11±5 versus 23±5 and 13±5 versus 24±5, P<0.05). With age glomerulosclerosis increased in obese ZSF1 rats (39±10 versus 53±14, P<0.01). Peritubular and glomerular endothelium were visualized on JG12-stained slides (Figure 8A). Compared with WKY and lean ZSF1 rats, the percentage of peritubular and glomerular endothelium decreased in obese ZSF1 rats (Figure 8B and 8C).

Discussion

The main findings of this study are (1) the obese ZSF1 rat strain is a suitable *in vivo* model for CRMS, sharing characteristics with the human syndrome during the earliest onset of disease, (2) in obese ZSF1 rats, CRMS induces microvascular fibrotic responses in heart and kidneys, associated with functional impairment of both organs.

Humans with metabolic derangements such as obesity, hypertension, hyperglycemia, and dyslipidemia—all recognized as important risk factors for CKD and cardiovascular disease[24, 25]—often present with preclinical diastolic dysfunction[26], diastolic heart failure, or HFpEF.[27, 28] In current and previous reports, we could validate that the obese ZSF1 rats share these characteristics with patients with metabolic syndrome[2]: obese ZSF1 rats are obese (65% and 45% increase compared with WKY and lean ZSF1 rats, respectively, Table

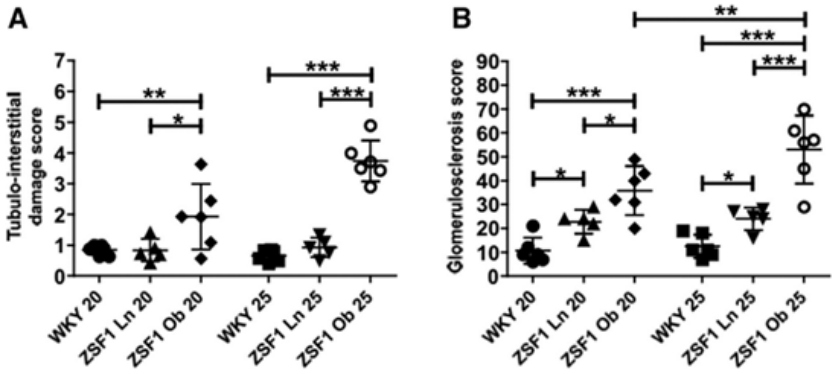

Figure 7: Increase in TI damage and glomerulosclerosis in the kidneys of obese ZSF1 rats compared with lean ZSF1 rats and WKY rats. TI damage **(A)** and glomerulosclerosis **(B)** scores for WKY, lean and obese ZSF1 rats at 20 and 25 weeks of age. Mean±SD. *P<0.05, **P<0.01, ***P<0.001.

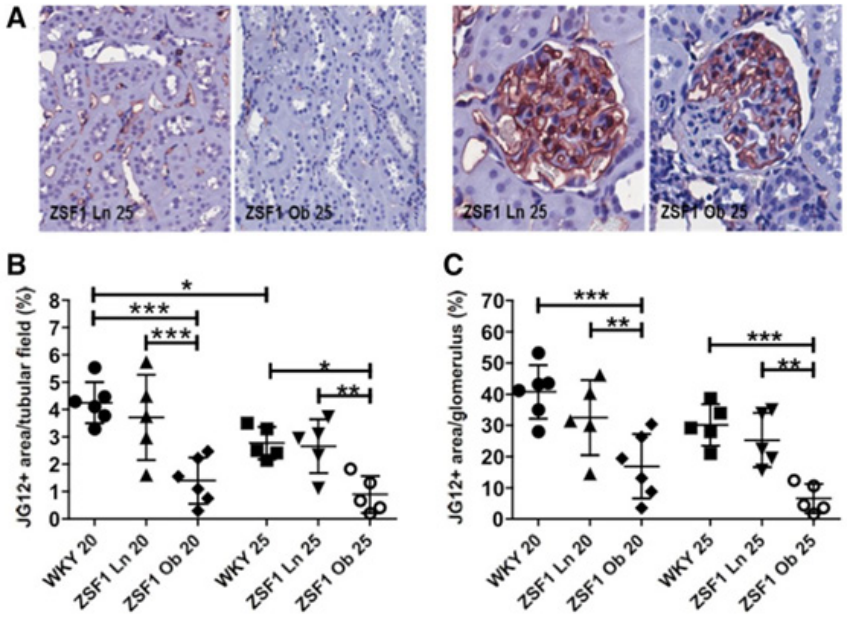

Figure 8: Rarefaction of the peritubular and glomerular vasculature in obese ZSF1 rats. (A) Representative images of JG12-stained renal sections from lean ZSF1 and obese ZSF1 rats. Quantified results depicting the JG12+ endothelial area (%) in the **(B)** peritubular and **(C)** glomerular vasculature determined in WKY, lean and obese ZSF1 rats at 20 and 25 weeks of age. Mean±SD. *P<0.05, **P<0.01, ***P<0.001.

1), hypertensive (46% and 19% increase in mean blood pressure compared with WKY and lean ZSF1 rats, Supplemental Table 2), and show elevated fasting plasma glucose levels (65% and 45% increase compared with WKY and lean ZSF1 rats, respectively)[9], whereas other studies have reported hypertriglyceridemia (increase of >25-fold) and hypercholesterolemia (increase of >5-fold) in obese versus lean ZSF1 rats.[10, 29]
Furthermore, CRMS in humans is defined by the presence of metabolic syndrome in addition to insulin resistance, microalbuminurina, and reduced renal function.[13] Current and previous findings demonstrate that obese ZSF1 rats develop proteinuria from 10 weeks onwards, whereas early signs of HFpEF were detected from 14 weeks onwards.[9] Similarly at 10 weeks, increased oral glucose tolerance and insulin resistance, glycosuria and significant weight gain can be detected.[9] These observations indicate that the presentation of metabolic risk factors accompanies the onset of renal dysfunction (signified by proteinuria) and precedes HFpEF development in obese ZSF1 rats, which is consistent with a pathophysiological course of CRMS in obese ZSF1 rats, in which metabolic and renal complications induce cardiac dysfunction.[18] On the basis of these combined data, we therefore propose obese ZSF1 rats as a small animal model for metabolic syndrome–induced CRS (and thus CRMS), in which the combined metabolic risk factors act together to trigger early onset and progression of CKD and HF, creating the downward spiral of disease progression that is so typical for patients with chronic CRS.[10]

CRMS was first suggested as a disease entity in 2004.[30] Already in this first publication, a relation with endothelial dysfunction was proposed.[30] Endothelial injury is implicated in CRS[20], whereas in HFpEF patients, vascular changes represented by endothelial dysfunction have been reported.[31] A direct link between heart failure, vascular activation, metabolic comorbidities, and CKD was presented by Shestakova *et al.*, who demonstrated a correlation between endothelial dysfunction and the hallmarks of HF in CRS patients with type 1 diabetes mellitus.[19] In line with these studies, our data show changes in the coronary microvascular bed of obese ZSF1 rats: endothelial and mural cells form atypical vascular patches of cells, with remarkable increases in proliferation rate. Not only do these structures lack functional organization, they also seem to act as origin sites of fibrosis, for we could demonstrate enriched deposition of fibrosis-associated extra cellular matrix components such as fibronectin and collagen type IV in these vascular foci.

In CRS rat models that use subtotal nephrectomy in combination with coronary ligation to initiate ischemic heart disease, a decrease in LV microvascular density was reported to be associated with systolic dysfunction.[32, 33] Other clinical and experimental studies provide

evidence that coronary microvascular rarefaction in diastolic and hypertrophic heart failure promotes tissue hypoxia, cell death, and fibrosis, all contributing to the progression from compensated hypertrophy to contractile dysfunction.[34, 35] In adults, vascular proliferation is part of the compensatory and repair response to local hypoxia and tissue damage in which endothelial cells proliferate and migrate into the ischemic injury site during macrophage influx and phagocytosis of necrotic tissue. As repair proceeds, dead tissue is replaced by granulation tissue, characterized by the deposition of a provisional matrix enriched in glycoproteins and fibronectin.[36, 37] The vascular foci that developed in obese ZSF1 rats resembled this process of scar formation with excessive endothelial cell proliferation, fibronectin deposition, and local recruitment of macrophages.

Vascular cells in the foci contribute to the formation of granulation matrix, demonstrated by deposition of the typical vascular basal membrane component collagen type IV. Collagen type IV is predominantly produced by pericytes and not by fibroblasts, as shown by quantitative polymerase chain reaction using *in vitro* human primary vascular cell types (Supplemental Figure 1B).

Extensive myocardial fibrosis is one of the hallmarks of CRMS. Previously, we reported that at 20 weeks, cardiac hypertrophy was increased in obese ZSF1 rats versus WKY and lean ZSF1 rats, but overall levels of myocardial fibrosis remained comparable between groups.[9] In contrast, glomerulosclerosis score in the kidneys (Figure 8B) was significantly increased in obese ZSF1 rats versus WKY and lean ZSF1 rats. Thus, the effect of metabolic risk factors on kidney fibrosis seems to precede the effects on fibrosis in the myocardium in the obese ZSF1 rats. In this study, we could demonstrate that onset of fibrosis is present in the subendocardial vascular foci at 20 and 25 weeks in obese ZSF1 rats. This was accompanied by vascular inflammation, yet another hallmark of CRMS.

On the basis of our observations to date, we hypothesize that the hyperproliferative vascular reaction in the heart of obese ZSF1 rats is part of a destructive response that leads to replacement of functional vascular structures by fibrotic tissue with semi and nonfunctional microvascular clusters, which may ultimately deteriorate into large fibrotic areas that are completely devoid of vascular support, in line with the previously reported vascular rarefaction phenotype. Additional studies are planned to further elucidate this highly dynamic process and to validate if microvascular hyperproliferation of pre-existing vessels indeed precedes fibrogenesis and vascular rarefaction in CRMS.

Potential impact of current findings on the field of CRMS research

Chronic CRS type 2, which is initiated by chronic cardiac dysfunction (such as congestive HF), and type 4, initiated by chronic renal dysfunction (resulting in LV hypertrophy and diastolic HF), are currently under-recognized syndromes in the cardiovascular research community in comparison with acute CRS types. This is largely because of the lack of a suitable animal model to mimic the human condition. However, the population of patients with chronic types of CRS is substantial: in adult patients with congestive HF, it has been reported that 31% of NYHA III and 39% of NYHA IV patients had renal dysfunction.[38] Recent findings presented in the PREVEND study also showed that early onset of renal dysfunction, indicated by albuminuria, is a strong predictor for new onset of HFpEF, but not HFrEF.[39] Others have also demonstrated that the prevalence of LV hypertrophy is significantly increased in patients with CKD from mild renal impairment onwards.[40] These findings are consistent with the concept that the synergy between renal and cardiac dysfunction is a driving factor in the early disease onset of HFpEF. An improved understanding of the disease mechanism of, in particular, chronic CRS would greatly aid in the development of new diagnostic and treatment options that are specifically targeted to this large subgroup of cardiac and renal patients.

The obese ZSF1 strain presents a suitable model to investigate the contribution of different disease pathways to CRMS, as the disease course resembles the onset phase of chronic CRS within the first 10 to 25 weeks of the animals' lifespan. In particular, studies that investigate the relationship between metabolic risk factors and endothelial dysfunction could shed further light on the contribution of vascular injury to HF in chronic CRMS.

Limitations of this study

The obese ZSF1 model described in this article is not suitable for studying type 1 and type 3 CRS because these forms require acute cardiac and renal failure to adequately mimic the human conditions, and may involve different disease mechanisms compared with the chronic forms (see review of disease pathogeneses of CRS subtypes).[18] A more suitable model for acute CRS would be surgical induction methods for myocardial infarction such as coronary ligation, and subtotal nephrectomy for severe renal dysfunction. Previous studies have indicated that a dual injury model to heart and kidneys is needed to produce a more robust acceleration of renal failure and heart failure with reduced ejection fraction that are typical for acute CRS.[41, 42] However, the causal relationship between metabolic risk factors and chronic CRS can be better studied in the ZSF1 model, as this would best imitate the natural course of the disease in patients with chronic CRS. The addition of obese ZSF1 rats

to our arsenal of animal models for CRS will greatly expand our means to adequately study mechanisms in the earliest phases of disease.

In addition to the proposed mechanism of vascular fibrosis–mediated CRMS, other disease mechanisms could trigger CRS, including low-cardiac output leading to impaired renal perfusion, which vice versa leads to kidney-mediated RAAS and sympathetic activation. Initial renal dysfunction could also induce chronic CRS via RAAS and sympathetic activation, in addition to Na^+ and H_2O overload, hypertension, accumulation of uremic toxins and calcium and phosphate abnormalities that all contribute to cardiovascular complications. Furthermore, renal impairment and subsequent dysregulation of erythropoietin contributes to anemia, which further aggravate hypoxia in both organs.[18] In this study, we have not specifically assessed the contribution of these mechanisms to CRS development in the obese ZSF1 model. However, cardiac output represented by the indexed cardiac output (cardiac index, in Table 3) is similar between the 3 groups at both time points assessed. In addition, obese ZSF1 rats are indeed hypertensive, and expression of AGTR1, the main receptor for RAAS-mediated effects on the cardiovascular system, was increased in LV sections of the obese ZSF1 group, particularly at the vascular foci. Further systematic evaluation will help identify for which specific pathological mechanisms of chronic CRS, the ZSF1 strain is a suitable research model.

In conclusion, this study demonstrates that the obese ZSF1 rat is a suitable *in vivo* model for CRMS, sharing many characteristics with the human CRS during the earliest onset of the disease, as triggered and mediated by metabolic risk factors. Further studies in the classic pathways of CRMS using this ZSF1 model will enhance our understanding of the contribution of microvascular and metabolic changes during the onset of CRMS.

References

1. Forman, DE, Butler, J, Wang, Y, Abraham, WT, O'Connor, CM, Gottlieb, SS, Loh, E, Massie, BM, Rich, MW, Stevenson, LW, Young, JB, Krumholz, HM: Incidence, predictors at admission, and impact of worsening renal function among patients hospitalized with heart failure. *J Am Coll Cardiol,* 43**:** 61-67, 2004.
2. Grundy, SM, Brewer, HB, Jr., Cleeman, JI, Smith, SC, Jr., Lenfant, C, American Heart, A, National Heart, L, Blood, I: Definition of metabolic syndrome: Report of the National Heart, Lung, and Blood Institute/American Heart Association conference on scientific issues related to definition. *Circulation,* 109**:** 433-438, 2004.
3. Raimundo, M, Lopes, JA: Metabolic syndrome, chronic kidney disease, and cardiovascular disease: a dynamic and life-threatening triad. *Cardiol Res Pract,* 2011**:** 747861, 2011.
4. Galassi, A, Reynolds, K, He, J: Metabolic syndrome and risk of cardiovascular disease: a meta-analysis. *Am J Med,* 119**:** 812-819, 2006.
5. Gami, AS, Witt, BJ, Howard, DE, Erwin, PJ, Gami, LA, Somers, VK, Montori, VM: Metabolic syndrome and risk of incident cardiovascular events and death: a systematic review and meta-analysis of longitudinal studies. *J Am Coll Cardiol,* 49**:** 403-414, 2007.
6. Kurella, M, Lo, JC, Chertow, GM: Metabolic syndrome and the risk for chronic kidney disease among nondiabetic adults. *J Am Soc Nephrol,* 16**:** 2134-2140, 2005.
7. Whaley-Connell, A, Pavey, BS, McCullough, PA, Saab, G, Li, S, McFarlane, SI, Chen, SC, Vassalotti, JA, Collins, AJ, Bakris, G, Sowers, JR, Investigators, K: Dysglycemia predicts cardiovascular and kidney disease in the Kidney Early Evaluation Program. *J Clin Hypertens (Greenwich),* 12**:** 51-58, 2010.
8. Bongartz, LG, Braam, B, Gaillard, CA, Cramer, MJ, Goldschmeding, R, Verhaar, MC, Doevendans, PA, Joles, JA: Target organ cross talk in cardiorenal syndrome: animal models. *Am J Physiol Renal Physiol,* 303**:** F1253-1263, 2012.
9. Hamdani, N, Franssen, C, Lourenco, A, Falcao-Pires, I, Fontoura, D, Leite, S, Plettig, L, Lopez, B, Ottenheijm, CA, Becher, PM, Gonzalez, A, Tschope, C, Diez, J, Linke, WA, Leite-Moreira, AF, Paulus, WJ: Myocardial titin hypophosphorylation importantly contributes to heart failure with preserved ejection fraction in a rat metabolic risk model. *Circ Heart Fail,* 6**:** 1239-1249, 2013.
10. Bilan, VP, Salah, EM, Bastacky, S, Jones, HB, Mayers, RM, Zinker, B, Poucher, SM, Tofovic, SP: Diabetic nephropathy and long-term treatment effects of rosiglitazone and enalapril in obese ZSF1 rats. *J Endocrinol,* 210**:** 293-308, 2011.
11. Griffin, KA, Abu-Naser, M, Abu-Amarah, I, Picken, M, Williamson, GA, Bidani, AK: Dynamic blood pressure load and nephropathy in the ZSF1 (fa/fa cp) model of type 2 diabetes. *Am J Physiol Renal Physiol,* 293**:** F1605-1613, 2007.
12. Leite, S, Oliveira-Pinto, J, Tavares-Silva, M, Abdellatif, M, Fontoura, D, Falcao-Pires, I, Leite-Moreira, AF, Lourenco, AP: Echocardiography and invasive hemodynamics during stress testing for diagnosis of heart failure with preserved ejection fraction: an experimental study. *Am J Physiol Heart Circ Physiol,* 308**:** H1556-1563, 2015.
13. Sowers, JR, Whaley-Connell, A, Hayden, MR: The Role of Overweight and Obesity in the Cardiorenal Syndrome. *Cardiorenal Med,* 1**:** 5-12, 2011.
14. André, PL, Inês, F-P, Rui, C, Dulce, F, Daniela, M, Nazha, H, Walter, P, Adelino, FL-M: Abstract 17471: The Obese Zsf1 Rat as a New Model of Heart Failure with Preserved Ejection Fraction Accompanying the Metabolic Syndrome. *Circulation,* 126**:** A17471-A17471, 2012.
15. Westermann, D, Lindner, D, Kasner, M, Zietsch, C, Savvatis, K, Escher, F, von Schlippenbach, J, Skurk, C, Steendijk, P, Riad, A, Poller, W, Schultheiss, HP, Tschope, C: Cardiac inflammation contributes to changes in the extracellular matrix in patients with heart failure and normal ejection fraction. *Circ Heart Fail,* 4**:** 44-52, 2011.
16. van Heerebeek, L, Hamdani, N, Falcao-Pires, I, Leite-Moreira, AF, Begieneman, MP, Bronzwaer, JG, van der Velden, J, Stienen, GJ, Laarman, GJ, Somsen, A, Verheugt, FW, Niessen, HW, Paulus, WJ: Low myocardial protein kinase G activity in heart failure with preserved ejection fraction. *Circulation,* 126**:** 830-839, 2012.
17. Paulus, WJ, Tschope, C: A novel paradigm for heart failure with preserved ejection fraction: comorbidities drive myocardial dysfunction and remodeling through coronary microvascular endothelial inflammation. *J Am Coll Cardiol,* 62**:** 263-271, 2013.
18. Ronco, C, Haapio, M, House, AA, Anavekar, N, Bellomo, R: Cardiorenal syndrome. *J Am Coll Cardiol,* 52**:** 1527-1539, 2008.
19. Shestakova, MV, Jarek-Martynowa, IR, Ivanishina, NS, Kuharenko, SS, Yadrihinskaya, MN, Aleksandrov, AA, Dedov, II: Role of endothelial dysfunction in the development of cardiorenal

syndrome in patients with type 1 diabetes mellitus. *Diabetes Res Clin Pract,* 68 Suppl1**:** S65-72, 2005.
20. Hatamizadeh, P, Fonarow, GC, Budoff, MJ, Darabian, S, Kovesdy, CP, Kalantar-Zadeh, K: Cardiorenal syndrome: pathophysiology and potential targets for clinical management. *Nat Rev Nephrol,* 9**:** 99-111, 2013.
21. Karnib, HH, Ziyadeh, FN: The cardiorenal syndrome in diabetes mellitus. *Diabetes Res Clin Pract,* 89**:** 201-208, 2010.
22. Leite-Moreira, AF, Correia-Pinto, J: Load as an acute determinant of end-diastolic pressure-volume relation. *Am J Physiol Heart Circ Physiol,* 280**:** H51-59, 2001.
23. van Dijk, CG, Nieuweboer, FE, Pei, JY, Xu, YJ, Burgisser, P, van Mulligen, E, el Azzouzi, H, Duncker, DJ, Verhaar, MC, Cheng, C: The complex mural cell: pericyte function in health and disease. *Int J Cardiol,* 190**:** 75-89, 2015.
24. Hall, JE, Crook, ED, Jones, DW, Wofford, MR, Dubbert, PM: Mechanisms of obesity-associated cardiovascular and renal disease. *Am J Med Sci,* 324**:** 127-137, 2002.
25. Cohen, JB, Cohen, DL: Cardiovascular and renal effects of weight reduction in obesity and the metabolic syndrome. *Curr Hypertens Rep,* 17**:** 34, 2015.
26. Correa de Sa, DD, Hodge, DO, Slusser, JP, Redfield, MM, Simari, RD, Burnett, JC, Chen, HH: Progression of preclinical diastolic dysfunction to the development of symptoms. *Heart,* 96**:** 528-532, 2010.
27. Afshinnia, F, Spitalewitz, S, Chou, SY, Gunsburg, DZ, Chadow, HL: Left ventricular geometry and renal function in hypertensive patients with diastolic heart failure. *Am J Kidney Dis,* 49**:** 227-236, 2007.
28. Ahmed, A, Rich, MW, Sanders, PW, Perry, GJ, Bakris, GL, Zile, MR, Love, TE, Aban, IB, Shlipak, MG: Chronic kidney disease associated mortality in diastolic versus systolic heart failure: a propensity matched study. *Am J Cardiol,* 99**:** 393-398, 2007.
29. Tofovic, SP, Kusaka, H, Kost, CK, Jr., Bastacky, S: Renal function and structure in diabetic, hypertensive, obese ZDFxSHHF-hybrid rats. *Ren Fail,* 22**:** 387-406, 2000.
30. El-Atat, FA, Stas, SN, McFarlane, SI, Sowers, JR: The relationship between hyperinsulinemia, hypertension and progressive renal disease. *J Am Soc Nephrol,* 15**:** 2816-2827, 2004.
31. Akiyama, E, Sugiyama, S, Matsuzawa, Y, Konishi, M, Suzuki, H, Nozaki, T, Ohba, K, Matsubara, J, Maeda, H, Horibata, Y, Sakamoto, K, Sugamura, K, Yamamuro, M, Sumida, H, Kaikita, K, Iwashita, S, Matsui, K, Kimura, K, Umemura, S, Ogawa, H: Incremental prognostic significance of peripheral endothelial dysfunction in patients with heart failure with normal left ventricular ejection fraction. *J Am Coll Cardiol,* 60**:** 1778-1786, 2012.
32. Windt, WA, Henning, RH, Kluppel, AC, Xu, Y, de Zeeuw, D, van Dokkum, RP: Myocardial infarction does not further impair renal damage in 5/6 nephrectomized rats. *Nephrol Dial Transplant,* 23**:** 3103-3110, 2008.
33. Dikow, R, Schmidt, U, Kihm, LP, Schaier, M, Schwenger, V, Gross, ML, Katus, HA, Zeier, M, Hardt, SE: Uremia aggravates left ventricular remodeling after myocardial infarction. *Am J Nephrol,* 32**:** 13-22, 2010.
34. Mohammed, SF, Hussain, S, Mirzoyev, SA, Edwards, WD, Maleszewski, JJ, Redfield, MM: Coronary microvascular rarefaction and myocardial fibrosis in heart failure with preserved ejection fraction. *Circulation,* 131**:** 550-559, 2015.
35. Oka, T, Akazawa, H, Naito, AT, Komuro, I: Angiogenesis and cardiac hypertrophy: maintenance of cardiac function and causative roles in heart failure. *Circ Res,* 114**:** 565-571, 2014.
36. Frangogiannis, NG, Smith, CW, Entman, ML: The inflammatory response in myocardial infarction. *Cardiovasc Res,* 53**:** 31-47, 2002.
37. Virag, JI, Murry, CE: Myofibroblast and endothelial cell proliferation during murine myocardial infarct repair. *Am J Pathol,* 163**:** 2433-2440, 2003.
38. McAlister, FA, Ezekowitz, J, Tonelli, M, Armstrong, PW: Renal insufficiency and heart failure: prognostic and therapeutic implications from a prospective cohort study. *Circulation,* 109**:** 1004-1009, 2004.
39. Brouwers, FP, de Boer, RA, van der Harst, P, Voors, AA, Gansevoort, RT, Bakker, SJ, Hillege, HL, van Veldhuisen, DJ, van Gilst, WH: Incidence and epidemiology of new onset heart failure with preserved vs. reduced ejection fraction in a community-based cohort: 11-year follow-up of PREVEND. *Eur Heart J,* 34**:** 1424-1431, 2013.
40. Greaves, K, Chen, R, Ge, L, Wei, M, Tong, B, Cai, N, Senior, R, Hemingway, H: Mild to moderate renal impairment is associated with increased left ventricular mass. *Int J Cardiol,* 124**:** 384-386, 2008.
41. van Dokkum, RP, Eijkelkamp, WB, Kluppel, AC, Henning, RH, van Goor, H, Citgez, M, Windt, WA, van Veldhuisen, DJ, de Graeff, PA, de Zeeuw, D: Myocardial infarction enhances progressive

renal damage in an experimental model for cardio-renal interaction. *J Am Soc Nephrol,* 15**:** 3103-3110, 2004.

42. Bongartz, LG, Joles, JA, Verhaar, MC, Cramer, MJ, Goldschmeding, R, Tilburgs, C, Gaillard, CA, Doevendans, PA, Braam, B: Subtotal nephrectomy plus coronary ligation leads to more pronounced damage in both organs than either nephrectomy or coronary ligation. *Am J Physiol Heart Circ Physiol,* 302**:** H845-854, 2012.

Supplemental data

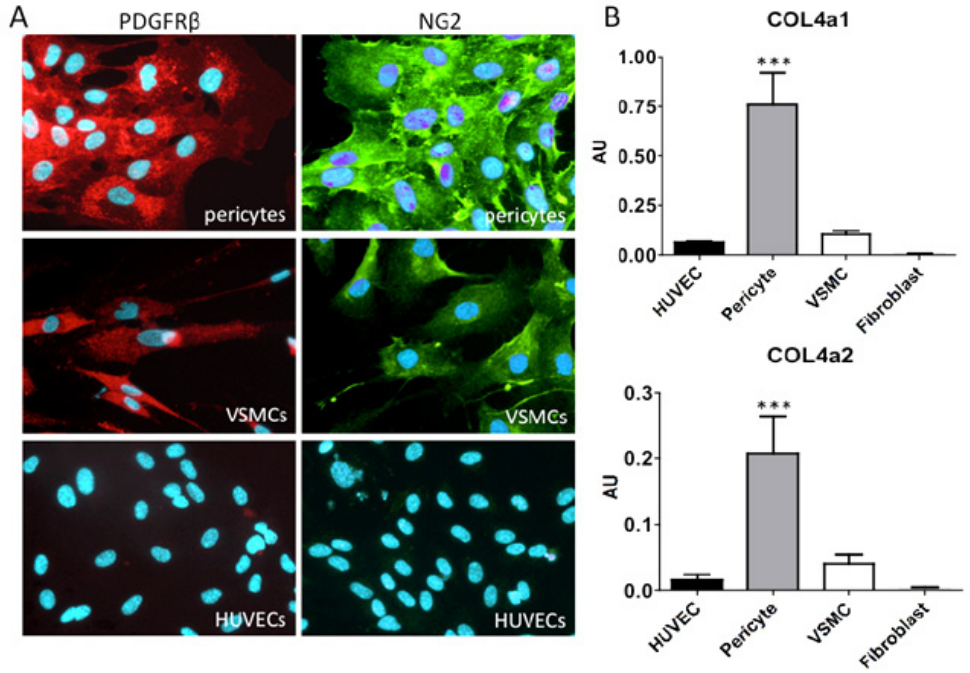

Supplemental Figure 1: NG2, PDGFRß, and COL4 expression in human vascular cell types. (A) Representative immunofluorescent staining of mural cells derived from human origin (pericytes and VSMCs) and HUVECs. NG2 (red), PDGFRß (green), and nuclei (blue). 20X magnification. **(B)** QPCR analysis of COL4a1 and COL4a2 expression levels in human derived vascular cells and fibroblasts. n=3, Mean±SD. ***P<0.001 versus all.

Supplemental Tables can be downloaded from:
http://circheartfailure.ahajournals.org/lookup/suppl/doi:10.1161/CIRCHEARTFAILURE.115.002760/-/DC1

Chapter 5

Limited synergy of obesity and hypertension, prevalent risk factors in onset and progression of HFpEF

Maarten M. Brandt*, Isabel T. N. Nguyen*, Merle M. Krebber, Jens van de Wouw, Michal Mokry, Maarten J. Cramer, Dirk J. Duncker, Marianne C. Verhaar, Jaap A. Joles‡, Caroline Cheng‡. (*‡ Authors contributed equally)

Journal of Cellular and Molecular Medicine, 2019; PMID: 31368189

Abstract

Obesity and hypertension are prevalent comorbidities in heart failure with preserved ejection fraction. It has been proposed that they act synergistically in development of heart failure. To clarify if and how this putative interaction contributes to development of diastolic dysfunction, lean and obese ZSF1 rats were treated with placebo, or deoxycorticosterone acetate implants plus 6% salt (DS) to induce sever hypertension. In addition to echocardiographic, metabolic, and hemodynamic analyses, immunohistochemistry and RNAseq were performed on left ventricles. Obesity lowered cardiac output and led to elevated E/e' ratios. DS did not affect cardiac output and minimally elevated E/e' ratios. Diastolic derangements in placebo-treated obese rats developed in absence of inflammation and fibrosis, yet in presence of oxidative stress and hypertrophic remodeling. In contrast, hypertension triggered apoptosis, inflammation, and fibrosis, with limited synergy of the comorbidities observed for inflammation and fibrosis. Transcriptional data suggested that these comorbidities exerted opposite effects on mitochondrial function. In placebo-treated obese rats, genes involved in fatty acid metabolism were upregulated, whereas DS induced a downregulation of genes involved in oxidative phosphorylation. Overall, limited interaction was observed between these comorbidities in development of diastolic dysfunction. Importantly, differences in comorbidity-induced cardiac remodeling emphasize the necessity for thorough phenotypical characterization.

Introduction

The chronic and progressive condition, in which the heart is unable to maintain cardiac output commensurate with the body's requirements, is referred to as heart failure (HF). Based on ejection fraction, HF can be divided into HF with reduced ejection fraction (HFrEF), marked by the inability to adequately contract during systole, and HF with preserved ejection fraction (HFpEF). HFpEF is associated with impaired cardiac relaxation and increased passive cardiac stiffness, resulting in elevated end-diastolic pressure and impaired left ventricle (LV) filling.[1] HFpEF accounts for over 50% of all HF cases in Europe and the United States of America, yet currently no effective treatment is available for this specific form of HF.[1]

This lack of evidence-based treatment options might find its origin in the complex, multifactorial disease etiology of HFpEF. Development and progression of HFpEF is associated with a high prevalence of non-cardiac comorbidities and in previous studies it was proposed that these comorbidities could provoke a state of chronic systemic inflammation, leading to coronary microvascular dysfunction, oxidative stress, enhanced cardiomyocyte stiffness and myocardial fibrosis.[2] Obesity and hypertension are both highly prevalent (84% and 60-80%, respectively) among HFpEF patients.[3, 4] It has been demonstrated that both comorbidities can individually contribute to development of diastolic dysfunction in rodent models. For example, deoxycorticosterone acetate- and salt-induced hypertensive rats developed perivascular fibrosis, and concentric cardiac hypertrophy accompanied by diastolic dysfunction in addition to hypertension.[5, 6] Similarly, in leptin-deficient murine obesity models, ob/ob mice were shown to develop concentric cardiac remodeling with increased cardiomyocyte size and diastolic dysfunction[7, 8], secondary to obesity and type 2 diabetes.[9] Importantly, it is estimated that at least 75% of the incidence of hypertension in the human population is related to obesity[10], and both comorbidities thus often present together. The current consensus is that metabolic- and hypertensive disease, like other HFpEF-associated comorbidities, contribute to the systemic state of inflammation[2], and as such, potentially act synergistically in development and progression of diastolic dysfunction. However, direct evidence for such a synergistic relation is lacking. More insight in the putative synergistic effects might not only provide a better understanding of the pathogenesis of HFpEF itself, but could also lead to novel insights in the poor performance of antihypertensive drug treatment alone in reducing morbidity or mortality in subsets of (obese) patients with HFpEF.[11]

Here we tested the hypothesis that metabolic- and hypertensive disease act synergistically in development and/or progression of HFpEF. For this purpose, male lean and obese ZSF1 rats, of which the latter were previously shown to develop diastolic dysfunction between

week 10 and 20 of natural aging[12, 13], were studied from 12 weeks of age. Both lean and obese rats were treated with deoxycorticosterone acetate implants plus high salt diet (DS) or placebo from 19 to 26 weeks of age to induce severe hypertension. DS treatment was limited to this period to prevent progression to HFrEF. In addition to echocardiographic, metabolic, and hemodynamic analyses, immunohistochemistry and RNAseq on LV apex tissue was performed, which enabled us to dissect which pathophysiological and transcriptional adaptations were associated with obesity and its associated biochemical aberrations, and which with DS-induced hypertension.

Methods

Ethics

All animal studies were approved by the Animal Ethics Committee of the University of Utrecht (CCD: AVD115002016462) and were in accordance with the Dutch Codes of Practice for the Care and Use of Animals for Scientific Purposes. Animal experiments were performed according to ARRIVE (Animal Research: Reporting of In Vivo Experiments) guidelines.

Animal Model

Nine-week old male lean (n=13) and obese (n=13) ZSF1 rats were obtained from Charles River (Kingston, MA) and housed in a temperature- and humidity-controlled environment with a 12-hour light/dark cycle. Rats had access to water and standard chow (CRM-E; Special Diet Services, Witham, Essex, UK) *ad libitum*. Starting at 12 weeks until 26 weeks of age, systolic blood pressure (SBP) measurements via tail-cuff plethysmography were done every two weeks. At 12 weeks and every two weeks from 18 to 26 weeks of age echocardiography was performed, whereas body weight was measured every week. At 19 weeks of age, lean and obese rats were randomized and either implanted with a deoxycorticosterone acetate pellet (35mg in lean, 50mg in obese; Innovative Research of America, Sarasota, Florida, USA) and fed a high salt diet (6% NaCl) or with a placebo pellet and fed a normal salt diet. At week 26, after the last measurements, the rats were terminated via exsanguination under deep anesthesia and organs were harvested and weighed (Figure 1A).

Echocardiography Evaluation

Rats were anesthetized with isoflurane (3.5-4% for induction and 2-2.5% for maintenance). Transthoracic echocardiography was performed with a digital ultrasound machine (model

Sonos 5500, Philips Research, Eindhoven, The Netherlands) and a 15-MHz linear array transducer (Hewlett Packard, Palo Alto, CA). The LV long-axis dimensions were recorded by 2D-echocardiography. Two-dimensional B-mode cine loops were recorded in the parasternal long-axis and the midpapillary short-axis views. Mitral flow velocity tracings were obtained with pulsed-wave Doppler above the mitral leaflets. Tissue Doppler Imaging (TDI) was used to obtain early (e') diastolic velocity at the medial mitral annulus. The recordings were averaged from 3 consecutive heartbeats.

Plasma measurements

Blood samples of 0.5 ml were drawn from the tail vein into EDTA anticoagulant-coated tubes, while the rats were under anesthesia. Plasma was extracted by centrifugation at 1500 x g for 15 min at 4°C and used for determination of plasma glucose, cholesterol and triglycerides (DiaSys Diagnostic Systems GmbH, Cholesterol FS, Triglycerides FS, Glucose GOD FS, Waterbury, Connecticut, USA).

Metabolic cage studies and TBARS measurements

Rats were housed individually in metabolic cages with access to food and water for 24 hours to collect urine. In urine samples, thiobarbituric acid-reactive substances (TBARS; TBARS assay kit, Cayman Chemical, Ann Arbor, Michigan, USA) were measured according to manufacturer's instructions.

Immunohistochemistry

Deparaffinized cardiac sections were subjected to 3% hydrogen peroxide in PBS for 30 min, followed by heat-induced antigen retrieval in citrate/HCl buffer (pH 6.0) for 15 min. To visualize capillaries, sections were first blocked in avidin and biotin blocking solution (Abcam, Cambridge, UK). Section were then incubated overnight at 4°C with biotin labelled anti-Lectin from *Bandeiraea simplicifolia* (1:200, Sigma, St. Louis, Missouri, USA), after which HRP-bound streptavidin (1:500, Bio-Rad, Veenendaal, the Netherlands) was added to the samples for 60 min. Finally, 3,3′-diaminobenzidine solution was applied to the sections twice, 6 min each. To visualize early apoptosis, sections were incubated for 60 min at room temperature (RT) with a primary antibody against active Caspase 3 (1:200, BD Biosciences, San Jose, California, USA), followed by 30 min incubation at RT with BrightVision PolyGoat-HRP-anti-Rabbit IgG (Immunologic BV, Duiven, the Netherlands). To visualize innate inflammation, sections were incubated for 60 min at RT with a primary antibody against CD68 (1:500, Abcam), followed by 30 min incubation at RT with Poly-Rabbit-anti-Mouse (Abcam) and 30 min incubation at RT with BrightVision PolyGoat-HRP-anti-Rabbit IgG. To

visualize adaptive immunity, sections were first blocked in avidin and biotin blocking solution. Thereafter, sections were incubated for 60 min at RT with a primary antibody against CD3 (1:200, Abcam), followed by 30 min incubation at RT with BrightVision PolyGoat-HRP-anti-Rabbit IgG. For all immunostainings (with the exception of lectin), finally NovaRed buffer was applied to the sections for 10 min, and a counterstaining was performed via a brief dip in hematoxylin. Late apoptosis was fluorescently visualized in deparaffinized cardiac sections, which were incubated 30 min at 37°C in a 20µg/mL proteinase K solution in 10mM Tris/HCL buffer (pH 8.0). After a brief wash, TUNEL labeling solution (Sigma) was applied according to manufacturer's instruction for 60 min at 37°C. Nuclei were counterstained with DAPI. For all immunostainings, four non-overlapping fields in the sub-endocardium were imaged and analyzed in a blinded fashion.

Gomori staining

Gomori staining was performed using the Reticulum Stain Kit (Diagnostic Biosystems, Pleasanton, California, USA) according to manufacturer's instructions. Slides were counterstained for 3 min using Nuclear Fast Red, and imaged. Cross-sectional areas of cardiomyocytes with clearly visible nuclei, and height to width ratios not exceeding 1:2, were measured in 4 non-overlapping fields in a blinded fashion using Clemex software.

Picrosirius red staining

Deparaffinized cardiac sections were stained with Picro Sirius red (Sigma) for 25 min, differentiated in 0.2 HCl and rinsed with aquadest, followed by dehydration. Twenty non-overlapping fields were imaged using a polarizing filter, followed by analysis in a blinded fashion using Adobe Photoshop and ImageJ software as described.[14]

Identification of gene expression

RNA sequencing was done as described.[15] Briefly, RNA was isolated from the cardiac apex using the RNeasy isolation kit (Qiagen, Hilden, Germany). NEXTflex Poly(A) Beads (PerkinElmer Applied Genomics, Waltham, Massachusetts, USA) were used to isolate polyadenylated mRNA, from which sequencing libraries were made using the Rapid Directional RNA-seq kit (NEXTflex). Libraries were sequenced using the Nextseq500 platform (Illumina, San Diego, California, USA), producing single end reads of 75bp. Reads were aligned to the rat reference genome. Picard's AddOrReplaceReadGroups (v1.98) was used to add read groups to the BAM files, which were sorted with Sambamba v0.4.5 and transcript abundances were quantified with HTSeq-count version 0.6.1p1 using the union mode. Subsequently, RPKMs were calculated with edgeR's RPKM function. Differentially

expressed genes in the transcriptome data were identified using the DESeq2 package with standard settings.[16]

Quantitative PCR analysis

Cardiac apex RNA was reverse transcribed into cDNA using iScript cDNA synthesis kit (Bioline, London, UK). Gene expression was assessed by qPCR using SensiFast SYBR & Fluorecein kit (Bioline) and primers as listed in Supplemental Table 1. Expression levels are relative to the averaged expression of housekeeping genes RPLP0, POLR2A, B2M, and YWHAZ.

Pathway analysis

RNAseq results were further analyzed using Ingenuity Pathway Analysis (IPA, Qiagen). IPA was used to identify both differences in pathway dynamics, and upstream regulators (growth factors and transcriptional regulators) of differentially expressed genes. P-values were calculated based on a right-tailed Fisher Exact Test, calculated by IPA.

Statistics

Data are presented as means ± SEM. Groups were compared by 2-way ANOVA or 2-way ANOVA for repeated measures, followed by Tukey post hoc test when appropriate. Statistical significance was accepted when $P<0.05$.

Results

ZSF1 rats develop diastolic dysfunction with a minimal effect of DS-induced hypertension

Male ZSF1 rats, heterozygous (lean) or homozygous (obese) for leptin receptor mutation, were studied from 12 to 26 weeks of age. Both lean and obese rats were treated with DS or placebo from 19 to 26 weeks of age and echocardiographic, metabolic, and hemodynamic analyses were performed every two weeks (Figure 1A). ZSF1 rats with leptin receptor deficiency had significant weight gain (Table 1). This weight gain was accompanied by elevated blood cholesterol and triglycerides, with no distinction between placebo- and DS-treated obese rats. An increase in blood glucose levels was observed in obese rats, which appeared to be attenuated by DS treatment. Systolic blood pressure was increased in both lean and obese DS-treated rats, with a synergistic elevation in DS-treated obese rats (Figure 1B).Obesity, in both placebo- and DS-treated rats, caused a minor reduction in ejection fraction (EF), yet in all conditions EF was preserved (>50%; Figure 1C).[17] Heart rate was reduced in both placebo- and DS-treated obese rats, and cardiac output (CO) tended to

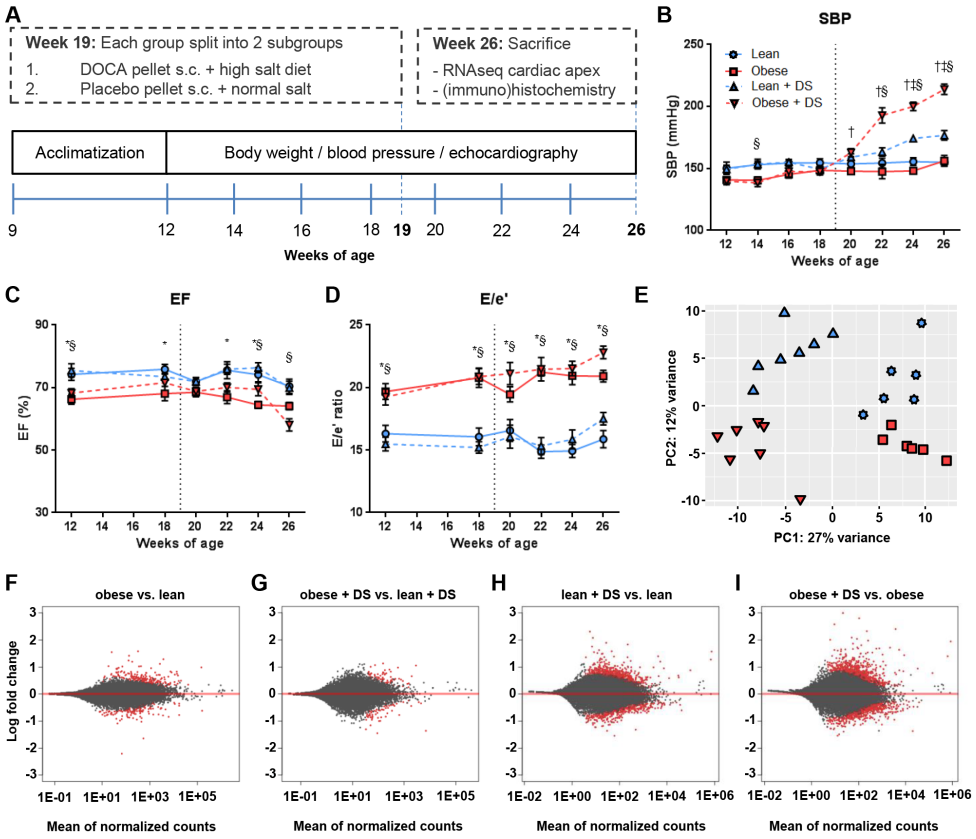

Figure 1: DS treatment leads to increased SBP and an intense cardiac transcriptional adaptation, whereas obesity triggers diastolic dysfunction (A) Graphical workflow, showing that male lean and obese ZSF1 rats were studied from 13 to 26 weeks of age. Both lean and obese rats were treated with DS or placebo from 19 to 26 weeks of age to trigger severe hypertension. Echocardiographic, metabolic, and hemodynamic analyses were done every two weeks, till sacrifice at the age of 26 weeks. Longitudinal plots of **(B)** systolic blood pressure (mmHg), **(C)** ejection fraction (%), and **(D)** E/e' ratio. n=6-7, * obese vs. lean, § obese+DS vs. lean+DS, ‡ lean+DS vs. lean, † obese+DS vs. obese P<0.05. **(E)** Principal component analysis of expression profiles in cardiac tissue. Symbols denoting subgroups panels B-E are shown in panel B. **(F-I)** Graphic display of differential gene expression in which log2FC is plotted against the mean of normalized counts. Red dots represent the differentially expressed genes (FDR<0.1), gray dots represent non-differentially expressed genes.

be lower in obese vs. lean (p=0.08) and in obese+DS vs. lean+DS (p=0.07). When corrected for body mass (cardiac index), placebo- and DS-treated obese rats appeared unable to match cardiac output to body mass. Obesity and DS-induced hypertension both tended to increase LV weight (LVW) and total heart weight (HW), but a significant increase was only observed in presence of both comorbidities. Illustrative for diastolic dysfunction, the ratio

Table 1: Parameters in lean and obese ZSF1 rats at 26 weeks of age

	Lean (n=6)	Lean+DS (n=7)	Obese (n=6)	Obese+DS (n=7)	p-values Obesity	DS	Interaction
Tibia length (mm)	40.8 ± 0.5	40.0 ± 0.4	38.1 ± 0.4*	39.1 ± 0.6	<0.05	0.93	0.05
Body weight (g)	443 ± 9	417 ± 10	584 ± 13*	607 ± 10§	<0.05	0.91	<0.05
Cholesterol (mM)	2.2 ± 0.1	2.1 ± 0.1	8.2 ± 0.8*	9.1 ± 0.7§	<0.05	0.46	0.34
Triglycerides (mM)	1.5 ± 0.2	1.1 ± 0.2	23.8 ± 4.0*	20.5 ± 2.5§	<0.05	0.44	0.53
Glucose (mM)	9.9 ± 0.5	9.1 ± 0.5	22.5 ± 2.6*	14.0 ± 1.6†	<0.05	<0.05	<0.05
SBP (mmHg)	153 ± 3	179 ± 4‡	150 ± 1	213 ± 5†§	<0.05	<0.05	<0.05
Heart rate (bpm)	381 ± 9	362 ± 8	308 ± 9*	292 ± 6§	<0.05	<0.05	0.81
SV (µl)	212 ± 19	217 ± 23	178 ± 19	187 ± 19	0.13	0.71	0.90
CO (ml/min)	81 ± 7	79 ± 8	55 ± 6	55 ± 5	<0.05	0.87	0.92
CI (ml/min/100g)	18.2 ± 1.6	18.7 ± 1.7	9.5 ± 1.2*	9.0 ± 0.9§	<0.05	0.99	0.73
EF (%)	73 ± 2	70 ± 3	65 ± 1*	59 ± 2†§	<0.05	<0.05	0.48
E/e'	15.9 ± 0.9	17.5 ± 0.6	20.5 ± 0.6*	22.9 ± 0.7†§	<0.05	<0.05	0.55
LVW (mg)	909 ± 27	1139 ± 64	1172 ± 66	1490 ± 116†§	<0.05	<0.05	0.58
HW (LV+RV; mg)	1338 ± 32	1459 ± 48	1474 ± 41	1684 ± 50†§	<0.05	<0.05	0.32

Values are means ± SEM, followed by main effect- (effect obesity / effect DS) and interaction p-values, as determined by 2-way ANOVA. SBP = systolic blood pressure, TL = tibia length, SV = stroke volume, CO = cardiac output, CI = cardiac index, LVW = left ventricle weight, HW = heart weight, RV = right ventricle. * obese vs. lean, § obese+DS vs. lean+DS, ‡ lean+DS vs. lean, † obese+DS vs. obese P<0.05.

between peak velocity of early mitral inflow and early diastolic mitral annulus velocity (E/e′) was increased in obese rats (Figure 1D). Surprisingly, both for the reduced cardiac index and the increased E/e' ratios, no interaction among the comorbidities was observed. In contrast to the functional findings, which were principally affected by obesity, RNAseq revealed that DS-induced hypertension caused the most predominant transcriptional variance (Figure 1E). In cardiac tissue of placebo-treated obese versus placebo-treated lean rats, and DS-treated obese versus DS-treated lean rats, a total of 410 and 146 genes were differentially expressed (FDR <0.1), respectively (Figure 1F-G, Supplemental Table 2-3). However, in DS-treated lean rats versus placebo-treated lean rats, and DS-treated obese rats versus placebo-treated obese rats, a total of 1258 and 1504 genes were differentially expressed (FDR<0.1), respectively (Figure 1H-I, Supplemental Table 4-5).

Obesity and DS-induced hypertension trigger adverse mitochondrial responses

Analyses of transcription profiles with Ingenuity Pathway Analysis (IPA) indicated that both risk factors had substantial, yet opposite effects on genes involved in mitochondrial function. In placebo-treated rats, enzymes involved in fatty acid metabolism and oxidative phosphorylation were upregulated in obese versus lean rats (Figure 2A-B). In contrast, both lean and obese DS-treated rats had an overall downregulation versus placebo-treated rats

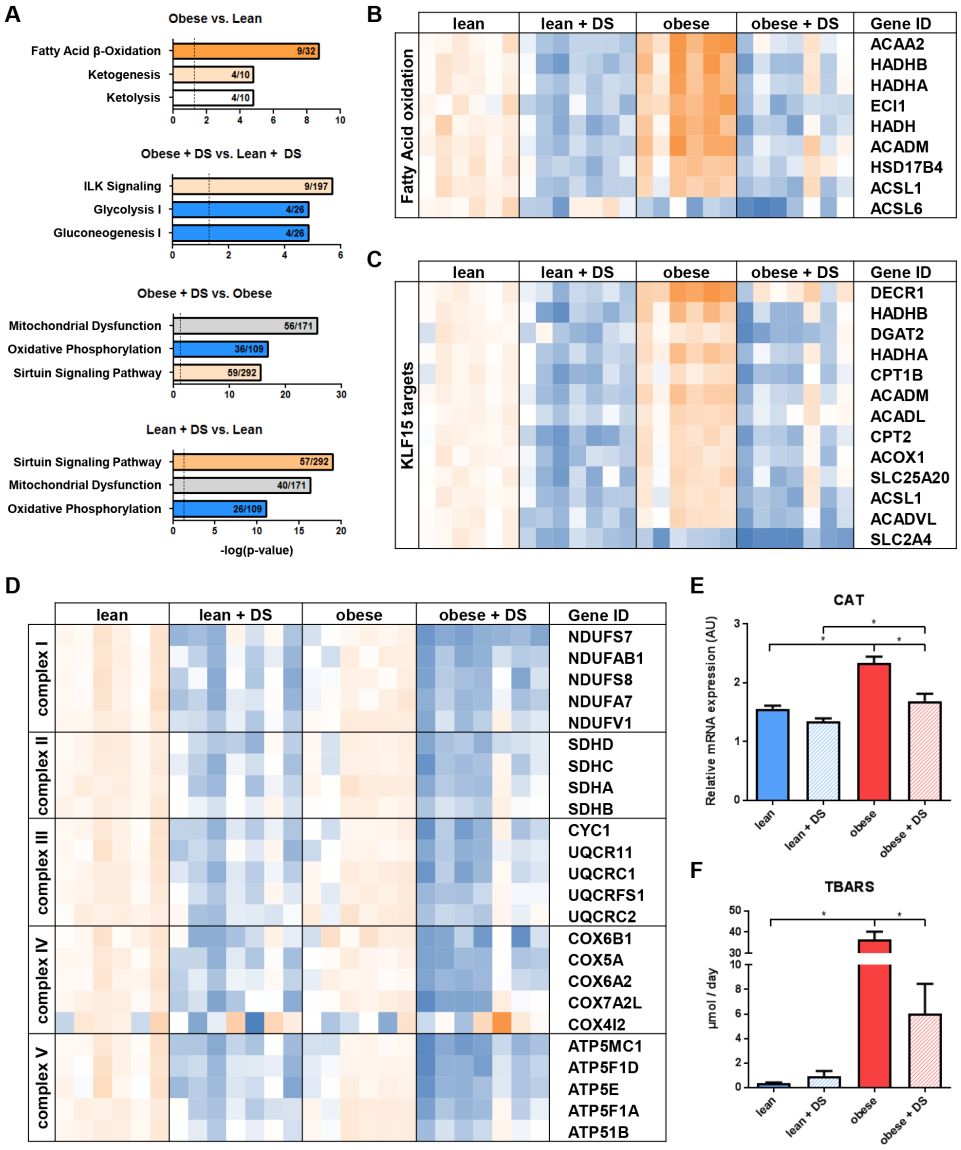

Figure 2: Pathway analysis revealed opposing mitochondrial responses to obesity and DS-induced hypertension. (A) Graphical visualization of 3 most affected pathways according to Ingenuity Pathway Analysis (orange and blue represent pathway activation and repression, respectively, grey represents no direction available). **(B)** Schematic presentation of RNAseq data for differentially expressed genes involved in FAO, **(C)** KLF15-induced transcription, **(D)** and oxidative phosphorylation. Shown is a color-based representation of the reads per kilobase million, relative to the average expression in the lean group, for each individual rat (orange and blue represent increased and decreased expression, relatively). **(E)** QPCR analysis of oxidative stress marker CAT. N=5-7, * P<0.05. **(F)** Analysis of urinary TBARS excretion as marker of systemic oxidative stress. N=6-7, * P<0.05.

of genes involved in oxidative phosphorylation, a phenomenon often observed in mitochondrial dysfunction (Figure 2A and D).[18, 19] IPA predicted that the transcriptional regulator Krüppel Like Factor 15 (KLF15), which has been described as a key regulator inducing mitochondrial fatty acid substrate usage[20], was the most active upstream regulator in placebo-treated obese versus lean rats (overlap p=2.66E-13/Z-score=2.95). Interestingly, it was among the most suppressed regulators in DS-treated rats (overlap p=5.37E-14/Z-score=-3.97 and overlap p=7.73E-17/Z-score=-3.70 in lean+DS vs. lean and obese+DS vs. obese, respectively; Figure 2C, Supplemental Table 6-8). qPCR analysis of established KLF15 targets Hydroxyacyl-CoA Dehydrogenase Trifunctional Multienzyme Complex Subunit Beta (HADHB), Acyl-CoA Dehydrogenase Medium Chain (ACADM), and 2,4 Dienoyl-CoA reductase (DECR1), substantiated this observation (Supplemental Figure 1).
RNAseq data also widely supported the DS-induced downregulation of genes coding for enzymes in oxidative phosphorylation, equally affecting the different complexes of the electron transport chain (Figure 2D). Remarkably, DS-induced downregulation of genes involved in oxidative phosphorylation was not accompanied by elevated transcription of oxidative stress responsive factor Catalase (CAT), whereas the increased transcription of fatty acid oxidation (FAO) genes in placebo-treated obese rats on the other hand was associated with elevated CAT expression (Figure 2E). Systemic oxidative stress, as measured by urinary excretion of thiobarbituric acid reactive substances (TBARS), followed a similar pattern, showing an elevation in placebo-treated obese rats (Figure 2F). The adaptations in transcription of mitochondrial genes raised the question whether this led to programmed cell death. Histological analysis of activated Caspase 3, a marker of early apoptosis, indicated no significant changes in sub-endocardial apoptosis (Supplemental Figure 2A and 2C), although the apoptotic effect of DS-induced hypertension showed a trend (p=0.05; Supplemental Table 9). A similar pattern was observed after labeling cells for late apoptosis, using Terminal Deoxynucleotidyl Transferase dUTP Nick End Labeling (TUNEL). Individually no differences were observed, although overall DS-induced hypertension stimulated apoptosis (Supplemental Figure 2B and 2D, Supplemental Table 9). Noteworthy, the apoptotic cells were predominantly found in patchy regions (Supplemental Figure 2E).

Cardiomyocyte hypertrophy is mostly associated with the presence of obesity

To get a better insight in myocardial hypertrophy in response to the comorbidities, the cross-sectional area of individual cardiomyocytes was studied. Presence of both comorbidities led to significant cardiomyocyte hypertrophy (Figure 3A-B). In contrast to the HW and LVW, which were affected by both DS-induced hypertension and obesity individually, obesity was

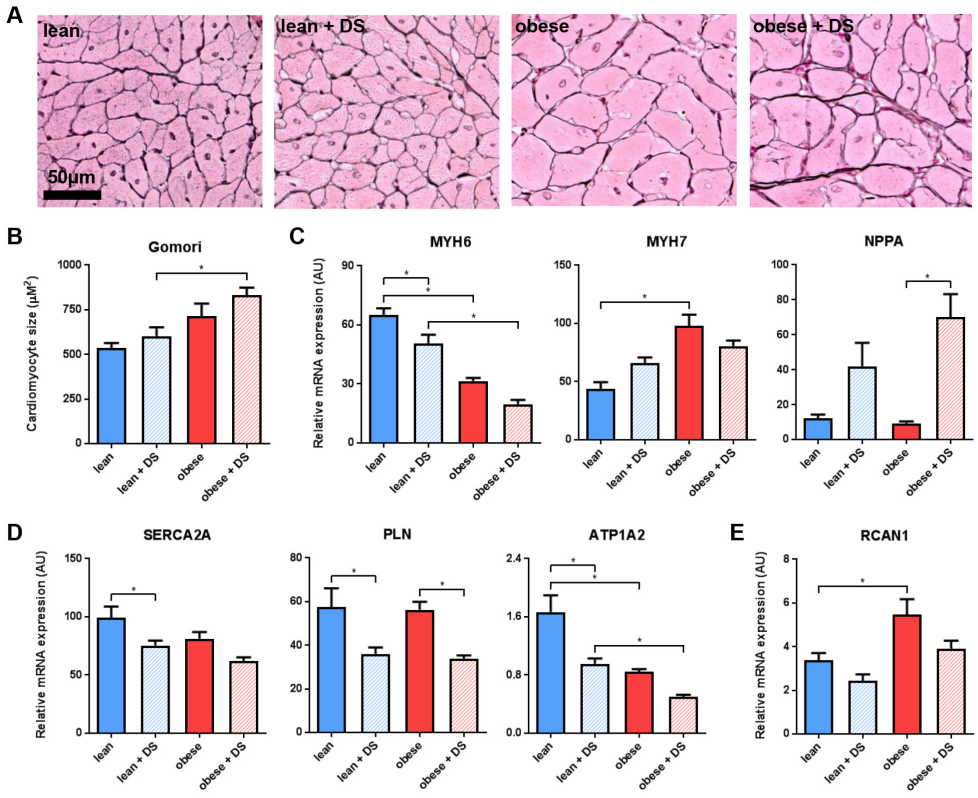

Figure 3: Immunohistochemistry and transcription analysis revealed DS- and obesity-induced cardiomyocyte hypertrophy. (A) Typical examples and **(B)** quantification of histological staining for cardiac hypertrophy (Gomori). N=4-6, * P<0.05. **(C)** QPCR analysis of cardiac transcription of hypertrophy markers MYH6, MYH7, and NPPA, **(D)** regulators of cytoplasmic Ca^{2+} levels SERCA2A, PLN, and ATP1A2, and **(E)** transcriptional target of Ca^{2+}-induced NFAT activation RCAN1. N=5-7, * P<0.05.

associated with an elevated cellular cross-sectional area, but no contribution of DS-induced hypertension was observed (Supplemental Table 9).

Transcription of Myosin Heavy Chain α (MYH6) and β (MYH7), defined markers for myocardial hypertrophy[21], resembled this predominant obesity-induced effect on cardiac remodeling. Obesity triggered a downregulation of MYH6, and an upregulation MYH7 (Figure 3C). DS-induced hypertension also reduced the expression of MYH6, though the effect size was more than a two-fold lower than that of obesity and appeared additive, not synergistic (Supplemental Table 9). Atrial natriuretic peptide (NPPA) on the other hand, like MYH6 and MYH7 a well-described hypertrophy marker, was upregulated solely in DS-treated rats. Transcriptional analysis demonstrated that expression of sarco/endoplasmic

reticulum Ca^{2+}-ATPase (SERCA2A) and phospholamban (PLN), both involved in calcium reuptake by the sarcoplasmic reticulum during diastole, was affected as well. SERCA2A expression was lowered by both comorbidities, whereas PLN appeared to be principally affected by DS-induced hypertension (Figure 3D). In line with SERCA2A, transcription of ATPase, Na^+/K^+ transporting alpha 2 (ATP1A2), was significantly lower in response to obesity and DS treatment. Of note, both for SERCA2A and ATP1A2, there was no interaction of the comorbidities (Figure 3D, Supplemental Table 9). Remarkably, Regulator of Calcineurin 1 (RCAN1), which is a direct Ca^{2+}-dependent transcriptional target of Nuclear Factor of Activated T-cells (NFAT), was solely upregulated in placebo-treated obese rats, whereas the opposite response was induced by DS (Figure 3E).

DS-induced hypertension and obesity in ZSF1 rats do not affect LV microvascular density

To evaluate whether DS-induced hypertension and obesity affect capillary density, a lectin staining was applied on LV cross sections. Surprisingly, no differences were observed in any of the conditions (Figure 4A-B). The absence of microvascular adaptations was substantiated by transcription levels of well-known affecters of microvascular stability Angiopoietin 1 and 2 (ANGPT1 and 2, respectively), and hypoxia associated factor Vascular endothelial Growth Factor A (VEGFA). transcription of vascular destabilizing factors ANGPT2 and VEGFA was not affected by the comorbidities (Figure 4C). Interestingly,

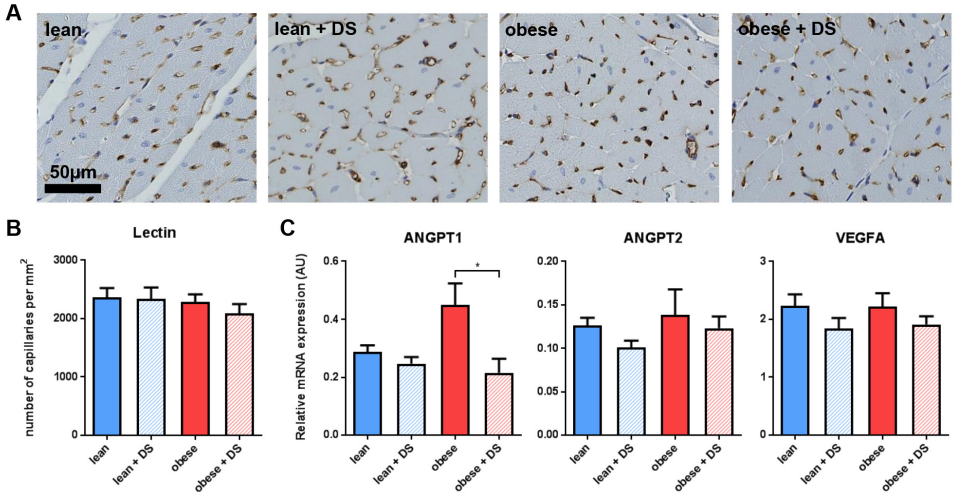

Figure 4: Immunohistochemistry and transcription analysis gave no indication for hypertension or obesity-induced LV microvascular changes. (A) Typical examples and **(B)** quantification of LV microvasculature (Lectin). N=4-6, * P<0.05. **(C)** QPCR analysis of cardiac transcription of factors involved in vascular remodeling ANGPT1, ANGPT2, and VEGFA. N=5-7, * P<0.05.

transcription of ANGPT1, which promotes vascular stability, was increased in placebo-treated obese rats, but not in DS-treated obese rats versus their respective lean counterparts.

DS-induced LV macrophage influx is aggravated by obesity

To assess the impact of DS-induced hypertension and obesity on the cardiac inflammatory state, presence of CD3+ T-cells and CD68+ macrophages was evaluated. The number of CD3+ T-cells, representing adaptive immunity, was low and not affected by obesity or DS-induced hypertension (Figure 5A and 5C, Supplemental Table 9). In contrast, presence of CD68+ macrophages, representing innate immunity, was markedly increased by DS-induced hypertension (Figure 5B and 5D, Supplemental Table 9). Obesity alone had no

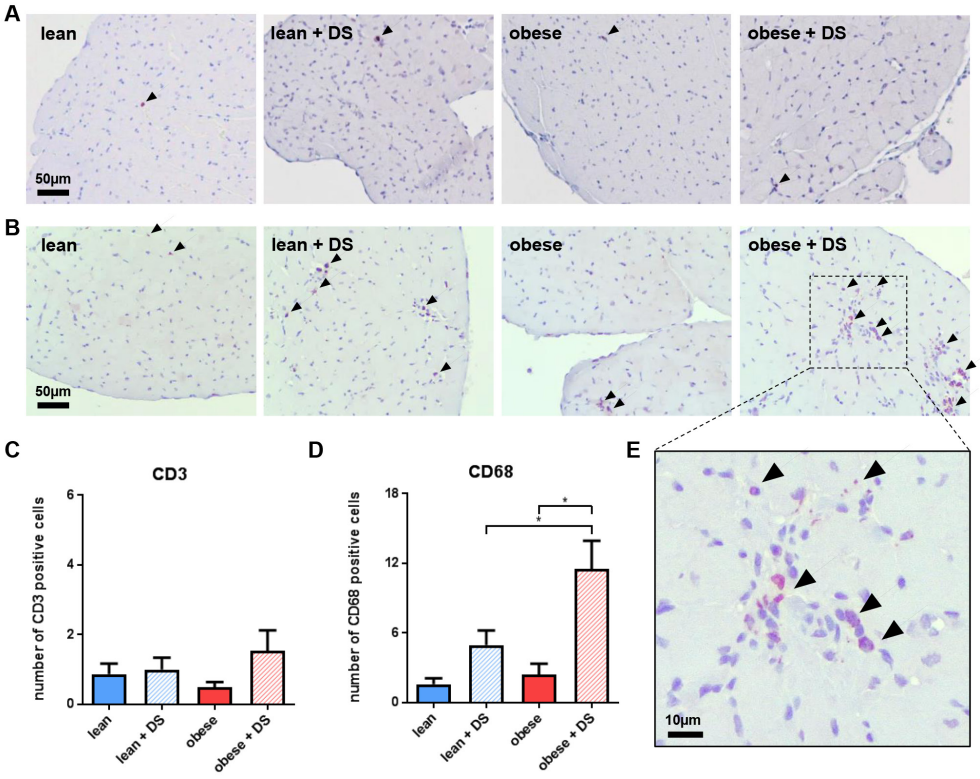

Figure 5: DS-induced LV macrophage influx is aggravated by obesity. (A) Typical examples of immunological staining for LV T cell (CD3) and **(B)** macrophage (CD68) presence. Positively labeled cells are depicted with an arrowhead. **(C)** Quantification of immunological staining for LV T cell (CD3) and **(D)** macrophage (CD68) presence. N=4-7, * P<0.05. **(E)** Magnified visualization of immunological CD68 labeling in DS-treated obese rats, illustrative for the observed DS-induced increase in apoptosis seen in regions with high cellular density.

effect, but in combination with DS-induced hypertension it significantly increased macrophage presence, showing a synergistic trend (interaction p=0.09). In line with the observed DS-induced apoptosis, macrophage presence was mostly seen in patchy clusters (Figure 5E).

DS-induced hypertension and obesity synergistically trigger TGFβ-induced LV fibrosis

To evaluate the impact of the comorbidities on the development and progression of fibrosis, collagen deposition was measured. Picro Sirius Red positivity in the placebo-treated obese ZSF1 rats was not different from the placebo-treated lean rats. In contrast, DS-induced hypertension triggered a profound fibrotic response. The DS-induced fibrosis appeared to be aggravated by obesity, although no significant interaction was observed (interaction p=0.31; Figure 6A-B, Supplemental Table 9). These findings were substantiated by qPCR validation of Collagen 1α1 (COL1A1), Collagen 3α1 (COL3A1), and Fibronectin (FN1) expression. Obesity alone had no effect, whereas DS-induced hypertension enhanced their transcription. This DS-induced upregulation was aggravated in the presence of obesity (Figure 6C) and significant synergy was observed for COL3A1 and FN1 (Supplemental Table 9). Based on the overall transcription profiles, IPA predicted high activity of Transforming Growth Factor (TGF) β1 (overlap p=2.81E-11/Z-score=4.01 and overlap p=2.95E-31/Z-score=6.24 in lean+DS vs. lean and obese+DS vs. obese, respectively) and TGFβ2 (overlap p=2.14E-4/Z-score=1.75 and overlap p=1.82E-6/Z-score=2.51 in lean+DS vs. lean and obese+DS vs. obese, respectively) signaling in the hearts of DS-treated versus placebo-treated rats (Supplemental Table 10-11). This predicted activation was accompanied by transcriptional upregulation of TGFβ1 and TGFβ2 (Figure 6D) upon DS-induced hypertension. Moreover, in addition to COL1A1, COL1A3 and FN1, various TGFβ target genes, including Periostin (POSTN) and Osteopontin 1 (SPP1) were upregulated (Figure 6E), of which the latter has recently been demonstrated to have predictive value for clinical outcome in HFpEF.[22]

Discussion

In line with previous reports[12, 13], ZSF1 rats with a homozygous leptin receptor mutation in our current study presented with metabolic derangements, including elevated body weight, hypercholesteremia, hyperglycemia, and hypertriglyceridemia. As anticipated, DS treatment triggered severe hypertension in both lean and obese ZSF1 rats, and the combination of these factors enabled us to study if and how obesity and hypertension interact in the development of diastolic dysfunction at a functional, histological, and transcriptional level. From this study we could conclude that (1) obesity-associated derangements had the most

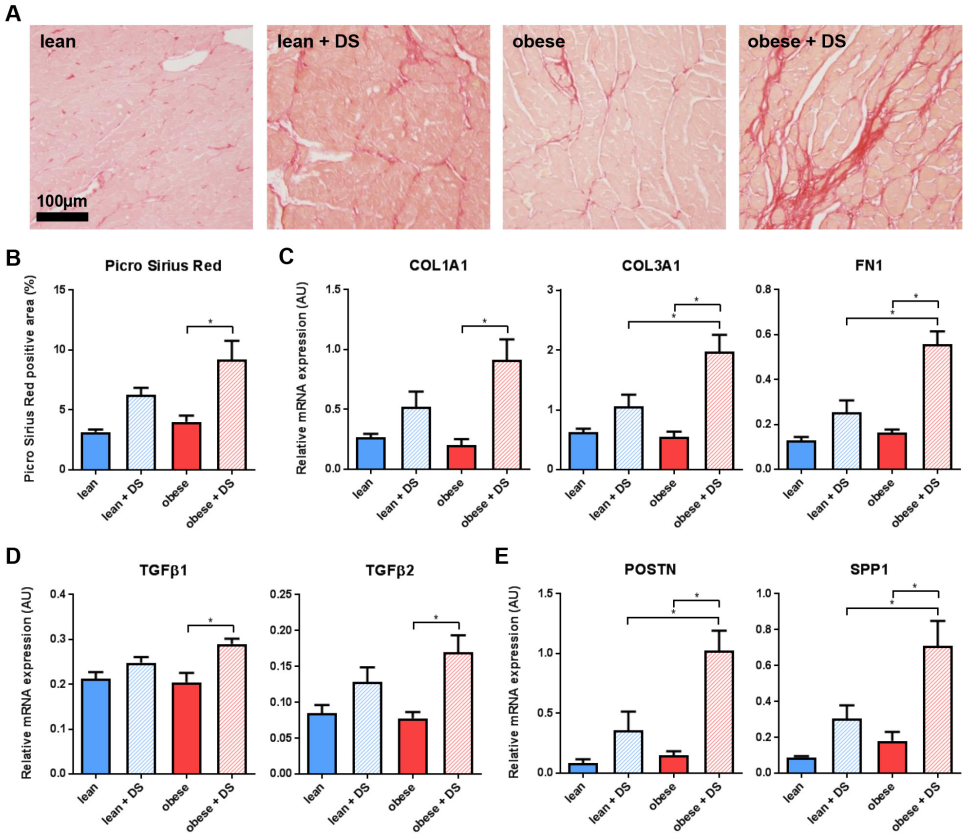

Figure 6: Synergistic effects of obesity and DS on LV TGFβ signaling and fibrosis. (A) Typical examples and **(B)** quantification of histological staining for cardiac collagen deposition (Picrosirius Red). N=6-7, * P<0.05. **(C)** QPCR analysis of cardiac transcription of extracellular matrix components COL1A1, COL3A1, and FN1, **(D)** activators of TGFβ signaling TGFβ1 and TGFβ2, and **(E)** transcriptional targets of TGFβ signaling POSTN and SPP1. N=5-7, * P<0.05.

predominant effect on development of diastolic dysfunction, with no synergy observed between obesity and DS-induced hypertension; (2) obesity also predominantly affected LV hypertrophic remodeling, which was associated with increased fetal gene expression and Ca^{2+}-mediated transcription; (3) capillary rarefaction was absent in all conditions, whereas inflammation and fibrosis occurred in response to DS-induced hypertension, with partial synergy observed if in combination with obesity; and that (4) obesity stimulated enhanced expression of genes involved in FAO, whereas DS treatment led to an overall downregulation of genes involved in oxidative phosphorylation, implying that the comorbidities triggered adverse mitochondrial responses. These findings do not support our initial hypothesis and illustrate important phenotypical differences in comorbidity-induced

cardiac adaptation. Moreover, these observations emphasize the need for thorough and individualized phenotypical characterization of HFpEF patients.[23]

Diastolic dysfunction, or more specifically, impaired active relaxation and reduced LV passive compliance leading to increased LV diastolic pressures, is a phenotypical hallmark of HFpEF.[24, 25] A well-defined echocardiographic parameter to define presence of diastolic dysfunction is the E/e' ratio[17], which was significantly elevated in both placebo- and DS-treated obese rats, compared with their lean counterparts. Similarly, obesity was strongly associated with a lower CO. Interestingly, DS-induced hypertension had no effect on CO and only a minor effect on E/e' ratio. Surprisingly, no functional interaction was observed between the comorbidities. These findings, indicating a relative mild contribution of hypertension on development and progression of diastolic dysfunction, and suggesting a more pronounced causal relation with metabolic derangements, could explain why antihypertensive treatment thus far has not established a major survival benefit in HFpEF patients.[11]

The lower CO in obese rats was principally the result of a lower heart rate, which is consistent with diabetes-induced lowering of resting heart rates[26], while – surprisingly – stroke volume was maintained even when both obesity and DS were present. Stroke volume was likely maintained as a result of the bradycardia-induced increase in diastolic filling time, thereby compensating for the impaired relaxation and the presence of concentric hypertrophy. The latter phenomenon has clinically been associated with an increased risk of morbidity and mortality in HFpEF patients.[27] In the ZSF1 rats, total HW and LVW reached statistical significance only when both comorbidities were present, although variance was individually affected both by obesity and DS. Remarkably, variance in cardiomyocyte cross-sectional area was solely affected by obesity, suggesting that the effect of DS treatment on HW might at least in part be secondary to a cellular hypertrophy-independent process, such as fibrosis. Transcriptional analysis supported this predominant obesity-induced myocardial maladaptation, which generally occurs in the presence of reinitiated fetal gene expression and elevated Ca^{2+}-induced transcription[21, 28]. In that regard, a clear obesity-driven switch from MYH6 to MYH7 was noticed, as well as elevated transcription of RCAN1, a defined target gene of the Ca^{2+}-responsive transcription factor NFAT.[29] The RNAseq data also underscored the notion that diastolic dysfunction-associated hypertrophy can develop in absence of severe cardiac afterload. In the ZSF1 rats, blood pressure- and wall stretch-responsive factor NPPA[30], was exclusively upregulated in DS-treated rats, whereas in placebo-treated obese rats with an apparent absence of elevated wall stretch, hypertrophy

developed. Since NPPA has been demonstrated to inhibit NFAT activation[28], this DS-induced upregulation of NPPA could explain why RCAN1 was not upregulated in DS-treated rats, even though crucial Ca^{2+}-handling genes (ATP1A2, SERCA2A, and PLN) were dysregulated upon DS-induced hypertension. Noteworthy, in none of the hypertrophy-related parameters, positive interaction was observed between hypertension and obesity.

In addition to cardiomyocyte hypertrophy, it has been proposed that HFpEF-associated comorbidities can induce systemic inflammation, leading to endothelial inflammation and oxidative stress, favoring monocyte extravasation, fibrosis, and microvascular rarefaction.[2] Fibrosis is suspected to result from monocyte-induced TGFβ secretion, and to actively contribute to LV stiffening[31], whereas a reduction in capillary density may impair oxygen delivery, limiting systolic and diastolic reserve function[32], yet could also lower NO availability which contributes to passive stiffness and LV hypertrophy via impaired Protein Kinase G activation.[2] In LV sections from HFpEF patients, indeed fibrosis and a lower capillary density were observed[32], but in line with our previous study[13], no capillary rarefaction was observed in any of the ZSF1 rats. From the current study it cannot be excluded that loss of capillaries develops at a later stage of the disease, although these data do suggest that it is not a prerequisite for the development of diastolic dysfunction. Interestingly, even in the absence of capillary rarefaction, a clear inflammatory and fibrotic response was observed. In contrast to the obesity-driven diastolic dysfunction and cardiomyocyte hypertrophy, inflammation and fibrosis predominantly occurred in DS-induced hypertensive rats. It has previously been shown that resident cardiac macrophages can respond to hypertension by activation of pro-inflammatory signaling[33], due to exposure to altered mechanical forces.[34] Additionally, DS-induced activation of mineralocorticoid receptors could also trigger cardiac inflammation and fibrosis, independent of hypertension[30, 35], implying that multiple mechanisms could orchestrate the observed response in the hypertensive rats. In placebo-treated obese rats, no inflammatory or fibrotic responses were observed, suggesting that the increased urinary TBARS excretion in these rats was presumably not derived from vascular and neutrophilic NADPH-induced oxidative stress.[36] Interestingly, obesity did significantly aggravate DS-induced macrophage presence and triggered upregulation of many extracellular matrix components with a TGFβ signature[37, 38], suggesting putative interaction with DS-induced hypertension for this particular aspect of LV adaptation. As obesity and DS-treatment also showed mild interaction in elevation of the systolic blood pressure, it cannot be excluded that the observed increase in inflammation and fibrosis is purely hypertension-driven. These data, however, do illustrate marked comorbidity-dependent phenotypical differences driving development of diastolic dysfunction.

The broad range of our analysis enabled us to dissect how functional differences in cardiac response to obesity-associated aberrations and DS-induced hypertension were reflected by the distinct transcription profiles. By comparing the transcriptome of placebo-treated obese rats with that of placebo-treated lean rats, the most abundant response came from elevated expression of genes encoding enzymes involved in FAO. Although cardiac hypertrophy is associated with decreased FAO and increased glucose metabolism[39], this finding was not completely unexpected considering the diabetic background of these rats.[40] Nonetheless, increased FAO is also evident in HFpEF patients[41], and due to the lower oxygen efficiency compared with glucose metabolism[42], this could result in a lower ATP bioavailability, which can contribute to hampered energy-consuming diastolic relaxation.[43] The increased FAO, which may partly occur in peroxisomes[44], might also be causally related to the observed elevation of oxidative stress. Since peroxisomes lack a respiratory chain, electrons from $FADH_2$ are transferred directly to O_2, generating H_2O_2 and heat.[44] In line with previous studies[45], obesity appeared to induce peroxisomal FAO, as illustrated by higher expression of peroxisomal-specific Acyl-Coenzyme A Oxidase 1 (ACOX1) and Acyl-CoA Dehydrogenase Very Long Chain (ACADVL). The upregulation of CAT in placebo-treated obese rats, which is predominantly involved in peroxisomal H_2O_2 conversion[44], substantiates the putative peroxisomal source of oxidative stress. Strikingly, when transcription profiles of DS-treated rats were compared with that of placebo-treated rats, an overall downregulation of factors involved in oxidative phosphorylation was observed, negatively modulating both fatty acid- and glucose oxidation. Others have shown that downregulation of only a minimal number of genes involved in oxidative phosphorylation could induce mitochondrial dysfunction.[18, 19] Mitochondrial dysfunction is causally related to myocardial cell-death[46, 47], which might explain the effect of DS on sub-endocardial TUNEL labeling. The relation between hypertension and mitochondrial dysfunction is well described.[48, 49] However, the present findings illustrate the adverse effects of two HFpEF comorbidities on energy homeostasis, indicating that in obese rats the mechanisms involved in metabolic derangements, with a putative role in development of diastolic dysfunction, are dependent on the presence or absence of hypertension. These observations emphasize the need for thorough phenotypical characterization of HFpEF patients.[23]

In summary, the present study shows, to our knowledge for the first time, how obesity and hypertension contribute to the development of diastolic dysfunction. Our data show that intrinsic metabolic derangements in ZSF1 rats have the most evident effect on development of diastolic dysfunction. However, from a mitochondrial-, fibrotic-, and inflammatory point of view, the presence of severe hypertension appears to have a major impact on disease

progression. When considering therapeutic interventions, it thus would seem extremely important to anticipate potential pathophysiological differences among HFpEF patients that were thus far grouped together based on the common denominator “preserved EF”. For instance, aiming for a switch from fatty acids towards more oxygen-efficient glucose metabolism, as was previously suggested in HFpEF[50], might provide an opening with promising therapeutic potential in obese patients, but may well be far less effective when applied to HFpEF patients with hypertension-induced mitochondrial dysfunction.

References

1. Borlaug, BA, Paulus, WJ: Heart failure with preserved ejection fraction: pathophysiology, diagnosis, and treatment. *Eur Heart J,* 32**:** 670-679, 2011.
2. Paulus, WJ, Tschope, C: A novel paradigm for heart failure with preserved ejection fraction: comorbidities drive myocardial dysfunction and remodeling through coronary microvascular endothelial inflammation. *J Am Coll Cardiol,* 62**:** 263-271, 2013.
3. Haass, M, Kitzman, DW, Anand, IS, Miller, A, Zile, MR, Massie, BM, Carson, PE: Body mass index and adverse cardiovascular outcomes in heart failure patients with preserved ejection fraction: results from the Irbesartan in Heart Failure with Preserved Ejection Fraction (I-PRESERVE) trial. *Circ Heart Fail,* 4**:** 324-331, 2011.
4. Dhingra, A, Garg, A, Kaur, S, Chopra, S, Batra, JS, Pandey, A, Chaanine, AH, Agarwal, SK: Epidemiology of heart failure with preserved ejection fraction. *Curr Heart Fail Rep,* 11**:** 354-365, 2014.
5. Grobe, JL, Mecca, AP, Mao, H, Katovich, MJ: Chronic angiotensin-(1-7) prevents cardiac fibrosis in DOCA-salt model of hypertension. *Am J Physiol Heart Circ Physiol,* 290**:** H2417-2423, 2006.
6. Allan, A, Fenning, A, Levick, S, Hoey, A, Brown, L: Reversal of cardiac dysfunction by selective ET-A receptor antagonism. *Br J Pharmacol,* 146**:** 846-853, 2005.
7. Barouch, LA, Berkowitz, DE, Harrison, RW, O'Donnell, CP, Hare, JM: Disruption of leptin signaling contributes to cardiac hypertrophy independently of body weight in mice. *Circulation,* 108**:** 754-759, 2003.
8. Dong, F, Zhang, X, Yang, X, Esberg, LB, Yang, H, Zhang, Z, Culver, B, Ren, J: Impaired cardiac contractile function in ventricular myocytes from leptin-deficient ob/ob obese mice. *J Endocrinol,* 188**:** 25-36, 2006.
9. Lindstrom, P: The physiology of obese-hyperglycemic mice [ob/ob mice]. *ScientificWorldJournal,* 7**:** 666-685, 2007.
10. Leggio, M, Lombardi, M, Caldarone, E, Severi, P, D'Emidio, S, Armeni, M, Bravi, V, Bendini, MG, Mazza, A: The relationship between obesity and hypertension: an updated comprehensive overview on vicious twins. *Hypertens Res,* 40**:** 947-963, 2017.
11. Tsioufis, C, Georgiopoulos, G, Oikonomou, D, Thomopoulos, C, Katsiki, N, Kasiakogias, A, Chrysochoou, C, Konstantinidis, D, Kalos, T, Tousoulis, D: Hypertension and Heart Failure with Preserved Ejection Fraction: Connecting the Dots. *Curr Vasc Pharmacol,* 16**:** 15-22, 2017.
12. Hamdani, N, Franssen, C, Lourenco, A, Falcao-Pires, I, Fontoura, D, Leite, S, Plettig, L, Lopez, B, Ottenheijm, CA, Becher, PM, Gonzalez, A, Tschope, C, Diez, J, Linke, WA, Leite-Moreira, AF, Paulus, WJ: Myocardial titin hypophosphorylation importantly contributes to heart failure with preserved ejection fraction in a rat metabolic risk model. *Circ Heart Fail,* 6**:** 1239-1249, 2013.
13. van Dijk, CG, Oosterhuis, NR, Xu, YJ, Brandt, M, Paulus, WJ, van Heerebeek, L, Duncker, DJ, Verhaar, MC, Fontoura, D, Lourenco, AP, Leite-Moreira, AF, Falcao-Pires, I, Joles, JA, Cheng, C: Distinct Endothelial Cell Responses in the Heart and Kidney Microvasculature Characterize the Progression of Heart Failure With Preserved Ejection Fraction in the Obese ZSF1 Rat With Cardiorenal Metabolic Syndrome. *Circ Heart Fail,* 9**:** e002760, 2016.
14. Bongartz, LG, Braam, B, Verhaar, MC, Cramer, MJ, Goldschmeding, R, Gaillard, CA, Doevendans, PA, Joles, JA: Transient nitric oxide reduction induces permanent cardiac systolic dysfunction and worsens kidney damage in rats with chronic kidney disease. *Am J Physiol Regul Integr Comp Physiol,* 298**:** R815-823, 2010.
15. Brandt, MM, Meddens, CA, Louzao-Martinez, L, van den Dungen, NAM, Lansu, NR, Nieuwenhuis, EES, Duncker, DJ, Verhaar, MC, Joles, JA, Mokry, M, Cheng, C: Chromatin Conformation Links Distal Target Genes to CKD Loci. *J Am Soc Nephrol,* 29**:** 462-476, 2018.
16. Love, MI, Huber, W, Anders, S: Moderated estimation of fold change and dispersion for RNA-seq data with DESeq2. *Genome Biol,* 15**:** 550, 2014.
17. Ponikowski, P, Voors, AA, Anker, SD, Bueno, H, Cleland, JG, Coats, AJ, Falk, V, Gonzalez-Juanatey, JR, Harjola, VP, Jankowska, EA, Jessup, M, Linde, C, Nihoyannopoulos, P, Parissis, JT, Pieske, B, Riley, JP, Rosano, GM, Ruilope, LM, Ruschitzka, F, Rutten, FH, van der Meer, P, Authors/Task Force, M, Document, R: 2016 ESC Guidelines for the diagnosis and treatment of acute and chronic heart failure: The Task Force for the diagnosis and treatment of acute and chronic heart failure of the European Society of Cardiology (ESC). Developed with the special contribution of the Heart Failure Association (HFA) of the ESC. *Eur J Heart Fail,* 18**:** 891-975, 2016.

18. Alaynick, WA, Kondo, RP, Xie, W, He, W, Dufour, CR, Downes, M, Jonker, JW, Giles, W, Naviaux, RK, Giguere, V, Evans, RM: ERRgamma directs and maintains the transition to oxidative metabolism in the postnatal heart. *Cell Metab,* 6**:** 13-24, 2007.
19. Arany, Z, He, H, Lin, J, Hoyer, K, Handschin, C, Toka, O, Ahmad, F, Matsui, T, Chin, S, Wu, PH, Rybkin, II, Shelton, JM, Manieri, M, Cinti, S, Schoen, FJ, Bassel-Duby, R, Rosenzweig, A, Ingwall, JS, Spiegelman, BM: Transcriptional coactivator PGC-1 alpha controls the energy state and contractile function of cardiac muscle. *Cell Metab,* 1**:** 259-271, 2005.
20. Prosdocimo, DA, John, JE, Zhang, L, Efraim, ES, Zhang, R, Liao, X, Jain, MK: KLF15 and PPARalpha Cooperate to Regulate Cardiomyocyte Lipid Gene Expression and Oxidation. *PPAR Res,* 2015**:** 201625, 2015.
21. Taegtmeyer, H, Sen, S, Vela, D: Return to the fetal gene program: a suggested metabolic link to gene expression in the heart. *Ann N Y Acad Sci,* 1188**:** 191-198, 2010.
22. Tromp, J, Khan, MA, Klip, IT, Meyer, S, de Boer, RA, Jaarsma, T, Hillege, H, van Veldhuisen, DJ, van der Meer, P, Voors, AA: Biomarker Profiles in Heart Failure Patients With Preserved and Reduced Ejection Fraction. *J Am Heart Assoc,* 6, 2017.
23. Shah, SJ, Kitzman, DW, Borlaug, BA, van Heerebeek, L, Zile, MR, Kass, DA, Paulus, WJ: Phenotype-Specific Treatment of Heart Failure With Preserved Ejection Fraction: A Multiorgan Roadmap. *Circulation,* 134**:** 73-90, 2016.
24. LeWinter, MM, Meyer, M: Mechanisms of diastolic dysfunction in heart failure with a preserved ejection fraction: If it's not one thing it's another. *Circ Heart Fail,* 6**:** 1112-1115, 2013.
25. Zile, MR, Gaasch, WH, Carroll, JD, Feldman, MD, Aurigemma, GP, Schaer, GL, Ghali, JK, Liebson, PR: Heart failure with a normal ejection fraction: is measurement of diastolic function necessary to make the diagnosis of diastolic heart failure? *Circulation,* 104**:** 779-782, 2001.
26. Malone, MA, Schocken, DD, Hanna, SK, Liang, X, Malone, JI: Diabetes-induced bradycardia is an intrinsic metabolic defect reversed by carnitine. *Metabolism,* 56**:** 1118-1123, 2007.
27. Zile, MR, Gottdiener, JS, Hetzel, SJ, McMurray, JJ, Komajda, M, McKelvie, R, Baicu, CF, Massie, BM, Carson, PE, Investigators, IP: Prevalence and significance of alterations in cardiac structure and function in patients with heart failure and a preserved ejection fraction. *Circulation,* 124**:** 2491-2501, 2011.
28. Nakamura, M, Sadoshima, J: Mechanisms of physiological and pathological cardiac hypertrophy. *Nat Rev Cardiol,* 15**:** 387-407, 2018.
29. Wu, H, Kao, SC, Barrientos, T, Baldwin, SH, Olson, EN, Crabtree, GR, Zhou, B, Chang, CP: Down syndrome critical region-1 is a transcriptional target of nuclear factor of activated T cells-c1 within the endocardium during heart development. *J Biol Chem,* 282**:** 30673-30679, 2007.
30. De Young, MB, Keller, JC, Graham, RM, Wildey, GM: Brefeldin A defines distinct pathways for atrial natriuretic factor secretion in neonatal rat atrial and ventricular myocytes. *Circ Res,* 74**:** 33-40, 1994.
31. Yamamoto, K, Masuyama, T, Sakata, Y, Nishikawa, N, Mano, T, Yoshida, J, Miwa, T, Sugawara, M, Yamaguchi, Y, Ookawara, T, Suzuki, K, Hori, M: Myocardial stiffness is determined by ventricular fibrosis, but not by compensatory or excessive hypertrophy in hypertensive heart. *Cardiovasc Res,* 55**:** 76-82, 2002.
32. Mohammed, SF, Hussain, S, Mirzoyev, SA, Edwards, WD, Maleszewski, JJ, Redfield, MM: Coronary microvascular rarefaction and myocardial fibrosis in heart failure with preserved ejection fraction. *Circulation,* 131**:** 550-559, 2015.
33. Wehner, S, Buchholz, BM, Schuchtrup, S, Rocke, A, Schaefer, N, Lysson, M, Hirner, A, Kalff, JC: Mechanical strain and TLR4 synergistically induce cell-specific inflammatory gene expression in intestinal smooth muscle cells and peritoneal macrophages. *Am J Physiol Gastrointest Liver Physiol,* 299**:** G1187-1197, 2010.
34. Solomon, SD, Biering-Sorensen, T: LA Strain When Ejection Fraction Is Preserved: A New Measure of Diastolic Function? *JACC Cardiovasc Imaging,* 10**:** 744-746, 2017.
35. Rickard, AJ, Morgan, J, Bienvenu, LA, Fletcher, EK, Cranston, GA, Shen, JZ, Reichelt, ME, Delbridge, LM, Young, MJ: Cardiomyocyte mineralocorticoid receptors are essential for deoxycorticosterone/salt-mediated inflammation and cardiac fibrosis. *Hypertension,* 60**:** 1443-1450, 2012.
36. Murdoch, CE, Chaubey, S, Zeng, L, Yu, B, Ivetic, A, Walker, SJ, Vanhoutte, D, Heymans, S, Grieve, DJ, Cave, AC, Brewer, AC, Zhang, M, Shah, AM: Endothelial NADPH oxidase-2 promotes interstitial cardiac fibrosis and diastolic dysfunction through proinflammatory effects and endothelial-mesenchymal transition. *J Am Coll Cardiol,* 63**:** 2734-2741, 2014.
37. Khalil, H, Kanisicak, O, Prasad, V, Correll, RN, Fu, X, Schips, T, Vagnozzi, RJ, Liu, R, Huynh, T, Lee, SJ, Karch, J, Molkentin, JD: Fibroblast-specific TGF-beta-Smad2/3 signaling underlies cardiac fibrosis. *J Clin Invest,* 127**:** 3770-3783, 2017.

38. Zahradka, P: Novel role for osteopontin in cardiac fibrosis. *Circ Res,* 102**:** 270-272, 2008.
39. Kolwicz, SC, Jr., Tian, R: Glucose metabolism and cardiac hypertrophy. *Cardiovasc Res,* 90**:** 194-201, 2011.
40. Abel, ED: Free fatty acid oxidation in insulin resistance and obesity. *Heart Metab,* 48**:** 5-10, 2010.
41. De Jong, KA, Lopaschuk, GD: Complex Energy Metabolic Changes in Heart Failure With Preserved Ejection Fraction and Heart Failure With Reduced Ejection Fraction. *Can J Cardiol,* 33**:** 860-871, 2017.
42. Fillmore, N, Mori, J, Lopaschuk, GD: Mitochondrial fatty acid oxidation alterations in heart failure, ischaemic heart disease and diabetic cardiomyopathy. *Br J Pharmacol,* 171**:** 2080-2090, 2014.
43. Pouleur, H: Diastolic dysfunction and myocardial energetics. *Eur Heart J,* 11 Suppl C**:** 30-34, 1990.
44. Lodhi, IJ, Semenkovich, CF: Peroxisomes: a nexus for lipid metabolism and cellular signaling. *Cell Metab,* 19**:** 380-392, 2014.
45. Thomassen, MS, Norseth, J, Christiansen, EN: Long-term effects of high-fat diets on peroxisomal beta-oxidation in male and female rats. *Lipids,* 20**:** 668-674, 1985.
46. Siwik, DA, Tzortzis, JD, Pimental, DR, Chang, DL, Pagano, PJ, Singh, K, Sawyer, DB, Colucci, WS: Inhibition of copper-zinc superoxide dismutase induces cell growth, hypertrophic phenotype, and apoptosis in neonatal rat cardiac myocytes in vitro. *Circ Res,* 85**:** 147-153, 1999.
47. Green, DR, Reed, JC: Mitochondria and apoptosis. *Science,* 281**:** 1309-1312, 1998.
48. Ventura-Clapier, R, Garnier, A, Veksler, V: Energy metabolism in heart failure. *J Physiol,* 555**:** 1-13, 2004.
49. Eirin, A, Lerman, A, Lerman, LO: Mitochondrial injury and dysfunction in hypertension-induced cardiac damage. *Eur Heart J,* 35**:** 3258-3266, 2014.
50. Lam, CSP, Voors, AA, de Boer, RA, Solomon, SD, van Veldhuisen, DJ: Heart failure with preserved ejection fraction: from mechanisms to therapies. *Eur Heart J,* 39**:** 2780-2792, 2018.

Supplemental data

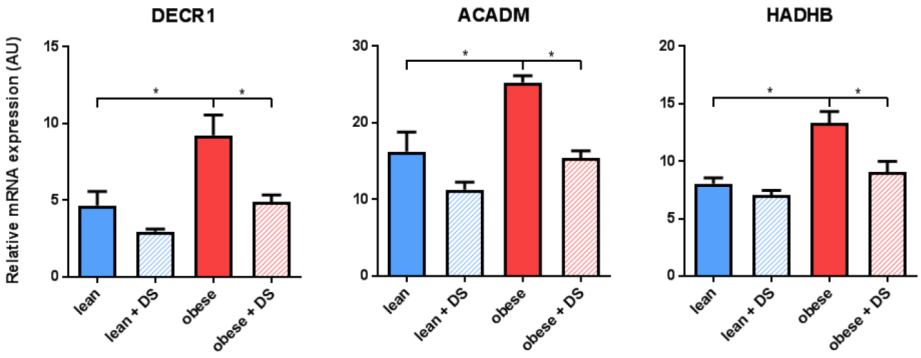

Supplemental Figure 1: Transcription of KLF15 target genes. (A) QPCR results showing expression levels of KLF15 targets DECR1, **(B)** ACADM, and **(C)** HADHB. N=5-7, * P<0.05.

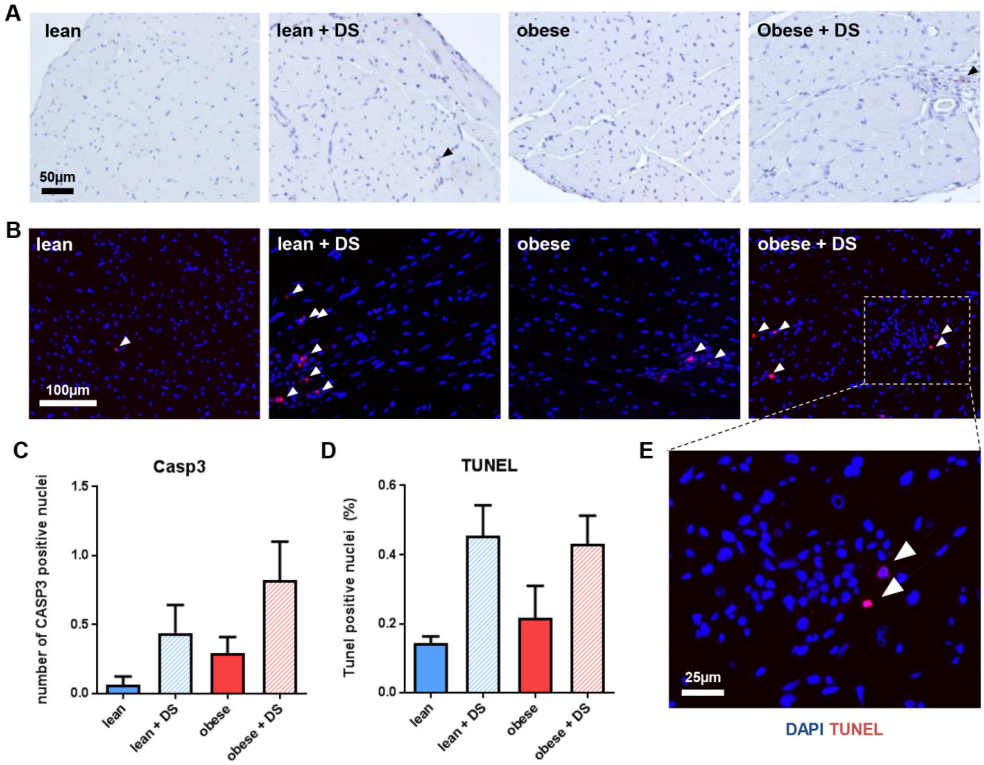

Supplemental Figure 2: Analysis of apoptosis by immunostaining. (A) Typical examples of histological analysis of LV early apoptosis (activated Caspase3) and **(B)** late apoptosis (TUNEL). Positively labeled cells are depicted with an arrowhead. **(C)** Quantification of histological staining for LV early (activated Caspase3) and **(D)** late (TUNEL) apoptosis. N=4-7. **(E)** Magnified visualization of immunological TUNEL labeling in DS-treated obese rats, illustrative for the observed DS-induced increase in apoptosis seen in regions with high cellular density.

Supplemental Tables can be downloaded from:
https://onlinelibrary.wiley.com/action/downloadSupplement?doi=10.1111%2Fjcmm.14542&file=jcmm14542-sup-0001-AppendixS1.docx

Chapter 6

Additional candidate genes for human atherosclerotic disease identified by annotation based on chromatin organization

Saskia Haitjema*, Claartje A. Meddens*, Sander W. van der Laan[1], Daniel Kofink, Magdalena Harakalova, Vinicius Tragante, Hassan Foroughi Asl, Jessica van Setten, Maarten M. Brandt, Joshua C. Bis, Christopher O'Donnell on behalf of the CHARGE Consortium, the METASTROKE Group of the International Stroke Genetics Consortium, Caroline Cheng, Ivana Isgum, Imo E. Hoefer, Johannes Waltenberger, Erik Biessen, J. Wouter Jukema, Pieter A.F.M. Doevendans, Edward E.S. Nieuwenhuis, Jeanette Erdmann, Johan L. M. Björkegren, Gerard Pasterkamp, Folkert W. Asselbergs, Hester M. den Ruijter, Michal Mokry. (* Authors contributed equally)

Circulation: Cardiovascular Genetics, 2017; PMID: 28320757

Abstract

As genome-wide association efforts, such as CARDIoGRAM and METASTROKE, are ongoing to reveal susceptibility loci for their underlying disease: atherosclerotic disease, identification of candidate genes explaining the associations of these loci has proven the main challenge. Many disease susceptibility loci co-localize with DNA regulatory elements, which influence gene expression through chromatin interactions. Therefore, the target genes of these regulatory elements can be considered candidate genes. Applying these biological principles, we used an alternative approach to annotate susceptibility loci and identify candidate genes for human atherosclerotic disease based on circular chromosome conformation capture followed by sequencing (4C-seq).In human monocytes and coronary endothelial cells we generated 63 chromatin interaction datasets for 37 active DNA regulatory elements that co-localize with known susceptibility loci for coronary artery disease (CARDIoGRAMplusC4D) and large artery stroke (METASTROKE). By 4C-seq we identified a physical 3D interaction with 326 candidate genes expressed in at least one of these cell types, of which 294 have not been reported before. We highlight 16 genes based on expression quantitative trait loci. Our findings provide additional candidate-gene annotation for 37 disease susceptibility loci for human atherosclerotic disease that are of potential interest to better understand the complex pathophysiology of cardiovascular diseases.

Introduction

Atherosclerosis is a chronic inflammatory disease of the lipid-rich vascular wall that underlies many cardiovascular diseases (CVD).[1] A large part of the disease burden of atherosclerosis can be traced back to coronary artery disease (CAD) and large artery stroke (LAS). Genome-wide association studies (GWAS) have helped to unravel the complex genomic background of these diseases, currently explaining about 10% of heritability.[2, 3] The current approach is to annotate a novel susceptibility locus with the gene at the nearest genomic position. Some alternative strategies also take into account gene expression or protein-protein interactions.[4, 5] A recent effort employing these bioinformatics-based approaches resulted in 98 new candidate genes for CAD.[6] In the last few years, the evidence that variants identified by GWAS also contribute to the disease pathogenesis by affecting the regulatory DNA sequences they reside in is growing.[7-9] These genetic variants may affect the activity of the DNA regulatory elements (DRE) and, under specific circumstances, lead to dysregulation of gene expression. This is mediated by long range 3D chromatin-chromatin interactions where the regulated candidate genes can be located up to ~1 MB away[10-12] – a distance much larger than is normally used to annotate candidate genes in GWAS. These candidate genes can be identified by capturing the physical

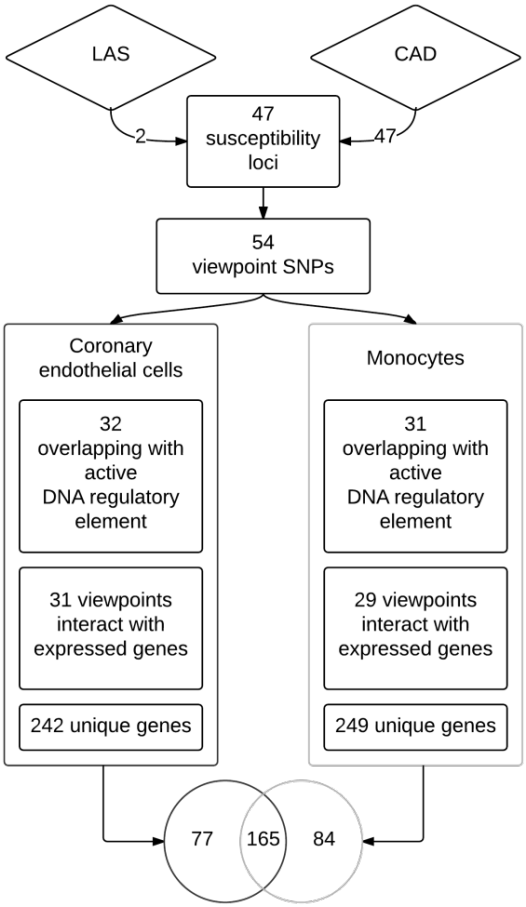

Figure 1 Flowchart of identification of candidate genes. Susceptibility loci indicates single nucleotide polymorphisms (SNPs) associated with risk of disease in METASTROKE and CARDIoGRAM. Viewpoint SNPs indicates SNPs used as focus point for primer design of the 4C experiment. CAD indicates coronary artery disease and LAS indicates large artery stroke.

chromatin-chromatin interaction between a known disease susceptibility locus and the promoter of the gene(s) it presumably regulates.[13] Here we systematically apply this principle (study design is summarized in Figure 1) to variants identified by large meta-analyses of GWAS for CAD and LAS; altogether assaying 47 previously identifiedsusceptibility loci.[2, 3] Atherosclerotic disease starts in the endothelial lining of the affected arteries and involves attraction and proliferation of monocytes.[14] Therefore, we studied 37 loci that co-localize with active DRE in human monocytes and/or in cardiac endothelial cells. We used circular chromosome conformation capture sequencing (4C-seq) to identify candidate genes based on their physical interaction with one of the active DRE.

Methods

Cell culture

Primary commercially available human cardiac endothelial cells (CEC) that were isolated by enzymatic detachment (Lonza Clonetics™) were cultured in RPMI-1640 with 10% FCS and standard supplements. Cells were harvested for 4C template preparation by trypsinisation at 60-80% confluence.

Monocyte isolation

Human peripheral blood was collected from a healthy donor in sodium-heparin tubes. Peripheral Blood Mononuclear Cells (PBMCs) were isolated by Ficoll-Paque gradient centrifugation. PMBCs were incubated with magnetic CD14+-microbeads (Milteny, order nr. 130-050-201) according to manufacturer's manual. Thereafter cells were magnetically separated by the AutoMACS™ Separator, the positive fraction (monocytes) was used for 4C template preparation.

Circular Chromosome Conformation Capture-Template preparation

The 4C template was prepared as previously described[13]. Summarized, $10x10^6$ cells were used per cell type (monocytes and CEC). Cells were crosslinked in 2% formaldehyde. After chromatin isolation, the chromatin was digested with *DpnII* (NEB, # R0543L). Digestion was stopped through heat inactivation of the restriction enzyme. Samples were diluted and ligated by T4 DNA ligase. The second digestion was carried out with CviQI (NEB, #R069S) and inactivated by phenol:chloroform extraction. The chromatin was diluted, for the final T4 ligation and the chromatin was purified. The quality of digestion and ligation was assessed on agarose gels.

Viewpoint selection and primer design

All SNPs from table 1 and 2 and the young-CAD SNP (rs16986953) from the CARDIoGRAMplusC4D paper[2] (n=47) and the two replicated SNPs (rs2383207 and rs2107595) from METASTROKE[3] were considered for viewpoint design (Supplemental Table 8). When the SNPs within the susceptibility locus were less than 15,000 bp apart (e.g. rs12740374, rs602633 and rs599839 in the *SORT1* region), only one SNP was selected as a viewpoint. Susceptibility loci that overlapped with active DRE were identified through FAIRE, the presence of H3K4Me1, H3K4Me3, H3K27Ac, H3K4Me2 or H3K9Ac, EP300 or CTCF binding sites or DNase hypersensitivity sites (Supplemental Table 9). DRE falling within the susceptibility locus coordinates were considered overlapping with the susceptibility locus. The primers were designed as was described previously.[13] Primer sequences are listed in Supplemental Table 8. In summary, primers were designed in a window of 5 kb up- and downstream from the associated SNP. Forward and reverse primers were designed at least 300 bp apart. Forward (reading) primers were designed on top of the first restriction enzyme site. The reverse (non-reading) primer was designed close to (max 100bp away from) the second restriction enzyme site. In case no primer pair could be designed within the initial window, the window was extended 5 kb up- and downstream (n=8). In the case of rs1561198 this did not result in a suitable primer, so a primer pair that was 299bp apart was selected for this viewpoint.

Circular Chromosome Conformation Capture- Sequencing library preparation

4C-sequencing library preparation was performed as described previously[13], with minor adaptations in order to make the protocol compatible with the large number of viewpoints: the PCR of 4C template was performed with 600 ng (monocytes) or 1,6 µg (coronary endothelial cells) of 4C template per reaction. 8 to 10 primer pairs were multiplexed in the initial PCR reaction (primer sequences are listed in Supplemental Table 8). Primers pairs were pooled according to primer efficiency (based on intensity on gel electrophoresis signal after PCR on test template). PCR products were purified after an initial PCR reaction of 6 cycles (reaction volume = 200 µL) and divided among 8-10 PCR reactions containing single primer pairs for another 26 cycles (reaction volume = 25 µL). Thereafter, PCR products derived from the same cells were pooled in equimolar amounts and a final 6 cycle PCR reaction containing 20 ng of pooled PCR product (reaction volume = 100 µL) was performed with primers that contained sequencing adaptor sequences. All fragments >700bp were removed using size selection on a 1% agarose gel follow by gel extraction of the selected products (Qiagen, #28704). Quality measures for the 4C library preparation and sequencing can be found in Supplemental Figure 1.

Sequencing

Libraries were sequenced using the HiSeq2500 platform (Illumina), according to the manufacturer's protocol, producing 50 bp single end reads.

Data analysis

The raw sequencing reads were de-multiplexed based on viewpoint specific primer sequences. Reads were then trimmed to 16 bases and mapped to an *in silico* generated library of fragends (fragment ends) neighboring all *DpnII* sites in human genome (NCBI37/hg19), using the custom Perl scripts. No mismatches were allowed during the mapping and the reads mapping to only one possible fragend were used for further analysis.

Identification of the interacting genes

First, we calculated the number of covered fragends within a running window of *k* fragends throughout the whole chromosome where the viewpoint is located. The *k* was set separately for every viewpoint so it contains on average 20 covered fragends in the area around the viewpoint (+/- 100kb). Next, we compared the number of covered fragends in each running window to the random distribution. The windows with significantly higher number of covered fragends compared to random distribution ($p<10^{-8}$ based on binominal cumulative distribution function; R *pbinom*) were considered as significant 4C-seq signal. The following criteria were defined for the identification of the candidate genes; i) the Transcriptional Start Site (TSS) co-localizes with a significant 4C-seq signal ($P<10^{-8}$) within 5 kbp; ii) the susceptibility variant or other variant in linkage disequilibrium (LD) co-localizes with a DNA regulatory element identified though FAIRE, the presence of H3K4Me1, H3K4Me3, H3K27Ac, H3K4Me2 or H3K9Ac, EP300 or CTCF binding sites or DNase hypersensitivity sites (Supplemental Table 9) in the cell type from which the 4C-seq signal originated and iii) the gene is expressed (RPKM > 0.5) in the assayed cell type.

Identification of gene expression

For monocyte expression, data from the ENCODE database were used (Supplemental Table 10).[15] For coronary endothelial cell expression, HMVECs (Lonza) were cultured on gelatine coated plates in EGM2-MV (Lonza) supplemented with penicillin and streptomycin. Subsequently, HMVECs were cultured for 20 hours in low serum medium (EBM + 0.5% FCS), followed by cell lysis and RNA isolation using the RNeasy isolation kit (Qiagen). Polyadenylated mRNA was isolated using Poly(A) Beads (NEXTflex). Sequencing libraries were made using the Rapid Directional RNA-Seq Kit (NEXTflex) and sequenced on Illumina NextSeq500 to produce single-end 75 base long reads (Utrecht Sequencing

Facility). Reads were aligned to the human reference genome GRCh37 using STAR version2.4.2a[16]. Read groups were added to the BAM files with Picard's AddOrReplaceReadGroups (v1.98). The BAM files are sorted with Sambamba v0.4.5 and transcript abundances are quantified with HTSeq-count version 0.6.1p1[17] using the union mode. Subsequently, reads per kilobase of transcript per million reads sequenced (RPKM's) are calculated with edgeR's rpkm() function.[18]

Pathway analysis

The interacting genes (with and without expressed CARDIoGRAMplusC4D/METASTROKE genes) were analyzed using QIAGEN's Ingenuity Pathway Analysis (IPA, 2015 winter version, QIAGEN Redwood City, www.qiagen.com/ingenuity). We used IPA to identify canonical biological pathways within the Ingenuity Knowledge Base to which the interacting genes were mapped. Limits were set to only direct relationships that were experimentally observed in humans. We performed six rounds of pathway analysis, three in each of the cell types: one with only CARDIoGRAMplusC4D/METASTROKE genes that were expressed in the cell type, one with the CARDIoGRAMplusC4D/METASTROKE genes supplemented by the newly identified genes and one with the novel genes only.

Tracks and plots

All tracks were accessed from the UCSC browser (hg19) (http://genome.ucsc.edu/). Regional plots were generated using LocusZoom version 1.3.[19]

Gene-based tests

Data for CAD were downloaded from the CARDIoGRAMplusC4D website (http://www.cardiogramplusc4d.org). We obtained summary statistics from GWAS on body mass index (BMI), blood lipids including LDL, HDL, total cholesterol and triglycerides, systolic and diastolic blood pressure, coronary calcification, fasting glucose, smoking behavior, and type 2 diabetes from public online resources and data on intima-media thickness and plaque-presence via data request (Supplemental Table 11). We used a VErsatile Gene-based Association Study (VEGAS) to calculate gene-based association statistics from the summary statistics of each interacting gene for each trait. The details of the methods applied by VEGAS have been described elsewhere.[20] In short, SNPs are mapped to the gene (in and around ±50kb from 5' and 3' gene borders), and using the GWAS p-value a gene-based test statistic is calculated corrected for the underlying population linkage disequilibrium structure. Finally using simulations an empirical gene-based *p*-value of association with the phenotype is calculated per gene. VEGAS results

were considered multiple testing significant if they were $P < 6.97x10^{-6}$ (0.05/22 phenotypes x 326 available genes in VEGAS).

eQTL analysis in STAGE

Within the STAGE study, patients undergoing coronary artery bypass grafting (CABG) surgery were sampled for seven different tissues, namely atherosclerotic arterial wall (AAW), internal mammary artery (IMA), liver, skeletal muscle (SM), subcutaneous fat (SF), visceral fat (VF), and fasting whole blood (WB) for RNA and DNA isolation.[21] Patients that were eligible for CABG and had no other severe systemic diseases (e.g. widespread cancer or active systemic inflammatory disease) were included. For quality control in genotyping, SNPs filtered for minor allele frequency MAF < 5%, Hardy-Weinberg equilibrium (HWE) p-value < $1x10^{-6}$, and call rate of 100%. Imputation was carried out using IMPUTE2 with 1000 Genomes EUR as the reference.[22] Quality control for imputed genotypes used additionally an IMPUTE2 INFO score filter < 0.3. After QC a total of 5,473,585 SNPs remained. The Ethical committee of the Karolinska Hospital approved the study, and all patients gave written informed consent after the nature and possible consequences of the study were explained. An expression trait was tested for association with each genotyped and imputed SNP using Kruskal-Wallis test and false discovery rate to correct for multiple testing as described before. First, all *cis*-pairs of SNPs within 50kb of the transcription start or end site for each gene were identified. Next, *cis* SNP-gene pairs were tested for association in all seven STAGE tissues using kruX.[23] The p-value for eQTL inclusion in kruX was set at 0.05. Finally, an empirical FDR estimate for each eQTL-gene pair was calculated using ten permutations by shuffling patient IDs on genotype data. As a result, the most significant eQTL-gene association in each tissue was reported.

eQTL analysis in Haploreg

Data on eQTL in healthy individuals were extracted from Haploreg version 4.1 (http://www.broadinstitute.org/mammals/haploreg/haploreg.php). The viewpoint SNPs and all SNPs in LD ($r^2 > 0.8$) were used as input. From the output, for each interacting gene, the most significant eQTL within each tissue was extracted.

eQTL analysis in CTMM circulating cells

CTMM circulating cells is a Dutch cohort from four different hospitals comprising of 714 patients undergoing coronary angiography of whom blood was stored. Monocytes were isolated by density centrifugation followed by positive magnetic bead isolation (CD14) and expression was measured using the Illumina humanHT-12 v3 Gene Expression BeadChip

Array. After removal of samples with a median intensity of <50, 370 patients were included in the analysis. The data were quantile normalized and and log2 transformed using the lumi R package.[24] Genotyping was performed using a customized Affymetrix Axiom Tx array containing 767,203 genetic markers. Community standard quality control was performed, filtering out samples with missingness >5%, outlying heterozygosity (± 4SD from the cohort mean) or inconsistent sex. Samples of non-European descent or those that were out of Hardy-Weinberg equilibrium ($p<5x10^{-5}$) were removed. In total, 622 were used in the current analysis. Untyped variants were imputed using a combined reference panel of the 1000 Genomes Project[25] and Genome of the Netherlands[26] totaling more than 90 million genetic variants across the genome. We used the software packages SHAPEIT[27] for phasing and IMPUTE2[22] for imputation. Prior to *cis*-eQTL analysis we filtered the imputed genotype data from CTMM based on MAF > 0.5%, HWE P > $1x10^{-6}$, Info-metric > 0.9, and only focused on those variants in LD (r2 >= 0.8) with the CAD associated variants. We then used fastQTL (v2.184)[28] to perform I-eQTL analyses using a fixed range (based on the 4C interactions) around each probeID available on the expression array.

Mouse knockout models

Murine gene names were mapped to the genes as follows. First, a custom data file was downloaded from the HUGO Gene Nomenclature Committee (http://www.genenames.org/cgi-bin/download) including the Approved gene name and the Mouse Genome Database ID from the Mouse Genome Informatics database and a file containing all available phenotypic information for all knockout mice was downloaded from MGI (ftp://ftp.informatics.jax.org/pub/reports/index.html#pheno). Next, for all approved gene names of genes identified through 4C-seq, the mouse phenotypes were looked up by linking the MGI IDs. If no linkage could be made for the MGI ID, this was coded as no available mouse model. If a mouse model was available, but no phenotype was found, this was coded as no available phenotype. If a mouse model was specifically coded as not showing any phenotype upon knockout, this was coded as a gene not resulting in any phenotype. Murine cardiovascular phenotypes were defined as a phenotype resulting in any of the following: impaired blood coagulation or abnormal platelets, abnormal glucose levels or homeostasis, abnormal vascular morphology, vascular remodeling or arterial differentiation, abnormal blood pressure, abnormal vasoconstriction, vasodilatation or vascular permeability, abnormal stress response of the heart, myocardial infarction, abnormal (circulating) lipid levels, abnormal fat morphology or amount, abnormal body weight, abnormal lipid droplet or fat cell size, abnormal macrophage response or inflammation, abnormal wound healing, arteritis, vasculitis, vascular occlusion or atherosclerosis.

Human knockout models

The interacting genes were extracted from the supplementary tables of the studies of Sulem *et al.* and MacArthur *et al.*.[29, 30] For each of the interacting genes, all SNPs and indels resulting in human functional knockouts were reported.

Drug targets

For the lookup of existing drugs that target any of the candidate genes, we used a custom built drug pipeline that searches for drug-gene interactions using DGIdb, which merged the most known drug-gene interaction databases, such as DrugBank and PharmGKB.[31-33] We removed redundant results using STITCH and WHO's INN.[34, 35] We tested overrepresentation of drug groups according to ATC codes using Fisher exact tests.[36]

Results

4C-seq identifies additional candidate genes

We identified 37 active DNA regulatory elements that co-localize with susceptibility loci for CAD or LAS. Twenty-six were active in both monocytes and coronary endothelial cells, 5 were only active in monocytes and 6 were only active in coronary endothelial cells (Supplemental Table 1). To identify the target genes of these active DRE, we generated 63 4C-seq interaction datasets. We applied the following criteria for the identification of candidate genes: I) the transcriptional start site (TSS) co-localizes with a significant 4C-seq signal ($P<10^{-8}$) within 5kb; II) the susceptibility variant or any other variant in LD ($r^2 \geq 0.8$) co-localizes with an active DRE signal in the cell type from with the 4C-seq signal was obtained and III) the gene is expressed (RPKM > 0.5) in the studied cell type. With this approach, we identified 326 candidate genes (Supplemental Table 1), 77 in human male coronary endothelial cells, 84 in human male monocytes and 165 in both cell types (Figure 1). In total, we identified 294 candidate genes that were not previously reported by the CAD and LAS GWAS (Supplemental Table 1). We replicated 235/242 (97.1%) of the chromatin interactions with expressed genes that were identified in male coronary endothelial cells in female coronary endothelial cells (Supplemental Table 1).

4C-seq identifies candidate genes in novel pathways

We performed cell-type specific pathway analysis of the candidate genes identified by 4C-seq combined with the candidate genes that were previously identified by the GWAS on CAD and LAS (Supplemental Table 2). Notably, these analyses revealed the *Hypoxia signaling in the cardiovascular system* pathway in monocytes (P = 0.01) and the NRF-

mediated oxidative stress response pathway (P = $4.68*10^{-4}$ and P = 0.026 in coronary endothelial cells and monocytes respectively, Supplemental Table 2). These pathways are both involved in the cellular response to oxidative stress. Additionally, the 4C-seq approach revealed *PTEN* (a player in the Hypoxia signaling in the cardiovascular system pathway) as a novel candidate gene (Supplemental Table 1). Although this gene was never reported via previous GWAS annotation, *PTEN* (phosphatase and tensin analog) was found to be a likely candidate gene based on dose-dependently upregulation by statins through higher peroxisome proliferator-activated receptor-gamma (PPAR gamma) activity.[37] A mutation of *PTEN* led to inflammatory plaque characteristics in human atherosclerotic plaque and increased stability of PTEN was found to ameliorate atherosclerosis.[38, 39] Furthermore, *PTEN* shares its upstream transcription regulator ZEB2 with *CDKN2A* and *CDKN2B* (enrichment P of overlap for ZEB2-regulated genes: $3.02x10^{-3}$ in monocytes and $3.06x10^{-3}$ in coronary endothelial cells). We reveal multiple novel pathways related to cardiovascular disease and we now show that *PTEN* physically interacts with a DRE at rs2246833 in monocytes (*P* interaction = $2.36x10^{-10}$).

Expression of identified genes is genotype dependent

DRE exert their function through regulation of gene expression. We explored this mechanism by studying expression quantitative trait loci: the GWAS SNPs (or a SNP in LD; r^2>0.8) that significantly affected the expression of the candidate genes identified by 4C-seq in the studied tissues (Table 1). For the candidate genes identified by 4C-seq in coronary endothelial cells, we performed lookups within eQTL data of atherosclerotic artery wall and internal mammary artery in the STAGE cohort of patients undergoing cardiac bypass surgery. We identified two eQTL (FDR<0.1) in atherosclerotic artery wall (rs9818870: *MRAS* and rs2281727: *SRR*, Supplemental Table 3a). The *SRR* gene, that has not been reported previously, encodes for the serine racemase enzyme that is an endogenous ligand of the glycine site of NDMA receptors in the brain. Blockage of this site was found to prevent stroke damage.[40] Interestingly, a set of twice the number of genes from the same genetic locus that were not identified by 4C-seq as a target gene resulted in no significant eQTL in STAGE. Using the HaploReg tool, we additionally examined expression in aorta, coronary artery and tibial artery tissue and identified another seven eQTL for genes that we identified in coronary endothelial cells (Supplemental Table 3b), of which *ARL3* and *FAM117B* were not reported before. Both genes are poorly studied in the context of cardiovascular disease. Within the *VAMP5-VAMP8-GGCX* locus we replicate rs1561198, that was previously reported to be an eQTL for *GGCX* in mammary artery by the CARDIoGRAMplusC4D

Table 1: Candidate genes identified by 4C-seq in coronary endothelial cells and/or monocytes

Chr	Susceptibility locus	4C-seq viewpoint(s)	Interacting genes	Cell type of identification		eQTL
				CEC	Monocytes	
1	MIA3	rs17464857	*AIDA*	√	√	
			BROX	√	√	
			MARC1	√		
			MIA3	√	√	
			TAF1A	√	√	
1	SORT1	rs12740374	*AMPD2*	√	√	
			ATXN7L2	√	√	
			CYB561D1	√	√	
			GNAI3	√	√	
			GNAT2	√		
			GSTM2	√	√	
			GSTM4	√	√	
			PSMA5	√	√	
			PSRC1	√	√	Monocytes
			SARS	√	√	
			SORT1	√	√	
2	APOB	rs515135	*LDAH*	√	√	
2	VAMP5-VAMP8-GGCX	rs1561198	*GGCX*	√	√	CEC
			C2orf68	√	√	
			ELMOD3	√	√	
			MAT2A	√	√	
			RETSAT	√	√	
			RNF181	√	√	
			TGOLN2	√	√	
			TMEM150A	√	√	
			USP39	√	√	
			VAMP5	√	√	
			VAMP8	√	√	Monocytes
2	WDR12	rs6725887	*CARF*		√	
			FAM117B	√	√	CEC/ Monocytes
			NBEAL1	√	√	CEC
			WDR12	√	√	
3	MRAS	rs9818870	*MRAS*	√	√	CEC
6	ANKS1A	rs12205331	*C6orf106*	√	√	
			RPS10	√	√	
			SNRPC	√	√	
			UHRF1BP1	√	√	
6	PHACTR1	rs9369640, rs12526453	*MYLIP*		√	
			PHACTR1	√	√	CEC
8	LPL	rs264	*INTS10*	√	√	
8	TRIB1	rs2954029	*TRIB1*	√	√	
9	CDKN2BAS	rs1333049, rs3217992, rs2383207	*CDKN2A*	√		

			CDKN2B	√	√	
10	CYP17A1-CNNM2-NT5C2	rs12413409	*ARL3*	√	√	CEC
			USMG5	√	√	Monocytes
10	CNNM2	rs12413409	*BORCS7*	√	√	
			WBP1L	√	√	
10	KIAA1462	rs2505083	*KIAA1462*	√		CEC
10	LIPA	rs11203042, rs2246833	*LIPA*	√	√	CEC/ Monocytes
13	COL4A1-COL4A2	rs4773144	*COL4A1*	√		
			COL4A2	√		
17	RAI1-PEMT-RASD1	rs12936587	*PEMT*	√	√	Monocytes
			RASD1	√	√	Monocytes
17	SMG6	rs2281727	*SRR*	√	√	CEC
			SMG6	√	√	
17	UBE2Z	rs15563	*CALCOCO2*	√	√	Monocytes
			KPNB1		√	
			UBE2Z	√	√	Monocytes
19	LDLR	rs1122608	*C19orf52*		√	
			CARM1		√	
			LDLR		√	
			SMARCA4		√	
			TSPAN16		√	
			YIPF2		√	

* Only genes that have their interacting viewpoint as eQTL or genes with a significant gene-based *P* value ($P < 6.97 \times 10^{-6}$ by gene-based test using VEGAS (corrected for multiple-testing 0.05/22 phenotypes x 326 available genes) are depicted. The full list of genes identified by 4C-seq can be found in Supplemental Table 1. Susceptibility locus indicates name of the locus as given by CARDIoGRAMplusC4D or METASTROKE; viewpoint indicates SNP used as the focus point for the primer design of the 4C experiment; Interacting gene represent genes physically interacting with viewpoint, determined by 4C-seq; Bolded genes indicate genes that have previously been reported by CARDIoGRAMplusC4D or METASTROKE; Chr: chromosome; eQTL: expression quantitative trait locus.

investigators in the ASAP study[41], as an eQTL for *GGCX* in aorta and tibial artery. For genes identified by 4C-seq in monocytes, we performed cis-eQTL analysis in monocytes from 370 patients undergoing coronary angiography for coronary artery atherosclerosis in the CTMM (Center for Translational Molecular Medicine) Circulating Cells cohort.[42] We identified four eQTL (FDR<0.1) of which the genes overlap with genes identified by 4C-seq in monocytes of these patients (rs12740374: *PSRC1*, rs1561198: *VAMP8*, rs2246833: *LIPA*, rs12413409: *USMG5*, Supplemental Table 3c). Previously, the CARDIoGRAMplusC4D investigators also identified rs1561198 as an eQTL for *VAMP8* in lymphoblastoid cells and skin in the MuTHER study.[43] Inclusion of the previously published cardiovascular cohort of Zeller *et al.* revealed five additional genes (Supplemental Table 3d).[44] The SNP that revealed the

strongest association with gene expression of PSRC1 in monocytes of CTMM (rs7528419) is in perfect LD (1.0) with rs12740374 in the *SORT1* region. Interestingly, whereas the minor allele of the latter SNP is known to increase SORT1 expression in liver, we found no such association between rs7528419 and SORT1 expression in monocytes (nominal P = 0.87). In addition, we found an association between higher PSRC1 expression in monocytes with a more severe atherosclerotic phenotype identified by a higher atherosclerotic burden, quantified using the SYNTAX score (P = 0.003). This association with high atherosclerosis burden could not solely be explained by LDL levels, the putative mechanism through which SORT1 expression affects cardiovascular disease phenotypes (P when corrected for circulating LDL levels = 0.01). Expression of PSRC1 in whole blood has previously been associated with cardiovascular disease in an Asian population.[45] Largely because the functional significance of the minor allele of rs12740374 as a transcription factor binding site that increases SORT1 expression directly, no further attention has been given to alternative candidate genes in the *SORT1* region. With our 4C-seq approach in monocytes, we here show first evidence that the expression of PSRC1, a candidate gene in the *SORT1* locus, is genotype-dependent expressed in monocytes and related to the severity of atherosclerosis. This example further supports the implication of our additionally identified candidate genes in cardiovascular disease.

Additional genetic annotation

We further explored current genetic knowledge for the candidate genes identified through 4C-seq (Table 1, Supplemental Table 4-7). First, if the candidate genes are effector genes of the DREs within CVD susceptibility loci, one would expect the genes to be enriched for (common) variants associated with CVD. Using the VEGAS algorithm, we concatenated GWAS p-values of all single-nucleotide polymorphisms (SNPs) in or within 50kb of a gene into a p-value for that particular gene. This way, we studied the genes identified by 4C-seq in published and unpublished GWAS data studying a total of 22 traits, either surrogate markers of atherosclerosis or known risk factors for cardiovascular disease (Supplemental Table 4). Of all 326 candidate genes, 33 showed a significant association ($P < 0.05/(22x326) = 6.97x10^{-6}$) with coronary artery disease in the CARDIoGRAMplusC4D GWAS and 149 were nominally associated with coronary artery disease in the CARDIoGRAMplusC4D GWAS (significant enrichment, 149/326: binomial $P = 2.9 \times 10^{-102}$). Additionally, we found 7 genes that were significantly associated with BMI in GIANT and 29 genes that were significantly associated with at least one lipid trait in GLGC. Second, we annotated the prioritized interacting genes from our 4C-seq experiment with phenotypic information of mouse models within the Mouse Genome Informatics database (MGI,

www.informatics.jax.org). We found murine phenotypic information on 144 mouse homologues (Supplemental Table 5). Knockout of 67 of them resulted in a phenotype related to cardiovascular disease (significant enrichment, 67/144: binomial $P = 1.36 \times 10^{-47}$), such as abnormal blood vessel morphology (*Col4a1, Cxcl12, Epor, Shc1, Tcf7l1*), altered circulating fatty acid levels (*Csf2, Kdm3a, Ldlr, Lipa, Pten*) and impaired vascular contractility (*Acta2*). Human variants in *ACTA2* are associated with early onset stroke and MI.[46] Knockout of two candidate gene murine homologues affected development of atherosclerotic lesions, namely *Ldlr* (accelerated development of atherosclerosis) and *Shc1* (resistance to diet-induced atherosclerosis). The p66 isoform of human SHC1 is implicated in reactive oxygen species generation and its knockdown in endothelial cells of obese mice attenuated production of these radicals and of fatty acids oxidation.[47] Third, we investigated the biological effect of human knockout variation of the candidate genes to study druggability. We queried two datasets of available information on SNPs and insertion/deletion variants that cause human functional knockouts.[29, 30] We found human knockouts, caused by nonsense, splice or frameshift variants, for 89 candidate genes (Supplemental Table 6). Fourth, using a custom-built drug discovery pipeline, we found available compounds to target 50 of the candidate genes (Supplemental Table 7a). These drugs showed a relative overrepresentation for usage as immunomodulating agents ($P = 0.012$ in coronary endothelial cells, $P < 0.001$ in monocytes) (Supplemental Table 7b). Together, these findings provide further evidence that by using the 4C-seq method we identified additional candidate target genes for human atherosclerotic disease.

Discussion

Based on 3D chromatin-chromatin interactions with DNA regulatory elements that co-localize with previously identified susceptibility loci, we present 294 additional candidate genes for CAD and LAS that are of potential interest in the pathophysiology of human atherosclerotic disease. This study is the first to systematically study the human chromatin interactions of the CARDIoGRAMplusC4D and METASTROKE loci. Many of the additional genes have not been implicated in atherosclerosis before. Our approach, from a DNA regulatory point of view, complements conventional methods for candidate gene identification of GWAS susceptibility, can help further unravel diseases with a complex genetic background, and pave the way for cell-type specific drug development.

We have highlighted the 4C candidate genes that we could annotate via additional analyses and that therefore have known or foreseeable effects on cardiovascular disease. Based on

tissue-specific pathway analyses, we highlighted *PTEN* that is known to be upregulated by statins and to possess effects on atherosclerosis.[37-39] Furthermore, based on eQTL studies, we identified *SRR*, the effect of which was previously implicated in stroke[40], and *USMG5*, that was previously associated with white matter hyperintensities in the brain.[48] Of special interest is the finding of an alternative mechanism by which the susceptibility locus that contains rs7528419 (*SORT1* region) may exert its effect. Using 4C-sequencing we identified a physical interaction between an active regulatory element that overlaps rs7528419 and *PSRC1* in monocytes. Moreover, we found an association between rs7528419 and the expression of PSRC1 in monocytes and an association between PSRC1 expression and atherosclerosis severity. This association was independent of LDL levels, which is the putative mechanism of rs12740374, a SNP in perfect LD (1.0) with rs7528419 that was previously found to increase SORT1 expression in liver.

Mapping the SNPs that identify susceptibility loci in GWAS to genes that affect a complex disease, such as cardiovascular disease, is a challenging task. By annotating the locus with the linearly closest gene, the 3D conformation of chromatin is inadvertently not taken into account. Many of the additional candidate genes we report are located outside the GWAS susceptibility loci. Using 5C (chromosome conformation capture carbon copy) the importance of studying 3D interactions has been highlighted previously; in a sample of 628 TSS from the ENCODE project only 7% of the over 1000 long-range looping interactions were with the nearest gene.[11] In a previous effort to identify candidate genes based on DNA regulatory mechanisms, 33 enhancers in the 9p21 locus were scrutinized.[49] Interestingly, the chromatin interaction between the enhancers identified by 3C (chromatin conformation capture) was found to be remodeled upon treatment with interferon-γ in HUVECs. In our 4C-seq experiment, we confirmed the physical chromatin-chromatin interaction between the 9p21 susceptibility locus and several candidate genes, among which interferons, in human coronary endothelial cells and monocytes. However, we found that these genes were not actively expressed in these cell types and therefore did not consider them any further.

There are some limitations to this study. First, there is no consensus about the gold standard approach to analysis of 4C-seq data. For example, we used a conservative cut-off for calling a chromatin-chromatin interaction ($P < 10^{-8}$). Altering this cut-off may result in more candidate genes. However, this likely leads to more false-positive results. We therefore report a quantitative measure for the p-value of the interaction of the DRE with the proposed candidate gene to enable the reader to take these considerations into account when interpreting the data. Second, while 4C-sequencing enables us to look at physical

interactions, these interactions do not necessarily mean that the expression in the studied tissue is in fact regulated by the association locus or even expressed. We therefore decided to only report only genes that are actively expressed in the studied tissues. Furthermore, we found no eQTL association between the SNP of interest and any of the genes in the vicinity of the genes that were identified by 4C-sequencing, indicating that the resolution of the technique is sufficient to distinguish between candidate genes and less relevant genes within a genomic region. A more accurate cell type-specific mapping of susceptibility loci to candidate genes in humans is of paramount importance for the development of specific compounds in the pharmaceutical industry. The genes we identified display only partial overlap between coronary endothelial cells and monocytes. This finding stresses the importance of cell-specific approaches in order to grasp the complex biology of atherosclerotic disease. It also highlights the possibility to develop cell-specific compounds to target atherosclerotic disease. Our results therefore underline the need to investigate cell type-specific 3D chromatin conformation in future functional follow-up of GWAS data.

References

1. Hansson, GK, Libby, P, Tabas, I: Inflammation and plaque vulnerability. *J Intern Med,* 278**:** 483-493, 2015.
2. Consortium, CAD, Deloukas, P, Kanoni, S, Willenborg, C, Farrall, M, Assimes, TL, Thompson, JR, Ingelsson, E, Saleheen, D, Erdmann, J, Goldstein, BA, Stirrups, K, Konig, IR, Cazier, JB, Johansson, A, Hall, AS, Lee, JY, Willer, CJ, Chambers, JC, Esko, T, Folkersen, L, Goel, A, Grundberg, E, Havulinna, AS, Ho, WK, Hopewell, JC, Eriksson, N, Kleber, ME, Kristiansson, K, Lundmark, P, Lyytikainen, LP, Rafelt, S, Shungin, D, Strawbridge, RJ, Thorleifsson, G, Tikkanen, E, Van Zuydam, N, Voight, BF, Waite, LL, Zhang, W, Ziegler, A, Absher, D, Altshuler, D, Balmforth, AJ, Barroso, I, Braund, PS, Burgdorf, C, Claudi-Boehm, S, Cox, D, Dimitriou, M, Do, R, Consortium, D, Consortium, C, Doney, AS, El Mokhtari, N, Eriksson, P, Fischer, K, Fontanillas, P, Franco-Cereceda, A, Gigante, B, Groop, L, Gustafsson, S, Hager, J, Hallmans, G, Han, BG, Hunt, SE, Kang, HM, Illig, T, Kessler, T, Knowles, JW, Kolovou, G, Kuusisto, J, Langenberg, C, Langford, C, Leander, K, Lokki, ML, Lundmark, A, McCarthy, MI, Meisinger, C, Melander, O, Mihailov, E, Maouche, S, Morris, AD, Muller-Nurasyid, M, Mu, TC, Nikus, K, Peden, JF, Rayner, NW, Rasheed, A, Rosinger, S, Rubin, D, Rumpf, MP, Schafer, A, Sivananthan, M, Song, C, Stewart, AF, Tan, ST, Thorgeirsson, G, van der Schoot, CE, Wagner, PJ, Wellcome Trust Case Control, C, Wells, GA, Wild, PS, Yang, TP, Amouyel, P, Arveiler, D, Basart, H, Boehnke, M, Boerwinkle, E, Brambilla, P, Cambien, F, Cupples, AL, de Faire, U, Dehghan, A, Diemert, P, Epstein, SE, Evans, A, Ferrario, MM, Ferrieres, J, Gauguier, D, Go, AS, Goodall, AH, Gudnason, V, Hazen, SL, Holm, H, Iribarren, C, Jang, Y, Kahonen, M, Kee, F, Kim, HS, Klopp, N, Koenig, W, Kratzer, W, Kuulasmaa, K, Laakso, M, Laaksonen, R, Lee, JY, Lind, L, Ouwehand, WH, Parish, S, Park, JE, Pedersen, NL, Peters, A, Quertermous, T, Rader, DJ, Salomaa, V, Schadt, E, Shah, SH, Sinisalo, J, Stark, K, Stefansson, K, Tregouet, DA, Virtamo, J, Wallentin, L, Wareham, N, Zimmermann, ME, Nieminen, MS, Hengstenberg, C, Sandhu, MS, Pastinen, T, Syvanen, AC, Hovingh, GK, Dedoussis, G, Franks, PW, Lehtimaki, T, Metspalu, A, Zalloua, PA, Siegbahn, A, Schreiber, S, Ripatti, S, Blankenberg, SS, Perola, M, Clarke, R, Boehm, BO, O'Donnell, C, Reilly, MP, Marz, W, Collins, R, Kathiresan, S, Hamsten, A, Kooner, JS, Thorsteinsdottir, U, Danesh, J, Palmer, CN, Roberts, R, Watkins, H, Schunkert, H, Samani, NJ: Large-scale association analysis identifies new risk loci for coronary artery disease. *Nat Genet,* 45**:** 25-33, 2013.
3. Traylor, M, Farrall, M, Holliday, EG, Sudlow, C, Hopewell, JC, Cheng, YC, Fornage, M, Ikram, MA, Malik, R, Bevan, S, Thorsteinsdottir, U, Nalls, MA, Longstreth, W, Wiggins, KL, Yadav, S, Parati, EA, Destefano, AL, Worrall, BB, Kittner, SJ, Khan, MS, Reiner, AP, Helgadottir, A, Achterberg, S, Fernandez-Cadenas, I, Abboud, S, Schmidt, R, Walters, M, Chen, WM, Ringelstein, EB, O'Donnell, M, Ho, WK, Pera, J, Lemmens, R, Norrving, B, Higgins, P, Benn, M, Sale, M, Kuhlenbaumer, G, Doney, AS, Vicente, AM, Delavaran, H, Algra, A, Davies, G, Oliveira, SA, Palmer, CN, Deary, I, Schmidt, H, Pandolfo, M, Montaner, J, Carty, C, de Bakker, PI, Kostulas, K, Ferro, JM, van Zuydam, NR, Valdimarsson, E, Nordestgaard, BG, Lindgren, A, Thijs, V, Slowik, A, Saleheen, D, Pare, G, Berger, K, Thorleifsson, G, Australian Stroke Genetics Collaborative, WTCCC, Hofman, A, Mosley, TH, Mitchell, BD, Furie, K, Clarke, R, Levi, C, Seshadri, S, Gschwendtner, A, Boncoraglio, GB, Sharma, P, Bis, JC, Gretarsdottir, S, Psaty, BM, Rothwell, PM, Rosand, J, Meschia, JF, Stefansson, K, Dichgans, M, Markus, HS, International Stroke Genetics, C: Genetic risk factors for ischaemic stroke and its subtypes (the METASTROKE collaboration): a meta-analysis of genome-wide association studies. *Lancet Neurol,* 11**:** 951-962, 2012.
4. Pers, TH, Karjalainen, JM, Chan, Y, Westra, HJ, Wood, AR, Yang, J, Lui, JC, Vedantam, S, Gustafsson, S, Esko, T, Frayling, T, Speliotes, EK, Genetic Investigation of, ATC, Boehnke, M, Raychaudhuri, S, Fehrmann, RS, Hirschhorn, JN, Franke, L: Biological interpretation of genome-wide association studies using predicted gene functions. *Nat Commun,* 6**:** 5890, 2015.
5. Rossin, EJ, Lage, K, Raychaudhuri, S, Xavier, RJ, Tatar, D, Benita, Y, International Inflammatory Bowel Disease Genetics, C, Cotsapas, C, Daly, MJ: Proteins encoded in genomic regions associated with immune-mediated disease physically interact and suggest underlying biology. *PLoS Genet,* 7**:** e1001273, 2011.
6. Braenne, I, Civelek, M, Vilne, B, Di Narzo, A, Johnson, AD, Zhao, Y, Reiz, B, Codoni, V, Webb, TR, Foroughi Asl, H, Hamby, SE, Zeng, L, Tregouet, DA, Hao, K, Topol, EJ, Schadt, EE, Yang, X, Samani, NJ, Bjorkegren, JL, Erdmann, J, Schunkert, H, Lusis, AJ, Leducq Consortium, CADGd: Prediction of Causal Candidate Genes in Coronary Artery Disease Loci. *Arterioscler Thromb Vasc Biol,* 35**:** 2207-2217, 2015.

7. Maurano, MT, Humbert, R, Rynes, E, Thurman, RE, Haugen, E, Wang, H, Reynolds, AP, Sandstrom, R, Qu, H, Brody, J, Shafer, A, Neri, F, Lee, K, Kutyavin, T, Stehling-Sun, S, Johnson, AK, Canfield, TK, Giste, E, Diegel, M, Bates, D, Hansen, RS, Neph, S, Sabo, PJ, Heimfeld, S, Raubitschek, A, Ziegler, S, Cotsapas, C, Sotoodehnia, N, Glass, I, Sunyaev, SR, Kaul, R, Stamatoyannopoulos, JA: Systematic localization of common disease-associated variation in regulatory DNA. *Science,* 337**:** 1190-1195, 2012.
8. Trynka, G, Sandor, C, Han, B, Xu, H, Stranger, BE, Liu, XS, Raychaudhuri, S: Chromatin marks identify critical cell types for fine mapping complex trait variants. *Nat Genet,* 45**:** 124-130, 2013.
9. Mokry, M, Middendorp, S, Wiegerinck, CL, Witte, M, Teunissen, H, Meddens, CA, Cuppen, E, Clevers, H, Nieuwenhuis, EE: Many inflammatory bowel disease risk loci include regions that regulate gene expression in immune cells and the intestinal epithelium. *Gastroenterology,* 146**:** 1040-1047, 2014.
10. de Laat, W, Klous, P, Kooren, J, Noordermeer, D, Palstra, RJ, Simonis, M, Splinter, E, Grosveld, F: Three-dimensional organization of gene expression in erythroid cells. *Curr Top Dev Biol,* 82**:** 117-139, 2008.
11. Sanyal, A, Lajoie, BR, Jain, G, Dekker, J: The long-range interaction landscape of gene promoters. *Nature,* 489**:** 109-113, 2012.
12. Hughes, JR, Roberts, N, McGowan, S, Hay, D, Giannoulatou, E, Lynch, M, De Gobbi, M, Taylor, S, Gibbons, R, Higgs, DR: Analysis of hundreds of cis-regulatory landscapes at high resolution in a single, high-throughput experiment. *Nat Genet,* 46**:** 205-212, 2014.
13. van de Werken, HJ, de Vree, PJ, Splinter, E, Holwerda, SJ, Klous, P, de Wit, E, de Laat, W: 4C technology: protocols and data analysis. *Methods Enzymol,* 513**:** 89-112, 2012.
14. Hansson, GK, Libby, P: The immune response in atherosclerosis: a double-edged sword. *Nat Rev Immunol,* 6**:** 508-519, 2006.
15. Consortium, EP: An integrated encyclopedia of DNA elements in the human genome. *Nature,* 489**:** 57-74, 2012.
16. Dobin, A, Davis, CA, Schlesinger, F, Drenkow, J, Zaleski, C, Jha, S, Batut, P, Chaisson, M, Gingeras, TR: STAR: ultrafast universal RNA-seq aligner. *Bioinformatics,* 29**:** 15-21, 2013.
17. Anders, S, Pyl, PT, Huber, W: HTSeq--a Python framework to work with high-throughput sequencing data. *Bioinformatics,* 31**:** 166-169, 2015.
18. Robinson, MD, McCarthy, DJ, Smyth, GK: edgeR: a Bioconductor package for differential expression analysis of digital gene expression data. *Bioinformatics,* 26**:** 139-140, 2010.
19. Pruim, RJ, Welch, RP, Sanna, S, Teslovich, TM, Chines, PS, Gliedt, TP, Boehnke, M, Abecasis, GR, Willer, CJ: LocusZoom: regional visualization of genome-wide association scan results. *Bioinformatics,* 26**:** 2336-2337, 2010.
20. Liu, JZ, McRae, AF, Nyholt, DR, Medland, SE, Wray, NR, Brown, KM, Investigators, A, Hayward, NK, Montgomery, GW, Visscher, PM, Martin, NG, Macgregor, S: A versatile gene-based test for genome-wide association studies. *Am J Hum Genet,* 87**:** 139-145, 2010.
21. Hagg, S, Skogsberg, J, Lundstrom, J, Noori, P, Nilsson, R, Zhong, H, Maleki, S, Shang, MM, Brinne, B, Bradshaw, M, Bajic, VB, Samnegard, A, Silveira, A, Kaplan, LM, Gigante, B, Leander, K, de Faire, U, Rosfors, S, Lockowandt, U, Liska, J, Konrad, P, Takolander, R, Franco-Cereceda, A, Schadt, EE, Ivert, T, Hamsten, A, Tegner, J, Bjorkegren, J: Multi-organ expression profiling uncovers a gene module in coronary artery disease involving transendothelial migration of leukocytes and LIM domain binding 2: the Stockholm Atherosclerosis Gene Expression (STAGE) study. *PLoS Genet,* 5**:** e1000754, 2009.
22. Howie, BN, Donnelly, P, Marchini, J: A flexible and accurate genotype imputation method for the next generation of genome-wide association studies. *PLoS Genet,* 5**:** e1000529, 2009.
23. Qi, J, Asl, HF, Bjorkegren, J, Michoel, T: kruX: matrix-based non-parametric eQTL discovery. *BMC Bioinformatics,* 15**:** 11, 2014.
24. Du, P, Kibbe, WA, Lin, SM: lumi: a pipeline for processing Illumina microarray. *Bioinformatics,* 24**:** 1547-1548, 2008.
25. Genomes Project, C, Abecasis, GR, Auton, A, Brooks, LD, DePristo, MA, Durbin, RM, Handsaker, RE, Kang, HM, Marth, GT, McVean, GA: An integrated map of genetic variation from 1,092 human genomes. *Nature,* 491**:** 56-65, 2012.
26. Genome of the Netherlands, C: Whole-genome sequence variation, population structure and demographic history of the Dutch population. *Nat Genet,* 46**:** 818-825, 2014.
27. Delaneau, O, Zagury, JF, Marchini, J: Improved whole-chromosome phasing for disease and population genetic studies. *Nat Methods,* 10**:** 5-6, 2013.
28. Ongen, H, Buil, A, Brown, AA, Dermitzakis, ET, Delaneau, O: Fast and efficient QTL mapper for thousands of molecular phenotypes. *Bioinformatics,* 32**:** 1479-1485, 2016.

29. Sulem, P, Helgason, H, Oddson, A, Stefansson, H, Gudjonsson, SA, Zink, F, Hjartarson, E, Sigurdsson, GT, Jonasdottir, A, Jonasdottir, A, Sigurdsson, A, Magnusson, OT, Kong, A, Helgason, A, Holm, H, Thorsteinsdottir, U, Masson, G, Gudbjartsson, DF, Stefansson, K: Identification of a large set of rare complete human knockouts. *Nat Genet,* 47**:** 448-452, 2015.
30. MacArthur, DG, Balasubramanian, S, Frankish, A, Huang, N, Morris, J, Walter, K, Jostins, L, Habegger, L, Pickrell, JK, Montgomery, SB, Albers, CA, Zhang, ZD, Conrad, DF, Lunter, G, Zheng, H, Ayub, Q, DePristo, MA, Banks, E, Hu, M, Handsaker, RE, Rosenfeld, JA, Fromer, M, Jin, M, Mu, XJ, Khurana, E, Ye, K, Kay, M, Saunders, GI, Suner, MM, Hunt, T, Barnes, IH, Amid, C, Carvalho-Silva, DR, Bignell, AH, Snow, C, Yngvadottir, B, Bumpstead, S, Cooper, DN, Xue, Y, Romero, IG, Genomes Project, C, Wang, J, Li, Y, Gibbs, RA, McCarroll, SA, Dermitzakis, ET, Pritchard, JK, Barrett, JC, Harrow, J, Hurles, ME, Gerstein, MB, Tyler-Smith, C: A systematic survey of loss-of-function variants in human protein-coding genes. *Science,* 335**:** 823-828, 2012.
31. Altman, RB: PharmGKB: a logical home for knowledge relating genotype to drug response phenotype. *Nat Genet,* 39**:** 426, 2007.
32. Griffith, M, Griffith, OL, Coffman, AC, Weible, JV, McMichael, JF, Spies, NC, Koval, J, Das, I, Callaway, MB, Eldred, JM, Miller, CA, Subramanian, J, Govindan, R, Kumar, RD, Bose, R, Ding, L, Walker, JR, Larson, DE, Dooling, DJ, Smith, SM, Ley, TJ, Mardis, ER, Wilson, RK: DGIdb: mining the druggable genome. *Nat Methods,* 10**:** 1209-1210, 2013.
33. Knox, C, Law, V, Jewison, T, Liu, P, Ly, S, Frolkis, A, Pon, A, Banco, K, Mak, C, Neveu, V, Djoumbou, Y, Eisner, R, Guo, AC, Wishart, DS: DrugBank 3.0: a comprehensive resource for 'omics' research on drugs. *Nucleic Acids Res,* 39**:** D1035-1041, 2011.
34. Kuhn, M, Szklarczyk, D, Franceschini, A, von Mering, C, Jensen, LJ, Bork, P: STITCH 3: zooming in on protein-chemical interactions. *Nucleic Acids Res,* 40**:** D876-880, 2012.
35. Van Bever, E, Wirtz, VJ, Azermai, M, De Loof, G, Christiaens, T, Nicolas, L, Van Bortel, L, Vander Stichele, R: Operational rules for the implementation of INN prescribing. *Int J Med Inform,* 83**:** 47-56, 2014.
36. Pahor, M, Chrischilles, EA, Guralnik, JM, Brown, SL, Wallace, RB, Carbonin, P: Drug data coding and analysis in epidemiologic studies. *Eur J Epidemiol,* 10**:** 405-411, 1994.
37. Teresi, RE, Planchon, SM, Waite, KA, Eng, C: Regulation of the PTEN promoter by statins and SREBP. *Hum Mol Genet,* 17**:** 919-928, 2008.
38. Muthalagan, E, Ganesh, RN, Sai Chandran, BV, Verma, SK: Phosphatase and tensin analog expression in arterial atherosclerotic lesions. *Indian J Pathol Microbiol,* 57**:** 427-430, 2014.
39. Dai, XY, Cai, Y, Mao, DD, Qi, YF, Tang, C, Xu, Q, Zhu, Y, Xu, MJ, Wang, X: Increased stability of phosphatase and tensin homolog by intermedin leading to scavenger receptor A inhibition of macrophages reduces atherosclerosis in apolipoprotein E-deficient mice. *J Mol Cell Cardiol,* 53**:** 509-520, 2012.
40. De Miranda, J, Santoro, A, Engelender, S, Wolosker, H: Human serine racemase: moleular cloning, genomic organization and functional analysis. *Gene,* 256**:** 183-188, 2000.
41. Folkersen, L, van't Hooft, F, Chernogubova, E, Agardh, HE, Hansson, GK, Hedin, U, Liska, J, Syvanen, AC, Paulsson-Berne, G, Franco-Cereceda, A, Hamsten, A, Gabrielsen, A, Eriksson, P, BiKe, groups, As: Association of genetic risk variants with expression of proximal genes identifies novel susceptibility genes for cardiovascular disease. *Circ Cardiovasc Genet,* 3**:** 365-373, 2010.
42. Hoefer, IE, Sels, JW, Jukema, JW, Bergheanu, S, Biessen, E, McClellan, E, Daemen, M, Doevendans, P, de Groot, P, Hillaert, M, Horsman, S, Ilhan, M, Kuiper, J, Pijls, N, Redekop, K, van der Spek, P, Stubbs, A, van de Veer, E, Waltenberger, J, van Zonneveld, AJ, Pasterkamp, G: Circulating cells as predictors of secondary manifestations of cardiovascular disease: design of the CIRCULATING CELLS study. *Clin Res Cardiol,* 102**:** 847-856, 2013.
43. Grundberg, E, Small, KS, Hedman, AK, Nica, AC, Buil, A, Keildson, S, Bell, JT, Yang, TP, Meduri, E, Barrett, A, Nisbett, J, Sekowska, M, Wilk, A, Shin, SY, Glass, D, Travers, M, Min, JL, Ring, S, Ho, K, Thorleifsson, G, Kong, A, Thorsteindottir, U, Ainali, C, Dimas, AS, Hassanali, N, Ingle, C, Knowles, D, Krestyaninova, M, Lowe, CE, Di Meglio, P, Montgomery, SB, Parts, L, Potter, S, Surdulescu, G, Tsaprouni, L, Tsoka, S, Bataille, V, Durbin, R, Nestle, FO, O'Rahilly, S, Soranzo, N, Lindgren, CM, Zondervan, KT, Ahmadi, KR, Schadt, EE, Stefansson, K, Smith, GD, McCarthy, MI, Deloukas, P, Dermitzakis, ET, Spector, TD, Multiple Tissue Human Expression Resource, C: Mapping cis- and trans-regulatory effects across multiple tissues in twins. *Nat Genet,* 44**:** 1084-1089, 2012.
44. Zeller, T, Wild, P, Szymczak, S, Rotival, M, Schillert, A, Castagne, R, Maouche, S, Germain, M, Lackner, K, Rossmann, H, Eleftheriadis, M, Sinning, CR, Schnabel, RB, Lubos, E, Mennerich, D, Rust, W, Perret, C, Proust, C, Nicaud, V, Loscalzo, J, Hubner, N, Tregouet, D, Munzel, T,

Ziegler, A, Tiret, L, Blankenberg, S, Cambien, F: Genetics and beyond--the transcriptome of human monocytes and disease susceptibility. *PLoS One,* 5**:** e10693, 2010.

45. Arvind, P, Nair, J, Jambunathan, S, Kakkar, VV, Shanker, J: CELSR2-PSRC1-SORT1 gene expression and association with coronary artery disease and plasma lipid levels in an Asian Indian cohort. *J Cardiol,* 64**:** 339-346, 2014.
46. Guo, DC, Papke, CL, Tran-Fadulu, V, Regalado, ES, Avidan, N, Johnson, RJ, Kim, DH, Pannu, H, Willing, MC, Sparks, E, Pyeritz, RE, Singh, MN, Dalman, RL, Grotta, JC, Marian, AJ, Boerwinkle, EA, Frazier, LQ, LeMaire, SA, Coselli, JS, Estrera, AL, Safi, HJ, Veeraraghavan, S, Muzny, DM, Wheeler, DA, Willerson, JT, Yu, RK, Shete, SS, Scherer, SE, Raman, CS, Buja, LM, Milewicz, DM: Mutations in smooth muscle alpha-actin (ACTA2) cause coronary artery disease, stroke, and Moyamoya disease, along with thoracic aortic disease. *Am J Hum Genet,* 84**:** 617-627, 2009.
47. Paneni, F, Costantino, S, Cosentino, F: p66(Shc)-induced redox changes drive endothelial insulin resistance. *Atherosclerosis,* 236**:** 426-429, 2014.
48. Lopez, LM, Hill, WD, Harris, SE, Valdes Hernandez, M, Munoz Maniega, S, Bastin, ME, Bailey, E, Smith, C, McBride, M, McClure, J, Graham, D, Dominiczak, A, Yang, Q, Fornage, M, Ikram, MA, Debette, S, Launer, L, Bis, JC, Schmidt, R, Seshadri, S, Porteous, DJ, Starr, J, Deary, IJ, Wardlaw, JM: Genes from a translational analysis support a multifactorial nature of white matter hyperintensities. *Stroke,* 46**:** 341-347, 2015.
49. Harismendy, O, Notani, D, Song, X, Rahim, NG, Tanasa, B, Heintzman, N, Ren, B, Fu, XD, Topol, EJ, Rosenfeld, MG, Frazer, KA: 9p21 DNA variants associated with coronary artery disease impair interferon-gamma signalling response. *Nature,* 470**:** 264-268, 2011.

Supplemental data

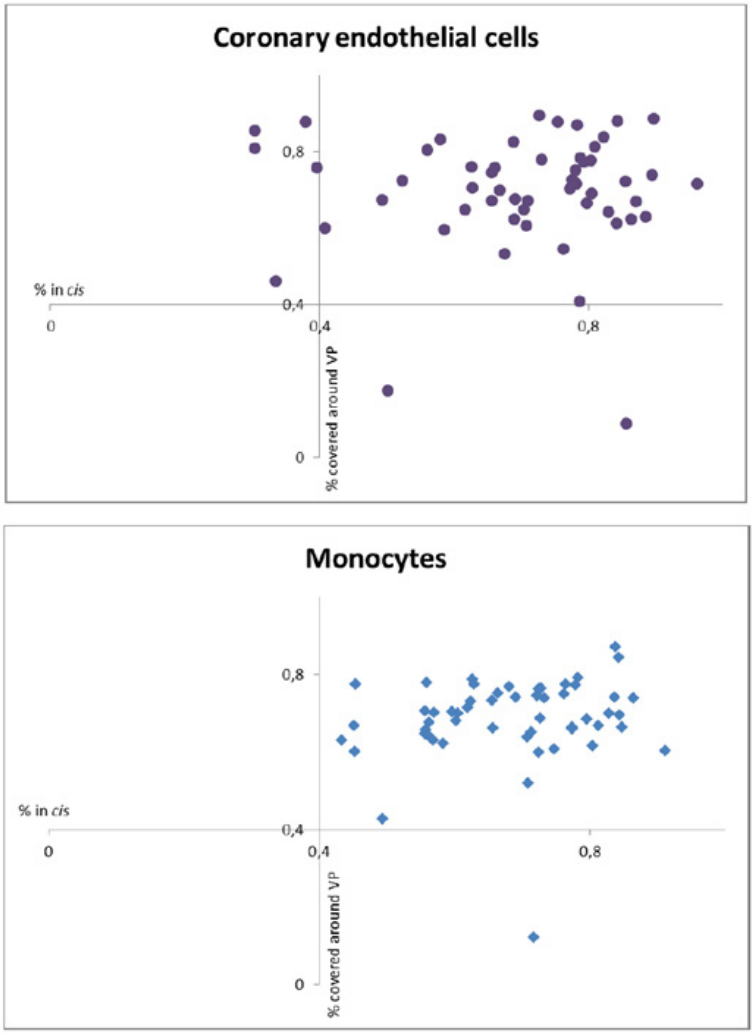

Supplemental Figure 1: Quality of 4C datasets of coronary endothelial cells and monocytes. The graphs show the quality measures of the 4C datasets. Y-axes shows the percentage of fragends covered around the viewpoint (measure for the complexity of the dataset), x-axes show the percentage of reads in cis i.e. the percentage of reads that map to the chromosome of the viewpoint (measure for the specificity of the dataset). Each dot represents one viewpoint.

Supplemental Tables can be downloaded from:
http://circgenetics.ahajournals.org/lookup/suppl/doi:10.1161/CIRCGENETICS.116.001664/-/DC1

Chapter 7

Chromatin conformation links distal target genes to chronic kidney disease loci

Maarten M. Brandt*, Claartje A. Meddens*, Laura Louzao-Martinez, Noortje A.M. van den Dungen, Nico R. Lansu, Edward E.S. Nieuwenhuis, Dirk J. Duncker, Marianne C. Verhaar, Jaap A. Joles, Michal Mokry‡, Caroline Cheng‡. (*‡ Authors contributed equally)

Journal of the American Society of Nephrology, 2018; PMID: 29093029

Abstract

Genome wide association studies (GWAS) identified many genetic risk factors for chronic kidney disease (CKD). However, linking common variants to genes that are causal for CKD etiology remains challenging. By adapting self-transcribing active regulatory region sequencing (STARR-seq), we demonstrated the perturbing effect of genetic variation on DNA regulatory elements (DRE). Variants in linkage with the CKD-associated SNP rs11959928 were shown to affect DRE function, illustrating that genes regulated by DREs colocalizing with CKD-associated variation can be dysregulated and therefore be considered as CKD candidate genes. To identify target genes of these DREs, we used circular chromosome conformation capture (4C) sequencing on glomerular endothelial cells and renal tubular epithelial cells. Our 4C analyses revealed interactions of CKD-associated susceptibility regions with the transcription start sites of 304 target genes. Overlap with multiple databases confirmed that many of these target genes are involved in kidney homeostasis. Expression quantitative trait loci analysis revealed that mRNA levels of many target genes are genotype dependent. Pathway analyses showed that target genes were enriched in processes crucial for renal function, identifying dysregulated geranylgeranyl diphosphate biosynthesis as a potential disease mechanism. Our data annotated multiple genes to previously reported CKD–associated SNPs and provided first time evidence for interaction between these loci and their target genes. This current pipeline provides a novel technique for hypothesis generation and complements classic GWAS interpretation. Future studies are required to specify the implications of our dataset and to further reveal the complex roles that common variants play in complex diseases such as CKD.

Introduction

Chronic kidney disease (CKD) is a condition marked by loss of kidney function, which can lead to end stage renal disease and is associated with a dramatic increase in cardiovascular disease-related morbidity and mortality.[1] Based on the latest report of the Center for Disease Control and Prevention (2007-2014), over 15% of the U.S. population is affected by CKD and the numbers are expected to rise. CKD incurs substantial rising medical costs in the U.S., with similar developments observed globally. Over the last decade, the findings of multiple genome wide association studies (GWASs) have established common DNA variants as genetic risk factors for CKD.[2, 3] However, functional annotation and explanation of these loci remains an issue. Currently, the functional annotation of GWAS data is mainly conducted by linking susceptibility loci by spatial proximity to the nearest gene.[4] For example, well-known single nucleotide polymorphisms (SNPs) that are associated with CKD include SNPs annotated with *ALMS1* and *UMOD*. *ALMS1* is required for medullar collecting duct ciliogenesis[5], whereas *UMOD* is involved in the inhibition of calcium oxalate crystallization in renal fluids and has an evolutionary role in protection from urinary tract infections.[6,7] Since these SNPs are located in coding regions of genes with important renal protective functions, it is conceivable that the genetic variation marked by these SNPs affects both genes, contributing to CKD pathogenesis. For many of the CKD associated susceptibility loci that are not directly located in or near protein coding regions, the causal contribution to disease etiology is far less straightforward.

New insights brought by epigenetic research have revealed the prevalence of DNA regulatory elements (DREs), such as enhancers and repressors, located in both coding- and non-protein-coding DNA regions (Figure 1A).[8] These DREs play a crucial role in regulating gene expression in a cell specific manner. Enhancer elements regulate transcription of their target genes through 3D chromatin interactions with transcriptional start sites (Figure 1B). Importantly, DREs can regulate expression levels of gene targets over a distance up to thousands of kilobase pairs (kbp)[9], far exceeding the current standard distance for GWAS annotation. Common genetic variation in DREs could be a causative factor in dysregulation of target gene expression, leading to disease or other phenotypes (Figure 1C-D). This was demonstrated previously for the SNP rs12913832, which was shown to modulate human pigmentation by affecting the enhancer regulation of the *OCA2* promoter.[10] Systematic mapping of the target genes of DREs that overlap with known CKD associated SNPs, could greatly improve our understanding of the complex genetics of CKD.

Here we used self-transcribing active regulatory region sequencing (STARR-seq) to evaluate the potential effect of CKD associated genetic variation on transcriptional regulation. In a proof of principle approach we cloned putative DREs located on the same

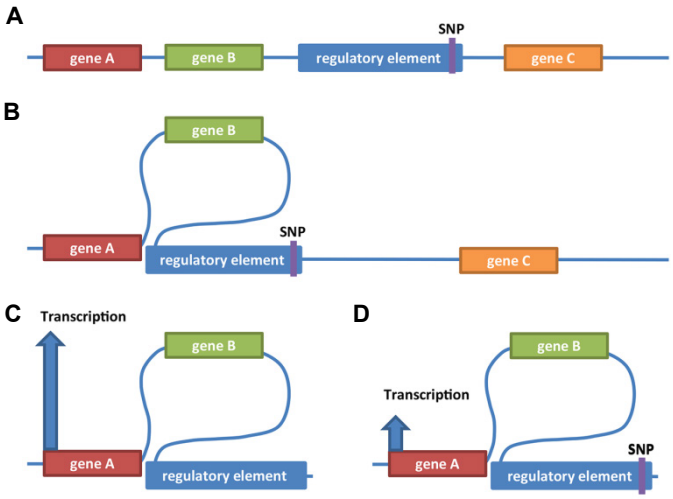

Figure 1: Genetic variation in DREs could be a causative factor in dysregulation of distal target gene expression. (A) Many of the susceptibility loci that are not located in protein coding regions, overlap with DREs such as enhancers and repressors. **(B)** DREs play a crucial role in regulating gene expression, in a cell specific manner, by modulating 3D chromatin interactions, and increasing spatial proximity of DREs with transcriptional start sites, thereby regulating transcription of genes on a non-linear DNA scale. **(C)** Distal transcriptional activity of DREs could be compromised **(D)** by genetic variation (represented by colocalization with disease-associated SNP).

linkage disequilibrium (LD) block as the CKD associated SNP rs11959928 from 20 donors in STARR-seq reporter plasmids. This approach enabled us to study the effect of all variants found on this susceptibility region in the donor pool on enhancer activity in primary human renal proximal tubular epithelial cells (HRPTECs), human renal glomerular endothelial cells (HRGECs), and the human embryonic kidney cell line HEK293a. The findings of this experiment illustrated how regulatory function could be affected by common small variants, thereby highlighting the relevance of studying downstream target genes of DREs overlapping with disease-associated susceptibility regions to add an additional layer to post GWAS analysis. Subsequently, we used circular chromosome conformation capture-sequencing (4C-seq) to identify putative candidate genes for CKD by examining 3D interactions between DREs that colocalize with CKD susceptibility loci and their target genes. This allowed us to study long range regulation of target gene promoters by cross-linking the folded and interacting DRE segments, followed by two restriction-ligation steps of the DNA strands and DNA sequencing. As transcriptional regulation is cell-type specific, and CKD pathogenesis is associated with reduced glomerular filtration rate as a result of tubulo-interstitial fibrosis as well as loss of peritubular and glomerular capillaries[11-13], we conducted the 4C-seq in HRPTECs and HRGECs. Chromatin interactions were studied in these primary cells from healthy donors to create an overview of genes interacting with CKD susceptibility loci. We conducted a systematic screen of 39 putative regulatory elements that colocalize with previously reported susceptibility regions for CKD. This led to the

identification of 304 target genes that are potentially transcriptionally affected by these CKD-associated SNPs. This study shows for the first time a direct interaction between CKD-associated common variant regions and the promoter regions of CKD-associated target genes. Although additional functional studies are needed to determine the exact mechanism of action, in its current form our data presents an extensive overview of potential target genes for the previously reported CKD-associated SNPs, providing new gene candidates for hypothesis-driven future studies.

Methods

Cell culture

Primary human renal glomerular endothelial cells (HRGECs; derived from human donor cell biobank Sciencell) and human renal proximal tubular epithelial cells (HRPTECs; Sciencell) were cultured on fibronectin and gelatin coated plates on ECM medium (supplemented with endothelial cell growth kit, and penicillin/streptomycin; Sciencell), and EpiCM medium (supplemented with epithelial cell growth kit, and penicillin/streptomycin; Sciencell) respectively. Human Embryonic Kidney Cells (HEK293a) were cultured on gelatin coated plates on DMEM (Lonza) supplemented with 10% fetal calf serum (Gibco) and 100U/ml penicillin/streptomycin (Lonza). All cells were cultured in 5% CO_2 at 37 ˚C. The experiments with primary cells were conducted with cells at passage 3.

STARR-seq reporter assay

DNA from 20 individual donors was isolated from whole blood obtained from the Mini Donor Service (positive approval from the medical ethics committee of the UMC Utrecht – protocol number 07/125) via salt precipitation. Regions (~1200 base pairs in size) containing DNase hypersensitivity sites overlapping with candidate variants (minor allele frequency>0.03) within the susceptibility locus were PCR amplified (primers in Supplemental Table 1), equimolarly pooled and cloned into pSTARR-seq_human vector (Addgene). The library complexity was verified by dilution series after transformation and was estimated to contain 50.000 individual reporter clones. 40 million cells were placed in 1600µl electroporation buffer (Bio-Rad) supplemented with 120µg (HEK293a) or 240µg (HRPTECs and HRGECs) library, after which electroporation mixture was divided over 16 2mm electroporation cuvettes (Bio-Rad), followed by electroporation with a square wave (110V/25ms for HEK293a, 125V/20ms for HRPTECs and HRGECs) using Gene Pulser Xcell™ (Bio-Rad). After electroporation cells were seeded in normal culture medium for 24h, followed by RNA extraction using the RNeasy isolation kit (Qiagen). The polyadenylated fraction of the total RNA was isolated using Dynabeads Oligo dT 25 (Thermo Fisher). The reporter specific

cDNA was synthesized and amplified according to standard STARR-seq protocols.[14] The amplified cDNA was subsequently fragmented (Covaris S2 ChIP seq programme (power peak 40, duty factor 5 cycle/burst 200)) and cleaned, followed by sequencing library preparation using NEXTflex ChIP-Seq library prep kit for Illumina sequencing. The libraries were sequenced on Illumina NextSeq500 platform to produce 75bp long single end reads.

4C-seq

4C template was prepared as previously described.[15] In summary, 10 million HRGECs or HRPTECs (both primary cells from healthy donors) were fixed in 2% formaldehyde, after which cells were lysed. The chromatin of the lysed cells was digested with the 4 base cutter DPNII (NEB), followed by ligation in a heavily diluted environment with T4 ligase (Roche). The ligated samples were de-crosslinked, followed by a second digestion with the 4 base cutter CvIQI (NEB). Next, samples were ligated once more in a diluted environment after which the chromatin was purified. The efficiency of each digestion and ligation step was validated on agarose gels. Viewpoints were selected based on the CKD susceptibility loci found in the GWASs of Y. Okada *et al.* (2012) and A. Köttgen *et al.* (2010). If multiple SNPs were found in a genomic region spanning less than 20kbp, only the SNP with the lowest P value was selected as viewpoint. To study the chromatin interactions of CKD associated susceptibility loci with 4C, primers were designed for each viewpoint as described previously.[15] Briefly, primers were designed within a 5kbp window surrounding the CKD associated SNP. Forward primers were designed in the first restriction site and the reversed primers were designed close to the second restriction site (<100bp), with a minimum distance of 300bp between the forward and the reversed primer. In case no suitable primers could be designed based on these specifications, either the window size surrounding the SNP was increased to 10kbp or the distance between the forward and reversed primer was reduced (Supplemental Table 8). 4C libraries were sequenced using the NextSeq500 platform (Illumina), producing single end reads of 75bp. The raw sequencing reads were then de-multiplexed based on viewpoint specific primer sequences. Reads were trimmed to 16 bases and mapped to an *in silico* generated library of fragends (fragment ends) neighboring all DpnII sites in human genome (NCBI37/hg19), using the custom Perl scripts.[16] No mismatches were allowed during the mapping. The reads mapping to only one possible fragend were used for further analysis.

Target gene identification

First, the number of covered fragends within a running window of *k* fragends throughout the whole chromosome was calculated (only the viewpoint's chromosome was taken into

account). The *k* was set separately for every viewpoint so it contained on average 20 covered fragends in the area around the viewpoint (+/- 100 kbp). Next, we compared the number of covered fragends in each running window to the theoretical random distribution. The windows with significantly higher number of covered fragends compared to random distribution ($p<10^{-8}$ based on binominal cumulative distribution function; R pbinom) were considered as a significant 4C signal. The following criteria were defined for the identification of the candidate genes: (1) The Transcriptional Start Site (TSS) colocalizes with a significant 4C-seq signal ($p<10^{-8}$) within 5kbp. (2) The susceptibility variant or other variant in linkage disequilibrium (LD) colocalizes with at least one of the published datasets that represent candidate regulatory sequences (Supplemental Table 3) in a similar cell type as from which the 4C signal was. (3) The candidate gene has been validated to be expressed by mRNA datasets.

Identification of gene expression

HRPTECs expression data was used from publically available datasets (NCBI Gene Expression Omnibus accession number GSE12792).[17] Expression data from microvascular endothelium was generated via RNA extraction from cultured microvascular endothelial cells in low serum medium (EBM-2 medium supplemented with 0.5% fetal calf serum) using the RNeasy isolation kit. Poly(A) Beads (NEXTflex) were used to isolate polyadenylated mRNA, from which sequencing libraries were made using the Rapid Directional RNA-seq kit (NEXTflex). Libraries were sequenced using the Nextseq500 platform (Illumina), producing single end reads of 75bp. Reads were aligned to the human reference genome GRCh37 using STAR version 2.4.2a. Picard's AddOrReplaceReadGroups (v1.98) was used to add read groups to the BAM files, which were sorted with Sambamba v0.4.5 and transcript abundances were quantified with HTSeq-count version 0.6.1p1 using the union mode. Subsequently, RPKMs were calculated with edgeR's RPKM function. Genes were accepted as expressed if probe intensity >6 or log2(RPKM) >-1 in HRPTECs and microvascular endothelium, respectively.

Haploblock localization

Haploview (Broad Institute) was used to download LD plots 500kb up- and downstream from CKD associated SNPs (pairwise comparisons of markers <2000kbp apart). From these LD plots, haploblocks, containing CKD associated SNPs, were extracted to evaluate target gene localization in relation to CKD associated susceptibility region.

Genetic annotation with OMIM

The Online Mendelian Inheritance in Man (OMIM) morbid map database was used to find mutant alleles that were associated with CKD. CKD associated traits were mapped based on the phenotype category queries 'renal', 'kidney', and 'nephro'. The gene set found in OMIM was used to identify known CKD associated genes in the list of genes generated via the 4C-seq approach.

Genetic annotation with MGI

The MGI database was used to find monogenic mutant murine alleles that led to CKD related traits. A data file containing the 'approved gene name' and the 'mouse genome database ID' was downloaded from the HUGO Gene Nomenclature Committee to identify the mutated murine genes in the MGI database that led to CKD related traits. CKD related traits were mapped based on the following phenotype categories: Abnormal kidney morphology, abnormal kidney angiogenesis, urine abnormalities, blood abnormalities, glomerulus abnormalities, renal tubules abnormalities, podocyte abnormalities, kidney cysts, abnormal renal filtration, other kidney related traits. The gene set found in MGI was used to identify known CKD associated genes in the list of genes generated via the 4C-seq approach.

eQTL study in GTEx portal

The GTEx portal database, containing data on eQTL in 449 genotyped donors with expression data in 44 different tissues was used to list genes that significantly correlated in their expression with CKD associated SNPs that colocalized with active DREs. Genes found via this approach were overlapped with the 4C-seq captured gene list to validate whether the 4C-seq approach indeed detected target genes that showed correlations in expression levels with the CKD associated SNPs.

Pathway analysis

Datasets were analyzed using QIAGEN's IPA. IPA was used to study both enrichment of 4C-seq identified genes in canonical pathways and upstream regulators of identified candidate genes, independently for HRGECs and HRPTECs. P-values were calculated based on a right-tailed Fisher Exact Test, calculated by IPA. Expression levels of upstream regulators of which target genes were found enriched in the candidate genes identified by 4C-seq were evaluated in a publically available micro-array dataset which was used to study gene expression in CKD in renal biopsy specimens (NCBI Gene Expression Omnibus accession number GSE66494).[18]

Results

STARR-seq demonstrates the effect of genetic variation on regulation of gene expression

To illustrate the effect of genetic variation on regulatory activity of DREs as an additional layer to GWAS interpretation, the STARR-seq reporter set-up was used to test the influence of common genetic variants colocalizing with possible DREs positioned on the haploblock marked by the CKD-associated SNP rs11959928. The STARR-seq reporter assay is based on a reporter plasmid containing a minimal promoter, followed by an incorporated candidate enhancer sequence.[14] The activity of each enhancer is reflected by its ability to induce the promoter activity leading to RNA transcription of the enhancers sequence (Figure 2A). The

A

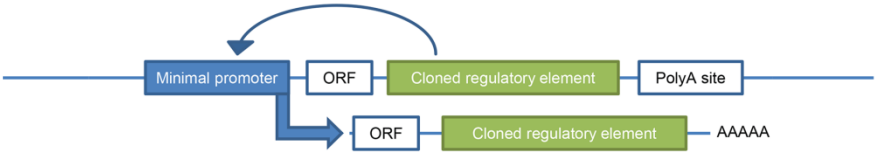

B

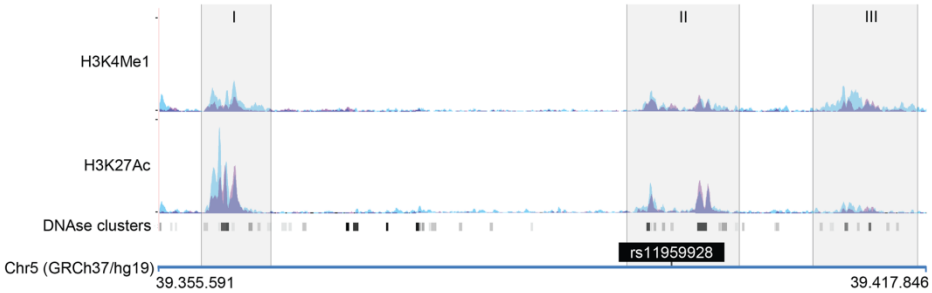

C

variant location	*reference*	*input 1*	*input 2*	*HRGECs 1*	*HRGECs 2*	*Δ HRGECs 1*	*Δ HRGECs 2*
chr5:39361231	A	72.8	69.1	100.0	100.0	27.2	30.9
chr5:39361273	T	74.8	71.2	100.0	100.0	25.2	28.8
chr5:39361303	G	36.5	31.8	17.8	3.2	-18.7	-28.6
chr5:39361359	A	70.2	64.8	100.0	99.1	29.8	34.3
chr5:39361573	A	48.9	45.2	100.0	99.6	51.1	54.4

variant location	*reference*	*input 1*	*input 2*	*HRPTECs 1*	*HRPTECs 2*	*Δ HRPTECs 1*	*Δ HRPTECs 2*
chr5:39361231	A	72.8	69.1	100.0	100.0	27.2	30.9
chr5:39361273	T	74.8	71.2	100.0	100.0	25.2	28.8
chr5:39361303	G	36.5	31.8	8.3	23.2	-28.1	-8.6
chr5:39361359	A	70.2	64.8	100.0	100.0	29.8	35.2
chr5:39361573	A	48.9	45.2	100.0	100.0	51.1	54.8

variant location	*reference*	*input 1*	*input 2*	*HEK293a 1*	*HEK293a 2*	*Δ HEK293a 1*	*Δ HEK293a 1*
chr5:39361231	A	72.8	69.1	100.0	100.0	27.2	30.9
chr5:39361273	T	74.8	71.2	100.0	100.0	25.2	28.8
chr5:39361303	G	36.5	31.8	9.1	19.8	-27.4	-12.1
chr5:39361359	A	70.2	64.8	100.0	100.0	29.8	35.2
chr5:39361573	A	48.9	45.2	98.9	100.0	50.0	54.8

◄ Figure 2: STARR-seq analysis illustrates the effect of CKD-associated genetic variation on transcriptional regulation. (A) The STARR-seq reporter principle is based on a reporter plasmid containing a minimal promotor, followed by a cloned candidate enhancer sequences. The activity of each enhancer is reflected by its ability to transcribe themselves. **(B)** Putative DREs, identified by H3K4Me1, H3K27Ac, and DNAse clusters (Human Umbilical Vein Endothelial Cells in blue, Human Epidermal Keratinocytes in pink, overlap in purple - adapted from USCS genome browser), located on the haploblock marked by CKD-associated SNP rs11959928 (I, II, III) were cloned into the STARR-seq plasmid from 20 individual donors. **(C)** The library of STARR-seq plasmids was transformed in HRGECs, HRPTECs and HEK293a, followed by RNA-seq of the produced enhancer RNA strands. Shown in replicate is the percentage of the reference allele in the input library, the percentage of the reference allele in cellular transcribed RNA, and the delta between the prevalence in the library versus transcribed RNA (found in region I).

advantage of this approach over luciferase reporter assays is that STARR-seq allows parallel (and thus "high throughput") assessment of all genomic variation in the enhancer regions located on this specific haploblock, as the effect of a variant on enhancer strength is reflected by its relative prevalence in transcribed RNA compared to its prevalence in the pool of reporter plasmids. Putative DREs located on the haploblock marked by the CKD-associated SNP rs11959928 (Figure 2B), containing at least three potential regulatory regions (I, II, III) as illustrated by H3K4Me1, H3K27Ac, and DNAse clusters in human umbilical vein endothelial cells and human epidermal keratinocytes (adapted from USCS genome browser), were cloned from 20 individual donors into one combined reporter library (Supplemental Table 1). This library was transformed in HRGECs, HRPTECs and HEK293a (the latter cell type was used an additional control), followed by sequencing of the produced enhancer derived RNA, as well as the library itself, enabling us to compare transcription frequency of each variable allele located in the enhancer sequences on the haploblock with its original frequency in the library (Supplemental Table 2). Via this approach, one particular region containing 5 variants was found to be strongly affected by allele specific activity in all three examined cell types (Figure 2C). Four of these variants had a reference allele frequency of 45.2-74.8% in the library input, yet virtually only the reference alleles were transcribed in all three cell types. The other allele had a wild-type penetrance of 31.8-36.5% in the library input, but its frequency was strongly reduced in the transcribed RNA. This example illustrates that disease-associated SNPs may not only affects gene coding sequences, but might also affect the transcriptional regulation of DRE target genes.

4C-seq leads to discovery of new target genes for CKD-associated SNPs

Building on the illustrative STARR-seq findings, 39 CKD associated susceptibility loci that colocalize with DREs were studied in HRGECs and HRPTECs in order to identify the target

genes of putative DREs.[2, 3] Activity of these DREs was assessed in renal epithelium and fetal renal tissue for HRPTECs and microvascular endothelium for HRGECs based on DNase hypersensitivity and H3K4me3 chromatin immunoprecipitation data (Supplemental Table 3). Of the 39 studied loci, 6 colocalize only with active DREs in renal epithelium, 5 colocalize only with active DREs in microvascular endothelium, and 28 loci colocalize with active DREs in both renal epithelium and microvascular endothelium. For the discovery of target genes of these regulatory elements, the TSSs that interacted with these loci were examined in HRPTECs and HRGECs using 4C-seq (Figure 3A-F). 67 chromatin interaction

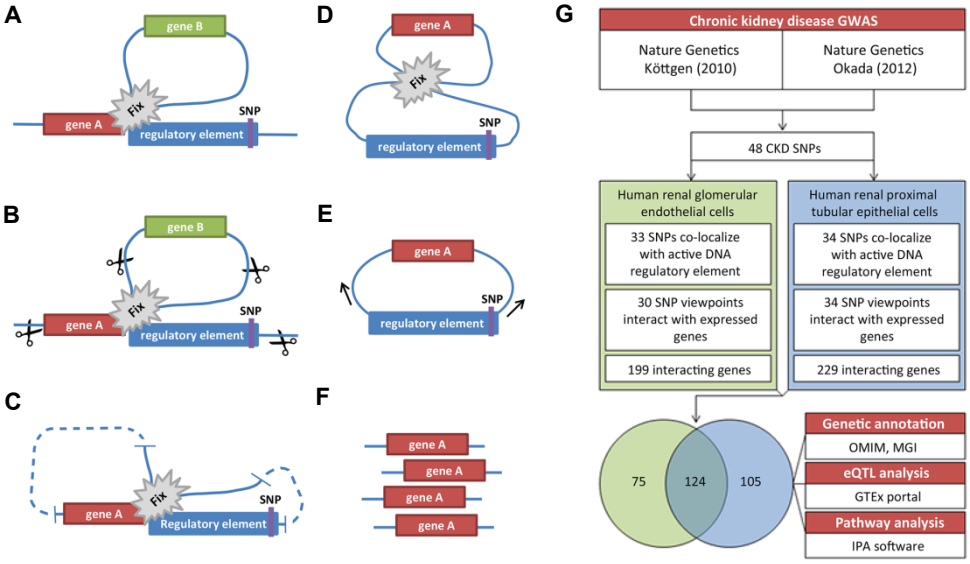

Figure 3: 4C-seq was used to study chromatin interactions leading to the discovery of 304 CKD target genes in total. The 3D chromatin conformation of the DREs was studied in detail based on 4C template, which was generated by fixing the chromatin structure **(A)**, followed by enzymatic (DPNI) digestion of the fixed chromatin **(B)**. The digested chromatin was ligated into circular fragments **(C)**, after which the chromatin was de-crosslinked **(D)**. The circular DNA molecules followed another round of enzymatic (CviQI) digestion and ligation, after which the 4C-seq library was prepared with primers that target sequences in close proximity of the CKD susceptibility loci **(E)**. This library was sequenced to identify genes that were physically interacting with CKD susceptibility loci **(F)**. **(G)** The 4C analysis was performed on 48 viewpoints based on CKD associated SNPs, of which in total 39 colocalized with DNase hypersensitivity or H3K04me3 ChIP-seq datasets (33 in HRGECs and 34 in HRPTECs with partial overlap of SNPs). Of these 39 studied viewpoints, only 36 (31 in HRGECs and 34 in HRPTECs with partial overlap of viewpoints) were interacting with a total of 304 target genes with validated expression in the assessed cell types. These 304 genes were subsequently processed for genetic annotation to renal failure associated traits in the online mendelian inheritance in man (OMIM) database and the mouse genome informatics (MGI) database, in addition to eQTL analysis in the GTEx portal database, and pathway analysis using Ingenuity Pathway Analysis (IPA) software.

A

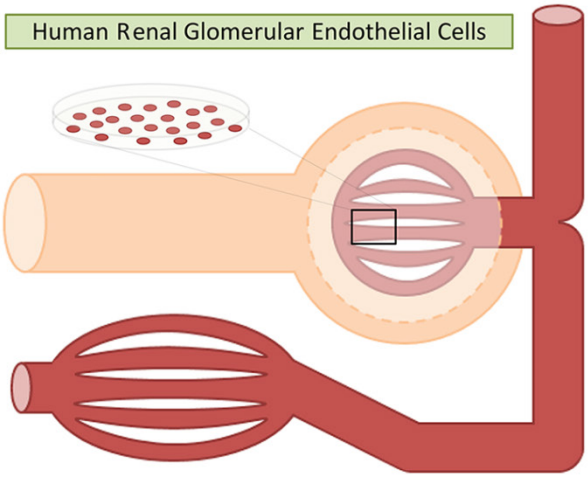

rs13069000 (chr. 3)***

Target genes	kbps
SLC25A26	680
LRIG1	248

rs16853722 (chr. 3)

Target genes	kbps
MECOM	287
ARPM1	337

rs347685 (chr. 3)

Target genes	kbps
RASA2	601
RNF7	350
ATP1B3	212
TFDP2	83
GK5	137
XRN1	360
ATR	491

B

rs267734 (chr. 1)

Target genes	kbps
ANP32E	744
APH1A	710
C1orf51	696
MRPS21	685
PRPF3	658
RPRD2	614
TARS2	492
ECM1	471
ADAMTSL4	430
MCL1	399
ENSA	350
GOLPH3L	282
CTSS	213
CTSK	171
ARNT	102
SETDB1	53
LASS2	4
ANXA9	3
FAM63A	28
PRUNE	29
C1orf56	69
CDC42SE1	81
MLLT11	81
GABPB2	92
SEMA6C	168
LYSMD1	187
SCNM1	187
VPS72	211
PIP5K1A	220
PSMD4	276

rs2049805 (chr. 1)

Target genes	kbps
EFNA1	95
RAG1AP1	87
DPM3	82
KRTCAP2	49
TRIM46	49
MUC1	32
THBS3	17
MTX1	16
GBAP	2
GBA	16
FAM189B	30
SCAMP3	37
CLK2	48
HCN3	52
FDPS	84
C1orf104	99
RUSC1	96
ASH1L	337
MIR555	121
LOC645676	337
MSTO1	385
YY1AP1	464
DAP3	464

rs1260326 (chr. 2) ns

Target genes	kbps
GTF3C2	151
EIF2B4	138
SNX17	138
ZNF513	127
PPM1G	98
FTHL3P	114
NRBP1	79
KRTCAP3	66
IFT172	18
FNDC4	13
C2orf16	68
ZNF512	75
CCDC121	121
GPN1	121
SUPT7L	156
SLC4A1AP	155

rs13538 (chr. 2) ns

Target genes	kbps
ALMS1	255
TPRKB	96
DUSP11	139
STAMBP	188
DGUOK	286
TET3	405
BOLA3	507
MOBKL1B	538
DCTN1	734

rs10937329 (chr. 3)***

Target genes	kbps
BCL6	261
LPP	217

rs13146355 (chr. 4)

Target genes	kbps
NUP54	342
SCARB2	277
STBD1	184
SHROOM3	56
CCNI	585
CCNG2	666

rs2725220 (chr. 4)**

Target genes	kbps
SPARCL1	509
PKD2	31
ABCG2	120
PPM1K	246
HERC6	340
HERC5	418
PIGY	485

rs17319721 (chr. 4)

Target genes	kbps
STBD1	141
SHROOM3	13

rs11959928 (chr. 5)

Target genes	kbps
RICTOR	323
DAB2	28
TTC33	1359

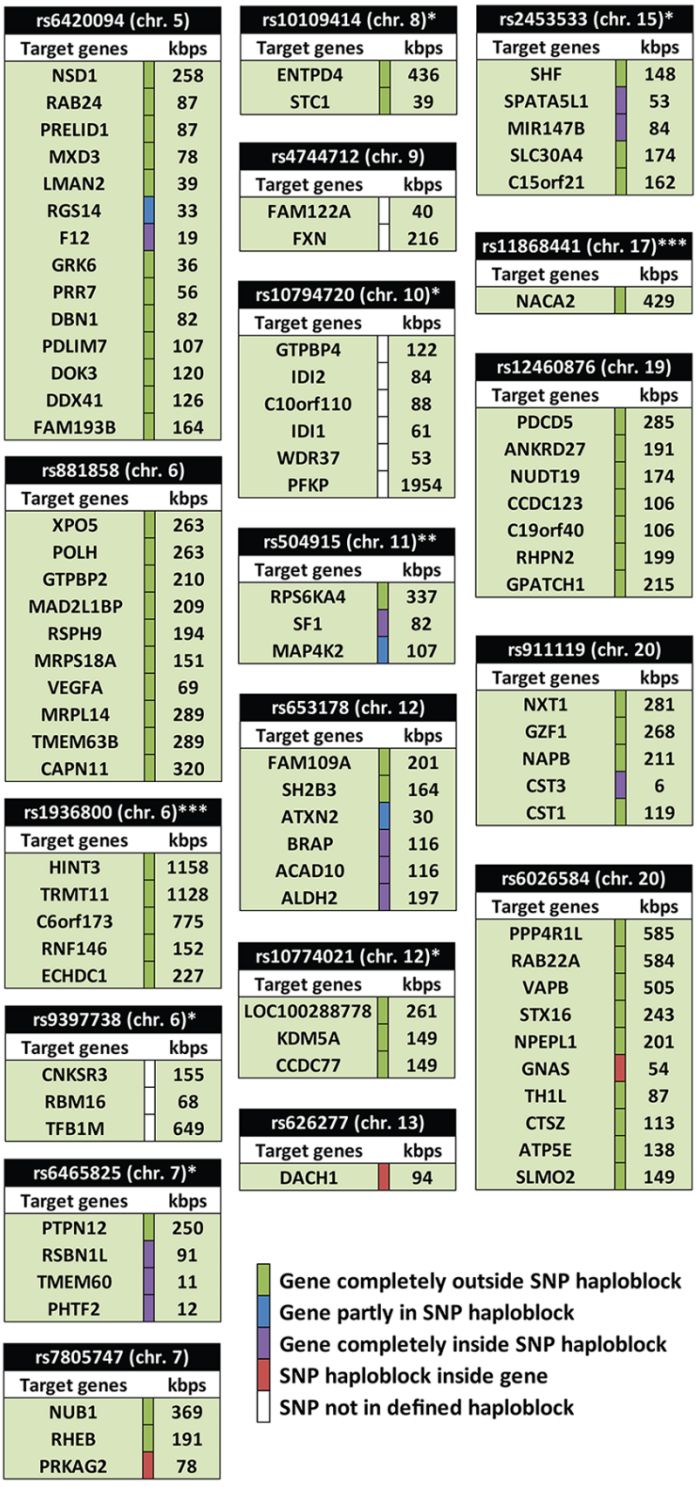

Figure 4: Analysis of chromatin interactions of CKD susceptibility loci using 4C-seq led to the discovery of 199 CKD target genes in human renal glomerular endothelial cells. (A) Chromatin interactions were studied in cultured HRGECs to define endothelial target genes of CKD suscep-tibility loci that colocalize with active regulatory elements. **(B)** Of a total of 33 replicated 4C datasets, based on CKD suscep-tibility loci that colocalize with active regulatory elements, 30 interacted with at least one target gene that was expressed in endothelium, which led to the identification of 199 CKD target genes. Studied SNPs are displayed ordered on position, followed by haploblock information and the SNP-TSS distance in kbps. *SNP solely associated with serum creatinine (estimated glomerular filtration rate), **SNP solely associated with serum urate, ***SNP solely associated with blood urea nitrogen, ^{ns}non-synonymous SNP.

A

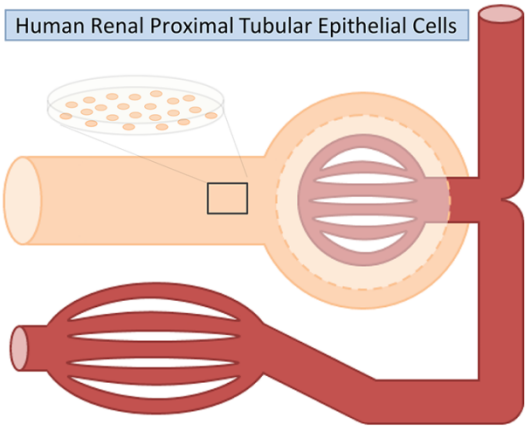

B

rs267734 (chr. 1)	
Target genes	kbps
NBPF10	5658
ANP32E	744
CA14	721
APH1A	710
C1orf54	706
PRPF3	658
RPRD2	614
TARS2	492
ECM1	471
ADAMTSL4	430
MCL1	399
ENSA	350
GOLPH3L	282
CTSS	213
CTSK	171
SETDB1	53
LASS2	4
ANXA9	3
FAM63A	28
PRUNE	29
C1orf56	69
CDC42SE1	81
SEMA6C	168
SCNM1	187
VPS72	211
PIP5K1A	220
PSMD4	276

rs2049805 (chr. 1)	
Target genes	kbps
ADAR	614
PMVK	285
PBXIP1	266
PYGO2	261
SHC1	252
CKS1B	248
FLAD1	239
LENEP	229
ZBTB7B	220
ADAM15	171
EFNA4	159
EFNA3	144
EFNA1	95
RAG1AP1	87
DPM3	82
TRIM46	49
MUC1	32
THBS3	17
MTX1	16
GBAP	2
GBA	16
FAM189B	30
SCAMP3	37
CLK2	48
PKLR	76
FDPS	84
RUSC1	96
ASH1L	337
MSTO1	385
YY1AP1	464
DAP3	464

rs1260326 (chr. 2) ns	
Target genes	kbps
AGBL5	456
SLC30A3	245
UCN	200
MPV17	185
GTF3C2	151
EIF2B4	138
SNX17	138
PPM1G	98
NRBP1	79
FNDC4	13
GCKR	11
GPN1	121
SUPT7L	156
SLC4A1AP	155
RBKS	382
BRE	383

rs13538 (chr. 2) ns	
Target genes	kbps
CCT7	407
FBXO41	370
ALMS1	255
NAT8	1
NAT8B	60
TPRKB	96
DUSP11	139
STAMBP	188
ACTG2	252
TET3	405
SLC4A5	702

rs16853722 (chr. 3)	
Target genes	kbps
MECOM	287
MYNN	340

rs11123170 (chr. 2)***	
Target genes	kbps
PRPF40A	39595

rs13069000 (chr. 3)***	
Target genes	kbps
LRIG1	248

rs347685 (chr. 3)	
Target genes	kbps
RASA2	601
RNF7	350
ATP1B3	212
TFDP2	83
ATR	491

rs10937329 (chr. 3)***	
Target genes	kbps
BCL6	261
LPP	217

rs3775948 (chr. 4)**	
Target genes	kbps
DRD5	212
SLC2A9	28
WDR1	123

rs17319721 (chr. 4)	
Target genes	kbps
NUP54	299
SCARB2	234
STBD1	141
CCNI	628
CCNG2	710

rs13146355 (chr. 4)	
Target genes	kbps
SDAD1	500
CXCL9	484
CXCL10	467
NUP54	342
SCARB2	277
STBD1	184
CCNI	585
CCNG2	666

rs6420094 (chr. 5)	
Target genes	kbps
UIMC1	384
FGFR4	304
NSD1	258
MXD3	78
LMAN2	39
RGS14	33
SLC34A1	6
F12	19
GRK6	36
PRR7	56
DBN1	82
PDLIM7	107
DOK3	120
DDX41	126
FAM193B	164
TMED9	202
B4GALT7	209

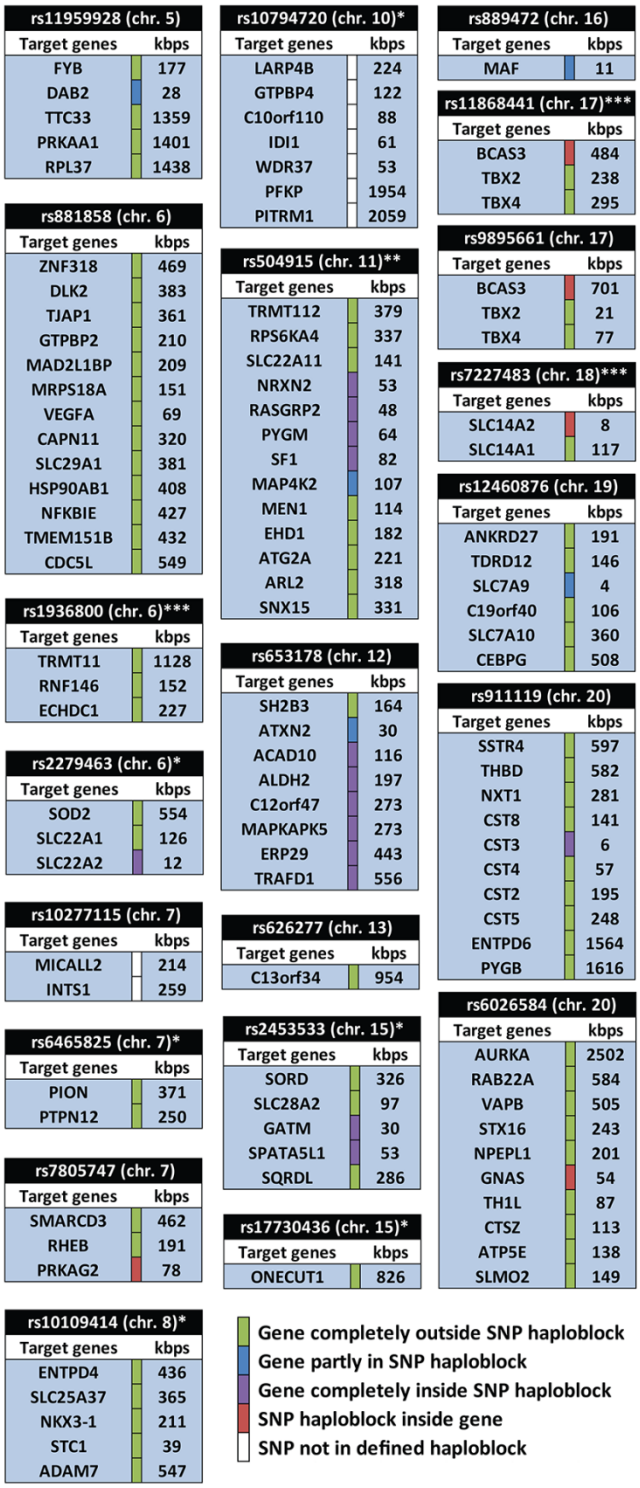

Figure 5: Analysis of chromatin interactions of CKD susceptibility loci using 4C-seq led to the discovery of 229 CKD target genes in human renal proximal tubular epithelial cells. Chromatin interactions were studied in cultured HRPTECs to define epithelial target genes of CKD susceptibility loci that colocalize with active regulatory elements. **(B)** Of a total of 34 4C datasets, based on CKD susceptibility loci that colocalize with active regulatory elements, 34 interacted with at least one target gene that was expressed in HRPTECs, which led to the identification of 229 CKD target genes in total. Studied SNPs are displayed ordered on position, followed by haploblock information and the SNP-TSS distance in kbps **(B)**. *SNP solely associated with serum creatinine (estimated glomerular filtration rate), **SNP solely associated with serum urate, ***SNP solely associated with blood urea nitrogen, ^{ns}non-synonymous SNP.

datasets were generated in twofold, of which only the replicated chromatin interactions were considered as candidate genes. These candidate genes were filtered per cell type for expression in that specific cell type, using in-house and public expression datasets (Figure 3G). This led to the discovery of 304 CKD target genes, of which 199 were found in HRGECs (Figure 4, Supplemental Table 4) and 229 in HRPTECs (Figure 5, Supplemental Table 5). Amongst the 199 target genes interacting in HRGECs and 229 target genes interacting in HRPTECs, 124 were identified in both cell types (Figure 3G). These 304 candidate genes all fulfilled the following three criteria: (1) The TSS of the candidate gene colocalizes with a significant 4C-seq signal ($P<10^{-8}$) within 5kbp. (2) The SNP or any other SNP in LD ($r>0.8$) colocalizes with active regulatory regions. (3) The candidate gene is expressed in the cell types of interest (reads per kilobase million reads sequenced (RPKMs) >-1 and probe intensity >6 for microvascular endothelium RNA-seq data and HRPTECs microarray data, respectively).[19] The TSS of the majority of candidate genes found with 4C (both expressed and non-expressed), were positioned within 500kbp from the lead SNP position (88% in HRGECs, 84% in HRPTECs), but occasionally interacting genes were found over 1000kbp from the SNP locus (7 in HRGECs, 23 in HRPTECs) (Supplemental Figure 1A-B).

Genetic annotation of candidates in OMIM and MGI demonstrates link with CKD

We evaluated if the identified candidates were associated with CKD, using the Online Mendelian Inheritance in Man (OMIM) and the Mouse Genome Informatics (MGI) database. The OMIM database is a catalogue of human genetic disorders that connects rare gene variants with phenotype. We established the overlap of our HRPTECs and HRGECs gene lists with the genes retrieved from the OMIM Morbid Map by searching for the keywords “kidney”, “renal” and “nephro”. Monogenetic defects in 5 CKD candidate genes were directly correlated with a renal disease phenotype, of which 2 are completely located on a different haploblock than the 4C viewpoint (table 1, green mark). The MGI database contains murine phenotypic information of mutant alleles. Analysis revealed that monogenetic silencing of 23 of the CKD candidate genes in mice, caused direct renal failure related traits, including albuminuria (*ALMS1, MPV17, SCARB2*), abnormal renal filtration rate (*SLC14A1*), and glomerular sclerosis (*CCNI, MPV17, VEGFA*) (table 2). Of the 23 renal failure traits associated target genes found with MGI, 13 are located entirely on a different haploblock than the 4C viewpoint (green mark).

eQTL analysis reveals genotype dependent expression of CKD candidate genes

A candidate gene with an expression level that is significantly correlated with co-occurrence of a SNP is likely to be transcriptionally regulated by a DRE affected by the SNP. These loci

Table 1: Overlapping genes in 4C-seq retrieved genes and CKD associated genes in OMIM.

Gene ID	*Phenotype*	*MIM Number*	*4C SNP*	*SNP-TSS (kbp)*	*HRGECs*	*HRPTECs*
MUC1	Medullary cystic kidney disease 1	158340	rs2049805	32	x	x
PKD2	Polycystic kidney disease 2	173910	rs2725220	31	x	
SCARB2	Epilepsy, progressive myoclonic 4, with or without renal failure	602257	rs13146355	277	x	x
SLC2A9	Hypouricemia	612076	rs3775948	28		x
SLC34A1	Nephrolithiasis/osteoporosis, hypophosphatemic	182309	rs6420094	6		x

Gene completely outside SNP haploblock
Gene completely inside SNP haploblock
SNP haploblock inside gene

Table 2: Overlapping genes in 4C-seq retrieved genes and CKD associated genes in MGI.

Gene ID	*Phenotype*	*4C SNP*	*SNP-TSS (kbp)*	*HRGECs*	*HRPTECs*
ALMS1	abnormal kidney morphology, urine-, renal tubules-, and other kidney related abnormalities	rs13538	255	x	x
ASH1L	glomerulus- and other kidney related abnormalities	rs2049805	337	x	x
CCNI	urine-, blood-, glomerulus-, podocyte-, and other kidney related abnormalities	rs13146355	585	x	x
CTSS	abnormal kidney angiogenesis	rs267734	213	x	x
DCTN1	blood abnormalities	rs13538	734	x	
GNAS	urine- and other kidney related abnormalities	rs6026584	54	x	x
GRK6	glomerulus- and other kidney related abnormalities	rs6420094	36	x	x
IFT172	abnormal kidney morphology, glomerulus abnormalities	rs1260326	18	x	
MAF	abnormal kidney morphology, renal tubules abnormalities	rs889472	11		x
MECOM	blood abnormalities	rs16853722	287	x	x
MPV17	abnormal kidney morphology and angiogenesis, urine-, blood-, glomerulus-, renal tubules-, and other kidney related abnormalities	rs1260326	185		x
PKD2	abnormal kidney morphology, kidney cysts, blood-, renal tubules-, and other kidney related abnormalities	rs2725220	31	x	
RNF7	abnormal kidney angiogenesis	rs347685	350	x	x
SCARB2	urine abnormalities	rs13146355	277	x	x
SHC1	abnormal kidney angiogenesis	rs2049805	252		x
SLC14A1	urine- and blood abnormalities, abnormal renal filtration	rs7227483	117		x
SLC14A2	urine abnormalities, abnormal renal filtration	rs7227483	8		x
SLC2A9	kidney cysts, urine-, blood-, renal tubules-, and other kidney related abnormalities	rs3775948	28		x
SLC4A5	urine abnormalities, abnormal renal filtration	rs13538	702		x
SLC7A9	renal tubules abnormalities	rs12460876	4		x
SOD2	blood abnormalities	rs2279463	554		x
THBD	abnormal kidney morphology	rs911119	582		x
VEGFA	abnormal kidney morphology and angiogenesis, blood-, glomerulus-, renal tubules-, and podocyte abnormalities	rs881858	69	x	x

Gene completely outside SNP haploblock
Gene partly in SNP haploblock
Gene completely inside SNP haploblock
SNP haploblock inside gene

that contribute to variation in gene expression levels, called expression quantitative trait loci (eQTL), are identified using GWAS and RNA-seq data of the target organ. To date, no large genome wide eQTL data of the human kidney has been published that allows adequate analysis of all CKD associated SNPs.[20] To evaluate if the expression levels of the CKD candidate genes are affected by CKD-associated SNPs, we used the Genotype-Tissue Expression (GTEx) database. Although GTEx so far only contains kidney specific expression data of 26 genotyped donors, which does not reach the GTEx threshold for eQTL analysis (>70), the database does include genotype- and expression-matched data of 449 donors for which eQTL analysis was conducted in 44 non-renal tissues, which is large enough to stratify most of the individual CKD SNPs and wild-type alleles assessed in our study. Of the 39 CKD associated susceptibility loci, 25 were annotated in GTEx. These 25 SNPs were significantly correlated with the expression of 54 genes, of which 48 physically interacted with the 4C-seq input loci (data not shown). Of these 48 captured target genes, 38 were actually expressed in HRPTECs and/or HRGECs and included 10 genes located on a completely different haploblock than the CKD-associated SNP (table 3, green mark). Thus, although the lack of genotype-kidney expression datasets prohibited us to study these eQTLs in renal tissue, this demonstrates the ability of the studied elements to establish a SNP dependent expression pattern of captured target genes in the 4C-seq approach. Interesting eQTL target genes also picked up by 4C-seq include the solute carriers *SLC28A2* and *SLC30A4* (rs2453533), and in relation to renal fibrosis, the genes encoding for the secreted proteases *CTSS* and *CTSK* (rs267734) (Figure 6A-B).

Pathway analysis reveals potentially disrupted mechanisms and regulators in CKD

Besides studying individual loci and interacting genes, we used Ingenuity Pathway Analysis (IPA, QIAGEN) to determine the pathways in which the CKD candidate genes are involved in. In both HRGECs and HRPTECs the 4C candidate genes were most significantly enriched in biosynthesis pathways (Supplemental Table 6 and 7), including the superpathway of geranylgeranyl diphosphate biosynthesis (p=4.17E-04, p=7.26E-04), and the trans, trans-farnesyl diphosphate biosynthesis pathway (p=6.63E-06, p=1.11E-03), respectively (Figure 7A-B). Interestingly, both molecular pathways are linked to the mevalonate pathway (Supplemental Figure 2). 4C-seq identified *FDPS* and *PMVK* (rs2049805), and *IDI1* and *IDI2* (rs10794720) as candidate genes in relation to the mevalonate pathway in CKD. In addition, IPA was used to identify upstream regulators of which the target genes were overrepresented amongst the CKD candidate genes. Targets of the transcription factors ATF6 (p=2.00E-03, p=4.50E-04) and FOXO4 (p=5.23E-05, p=1.24E-04) were significantly enriched in the CKD candidates in both HRGECs and HRPTECs respectively, whereas

Table 3: Overlapping genes in 4C-seq retrieved genes and eQTL genes derived from GTEx portal.

eQTL	*Gene ID*	*SNP-TSS (kbp)*	*eQTL in (tissue):*	*HRGECs*	*HRPTECs*
rs10794720	IDI2	84	Muscle	x	
	NUDT19	174	Artery, Nerve	x	
rs12460876	SLC7A9	4	Adipose, Skin, Thyroid, Nerve, Lung		x
	TDRD12	146	Testis		x
	SNX17	138	Muscle	x	x
rs1260326	FNDC4	13	Thyroid	x	x
	NRBP1	79	Adipose, Testis	x	x
	KRTCAP3	66	Adrenal gland	x	
	ALMS1	255	Pancreas	x	x
rs13538	TPRKB	96	Artery	x	x
	NAT8	1	Adipose, Thyroid, Skin, Esophagus, Pancreas, Artery, Brain		x
	THBS3	17	Whole Blood, Thyroid, Esophagus, Colon, Lung, Stomach, Testis, Spleen	x	x
	GBA	16	Esophagus, Nerve, Thyroid	x	x
rs2049805	MUC1	32	Esophagus	x	x
	FAM189B	30	Thyroid	x	x
	EFNA1	95	Skin	x	x
	HCN3	52	Nerve	x	
	SPATA5L1	53	Nerve, Adipose, Esophagus, Thyroid, Whole Blood, Artery, Muscle, Heart	x	x
rs2453533	SLC30A4	174	Adipose	x	
	GATM	30	Thyroid, Muscle, Esophagus, Lung, Skin, Whole blood		x
	SLC28A2	97	Nerve, Thyroid, Adrenal gland, Colon, Ovary		x
	ANXA9	3	Skin, Testis	x	x
rs267734	CTSS	213	Adipose, Skin, Artery, Muscle, Thyroid, Nerve, Esophagus	x	x
	CTSK	171	Whole blood	x	x
	ARNT	102	Whole blood	x	
rs2725220	PKD2	31	Testis, Esophagus	x	
rs4744712	FAM122A	40	Artery	x	
rs504915	MEN1	114	Testis		x
	NRXN2	53	Lung, Artery, Esophagus, Nerve, Adipose, Muscle, Skin		x
	RGS14	33	Skin, Artery, Testis	x	x
rs6420094	FGFR4	304	Nerve		x
	SLC34A1	6	Esophagus		x
rs6465825	RSBN1L	91	Brain	x	
	TMEM60	11	Artery, Testis	x	
rs653178	ALDH2	197	Skin	x	x
rs911119	CST3	6	Testis, Lung, Whole blood, Nerve	x	x
rs9895661	TBX2	238	Artery		x

Gene completely outside SNP haploblock
Gene partly in SNP haploblock
Gene completely inside SNP haploblock
SNP haploblock inside gene
SNP not in defined haploblock

targets of HNF4α were only enriched in HRPTECs (p=3.76E-02). It was previously shown that HNF4α was crucial for establishing and maintaining transcriptional enhancer elements in the renal proximal tubule and that sub-optimal DNA binding properties amongst others led to transcriptional dysregulation of a variety of solute carriers.[21] Interestingly, from publically

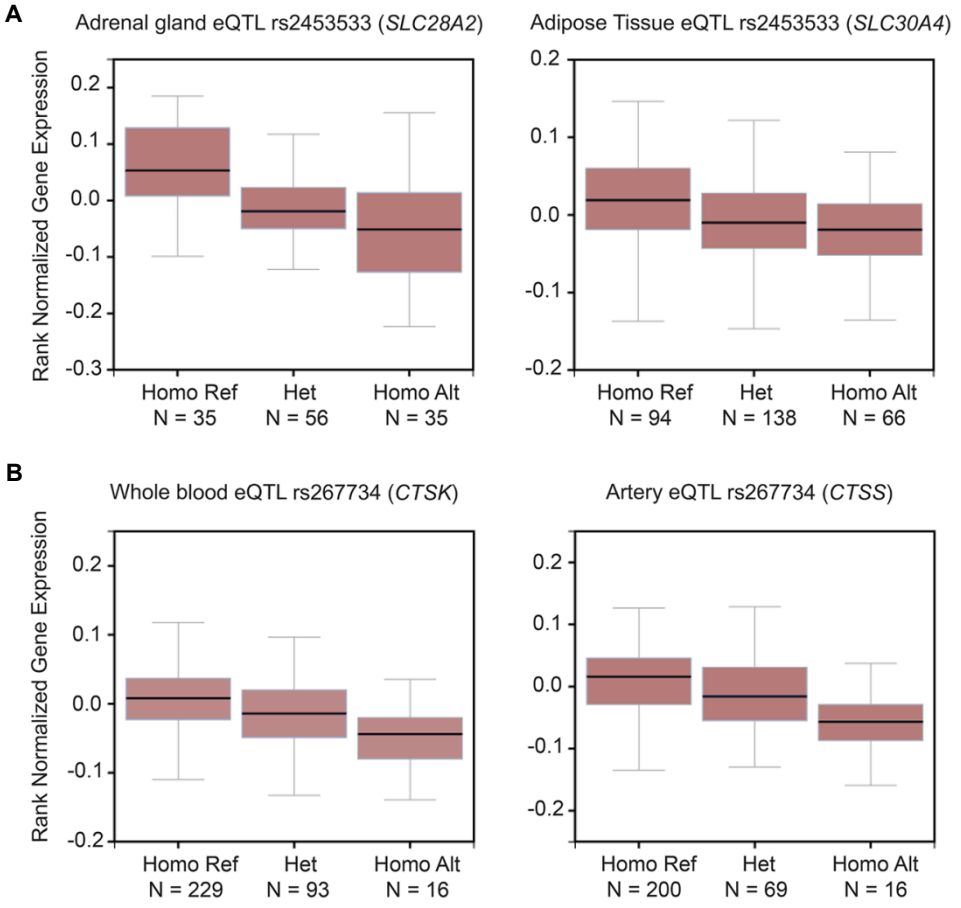

Figure 6: Expression levels of 4C-seq captured genes are correlated with the associated CKD SNP. (A) The expression level of solute carriers *SLC28A2* and *SLC30A4* is lower in the presence of the heterozygous (Het) and homozygous alternative (Homo Alt) allele (rs2453533), compared to the homozygous reference (Homo Ref) "wildtype" allele, p-value 6.8E-10 and 1.9E-05, respectively (adjusted from GTEx portal)**. (B)** Similarly, the expression levels of the secreted proteases *CTSS* and *CTSK* are lower in the presence of the heterozygous and homozygous alternative allele (rs267734), compared to the homozygous reference allele, p-value 1.4E-07 and 0.5E-06, respectively (adjusted from GTEx portal). SNP-target gene pair p-values were based on matrix eQTL analysis in linear regression mode, as described by the GTEx consortium.[22]

available micro-array data (NCBI Gene Expression Omnibus accession number GSE66494)[18] all three transcription factors were found to be significantly upregulated in renal biopsies from patients with CKD compared to healthy controls (Figure 7C), suggesting these three factors are potentially key regulators in CKD.

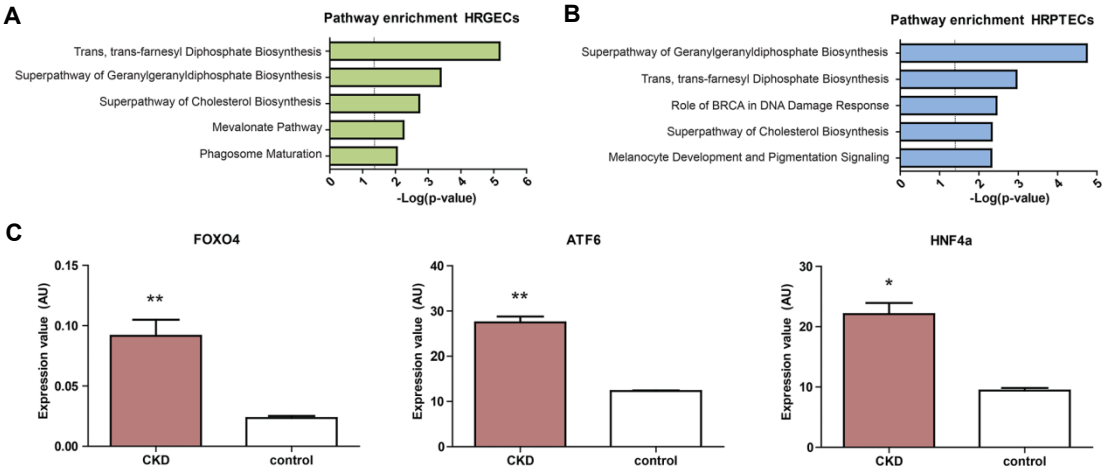

Figure 7: CKD candidate genes are enriched in pathways of biosynthesis, microangiopathy and molecular transport. IPA revealed that CKD candidate genes in both HRGECs **(A)** and HRPTECs **(B)** were most enriched in biosynthesis pathways, including the superpathway of geranylgeranyl diphosphate biosynthesis, and the trans, trans-farnesyl diphosphate biosynthesis pathway. These pathways play crucial roles in protein reuptake in HRPTECs. P-values were calculated by a right-tailed Fisher Exact Test. **(C)** Upstream regulators, identified by IPA based on the enrichment of their target genes in the 4C-seq derived candidates, were significantly higher expressed in renal biopsy specimens from CKD patients (derived from GSE66494). *p<0.05, **p<0.001, p-values were calculated by a non-parametric t-test.

Discussion

The main findings of the study are: (1) CKD-associated variation can affect transcriptional regulation, as demonstrated in a proof of principle approach for rs11959928 using STARR-seq. (2) CKD-associated loci interact with promoter regions of target genes via 3D chromatin folding. By taking this DNA regulatory information into account in GWAS annotation, we found many novel CKD candidate genes. (3) Multiple SNP-target genes sets can be distinguished. (4) The identified target genes can be linked to CKD in human and murine disease databases (OMIM and MGI). (5) eQTL analysis reveals that expression of many target genes are genotype dependent. (6) HRGECs and HRPTECs-derived target genes share trans, trans-farnesyl diphosphate biosynthesis pathway as a common molecular mechanism. Combined, our data annotated multiple new genes to previously reported CKD–associated SNPs and provided first time evidence for direct interaction between these common variant regions and their targets. Future studies are now required to pinpoint causal

genetic variant(s) at each locus, allowing a deeper understanding of their associated disease mechanisms and their relevance in kidney disease.

Previously reported GWASs for CKD-associated SNPs used classic annotation based on spatial proximity principles to identify affected target genes.[4] This includes annotation of SNPs based on location in coding regions or in close proximity of TSS (taking into account that the average promotor is 100-1000bp long), but also taking into consideration that these SNPs could be markers for less common variants in gene bodies. Using STARR-seq analysis, variants in LD with the CKD-associated SNP rs11959928 were shown to affect activity of a DRE in an allele specific manner, emphasizing that not only protein coding variants, but also variants located in regulatory regions could be at the basis of development or progression of complex diseases. Therefore, we examined the 3D folded state of the chromatin by 4C-seq to list genes that interact with DREs in LD with CKD associated SNPs. This approach led to the identification of 304 CKD candidate genes of which many are not directly located near the associated susceptibility loci. Most enhancers are located several hundreds, sometimes even thousands kbp from their target genes.[9] In our study, the majority of the SNPs are located between 100-500kbp from the target genes' TSS, supporting the idea that the interactions observed in the 4C-seq approach are enhancer-target gene interactions. The effect of common genetic variants in DNA regulatory elements is relatively low[23], therefore it is unlikely that the CKD associated SNPs in these elements will result in creating new or completely ablating 3D DRE-gene interactions. Rather, dysregulation in the expression of a gene profile that is part of the regulation of kidney homeostasis in healthy individuals, is more likely the contributing factor in CKD etiology. The 4C-seq approach helps interpreting genetic variants as a determining factor of the expression levels of interacting targets in the pathogenesis of CKD.

By overlapping our 304 CKD target genes with datasets provided by OMIM and MGI, we confirmed their relevance to kidney disease: Analysis with the MGI database showed that mice deficient for the CKD candidate genes *MPV17*, *CCNI*, *ASH1L* and *SLC4A5* suffer from renal failure related traits.[24-27] These genes are located 185kbp (rs1260326), 585kbp (rs13246355), 337kbp (rs2049805), and 702kbp (rs13538) from the CKD associated SNP respectively. In addition, validation of the 4C-seq approach was provided by analysis in the OMIM dataset, which demonstrated that multiple target genes were linked to CKD associated traits in human. For example, *MUC1 and PKD2* were identified by 4C-seq, as a result of the interaction of their promoter regions with regulatory domains that colocalize with rs2049805 and rs2725220, respectively. *MUC1* encodes the protein mucin-1, which is a membrane anchored mucoprotein involved in providing a protective barrier against

pathogens. A frameshift mutation in *MUC1*, leading to a novel stop codon, induced medullar cystic kidney disease type 1 (MIM: 158340).[28] *PKD2* encodes the polycystin-2 protein, which is involved in renal calcium transport and calcium signaling. Mutations in the gene, leading to loss of function, causes the formation of fluid-filled cysts, eventually leading to progressive destruction of the renal parenchyma (MIM: 173910)[29], but was recently also demonstrated to be involved in branching and network formation of lymphatic endothelium which plays a crucial role in renal function.[30, 31] Such examples illustrate the potential relevance of the candidate genes identified by 4C-seq for renal function, and provide clear evidence for the functional association between the investigated SNP regions and their corresponding 4C-seq captured genes in (human) CKD.

Evidence for the transcription regulatory function of the CKD-associated SNP regions was provided by GTEx database analysis. Many of the CKD susceptibility loci were eQTLs, showing a significant correlation between SNP genotypes and expression level of linked target genes in a variety of tissues. These eQTL target genes include *CTSS* and *CTSK*, coding for cathepsin S and K respectively, both downregulated in the presence of rs267734. Cathepsins are potent proteases and the negative correlation between rs267734 and cathepsin S and K expression might be relevant in relation to renal fibrosis, which is critically involved in CKD progression. In a bleomycin lung fibrosis model it was shown that cathepsin K deficient mice had more severe lung fibrosis than wild-type mice.[32] Furthermore, it was observed that pharmacological inhibition of cathepsin activity in mice with unilateral ureteral obstruction induced renal fibrosis led to a worse outcome[33], indicating that reduced expression of cathepsin S and K in the presence of rs267734 could contribute to CKD.

Pathway analysis demonstrated enrichment of 4C-seq captured genes in multiple biosynthesis pathways involved in the generation of isoprenoid pyrophosphates. Interestingly, this enrichment was observed in HRGECs, and HRPTECs, though with different identified target genes per cell type. Isoprenoid pyrophosphates are indispensable for renal proximal tubular protein reabsorption, as inhibition of 3-hydroxy-3-methylglutaryl CoA reductase in de mevalonate pathway leads to reduced prenylation of GTP binding proteins involved in receptor mediated endocytosis, eventually resulting in proteinuria.[34] Similarly, altered levels of prenylation of RhoA affects eNOS activity in endothelial cells, resulting in imbalance of ROS levels, contributing to the endothelial dysfunction reported in CKD onset.[35]

In our systemic approach, besides the non-coding variants, we also included 2 non-synonymous SNPs (SNPs in gene coding regions that alter protein sequence: rs1260326 in

GCKR and rs13538 in *NAT8*) were amongst the studied regions. Presumably, the affected genes are involved in the associated disease phenotype. Especially reports on *NAT8* activity in association with kidney disease seem convincing.[36-38] However, it was previously demonstrated that DREs can also be located in coding regions[39], and it remains of interest that by 4C-seq we found interactions of this locus with TSS of multiple other genes of which the expression levels according to GTEx are significantly associated with the occurrence of the variant. The incorporation of regulatory information provides an additional layer in post-GWAS data to aid in our interpretation of these GWAS datasets, but certainly does not replace the candidate genes identified based on spatial proximity such as *NAT8*. Along the same lines, several SNPs associated with a single trait were included. Several SNPs are solely associated with serum creatinine (estimated glomerular filtration rate). Although these SNPs might be causally associated with CKD, they might also affect creatinine production/secretion independent of renal function. Rs91119 is only associated with serum cystatin C (estimated glomerular filtration rate), and is located directly within the CST locus. Again, this SNP does not necessarily have to be causally associated with CKD, but could also be involved in the dynamics of cystatin C production. The same is true for SNPs solely associated with serum urate or blood urea nitrogen, although the authors that identified SNPs associated with the latter group had corrected for non-renal factors.[3]

In conclusion, taking the 3D structure of chromatin into account, we have identified 304 putative CKD candidate genes of DREs that colocalize with CKD susceptibility loci. In this hypothesis generation-driven approach, we present a new method of GWAS interpretation based on DRE target gene identification by 4C analysis that complements the classic methods of candidate gene identification. In addition, incorporation of the adapted STARR-seq method up or down stream of the 4C pipeline, would further narrow down the identification of causal variants in DNA regulatory function, and help us to greatly expand our understanding of the role that common low risk variants play in the onset of complex diseases such as CKD.

References

1. Levey, AS, Beto, JA, Coronado, BE, Eknoyan, G, Foley, RN, Kasiske, BL, Klag, MJ, Mailloux, LU, Manske, CL, Meyer, KB, Parfrey, PS, Pfeffer, MA, Wenger, NK, Wilson, PW, Wright, JT, Jr.: Controlling the epidemic of cardiovascular disease in chronic renal disease: what do we know? What do we need to learn? Where do we go from here? National Kidney Foundation Task Force on Cardiovascular Disease. *Am J Kidney Dis,* 32**:** 853-906, 1998.
2. Kottgen, A, Pattaro, C, Boger, CA, Fuchsberger, C, Olden, M, Glazer, NL, Parsa, A, Gao, X, Yang, Q, Smith, AV, O'Connell, JR, Li, M, Schmidt, H, Tanaka, T, Isaacs, A, Ketkar, S, Hwang, SJ, Johnson, AD, Dehghan, A, Teumer, A, Pare, G, Atkinson, EJ, Zeller, T, Lohman, K, Cornelis, MC, Probst-Hensch, NM, Kronenberg, F, Tonjes, A, Hayward, C, Aspelund, T, Eiriksdottir, G, Launer, LJ, Harris, TB, Rampersaud, E, Mitchell, BD, Arking, DE, Boerwinkle, E, Struchalin, M, Cavalieri, M, Singleton, A, Giallauria, F, Metter, J, de Boer, IH, Haritunians, T, Lumley, T, Siscovick, D, Psaty, BM, Zillikens, MC, Oostra, BA, Feitosa, M, Province, M, de Andrade, M, Turner, ST, Schillert, A, Ziegler, A, Wild, PS, Schnabel, RB, Wilde, S, Munzel, TF, Leak, TS, Illig, T, Klopp, N, Meisinger, C, Wichmann, HE, Koenig, W, Zgaga, L, Zemunik, T, Kolcic, I, Minelli, C, Hu, FB, Johansson, A, Igl, W, Zaboli, G, Wild, SH, Wright, AF, Campbell, H, Ellinghaus, D, Schreiber, S, Aulchenko, YS, Felix, JF, Rivadeneira, F, Uitterlinden, AG, Hofman, A, Imboden, M, Nitsch, D, Brandstatter, A, Kollerits, B, Kedenko, L, Magi, R, Stumvoll, M, Kovacs, P, Boban, M, Campbell, S, Endlich, K, Volzke, H, Kroemer, HK, Nauck, M, Volker, U, Polasek, O, Vitart, V, Badola, S, Parker, AN, Ridker, PM, Kardia, SL, Blankenberg, S, Liu, Y, Curhan, GC, Franke, A, Rochat, T, Paulweber, B, Prokopenko, I, Wang, W, Gudnason, V, Shuldiner, AR, Coresh, J, Schmidt, R, Ferrucci, L, Shlipak, MG, van Duijn, CM, Borecki, I, Kramer, BK, Rudan, I, Gyllensten, U, Wilson, JF, Witteman, JC, Pramstaller, PP, Rettig, R, Hastie, N, Chasman, DI, Kao, WH, Heid, IM, Fox, CS: New loci associated with kidney function and chronic kidney disease. *Nat Genet,* 42**:** 376-384, 2010.
3. Okada, Y, Sim, X, Go, MJ, Wu, JY, Gu, D, Takeuchi, F, Takahashi, A, Maeda, S, Tsunoda, T, Chen, P, Lim, SC, Wong, TY, Liu, J, Young, TL, Aung, T, Seielstad, M, Teo, YY, Kim, YJ, Lee, JY, Han, BG, Kang, D, Chen, CH, Tsai, FJ, Chang, LC, Fann, SJ, Mei, H, Rao, DC, Hixson, JE, Chen, S, Katsuya, T, Isono, M, Ogihara, T, Chambers, JC, Zhang, W, Kooner, JS, KidneyGen, C, Consortium, CK, Albrecht, E, consortium, G, Yamamoto, K, Kubo, M, Nakamura, Y, Kamatani, N, Kato, N, He, J, Chen, YT, Cho, YS, Tai, ES, Tanaka, T: Meta-analysis identifies multiple loci associated with kidney function-related traits in east Asian populations. *Nat Genet,* 44**:** 904-909, 2012.
4. Raychaudhuri, S, Plenge, RM, Rossin, EJ, Ng, AC, International Schizophrenia, C, Purcell, SM, Sklar, P, Scolnick, EM, Xavier, RJ, Altshuler, D, Daly, MJ: Identifying relationships among genomic disease regions: predicting genes at pathogenic SNP associations and rare deletions. *PLoS Genet,* 5**:** e1000534, 2009.
5. Li, G, Vega, R, Nelms, K, Gekakis, N, Goodnow, C, McNamara, P, Wu, H, Hong, NA, Glynne, R: A role for Alstrom syndrome protein, alms1, in kidney ciliogenesis and cellular quiescence. *PLoS Genet,* 3**:** e8, 2007.
6. Mo, L, Huang, HY, Zhu, XH, Shapiro, E, Hasty, DL, Wu, XR: Tamm-Horsfall protein is a critical renal defense factor protecting against calcium oxalate crystal formation. *Kidney Int,* 66**:** 1159-1166, 2004.
7. Ghirotto, S, Tassi, F, Barbujani, G, Pattini, L, Hayward, C, Vollenweider, P, Bochud, M, Rampoldi, L, Devuyst, O: The Uromodulin Gene Locus Shows Evidence of Pathogen Adaptation through Human Evolution. *J Am Soc Nephrol*, 2016.
8. Maurano, MT, Humbert, R, Rynes, E, Thurman, RE, Haugen, E, Wang, H, Reynolds, AP, Sandstrom, R, Qu, H, Brody, J, Shafer, A, Neri, F, Lee, K, Kutyavin, T, Stehling-Sun, S, Johnson, AK, Canfield, TK, Giste, E, Diegel, M, Bates, D, Hansen, RS, Neph, S, Sabo, PJ, Heimfeld, S, Raubitschek, A, Ziegler, S, Cotsapas, C, Sotoodehnia, N, Glass, I, Sunyaev, SR, Kaul, R, Stamatoyannopoulos, JA: Systematic localization of common disease-associated variation in regulatory DNA. *Science,* 337**:** 1190-1195, 2012.
9. Williamson, I, Hill, RE, Bickmore, WA: Enhancers: from developmental genetics to the genetics of common human disease. *Dev Cell,* 21**:** 17-19, 2011.
10. Visser, M, Kayser, M, Palstra, RJ: HERC2 rs12913832 modulates human pigmentation by attenuating chromatin-loop formation between a long-range enhancer and the OCA2 promoter. *Genome Res,* 22**:** 446-455, 2012.
11. Bohle, A, Grund, KE, Mackensen, S, Tolon, M: Correlations between renal interstitium and level of serum creatinine. Morphometric investigations of biopsies in perimembranous glomerulonephritis. *Virchows Arch A Pathol Anat Histol,* 373**:** 15-22, 1977.

12. Nangaku, M: Chronic hypoxia and tubulointerstitial injury: a final common pathway to end-stage renal failure. *J Am Soc Nephrol,* 17**:** 17-25, 2006.
13. Kozakowski, N, Herkner, H, Bohmig, GA, Regele, H, Kornauth, C, Bond, G, Kikic, Z: The diffuse extent of peritubular capillaritis in renal allograft rejection is an independent risk factor for graft loss. *Kidney Int,* 88**:** 332-340, 2015.
14. Arnold, CD, Gerlach, D, Stelzer, C, Boryn, LM, Rath, M, Stark, A: Genome-wide quantitative enhancer activity maps identified by STARR-seq. *Science,* 339**:** 1074-1077, 2013.
15. van de Werken, HJ, de Vree, PJ, Splinter, E, Holwerda, SJ, Klous, P, de Wit, E, de Laat, W: 4C technology: protocols and data analysis. *Methods Enzymol,* 513**:** 89-112, 2012.
16. Ji, H, Jiang, H, Ma, W, Johnson, DS, Myers, RM, Wong, WH: An integrated software system for analyzing ChIP-chip and ChIP-seq data. *Nat Biotechnol,* 26**:** 1293-1300, 2008.
17. Beyer, S, Kristensen, MM, Jensen, KS, Johansen, JV, Staller, P: The histone demethylases JMJD1A and JMJD2B are transcriptional targets of hypoxia-inducible factor HIF. *J Biol Chem,* 283**:** 36542-36552, 2008.
18. Nakagawa, S, Nishihara, K, Miyata, H, Shinke, H, Tomita, E, Kajiwara, M, Matsubara, T, Iehara, N, Igarashi, Y, Yamada, H, Fukatsu, A, Yanagita, M, Matsubara, K, Masuda, S: Molecular Markers of Tubulointerstitial Fibrosis and Tubular Cell Damage in Patients with Chronic Kidney Disease. *PLoS One,* 10**:** e0136994, 2015.
19. Mokry, M, Hatzis, P, Schuijers, J, Lansu, N, Ruzius, FP, Clevers, H, Cuppen, E: Integrated genome-wide analysis of transcription factor occupancy, RNA polymerase II binding and steady-state RNA levels identify differentially regulated functional gene classes. *Nucleic Acids Res,* 40**:** 148-158, 2012.
20. Keller, BJ, Martini, S, Sedor, JR, Kretzler, M: A systems view of genetics in chronic kidney disease. *Kidney Int,* 81**:** 14-21, 2012.
21. Martovetsky, G, Tee, JB, Nigam, SK: Hepatocyte nuclear factors 4alpha and 1alpha regulate kidney developmental expression of drug-metabolizing enzymes and drug transporters. *Mol Pharmacol,* 84**:** 808-823, 2013.
22. Consortium, GT: Human genomics. The Genotype-Tissue Expression (GTEx) pilot analysis: multitissue gene regulation in humans. *Science,* 348**:** 648-660, 2015.
23. Vernot, B, Stergachis, AB, Maurano, MT, Vierstra, J, Neph, S, Thurman, RE, Stamatoyannopoulos, JA, Akey, JM: Personal and population genomics of human regulatory variation. *Genome Res,* 22**:** 1689-1697, 2012.
24. Viscomi, C, Spinazzola, A, Maggioni, M, Fernandez-Vizarra, E, Massa, V, Pagano, C, Vettor, R, Mora, M, Zeviani, M: Early-onset liver mtDNA depletion and late-onset proteinuric nephropathy in Mpv17 knockout mice. *Hum Mol Genet,* 18**:** 12-26, 2009.
25. Griffin, SV, Olivier, JP, Pippin, JW, Roberts, JM, Shankland, SJ: Cyclin I protects podocytes from apoptosis. *J Biol Chem,* 281**:** 28048-28057, 2006.
26. Xia, M, Liu, J, Wu, X, Liu, S, Li, G, Han, C, Song, L, Li, Z, Wang, Q, Wang, J, Xu, T, Cao, X: Histone methyltransferase Ash1l suppresses interleukin-6 production and inflammatory autoimmune diseases by inducing the ubiquitin-editing enzyme A20. *Immunity,* 39**:** 470-481, 2013.
27. Groger, N, Vitzthum, H, Frohlich, H, Kruger, M, Ehmke, H, Braun, T, Boettger, T: Targeted mutation of SLC4A5 induces arterial hypertension and renal metabolic acidosis. *Hum Mol Genet,* 21**:** 1025-1036, 2012.
28. Kirby, A, Gnirke, A, Jaffe, DB, Baresova, V, Pochet, N, Blumenstiel, B, Ye, C, Aird, D, Stevens, C, Robinson, JT, Cabili, MN, Gat-Viks, I, Kelliher, E, Daza, R, DeFelice, M, Hulkova, H, Sovova, J, Vylet'al, P, Antignac, C, Guttman, M, Handsaker, RE, Perrin, D, Steelman, S, Sigurdsson, S, Scheinman, SJ, Sougnez, C, Cibulskis, K, Parkin, M, Green, T, Rossin, E, Zody, MC, Xavier, RJ, Pollak, MR, Alper, SL, Lindblad-Toh, K, Gabriel, S, Hart, PS, Regev, A, Nusbaum, C, Kmoch, S, Bleyer, AJ, Lander, ES, Daly, MJ: Mutations causing medullary cystic kidney disease type 1 lie in a large VNTR in MUC1 missed by massively parallel sequencing. *Nat Genet,* 45**:** 299-303, 2013.
29. Koptides, M, Hadjimichael, C, Koupepidou, P, Pierides, A, Constantinou Deltas, C: Germinal and somatic mutations in the PKD2 gene of renal cysts in autosomal dominant polycystic kidney disease. *Hum Mol Genet,* 8**:** 509-513, 1999.
30. Stolarczyk, J, Carone, FA: Effects of renal lymphatic occlusion and venous constriction on renal function. *Am J Pathol,* 78**:** 285-296, 1975.
31. Outeda, P, Huso, DL, Fisher, SA, Halushka, MK, Kim, H, Qian, F, Germino, GG, Watnick, T: Polycystin signaling is required for directed endothelial cell migration and lymphatic development. *Cell Rep,* 7**:** 634-644, 2014.
32. Buhling, F, Rocken, C, Brasch, F, Hartig, R, Yasuda, Y, Saftig, P, Bromme, D, Welte, T: Pivotal role of cathepsin K in lung fibrosis. *Am J Pathol,* 164**:** 2203-2216, 2004.

33. Lopez-Guisa, JM, Cai, X, Collins, SJ, Yamaguchi, I, Okamura, DM, Bugge, TH, Isacke, CM, Emson, CL, Turner, SM, Shankland, SJ, Eddy, AA: Mannose receptor 2 attenuates renal fibrosis. *J Am Soc Nephrol,* 23**:** 236-251, 2012.
34. Sidaway, JE, Davidson, RG, McTaggart, F, Orton, TC, Scott, RC, Smith, GJ, Brunskill, NJ: Inhibitors of 3-hydroxy-3-methylglutaryl-CoA reductase reduce receptor-mediated endocytosis in opossum kidney cells. *J Am Soc Nephrol,* 15**:** 2258-2265, 2004.
35. Eelen, G, de Zeeuw, P, Simons, M, Carmeliet, P: Endothelial cell metabolism in normal and diseased vasculature. *Circ Res,* 116**:** 1231-1244, 2015.
36. Chambers, JC, Zhang, W, Lord, GM, van der Harst, P, Lawlor, DA, Sehmi, JS, Gale, DP, Wass, MN, Ahmadi, KR, Bakker, SJ, Beckmann, J, Bilo, HJ, Bochud, M, Brown, MJ, Caulfield, MJ, Connell, JM, Cook, HT, Cotlarciuc, I, Davey Smith, G, de Silva, R, Deng, G, Devuyst, O, Dikkeschei, LD, Dimkovic, N, Dockrell, M, Dominiczak, A, Ebrahim, S, Eggermann, T, Farrall, M, Ferrucci, L, Floege, J, Forouhi, NG, Gansevoort, RT, Han, X, Hedblad, B, Homan van der Heide, JJ, Hepkema, BG, Hernandez-Fuentes, M, Hypponen, E, Johnson, T, de Jong, PE, Kleefstra, N, Lagou, V, Lapsley, M, Li, Y, Loos, RJ, Luan, J, Luttropp, K, Marechal, C, Melander, O, Munroe, PB, Nordfors, L, Parsa, A, Peltonen, L, Penninx, BW, Perucha, E, Pouta, A, Prokopenko, I, Roderick, PJ, Ruokonen, A, Samani, NJ, Sanna, S, Schalling, M, Schlessinger, D, Schlieper, G, Seelen, MA, Shuldiner, AR, Sjogren, M, Smit, JH, Snieder, H, Soranzo, N, Spector, TD, Stenvinkel, P, Sternberg, MJ, Swaminathan, R, Tanaka, T, Ubink-Veltmaat, LJ, Uda, M, Vollenweider, P, Wallace, C, Waterworth, D, Zerres, K, Waeber, G, Wareham, NJ, Maxwell, PH, McCarthy, MI, Jarvelin, MR, Mooser, V, Abecasis, GR, Lightstone, L, Scott, J, Navis, G, Elliott, P, Kooner, JS: Genetic loci influencing kidney function and chronic kidney disease. *Nat Genet,* 42**:** 373-375, 2010.
37. Suhre, K, Shin, SY, Petersen, AK, Mohney, RP, Meredith, D, Wagele, B, Altmaier, E, CardioGram, Deloukas, P, Erdmann, J, Grundberg, E, Hammond, CJ, de Angelis, MH, Kastenmuller, G, Kottgen, A, Kronenberg, F, Mangino, M, Meisinger, C, Meitinger, T, Mewes, HW, Milburn, MV, Prehn, C, Raffler, J, Ried, JS, Romisch-Margl, W, Samani, NJ, Small, KS, Wichmann, HE, Zhai, G, Illig, T, Spector, TD, Adamski, J, Soranzo, N, Gieger, C: Human metabolic individuality in biomedical and pharmaceutical research. *Nature,* 477**:** 54-60, 2011.
38. Yu, B, Zheng, Y, Alexander, D, Morrison, AC, Coresh, J, Boerwinkle, E: Genetic determinants influencing human serum metabolome among African Americans. *PLoS Genet,* 10**:** e1004212, 2014.
39. Birnbaum, RY, Clowney, EJ, Agamy, O, Kim, MJ, Zhao, J, Yamanaka, T, Pappalardo, Z, Clarke, SL, Wenger, AM, Nguyen, L, Gurrieri, F, Everman, DB, Schwartz, CE, Birk, OS, Bejerano, G, Lomvardas, S, Ahituv, N: Coding exons function as tissue-specific enhancers of nearby genes. *Genome Res,* 22**:** 1059-1068, 2012.

Supplemental data

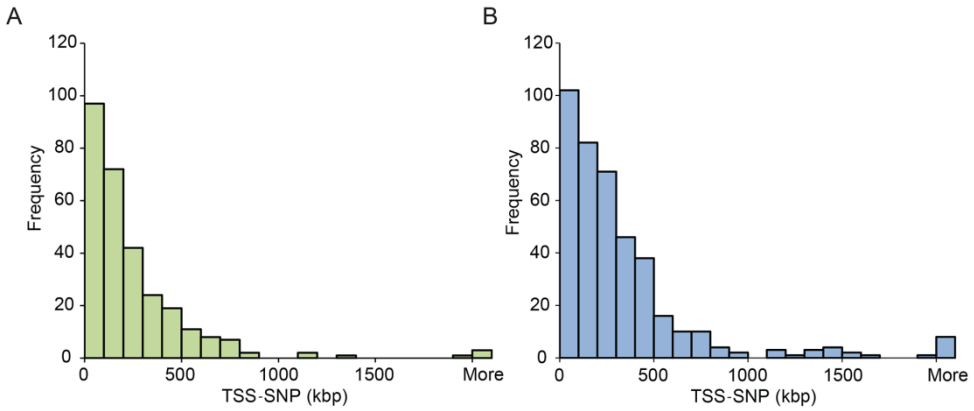

Supplemental Figure 1: The majority of genes identified with 4C-seq were positioned up to 500kbp from the CKD associated SNP locus. **(A)** Graph indicates the distance from the SNP to the TSS of the target genes found with 4C in HRGECs (X-axis), expressed as the number of target genes (frequency on Y-axis) per 100kbp. The majority of target genes was positioned up to 500kbp from the SNP, but occasionally candidate genes were found at locations over 1.5mb from the SNP locus. **(B)** The TSS of the majority of candidate genes found with 4C in HRPTECs was positioned up to 500kbp from the SNP position, but some candidate genes were found at locations over 1.5mbp from the SNP locus.

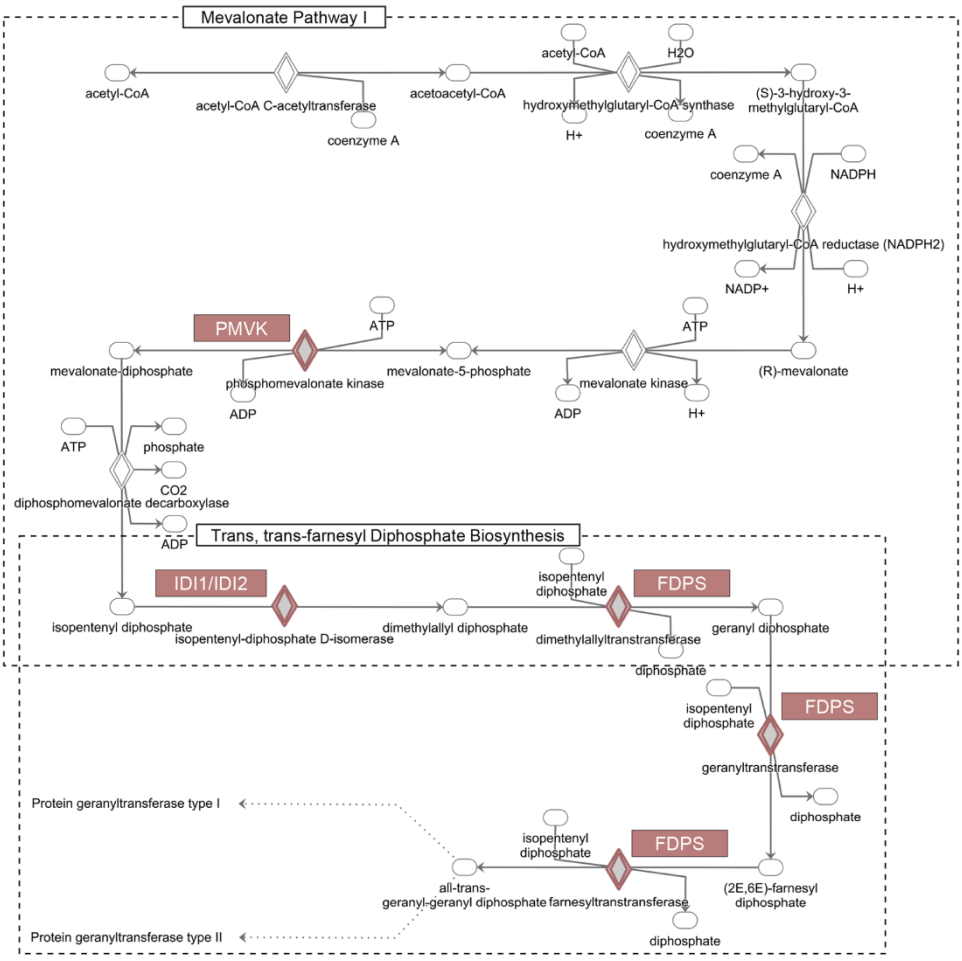

Supplemental Figure 2: Target genes of DREs colocalizing with CKD-associated SNPs, highlighted in red, are enriched in the mevalonate pathway and the trans, trans-farnesyl diphosphate biosynthesis pathway (adapted from IPA).

Supplemental Tables can be downloaded from:
http://jasn.asnjournals.org/lookup/suppl/doi:10.1681/ASN.2016080875/-/DCSupplemental.

Chapter 8

General discussion and summary

General discussion and summary

Cardiovascular diseases are the leading cause of disease burden and deaths globally.[1] The term cardiovascular disease covers a broad domain of acute and chronic disruptions of vascular and cardiac function, which are often interrelated. In contrast to what the term suggests, cardiovascular diseases are not tightly framed concerning only the heart and vessels. The kidneys for instance are bidirectionally related to cardiovascular homeostasis, not only functionally depending on it, but also playing a crucial role in maintaining this homeostasis.[2] Moreover, considering that every cell in the body depends on oxygen and nutrients, whose transport is facilitated by the cardiovascular system, it is not surprising that dysregulation of this system can both have a causal-, and a contributing role in organism-wide pathological conditions, varying from development of exercise intolerance to tumorigenesis facilitated by excessive vascular growth. Over the years, a plethora of studies has focussed on the many different aspects of cardiovascular- and renal disease, which has not only led to better insights into the existence and management of risk factors, but has also provided the intellectual basis for successful therapeutic interventions. Unfortunately, many mechanisms underlying development and progression of these diseases are still poorly understood, and the aim of this thesis was therefore to provide novel insights in the molecular regulation of renal and cardiovascular homeostasis.

Endothelial FZD5 signaling and therapeutic potential of its modulation

Dysregulation of vascular growth is associated with the onset and progression of many diseases and restoration of the angiogenic balance might provide an opening with far-reaching therapeutic potential.[3] Over the past decades, a lot of progress has been made in unraveling the pathways involved in regulating vascular quiescence and angiogenesis. This led to the development of treatment strategies aiming for instance to enhance collateral vessel formation in myocardial ischemia[4], and to block detrimental angiogenesis as observed in atherosclerosis and tumorigenesis.[5] Although some of these therapies are now implemented in standard treatment protocols, our incomplete knowledge of vascular growth often leads to unexpected and undesirable outcomes. Anti-angiogenic therapy in cancer for instance, often faces therapeutic resistance due to upregulation of alternative angiogenic pathways and selection of tumor cells capable of growing in a low oxygen environment.[6, 7] In addition to current therapeutic barriers, graft vascularization comes as one of the most predominant challenges in regenerative medicine, and the current incomplete knowledge of angiogenesis limits progression in this field to avascular applications.[8] Overall, these shortcomings in current medicine underscore the necessity to further explore the

mechanisms involved in regulation of vascular growth and stabilization. In previous studies it has been suggested that WNT receptor Frizzled 5 (FZD5) might be an important regulator in angiogenesis.[9] FZD5 knockout mice have previously been shown to die in utero with severe defects in yolk sac and placenta angiogenesis.[9] However, the mechanism underlying the poor vascular phenotype in absence of this receptor had not been elucidated.

In **chapter 2** we show that WNT5a is able to activate FZD5-mediated phosphorylation of Dishevelled in endothelial cells and that siRNA-mediated knockdown of this receptor attenuated angiogenesis in an *in vitro* 3D co-culture model. These findings reveal the direct role of endothelial FZD5 in angiogenesis, superimposing the reported defect in chorionic branching morphogenesis to which part of the murine FZD5 full body knockout phenotype had previously been ascribed.[10] **Chapter 2** furthermore illustrates that blockade of endothelial FZD5 expression induced upregulation of VEGFr1 and Angpt2. Angpt2 by itself is known to have a positive effect on neovessel formation, as it antagonizes binding of Angpt1 to the endothelial Tie2 receptor, leading to pericyte detachment and destabilization of the endothelium, thereby potentiating the actions of pro-angiogenic factors.[11, 12] However, in the absence of VEGFa, or in the presence of elevated levels of the VEGFa decoy receptor VEGFr1, Angpt2-induced destabilization eventually proceeds to vascular regression.[13, 14] Using various pharmacological- and siRNA-mediated inhibitory experiments, we demonstrated that the upregulation of VEGFr1 and Angpt2 did not depend on dysregulation of well-described WNT/β-catenin, WNT/Ca^{2+} and WNT/planar cell polarity signaling. Instead, we found that in absence of FZD5, Ca^{2+}-independent Protein Kinase C induced Ets1-mediated transcription of these vascular regression-associated factors. In parallel with our findings, a genome-wide CRISPR-Cas9 study recently demonstrated that FZD5 is a potentially druggable target in specific subtypes of pancreatic tumors.[15] Signaling via FZD5 in these tumor cells was shown to induce β-catenin-mediated proliferation and treatment of these pancreatic adenocarcinoma cells with FZD5 antibodies led to inhibited cell growth, both *in vitro* and in xenograft models *in vivo*.[15] Although these pancreatic adenocarcinoma tumors are not excessively vascularized, they were previously shown to depend on angiogenesis for growth.[16, 17] Our data demonstrate the importance of FZD5 for endothelial cells during angiogenesis and future studies should be aimed at elucidating whether targeting FZD5 in these pancreatic tumors, beside its inhibitory effect on growth of pancreatic adenocarcinoma cells, provides an additional effect on tumor angiogenesis without affecting the healthy vasculature.

Characterization of endothelium-induced pericyte differentiation

Pericytes play a major role in capillary stabilization, a function for which they rely on well-orchestrated and bidirectional cross talk with the endothelium.[18] Considering their role in maintaining vascular quiescence, pericytes are inseparable from the process of neovascularization and in our attempts to get a better appreciation of this process, it is thus essential that we do not limit our scope to the endothelium. Moreover, novel insights in pericyte function and their interaction with the endothelium could not only have a beneficial impact on angiogenic- and regenerative medicine applications, but might also provide a better understanding of pathological conditions such as organ fibrosis, in which disturbed vascular crosstalk has been suggested to be causally involved in progression towards organ failure.[19-21]

To get a better appreciation of pericyte function and the effect of interaction with endothelial cells hereon, we compared the transcriptome of pericytes cultured in absence, and in direct presence of microvascular endothelial cells. In **chapter 3** we describe the capillary niche-dependent differentiation of pericytes. The sonic hedgehog transcription factor Zinc Finger Protein GLI1 (GLI1), which was previously described to mark immature pericyte progenitors[21], was significantly reduced in co-cultured pericytes. In contrast, well-validated pericyte markers[22], including Chondroitin Sulfate Proteoglycan 4 (NG2), Alpha Smooth Muscle Actin 2 (ACTA2), Melanoma Cell Adhesion Molecule (CD146) and Nestin (NES), were highly upregulated upon direct interaction with endothelial cells, underscoring the importance of direct endothelial interaction for pericyte maturation. **Chapter 3** furthermore describes how endothelial cells stimulate pericyte proliferation and survival. Although it had previously been suggested that this was a VEGFa-dependent phenomenon[23], we could not confirm this finding in our study. In contrast, both pathway analysis and siRNA-mediated interventions demonstrated the significant proliferative contribution of Heparin-binding EGF-like growth factor (HB-EGF) and fibroblast growth factor 2 (FGF2), which unlike VEGFa were upregulated in co-cultured pericytes. In line with our findings, both factors have previously been shown to stimulate proliferation in a variety of cell types and our data suggest the existence of an endothelial-induced autocrine proliferation signaling axis in pericytes.[24-26] Similarly, our findings confirmed the importance of the endothelial-derived Platelet Derived Growth Factor β. This well-described pericyte mitogen was upregulated in co-cultured endothelial cells[27], and siRNA-mediated knockdown significantly reduced proliferation of pericytes. Moreover, **chapter 3** illustrates that in addition to pericyte maturation and proliferation, direct interaction with endothelial cells has a major suppressive effect on extracellular matrix synthesis, as evidenced by an overall downregulation of Fibronectin (FN1), Alpha- and Beta Laminins (LAMAs and LAMBs, respectively), and

numerous Collagen isoforms. In previous studies, renal- and cardiac tissue resident pericytes were shown to be major contributors to injury-induced fibrosis and their detachment from the endothelium was shown to coincide both with capillary rarefaction and differentiation towards ECM-producing myofibroblasts.[21] Whether injury-induced stimulation, or loss of endothelial interaction drove this differentiation is not completely understood, but since ablation of these cells substantially ameliorated cardiac- and renal fibrosis[21], they seem promising targets for future therapeutic interventions. Our findings argue that differentiation into a scarring phenotype might at least in part be secondary to loss of direct interaction with the endothelium, and that future interventions, aiming for prevention of initial pericyte detachment, have the potential to act as a double-edged sword - not only stabilizing capillaries and thus preventing capillary rarefaction and local ischemia, but also limiting differentiation of pericytes into ECM-producing cells.

ZSF1 rats as animal model of comorbidity-induced diastolic dysfunction

To facilitate the distribution of oxygen- and nutrients throughout the body, the vascular system relies on proper cardiac function. The chronic and progressive condition, in which the heart is unable to maintain cardiac output commensurate with the body's requirements, is referred to as heart failure (HF). Based on ejection fraction, HF can be divided into HF with reduced ejection fraction (HFrEF) and HF with preserved ejection fraction (HFpEF). HFrEF is associated with systolic impairments, whereas HFpEF results from diastolic dysfunction. Both HFrEF and HFpEF are associated with the presence of multiple systemic comorbidities, including chronic kidney disease (CKD) and hypertension.[28] In general, systemic impairments in HFrEF are largely driven by a primary defect in systolic function.[29] Since these primary defects, such as loss of muscle mass due to a coronary artery obstruction, can properly be induced in animal models, the etiology of HFrEF is relatively well studied and major therapeutic progress has been made in reducing its mortality over the last decades.[30] Conversely, the etiology of HFpEF is still poorly understood and common successful therapeutics for treatment of HFrEF, such as angiotensin-converting enzyme inhibitors and β-blockers, have shown no significant impact on clinical outcomes in HFpEF.[31] Moreover, it remains unclear how the associated comorbidities contribute to the development of the different aspects of diastolic dysfunction and identification as well as characterization of animal models that develop HFpEF, driven by relevant systemic impairments, could provide novel pathological insights and may lead to therapeutic opportunities.

In **chapter 4** we describe the obese Zucker spontaneously hypertensive fatty (ZSF1) rat strain, which has been reported as a suitable *in vivo* model to study HFpEF development in presence of renal- and metabolic derangements.[32] At the age of 25 weeks, these rats had

substantially increased body weight, showed elevated fasting plasma glucose levels, and a decline in renal function as evidenced by severe proteinuria. Renal dysfunction was accompanied by glomerular sclerosis and capillary rarefaction, and in addition to the metabolic- and renal derangements, the ratio between peak velocity of early mitral inflow and early diastolic mitral annulus velocity (E/e') was significantly elevated, indicative of diastolic dysfunction. Moreover, LV mass, left atria and lung weight were increased, typically resembling clinical features of HFpEF.[33] In **chapter 4** we report that progression of diastolic dysfunction in obese ZSF1 rats was not accompanied by capillary rarefaction. Instead, development of fibrotic patches with highly proliferative and disorganized microvascular clusters was observed in the LV subendocardium. In a previous study, cardiac biopsies from HFpEF patients were shown to contain clear interstitial fibrosis, yet in contrast to our findings, capillary density was reduced.[34] Although additional studies are required to further elucidate this dynamic process, we hypothesize that the cardiac hyperproliferative vascular response in obese ZSF1 rats was part of a maladaptive response that leads to replacement of functional vascular structures by fibrotic tissue with semi- and nonfunctional microvascular clusters, which may ultimately deteriorate into the previously reported fibrotic areas that are devoid of vascular support. In **chapter 4** we also illustrate that the fibrotic foci are not only enriched in endothelial cells, but also in NG2- and PDGFRβ-positive pericytes. Remarkably, these pericytes were atypically organized, showing limited vascular coverage. Double staining for PDGFRβ-positive pericytes and Collagen type 4 (COL4), a vascular basement membrane component predominantly produced by pericytes, demonstrated a robust COL4 deposition in the fibrotic foci, indicative for a potential fibrotic contribution of pericytes, which has also been described in **chapter 3**. Future studies are planned in which we aim to get a better appreciation of the putative role of pericytes in HFpEF-associated cardiac fibrosis.

Limited synergy between obesity and hypertension in development of diastolic dysfunction

In previous studies it has been proposed that presence of non-cardiac comorbidities could provoke a state of chronic systemic inflammation, leading to coronary microvascular dysfunction and myocardial fibrosis.[35] Fibrosis is suspected to limit LV relaxation, whereas microvascular dysfunction lowers NO availability, which causes impaired myocardial Protein Kinase G (PKG) activity, leading to cardiomyocyte hypertrophy and Titin (TTN) hypophosphorylation.[35] This hypophosphorylation of TTN was also evident in cardiomyocytes from obese ZSF1 rats, and was experimentally shown to be a major contributor to cardiac stiffness.[32] Based on this proposed mechanism, several successful pre-clinical studies paved the road for a multitude of large clinical trials aiming to improve perspectives of HFpEF patients. For instance, phosphodiesterase-5 inhibitor sildenafil and

guanylate cyclase stimulator veriguat were used to stimulate myocardial PKG activity[36, 37], whereas the mineralocorticoid receptor antagonists spironolactone on the other hand, was supposed to limit both endothelial dysfunction and myocardial fibrosis.[38] Unfortunately, none of the HFpEF-related clinical trials so far led to significant improvement of exercise capacity or clinical status. It is currently believed that this lack of success might find its origin in the phenotypical diversity among HFpEF patients and personalized therapeutic strategies are therefore proposed.[39] In order to successfully implement personalized medicine, it is of the essence that we get a better appreciation of phenotypical differences among HFpEF patients, and how these, for instance, relate to presence of different comorbidities.[31]

In **chapter 5** we studied the superimposing effect of deoxycorticosterone acetate- and high salt diet- (DS) induced hypertension on diastolic dysfunction in lean and obese ZSF1 rats discussed in **chapter 4**. This not only enabled us to dissect which adaptations were associated with obesity and its associated biochemical aberrations, and which were associated with hypertension, but also to directly study their putative interaction. We found that obesity-associated derangements had the most predominant effect on development of diastolic dysfunction, lowering of cardiac output, and cardiomyocyte hypertrophy, with only a limited additive effect of hypertension. Not only are these findings in line with observations from the MONICA registry and the ALL-HAT trial[40, 41], which showed a larger contribution of obesity to HFpEF development than hypertension, they also illustrate why blood pressure lowering drugs alone did not reduce morbidity and mortality in HFpEF patients.[42] Other findings in **chapter 5** further support that, when considering therapeutic interventions, it is extremely important to anticipate potential pathophysiological differences among HF patients that were thus far grouped based on the common denominator “preserved ejection fraction”. For instance, cardiac inflammation and subsequent fibrosis, unlike diastolic dysfunction and hypertrophy, were predominantly driven by DS-induced hypertension, with partial synergy observed when combined with obesity. Although hypertension-induced fibrosis was accompanied by only a mild increase in diastolic dysfunction, it has previously been shown to be an independent predictor of morbidity and mortality in HFpEF[43, 44], suggesting that mineralocorticoid receptor antagonists could in essence have beneficial effects in HFpEF patients, provided that they are evaluated and used in relevant patient subsets. Similarly, in **chapter 5** we also demonstrate that obesity stimulated enhanced expression of genes involved in fatty acid oxidation, whereas DS-induced hypertension led to an overall downregulation of genes involved in oxidative phosphorylation, implying that the comorbidities triggered adverse mitochondrial responses. Aiming for a therapeutic switch from fatty acids towards more oxygen-efficient glucose metabolism[45], as was previously suggested for HFpEF[46], might provide a promising opportunity for obese patients, but may

well be far less effective when applied to HFpEF patients with hypertension-induced mitochondrial dysfunction. In summary, **chapter 5** illustrates the limited interaction among obesity and hypertension, and implies that, in order to successfully attenuate or reverse disease progression, differences in comorbidity-induced cardiac remodeling require personalized interventions, according to the differences in HFpEF phenotypes.

Chromatin organisation-based annotation of candidate genes in atherosclerosis and CKD

Although cardiovascular- and renal disease are heavily influenced by environmental factors, genome wide association studies (GWASs) have also identified many common genetic variants or single nucleotide polymorphisms (SNPs) that are associated with onset and progression of these pathological conditions.[47-50] Among the disease-associated variants, non-synonymous SNPs (affecting protein sequence) are exceptionally rare and functional annotation of most risk loci therefore till date remains an issue. Annotation has thus far mainly been conducted by linking risk loci to genes at the nearest genomic position based on linear spatial proximity, taking into consideration that disease-associated SNPs could be markers for less common non-synonymous variants.[51] Unfortunately, this approach has only partially been able to explain genetic variation-induced disease development. Recent epigenetic studies have revealed that our genetic material is packed with DNA regulatory elements (DREs), such as promoters, enhancers and repressors, located in both coding- and non-protein-coding DNA regions.[52] These DREs play a crucial role in transcriptional regulation in a cell type- and circumstance-specific manner and growing evidence suggests that variants residing in regulatory sequences, in addition to non-synonymous variants, could contribute to pathogenesis.[53] Systematic mapping of genes that are transcriptionally regulated by DREs that colocalize with disease-associated common variants could greatly improve our understanding of the complex genetics involved in cardiovascular- and renal disease.

In **chapter 6** and **chapter 7** we used circular chromosome conformation capture sequencing (4C-seq), which enabled us to identify genes that physically interacted with DREs colocalizing with atherosclerosis- and CKD-associated risk loci, respectively. Since transcriptional regulation might differ among individual cell-types, 3D chromatin interactions in relation to atherosclerotic disease were evaluated in microvascular endothelial cells and monocytes. In these cells we found 37 active DREs that colocalized with SNPs associated with coronary artery disease and stroke. Both are conditions to which a large part of the disease burden of atherosclerosis can be traced back to. These 37 active DREs were shown to physically interact with a total of 326 candidate genes, of which 296 had not been reported before. In **chapter 7**, we employed a similar approach to identify candidate genes

for SNPs associated with CKD, using renal proximal tubule epithelial cells and glomerular endothelial cells. In these cells we studied 36 CKD-associated SNPs that colocalized with active DREs. In total, these 36 risk loci interacted with a total of 304 candidate genes.

The physical interactions identified by 4C-seq, do not per se mean that expression of the captured genes is affected by the associated loci. However, evaluation of known expression quantitative trait loci (eQTL) substantiated this putative regulatory relation between many studied risk loci and the identified candidate genes. In **chapter 7** we used the Genotype-Tissue Expression (GTEx) database. We found that among the studied CKD-associated risk loci, 25 were highly correlated with differential expression of 54 different genes. Of these 54 genes, the promoter regions of 48 genes were captured by 4C-seq, and although the lack of kidney-specific expression data from genotyped donors in GTEx did not allow us to study these eQTL in renal tissue, it did provide direct evidence for the hypothesized transcriptional regulation by the studied risk loci and showed that 4C-seq enabled us to capture relevant target genes. In **chapter 7** we further substantiated the causal role of common variants in transcriptional regulation by applying self-transcribing active regulatory region sequencing (STARR-seq).[54] In a proof of principle approach, studying the CKD risk locus marked by rs11959928, this technique enabled us to pinpoint specific variants that colocalized with DREs in this locus and affected transcriptional activity. For coronary artery disease on the other hand, eQTL analysis could be performed in monocytes and the vasculature, resembling the tissue in which the initial 4C-seq was performed. In line with the findings from the CKD study, in **chapter 6** we report a variety of atherosclerosis-associated risk loci that were shown to affect transcriptional regulation of many genes captured with 4C. Of particular interest was the coronary artery disease-associated variant rs12740374. The minor T allele of rs12740374 creates a CCAAT/enhancer binding protein (C/EBP) transcription factor binding site which was previously demonstrated to elevate liver sortilin 1 (SORT1) expression.[55] Various *in vitro* and *in vivo* studies demonstrated that overexpression of SORT1 resulted enhanced low-density-lipoprotein (LDL) clearance, whereas SORT1 deficiency, mimicking the effect of the rs12740374 risk allele, led to impaired LDL clearance[56, 57]. Largely because of this clear effect that appears to explain much of the causal relation with atherosclerosis, no further attention has been given to alternative candidate genes for this risk locus. Remarkably, SORT1 expression was not affected by rs12740374 in monocytes, whereas expression of proline and serine rich coiled-coil 1 (PSRC1), which was captured by 4C-seq, was genotype-dependent. Interestingly, the expression of PSRC1 also correlated with atherosclerosis severity independent of LDL levels, the putative mechanism through which dysregulation of SORT1 acts, suggesting that in addition to SORT1, PSRC1 could be considered as a promising candidate for future

mechanistic studies in atherogenesis. Using various online databases containing human and murine phenotypic information on monogenetic mutations, we furthermore found that many of the identified candidate genes were strongly associated with different aspects of the studied disorders. Phosphatase and tensin analog (PTEN) for instance, of which the promoter region interacted with the atherosclerosis-associated LIPA risk locus (rs2246833), has previously been correlated with inflammatory plaque characteristics and intimal smooth muscle cell proliferation[58], whereas increased stability of PTEN on the other hand appears to ameliorate atherosclerosis (**chapter 6**).[59] Similarly, Mucin-1 (MUC1) physically interacted with the CKD-associated variant rs2049805, which was also shown to be an eQTL for MUC1. MUC1 is a membrane-anchored mucoprotein, in which a pre-mature stop codon-inducing frame shift mutation has previously been demonstrated to result in medullar cystic kidney disease type 1 (**chapter 7**).[60] These illustrative examples highlight the indispensable nature of both factors, and underscore that genetic variation-induced dysregulation of their expression might very well contribute to pathogenesis. Overall, our findings reported in **chapter 6** and **chapter 7** annotated multiple genes to previously reported CKD-associated SNPs and provided evidence for interaction between these loci and their target genes. This pipeline provides a novel technique for hypothesis generation and complements classic GWAS interpretation. Future studies are required to specify the implications of our findings, focusing both on the mechanism by which the newly annotated genes might contribute to disease, as well as on applying STARR-seq more broadly to specifically identify disease causing variants, rather than variants marking risk loci. Moreover, in future studies these techniques could also be applied to further dissect the role of genetics in the renocardiac- and cardiorenal syndrome. It has for instance been demonstrated that the cardiac transcriptome is heavily influenced by CKD-associated circulating factors, such as Endothelin 1 and Angiotensin II, as well as accumulating renal toxins.[61] This implies that these factors have a profound effect on DRE activity in cardiomyocytes, cardiac fibroblast or coronary endothelium. Mapping those responsive regulatory elements, followed by STARR-seq and 4C-seq analysis of colocalizing heart failure-associated risk loci, could contribute to our understanding of renal dysfunction-induced heart failure. Similarly, studying CKD-associated risk loci colocalizing with DREs affected for instance by low oxygen levels, mimicking heart failure-induced renal hypoperfusion, might provide a better appreciation of the complex interplay between the heart and kidney during disease.

Future perspectives

The studies presented in this thesis aimed to provide novel insights in the molecular regulation of renal and cardiovascular homeostasis. With these proceeding insights, several

new questions arose that should be pursued in future studies. Firstly, the *in vitro* studies on the role of endothelial FZD5 signaling, described in **chapter 2,** illustrate the importance of this receptor in vascular growth. The finding that *in vivo* blockade of this receptor with FZD5 antibodies also attenuated growth of ring finger protein 43 (RNF43) mutant pancreatic tumors[15], raised the question whether part of this effect was the result of the inhibition of angiogenesis. Simple but effective ways to assess the impact of FZD5 antibodies on tumor angiogenesis would be to focus more on the tumor vasculature in response to the FZD5 antibodies rather than tumor size only, or to implant a non-RNF43 mutant tumor in immunodeficient mice instead of the originally used HPAF-II xenografts and evaluate overall tumor growth over time, with and without infusion of FZD5 antibodies. Not only would this lead us to a more comprehensive understanding of the working mechanism of these FZD5 antibodies as therapeutic agent against RNF43 mutant tumors, it could also provide valuable insights on the potential of FZD5 inhibition in a more general approach to block tumor angiogenesis. Secondly, the combined results from **chapter 3** and **chapter 4**, in which we illustrate that pericytes need stable interaction with endothelium to suppress a fibrotic phenotype, and that subendocardial fibrotic foci in obese ZSF1 rats are enriched in atypically organized pericytes, respectively, made us wonder to what extent these pericytes are causally related to the development of these fibrotic foci. In future experiments, using a single-cell sequencing approach on LV material from lean and obese ZSF1 rats, it might be possible to distinguish different subsets of cardiac pericytes, which would enable us to evaluate their putative fibrotic nature in obese rats in more detail. This approach would furthermore complement our current findings described in **chapter 5**, providing a better appreciation of cell type-specific adaptations involved in development of diastolic dysfunction. Finally, in our attempts to get a better appreciation of the effect of CKD-associated common variants on transcriptional regulation, described in **chapter 7**, we found a particular region marked by the CKD-associated SNP rs11959928, in which five variants significantly affected transcription. As these five variants are in high linkage disequilibrium with each other, it is possible that not all of them are actively involved in transcriptional regulation. Using site-directed mutagenesis, the variants causing transcriptional dysregulation identified with STARR-seq should one-by-one be replicated, which would enable us to individually assess their impact on transcription. Subsequently, we should replicate variants affecting transcription into the genome of human primary renal cells and verify which of the candidate genes, that we identified with 4C-seq, are in fact transcriptionally regulated by this CKD risk locus. This strategy would allow us to empirically select candidate genes for functional follow-up studies, and may lead us to a better understanding of disease-associated common variants.

References

1. Roth, GA, Johnson, C, Abajobir, A, Abd-Allah, F, Abera, SF, Abyu, G, Ahmed, M, Aksut, B, Alam, T, Alam, K, Alla, F, Alvis-Guzman, N, Amrock, S, Ansari, H, Arnlov, J, Asayesh, H, Atey, TM, Avila-Burgos, L, Awasthi, A, Banerjee, A, Barac, A, Barnighausen, T, Barregard, L, Bedi, N, Belay Ketema, E, Bennett, D, Berhe, G, Bhutta, Z, Bitew, S, Carapetis, J, Carrero, JJ, Malta, DC, Castaneda-Orjuela, CA, Castillo-Rivas, J, Catala-Lopez, F, Choi, JY, Christensen, H, Cirillo, M, Cooper, L, Jr., Criqui, M, Cundiff, D, Damasceno, A, Dandona, L, Dandona, R, Davletov, K, Dharmaratne, S, Dorairaj, P, Dubey, M, Ehrenkranz, R, El Sayed Zaki, M, Faraon, EJA, Esteghamati, A, Farid, T, Farvid, M, Feigin, V, Ding, EL, Fowkes, G, Gebrehiwot, T, Gillum, R, Gold, A, Gona, P, Gupta, R, Habtewold, TD, Hafezi-Nejad, N, Hailu, T, Hailu, GB, Hankey, G, Hassen, HY, Abate, KH, Havmoeller, R, Hay, SI, Horino, M, Hotez, PJ, Jacobsen, K, James, S, Javanbakht, M, Jeemon, P, John, D, Jonas, J, Kalkonde, Y, Karimkhani, C, Kasaeian, A, Khader, Y, Khan, A, Khang, YH, Khera, S, Khoja, AT, Khubchandani, J, Kim, D, Kolte, D, Kosen, S, Krohn, KJ, Kumar, GA, Kwan, GF, Lal, DK, Larsson, A, Linn, S, Lopez, A, Lotufo, PA, El Razek, HMA, Malekzadeh, R, Mazidi, M, Meier, T, Meles, KG, Mensah, G, Meretoja, A, Mezgebe, H, Miller, T, Mirrakhimov, E, Mohammed, S, Moran, AE, Musa, KI, Narula, J, Neal, B, Ngalesoni, F, Nguyen, G, Obermeyer, CM, Owolabi, M, Patton, G, Pedro, J, Qato, D, Qorbani, M, Rahimi, K, Rai, RK, Rawaf, S, Ribeiro, A, Safiri, S, Salomon, JA, Santos, I, Santric Milicevic, M, Sartorius, B, Schutte, A, Sepanlou, S, Shaikh, MA, Shin, MJ, Shishehbor, M, Shore, H, Silva, DAS, Sobngwi, E, Stranges, S, Swaminathan, S, Tabares-Seisdedos, R, Tadele Atnafu, N, Tesfay, F, Thakur, JS, Thrift, A, Topor-Madry, R, Truelsen, T, Tyrovolas, S, Ukwaja, KN, Uthman, O, Vasankari, T, Vlassov, V, Vollset, SE, Wakayo, T, Watkins, D, Weintraub, R, Werdecker, A, Westerman, R, Wiysonge, CS, Wolfe, C, Workicho, A, Xu, G, Yano, Y, Yip, P, Yonemoto, N, Younis, M, Yu, C, Vos, T, Naghavi, M, Murray, C: Global, Regional, and National Burden of Cardiovascular Diseases for 10 Causes, 1990 to 2015. *J Am Coll Cardiol,* 70**:** 1-25, 2017.
2. Shamseddin, MK, Parfrey, PS: Mechanisms of the cardiorenal syndromes. *Nat Rev Nephrol,* 5**:** 641-649, 2009.
3. Carmeliet, P: Angiogenesis in health and disease. *Nat Med,* 9**:** 653-660, 2003.
4. Degen, A, Millenaar, D, Schirmer, SH: Therapeutic approaches in the stimulation of the coronary collateral circulation. *Curr Cardiol Rev,* 10**:** 65-72, 2014.
5. Vasudev, NS, Reynolds, AR: Anti-angiogenic therapy for cancer: current progress, unresolved questions and future directions. *Angiogenesis,* 17**:** 471-494, 2014.
6. Casanovas, O, Hicklin, DJ, Bergers, G, Hanahan, D: Drug resistance by evasion of antiangiogenic targeting of VEGF signaling in late-stage pancreatic islet tumors. *Cancer Cell,* 8**:** 299-309, 2005.
7. Shojaei, F: Anti-angiogenesis therapy in cancer: current challenges and future perspectives. *Cancer Lett,* 320**:** 130-137, 2012.
8. Banfi, A, Holnthoner, W, Martino, MM, Yla-Herttuala, S: Editorial: Vascularization for Regenerative Medicine. *Front Bioeng Biotechnol,* 6**:** 175, 2018.
9. Ishikawa, T, Tamai, Y, Zorn, AM, Yoshida, H, Seldin, MF, Nishikawa, S, Taketo, MM: Mouse Wnt receptor gene Fzd5 is essential for yolk sac and placental angiogenesis. *Development,* 128**:** 25-33, 2001.
10. Lu, J, Zhang, S, Nakano, H, Simmons, DG, Wang, S, Kong, S, Wang, Q, Shen, L, Tu, Z, Wang, W, Wang, B, Wang, H, Wang, Y, van Es, JH, Clevers, H, Leone, G, Cross, JC, Wang, H: A positive feedback loop involving Gcm1 and Fzd5 directs chorionic branching morphogenesis in the placenta. *PLoS Biol,* 11**:** e1001536, 2013.
11. Rennel, ES, Regula, JT, Harper, SJ, Thomas, M, Klein, C, Bates, DO: A human neutralizing antibody specific to Ang-2 inhibits ocular angiogenesis. *Microcirculation,* 18**:** 598-607, 2011.
12. White, RR, Shan, S, Rusconi, CP, Shetty, G, Dewhirst, MW, Kontos, CD, Sullenger, BA: Inhibition of rat corneal angiogenesis by a nuclease-resistant RNA aptamer specific for angiopoietin-2. *Proc Natl Acad Sci U S A,* 100**:** 5028-5033, 2003.
13. Lobov, IB, Brooks, PC, Lang, RA: Angiopoietin-2 displays VEGF-dependent modulation of capillary structure and endothelial cell survival in vivo. *Proc Natl Acad Sci U S A,* 99**:** 11205-11210, 2002.
14. Zygmunt, T, Gay, CM, Blondelle, J, Singh, MK, Flaherty, KM, Means, PC, Herwig, L, Krudewig, A, Belting, HG, Affolter, M, Epstein, JA, Torres-Vazquez, J: Semaphorin-PlexinD1 signaling limits angiogenic potential via the VEGF decoy receptor sFlt1. *Dev Cell,* 21**:** 301-314, 2011.
15. Steinhart, Z, Pavlovic, Z, Chandrashekhar, M, Hart, T, Wang, X, Zhang, X, Robitaille, M, Brown, KR, Jaksani, S, Overmeer, R, Boj, SF, Adams, J, Pan, J, Clevers, H, Sidhu, S, Moffat, J, Angers,

S: Genome-wide CRISPR screens reveal a Wnt-FZD5 signaling circuit as a druggable vulnerability of RNF43-mutant pancreatic tumors. *Nat Med,* 23**:** 60-68, 2017.
16. Hotz, HG, Gill, PS, Masood, R, Hotz, B, Buhr, HJ, Foitzik, T, Hines, OJ, Reber, HA: Specific targeting of tumor vasculature by diphtheria toxin-vascular endothelial growth factor fusion protein reduces angiogenesis and growth of pancreatic cancer. *J Gastrointest Surg,* 6**:** 159-166; discussion 166, 2002.
17. Hotz, HG, Reber, HA, Hotz, B, Sanghavi, PC, Yu, T, Foitzik, T, Buhr, HJ, Hines, OJ: Angiogenesis inhibitor TNP-470 reduces human pancreatic cancer growth. *J Gastrointest Surg,* 5**:** 131-138, 2001.
18. Jain, RK: Molecular regulation of vessel maturation. *Nat Med,* 9**:** 685-693, 2003.
19. Lin, SL, Kisseleva, T, Brenner, DA, Duffield, JS: Pericytes and perivascular fibroblasts are the primary source of collagen-producing cells in obstructive fibrosis of the kidney. *Am J Pathol,* 173**:** 1617-1627, 2008.
20. Humphreys, BD, Lin, SL, Kobayashi, A, Hudson, TE, Nowlin, BT, Bonventre, JV, Valerius, MT, McMahon, AP, Duffield, JS: Fate tracing reveals the pericyte and not epithelial origin of myofibroblasts in kidney fibrosis. *Am J Pathol,* 176**:** 85-97, 2010.
21. Kramann, R, Schneider, RK, DiRocco, DP, Machado, F, Fleig, S, Bondzie, PA, Henderson, JM, Ebert, BL, Humphreys, BD: Perivascular Gli1+ progenitors are key contributors to injury-induced organ fibrosis. *Cell Stem Cell,* 16**:** 51-66, 2015.
22. van Dijk, CG, Nieuweboer, FE, Pei, JY, Xu, YJ, Burgisser, P, van Mulligen, E, el Azzouzi, H, Duncker, DJ, Verhaar, MC, Cheng, C: The complex mural cell: pericyte function in health and disease. *Int J Cardiol,* 190**:** 75-89, 2015.
23. Yamagishi, S, Yonekura, H, Yamamoto, Y, Fujimori, H, Sakurai, S, Tanaka, N, Yamamoto, H: Vascular endothelial growth factor acts as a pericyte mitogen under hypoxic conditions. *Lab Invest,* 79**:** 501-509, 1999.
24. Papetti, M, Shujath, J, Riley, KN, Herman, IM: FGF-2 antagonizes the TGF-beta1-mediated induction of pericyte alpha-smooth muscle actin expression: a role for myf-5 and Smad-mediated signaling pathways. *Invest Ophthalmol Vis Sci,* 44**:** 4994-5005, 2003.
25. Hosaka, K, Yang, Y, Nakamura, M, Andersson, P, Yang, X, Zhang, Y, Seki, T, Scherzer, M, Dubey, O, Wang, X, Cao, Y: Dual roles of endothelial FGF-2-FGFR1-PDGF-BB and perivascular FGF-2-FGFR2-PDGFRbeta signaling pathways in tumor vascular remodeling. *Cell Discov,* 4**:** 3, 2018.
26. Yu, X, Radulescu, A, Chen, CL, James, IO, Besner, GE: Heparin-binding EGF-like growth factor protects pericytes from injury. *J Surg Res,* 172**:** 165-176, 2012.
27. Hellstrom, M, Gerhardt, H, Kalen, M, Li, X, Eriksson, U, Wolburg, H, Betsholtz, C: Lack of pericytes leads to endothelial hyperplasia and abnormal vascular morphogenesis. *J Cell Biol,* 153**:** 543-553, 2001.
28. Mentz, RJ, Kelly, JP, von Lueder, TG, Voors, AA, Lam, CS, Cowie, MR, Kjeldsen, K, Jankowska, EA, Atar, D, Butler, J, Fiuzat, M, Zannad, F, Pitt, B, O'Connor, CM: Noncardiac comorbidities in heart failure with reduced versus preserved ejection fraction. *J Am Coll Cardiol,* 64**:** 2281-2293, 2014.
29. Roh, J, Houstis, N, Rosenzweig, A: Why Don't We Have Proven Treatments for HFpEF? *Circ Res,* 120**:** 1243-1245, 2017.
30. Ponikowski, P, Voors, AA, Anker, SD, Bueno, H, Cleland, JG, Coats, AJ, Falk, V, Gonzalez-Juanatey, JR, Harjola, VP, Jankowska, EA, Jessup, M, Linde, C, Nihoyannopoulos, P, Parissis, JT, Pieske, B, Riley, JP, Rosano, GM, Ruilope, LM, Ruschitzka, F, Rutten, FH, van der Meer, P, Authors/Task Force, M, Document, R: 2016 ESC Guidelines for the diagnosis and treatment of acute and chronic heart failure: The Task Force for the diagnosis and treatment of acute and chronic heart failure of the European Society of Cardiology (ESC). Developed with the special contribution of the Heart Failure Association (HFA) of the ESC. *Eur J Heart Fail,* 18**:** 891-975, 2016.
31. Silverman, DN, Shah, SJ: Treatment of Heart Failure With Preserved Ejection Fraction (HFpEF): the Phenotype-Guided Approach. *Curr Treat Options Cardiovasc Med,* 21**:** 20, 2019.
32. Hamdani, N, Franssen, C, Lourenco, A, Falcao-Pires, I, Fontoura, D, Leite, S, Plettig, L, Lopez, B, Ottenheijm, CA, Becher, PM, Gonzalez, A, Tschope, C, Diez, J, Linke, WA, Leite-Moreira, AF, Paulus, WJ: Myocardial titin hypophosphorylation importantly contributes to heart failure with preserved ejection fraction in a rat metabolic risk model. *Circ Heart Fail,* 6**:** 1239-1249, 2013.
33. Shah, SJ, Katz, DH, Deo, RC: Phenotypic spectrum of heart failure with preserved ejection fraction. *Heart Fail Clin,* 10**:** 407-418, 2014.

34. Mohammed, SF, Hussain, S, Mirzoyev, SA, Edwards, WD, Maleszewski, JJ, Redfield, MM: Coronary microvascular rarefaction and myocardial fibrosis in heart failure with preserved ejection fraction. *Circulation,* 131**:** 550-559, 2015.
35. Paulus, WJ, Tschope, C: A novel paradigm for heart failure with preserved ejection fraction: comorbidities drive myocardial dysfunction and remodeling through coronary microvascular endothelial inflammation. *J Am Coll Cardiol,* 62**:** 263-271, 2013.
36. Redfield, MM, Chen, HH, Borlaug, BA, Semigran, MJ, Lee, KL, Lewis, G, LeWinter, MM, Rouleau, JL, Bull, DA, Mann, DL, Deswal, A, Stevenson, LW, Givertz, MM, Ofili, EO, O'Connor, CM, Felker, GM, Goldsmith, SR, Bart, BA, McNulty, SE, Ibarra, JC, Lin, G, Oh, JK, Patel, MR, Kim, RJ, Tracy, RP, Velazquez, EJ, Anstrom, KJ, Hernandez, AF, Mascette, AM, Braunwald, E, Trial, R: Effect of phosphodiesterase-5 inhibition on exercise capacity and clinical status in heart failure with preserved ejection fraction: a randomized clinical trial. *JAMA,* 309**:** 1268-1277, 2013.
37. Pieske, B, Maggioni, AP, Lam, CSP, Pieske-Kraigher, E, Filippatos, G, Butler, J, Ponikowski, P, Shah, SJ, Solomon, SD, Scalise, AV, Mueller, K, Roessig, L, Gheorghiade, M: Vericiguat in patients with worsening chronic heart failure and preserved ejection fraction: results of the SOluble guanylate Cyclase stimulatoR in heArT failurE patientS with PRESERVED EF (SOCRATES-PRESERVED) study. *Eur Heart J,* 38**:** 1119-1127, 2017.
38. Pitt, B, Pfeffer, MA, Assmann, SF, Boineau, R, Anand, IS, Claggett, B, Clausell, N, Desai, AS, Diaz, R, Fleg, JL, Gordeev, I, Harty, B, Heitner, JF, Kenwood, CT, Lewis, EF, O'Meara, E, Probstfield, JL, Shaburishvili, T, Shah, SJ, Solomon, SD, Sweitzer, NK, Yang, S, McKinlay, SM, Investigators, T: Spironolactone for heart failure with preserved ejection fraction. *N Engl J Med,* 370**:** 1383-1392, 2014.
39. Shah, SJ: Precision Medicine for Heart Failure with Preserved Ejection Fraction: An Overview. *J Cardiovasc Transl Res,* 10**:** 233-244, 2017.
40. Stritzke, J, Markus, MR, Duderstadt, S, Lieb, W, Luchner, A, Doring, A, Keil, U, Hense, HW, Schunkert, H, Investigators, MK: The aging process of the heart: obesity is the main risk factor for left atrial enlargement during aging the MONICA/KORA (monitoring of trends and determinations in cardiovascular disease/cooperative research in the region of Augsburg) study. *J Am Coll Cardiol,* 54**:** 1982-1989, 2009.
41. Davis, BR, Kostis, JB, Simpson, LM, Black, HR, Cushman, WC, Einhorn, PT, Farber, MA, Ford, CE, Levy, D, Massie, BM, Nawaz, S, Group, ACR: Heart failure with preserved and reduced left ventricular ejection fraction in the antihypertensive and lipid-lowering treatment to prevent heart attack trial. *Circulation,* 118**:** 2259-2267, 2008.
42. Tsioufis, C, Georgiopoulos, G, Oikonomou, D, Thomopoulos, C, Katsiki, N, Kasiakogias, A, Chrysochoou, C, Konstantinidis, D, Kalos, T, Tousoulis, D: Hypertension and Heart Failure with Preserved Ejection Fraction: Connecting the Dots. *Curr Vasc Pharmacol,* 16**:** 15-22, 2017.
43. Kato, S, Saito, N, Kirigaya, H, Gyotoku, D, Iinuma, N, Kusakawa, Y, Iguchi, K, Nakachi, T, Fukui, K, Futaki, M, Iwasawa, T, Taguri, M, Kimura, K, Umemura, S: Prognostic significance of quantitative assessment of focal myocardial fibrosis in patients with heart failure with preserved ejection fraction. *Int J Cardiol,* 191**:** 314-319, 2015.
44. Su, MY, Lin, LY, Tseng, YH, Chang, CC, Wu, CK, Lin, JL, Tseng, WY: CMR-verified diffuse myocardial fibrosis is associated with diastolic dysfunction in HFpEF. *JACC Cardiovasc Imaging,* 7**:** 991-997, 2014.
45. Kessler, G, Friedman, J: Metabolism of fatty acids and glucose. *Circulation,* 98**:** 1351, 1998.
46. Lam, CSP, Voors, AA, de Boer, RA, Solomon, SD, van Veldhuisen, DJ: Heart failure with preserved ejection fraction: from mechanisms to therapies. *Eur Heart J,* 39**:** 2780-2792, 2018.
47. Kottgen, A, Pattaro, C, Boger, CA, Fuchsberger, C, Olden, M, Glazer, NL, Parsa, A, Gao, X, Yang, Q, Smith, AV, O'Connell, JR, Li, M, Schmidt, H, Tanaka, T, Isaacs, A, Ketkar, S, Hwang, SJ, Johnson, AD, Dehghan, A, Teumer, A, Pare, G, Atkinson, EJ, Zeller, T, Lohman, K, Cornelis, MC, Probst-Hensch, NM, Kronenberg, F, Tonjes, A, Hayward, C, Aspelund, T, Eiriksdottir, G, Launer, LJ, Harris, TB, Rampersaud, E, Mitchell, BD, Arking, DE, Boerwinkle, E, Struchalin, M, Cavalieri, M, Singleton, A, Giallauria, F, Metter, J, de Boer, IH, Haritunians, T, Lumley, T, Siscovick, D, Psaty, BM, Zillikens, MC, Oostra, BA, Feitosa, M, Province, M, de Andrade, M, Turner, ST, Schillert, A, Ziegler, A, Wild, PS, Schnabel, RB, Wilde, S, Munzel, TF, Leak, TS, Illig, T, Klopp, N, Meisinger, C, Wichmann, HE, Koenig, W, Zgaga, L, Zemunik, T, Kolcic, I, Minelli, C, Hu, FB, Johansson, A, Igl, W, Zaboli, G, Wild, SH, Wright, AF, Campbell, H, Ellinghaus, D, Schreiber, S, Aulchenko, YS, Felix, JF, Rivadeneira, F, Uitterlinden, AG, Hofman, A, Imboden, M, Nitsch, D, Brandstatter, A, Kollerits, B, Kedenko, L, Magi, R, Stumvoll, M, Kovacs, P, Boban, M, Campbell, S, Endlich, K, Volzke, H, Kroemer, HK, Nauck,

M, Volker, U, Polasek, O, Vitart, V, Badola, S, Parker, AN, Ridker, PM, Kardia, SL, Blankenberg, S, Liu, Y, Curhan, GC, Franke, A, Rochat, T, Paulweber, B, Prokopenko, I, Wang, W, Gudnason, V, Shuldiner, AR, Coresh, J, Schmidt, R, Ferrucci, L, Shlipak, MG, van Duijn, CM, Borecki, I, Kramer, BK, Rudan, I, Gyllensten, U, Wilson, JF, Witteman, JC, Pramstaller, PP, Rettig, R, Hastie, N, Chasman, DI, Kao, WH, Heid, IM, Fox, CS: New loci associated with kidney function and chronic kidney disease. *Nat Genet,* 42**:** 376-384, 2010.

48. Okada, Y, Sim, X, Go, MJ, Wu, JY, Gu, D, Takeuchi, F, Takahashi, A, Maeda, S, Tsunoda, T, Chen, P, Lim, SC, Wong, TY, Liu, J, Young, TL, Aung, T, Seielstad, M, Teo, YY, Kim, YJ, Lee, JY, Han, BG, Kang, D, Chen, CH, Tsai, FJ, Chang, LC, Fann, SJ, Mei, H, Rao, DC, Hixson, JE, Chen, S, Katsuya, T, Isono, M, Ogihara, T, Chambers, JC, Zhang, W, Kooner, JS, KidneyGen, C, Consortium, CK, Albrecht, E, consortium, G, Yamamoto, K, Kubo, M, Nakamura, Y, Kamatani, N, Kato, N, He, J, Chen, YT, Cho, YS, Tai, ES, Tanaka, T: Meta-analysis identifies multiple loci associated with kidney function-related traits in east Asian populations. *Nat Genet,* 44**:** 904-909, 2012.
49. Consortium, CAD, Deloukas, P, Kanoni, S, Willenborg, C, Farrall, M, Assimes, TL, Thompson, JR, Ingelsson, E, Saleheen, D, Erdmann, J, Goldstein, BA, Stirrups, K, Konig, IR, Cazier, JB, Johansson, A, Hall, AS, Lee, JY, Willer, CJ, Chambers, JC, Esko, T, Folkersen, L, Goel, A, Grundberg, E, Havulinna, AS, Ho, WK, Hopewell, JC, Eriksson, N, Kleber, ME, Kristiansson, K, Lundmark, P, Lyytikainen, LP, Rafelt, S, Shungin, D, Strawbridge, RJ, Thorleifsson, G, Tikkanen, E, Van Zuydam, N, Voight, BF, Waite, LL, Zhang, W, Ziegler, A, Absher, D, Altshuler, D, Balmforth, AJ, Barroso, I, Braund, PS, Burgdorf, C, Claudi-Boehm, S, Cox, D, Dimitriou, M, Do, R, Consortium, D, Consortium, C, Doney, AS, El Mokhtari, N, Eriksson, P, Fischer, K, Fontanillas, P, Franco-Cereceda, A, Gigante, B, Groop, L, Gustafsson, S, Hager, J, Hallmans, G, Han, BG, Hunt, SE, Kang, HM, Illig, T, Kessler, T, Knowles, JW, Kolovou, G, Kuusisto, J, Langenberg, C, Langford, C, Leander, K, Lokki, ML, Lundmark, A, McCarthy, MI, Meisinger, C, Melander, O, Mihailov, E, Maouche, S, Morris, AD, Muller-Nurasyid, M, Mu, TC, Nikus, K, Peden, JF, Rayner, NW, Rasheed, A, Rosinger, S, Rubin, D, Rumpf, MP, Schafer, A, Sivananthan, M, Song, C, Stewart, AF, Tan, ST, Thorgeirsson, G, van der Schoot, CE, Wagner, PJ, Wellcome Trust Case Control, C, Wells, GA, Wild, PS, Yang, TP, Amouyel, P, Arveiler, D, Basart, H, Boehnke, M, Boerwinkle, E, Brambilla, P, Cambien, F, Cupples, AL, de Faire, U, Dehghan, A, Diemert, P, Epstein, SE, Evans, A, Ferrario, MM, Ferrieres, J, Gauguier, D, Go, AS, Goodall, AH, Gudnason, V, Hazen, SL, Holm, H, Iribarren, C, Jang, Y, Kahonen, M, Kee, F, Kim, HS, Klopp, N, Koenig, W, Kratzer, W, Kuulasmaa, K, Laakso, M, Laaksonen, R, Lee, JY, Lind, L, Ouwehand, WH, Parish, S, Park, JE, Pedersen, NL, Peters, A, Quertermous, T, Rader, DJ, Salomaa, V, Schadt, E, Shah, SH, Sinisalo, J, Stark, K, Stefansson, K, Tregouet, DA, Virtamo, J, Wallentin, L, Wareham, N, Zimmermann, ME, Nieminen, MS, Hengstenberg, C, Sandhu, MS, Pastinen, T, Syvanen, AC, Hovingh, GK, Dedoussis, G, Franks, PW, Lehtimaki, T, Metspalu, A, Zalloua, PA, Siegbahn, A, Schreiber, S, Ripatti, S, Blankenberg, SS, Perola, M, Clarke, R, Boehm, BO, O'Donnell, C, Reilly, MP, Marz, W, Collins, R, Kathiresan, S, Hamsten, A, Kooner, JS, Thorsteinsdottir, U, Danesh, J, Palmer, CN, Roberts, R, Watkins, H, Schunkert, H, Samani, NJ: Large-scale association analysis identifies new risk loci for coronary artery disease. *Nat Genet,* 45**:** 25-33, 2013.
50. Traylor, M, Farrall, M, Holliday, EG, Sudlow, C, Hopewell, JC, Cheng, YC, Fornage, M, Ikram, MA, Malik, R, Bevan, S, Thorsteinsdottir, U, Nalls, MA, Longstreth, W, Wiggins, KL, Yadav, S, Parati, EA, Destefano, AL, Worrall, BB, Kittner, SJ, Khan, MS, Reiner, AP, Helgadottir, A, Achterberg, S, Fernandez-Cadenas, I, Abboud, S, Schmidt, R, Walters, M, Chen, WM, Ringelstein, EB, O'Donnell, M, Ho, WK, Pera, J, Lemmens, R, Norrving, B, Higgins, P, Benn, M, Sale, M, Kuhlenbaumer, G, Doney, AS, Vicente, AM, Delavaran, H, Algra, A, Davies, G, Oliveira, SA, Palmer, CN, Deary, I, Schmidt, H, Pandolfo, M, Montaner, J, Carty, C, de Bakker, PI, Kostulas, K, Ferro, JM, van Zuydam, NR, Valdimarsson, E, Nordestgaard, BG, Lindgren, A, Thijs, V, Slowik, A, Saleheen, D, Pare, G, Berger, K, Thorleifsson, G, Australian Stroke Genetics Collaborative, WTCCC, Hofman, A, Mosley, TH, Mitchell, BD, Furie, K, Clarke, R, Levi, C, Seshadri, S, Gschwendtner, A, Boncoraglio, GB, Sharma, P, Bis, JC, Gretarsdottir, S, Psaty, BM, Rothwell, PM, Rosand, J, Meschia, JF, Stefansson, K, Dichgans, M, Markus, HS, International Stroke Genetics, C: Genetic risk factors for ischaemic stroke and its subtypes (the METASTROKE collaboration): a meta-analysis of genome-wide association studies. *Lancet Neurol,* 11**:** 951-962, 2012.
51. Raychaudhuri, S, Plenge, RM, Rossin, EJ, Ng, AC, International Schizophrenia, C, Purcell, SM, Sklar, P, Scolnick, EM, Xavier, RJ, Altshuler, D, Daly, MJ: Identifying relationships among genomic disease regions: predicting genes at pathogenic SNP associations and rare deletions. *PLoS Genet,* 5**:** e1000534, 2009.

52. Maurano, MT, Humbert, R, Rynes, E, Thurman, RE, Haugen, E, Wang, H, Reynolds, AP, Sandstrom, R, Qu, H, Brody, J, Shafer, A, Neri, F, Lee, K, Kutyavin, T, Stehling-Sun, S, Johnson, AK, Canfield, TK, Giste, E, Diegel, M, Bates, D, Hansen, RS, Neph, S, Sabo, PJ, Heimfeld, S, Raubitschek, A, Ziegler, S, Cotsapas, C, Sotoodehnia, N, Glass, I, Sunyaev, SR, Kaul, R, Stamatoyannopoulos, JA: Systematic localization of common disease-associated variation in regulatory DNA. *Science,* 337**:** 1190-1195, 2012.
53. Visser, M, Kayser, M, Palstra, RJ: HERC2 rs12913832 modulates human pigmentation by attenuating chromatin-loop formation between a long-range enhancer and the OCA2 promoter. *Genome Res,* 22**:** 446-455, 2012.
54. Arnold, CD, Gerlach, D, Stelzer, C, Boryn, LM, Rath, M, Stark, A: Genome-wide quantitative enhancer activity maps identified by STARR-seq. *Science,* 339**:** 1074-1077, 2013.
55. Musunuru, K, Strong, A, Frank-Kamenetsky, M, Lee, NE, Ahfeldt, T, Sachs, KV, Li, X, Li, H, Kuperwasser, N, Ruda, VM, Pirruccello, JP, Muchmore, B, Prokunina-Olsson, L, Hall, JL, Schadt, EE, Morales, CR, Lund-Katz, S, Phillips, MC, Wong, J, Cantley, W, Racie, T, Ejebe, KG, Orho-Melander, M, Melander, O, Koteliansky, V, Fitzgerald, K, Krauss, RM, Cowan, CA, Kathiresan, S, Rader, DJ: From noncoding variant to phenotype via SORT1 at the 1p13 cholesterol locus. *Nature,* 466**:** 714-719, 2010.
56. Linsel-Nitschke, P, Heeren, J, Aherrahrou, Z, Bruse, P, Gieger, C, Illig, T, Prokisch, H, Heim, K, Doering, A, Peters, A, Meitinger, T, Wichmann, HE, Hinney, A, Reinehr, T, Roth, C, Ortlepp, JR, Soufi, M, Sattler, AM, Schaefer, J, Stark, K, Hengstenberg, C, Schaefer, A, Schreiber, S, Kronenberg, F, Samani, NJ, Schunkert, H, Erdmann, J: Genetic variation at chromosome 1p13.3 affects sortilin mRNA expression, cellular LDL-uptake and serum LDL levels which translates to the risk of coronary artery disease. *Atherosclerosis,* 208**:** 183-189, 2010.
57. Strong, A, Ding, Q, Edmondson, AC, Millar, JS, Sachs, KV, Li, X, Kumaravel, A, Wang, MY, Ai, D, Guo, L, Alexander, ET, Nguyen, D, Lund-Katz, S, Phillips, MC, Morales, CR, Tall, AR, Kathiresan, S, Fisher, EA, Musunuru, K, Rader, DJ: Hepatic sortilin regulates both apolipoprotein B secretion and LDL catabolism. *J Clin Invest,* 122**:** 2807-2816, 2012.
58. Muthalagan, E, Ganesh, RN, Sai Chandran, BV, Verma, SK: Phosphatase and tensin analog expression in arterial atherosclerotic lesions. *Indian J Pathol Microbiol,* 57**:** 427-430, 2014.
59. Dai, XY, Cai, Y, Mao, DD, Qi, YF, Tang, C, Xu, Q, Zhu, Y, Xu, MJ, Wang, X: Increased stability of phosphatase and tensin homolog by intermedin leading to scavenger receptor A inhibition of macrophages reduces atherosclerosis in apolipoprotein E-deficient mice. *J Mol Cell Cardiol,* 53**:** 509-520, 2012.
60. Kirby, A, Gnirke, A, Jaffe, DB, Baresova, V, Pochet, N, Blumenstiel, B, Ye, C, Aird, D, Stevens, C, Robinson, JT, Cabili, MN, Gat-Viks, I, Kelliher, E, Daza, R, DeFelice, M, Hulkova, H, Sovova, J, Vylet'al, P, Antignac, C, Guttman, M, Handsaker, RE, Perrin, D, Steelman, S, Sigurdsson, S, Scheinman, SJ, Sougnez, C, Cibulskis, K, Parkin, M, Green, T, Rossin, E, Zody, MC, Xavier, RJ, Pollak, MR, Alper, SL, Lindblad-Toh, K, Gabriel, S, Hart, PS, Regev, A, Nusbaum, C, Kmoch, S, Bleyer, AJ, Lander, ES, Daly, MJ: Mutations causing medullary cystic kidney disease type 1 lie in a large VNTR in MUC1 missed by massively parallel sequencing. *Nat Genet,* 45**:** 299-303, 2013.
61. Dang, MQ, Zhao, XC, Lai, S, Wang, X, Wang, L, Zhang, YL, Liu, Y, Yu, XH, Liu, Y, Li, HH, Xia, YL: Gene expression profile in the early stage of angiotensin II-induced cardiac remodeling: a time series microarray study in a mouse model. *Cell Physiol Biochem,* 35**:** 467-476, 2015.

Appendix

Nederlandse samenvatting

Cellen zijn fundamentele biologische eenheden die voor hun functie afhankelijk zijn van zuurstof en voedingsstoffen. Met het ontstaan van complexe organismen, opgebouwd uit miljoenen cellen, ontwikkelde zich gaandeweg het probleem dat de opname van zuurstof en voedingsstoffen niet meer simpelweg uit de omgeving van het organisme plaats kon vinden omdat de diffusie afstand daarvoor te groot werd. Om in de behoefte van alle cellen te kunnen blijven voorzien zijn complexe organismen, de mens inclusief, uitgerust met een cardiovasculair systeem, waarin het hart als pomp fungeert om het voedingsstof- en zuurstofdragende bloed via een ongekend stelsel van bloedvaten tot aan de meest inwendig gelegen cellen te transporteren. Met deze elementaire rol van het cardiovasculaire systeem in het achterhoofd, is het niet moeilijk voor te stellen dat zowel acute als chronische verstoringen van hart- en vaatfunctie een enorme impact kunnen hebben op het algehele welzijn, en ondanks de grote medische vooruitgang van de afgelopen decennia, dit wereldwijd nog steeds een belangrijke oorzaak is van ziekte en sterfte. Deze verstoringen van hart- en vaatfunctie, die worden geclusterd onder de noemer hart- en vaatziekten, zijn vaak niet op zichzelf staand en gaan veelal gepaard met functionele verstoringen van andere organen. De nieren zijn daarvan een sprekend voorbeeld. Niet alleen zijn de nieren functioneel afhankelijk van cardiovasculaire homeostase, ze spelen ook een cruciale rol bij het handhaven daarvan. In de loop der jaren heeft een groot aantal onderzoeken zich gericht op de vele verschillende aspecten van zowel cardiovasculaire, als renale dysfunctie, welke niet alleen hebben geleid tot betere inzichten in het bestaan en het beheersen van risicofactoren, maar ook de intellectuele basis hebben gelegd voor succesvolle therapeutische interventies. Helaas zijn echter nog steeds veel mechanismen die ten grondslag liggen aan cardiovasculaire ziekten niet, of slechts ten dele bekend, en het doel van dit proefschrift was dan ook om nieuw inzicht te verschaffen in de moleculaire regulatie van renale en cardiovasculaire homeostase.

Al tijdens de primaire fase van de embryonale ontwikkeling is het essentieel dat een functioneel netwerk van bloedvaten ontwikkeld. De basis hiervoor wordt gelegd door vasculogenese, waarbij angioblasten differentiëren in endotheelcellen welke een primair tubulair netwerk vormen. Vanuit dit netwerk groeit de vaatboom zowel prenataal als postnataal proportioneel mee met het ontwikkelende organisme via angiogenese, een strak gecontroleerd proces waarbij endotheelcellen vanuit het bestaande vaatnetwerk delen en migreren in de richting van een zuurstofarm gebied. Na volgroeiing van een individu, wordt de activiteit van angiogenese beperkt tot nieuwgroei van weefsel, bijvoorbeeld aanmaak van nieuwe spieren. Dit kan echter ook in pathologisch verband gebeuren, zoals het geval is bij

tumorgroei. De delende cellen van de tumor zijn net als alle andere cellen afhankelijk van voedingsstoffen en zuurstof, waarin ze worden voorzien door ingroei van nieuwe vaten. Het remmen van angiogenese wordt momenteel gezien als een mogelijke ingang om tumorgroei te reduceren. Visa versa, is in sommige gevallen juist aanwas van nieuwe bloedvaten gewenst, zoals bijvoorbeeld in het zuurstofarme gebied dat ontstaat na een hartinfarct. Tot op heden zijn we echter pas beperkt in staat om angiogenese op een therapeutisch verantwoorde wijze in ons voordeel te gebruiken, deels ten gevolge van een nog ontwikkelende kennis van de moleculaire signalering cascades die angiogenese reguleren. Om hier een beter inzicht in te krijgen is in **hoofdstuk 2** de rol van Frizzled 5 (FZD5) in angiogenese bestudeerd. Uit eerdere studies is gebleken dat deze receptor onmisbaar is voor het ontwikkelen van een functioneel vasculair netwerk, maar de exacte wijze waarop FZD5 hieraan bijdraagt was tot op heden niet bekend. Uit onze studie is gebleken dat het verlagen van de aanwezigheid van FZD5 in endotheelcellen ervoor zorgde dat de cellen niet alleen stopten met delen, maar ook minder in staat waren te migreren, en als gevolg daarvan ook geen nieuwe vaatjes meer konden vormen. Tegelijkertijd leidde een lagere aanwezigheid van FZD5 tot een verhoogde aanmaak van Vascular Endothelial Growth Factor Receptor 1 en Angiopoietin 2, welke respectievelijk zorgen voor een verminderde gevoeligheid voor pro-angiogenese signalen uit zuurstofarme gebieden en een vermindering van vaatstabilisatie.

Deze vaatstabilisatie is een belangrijk onderdeel van angiogenese. Enerzijds zorgt het ervoor dat nieuw gevormde vaatjes niet direct desintegreren, en anderzijds voorkomt het overmatige gevoeligheid voor pro-angiogenese factoren. Deze stabilisatie van endotheelcellen komt voor een groot deel op het conto van perivasculaire cellen, genaamd pericyten. In de literatuur is al veel geschreven over de wijze waarop deze pericyten het endotheel, en daarmee angiogenese beïnvloeden, maar tegelijkertijd is nog relatief weinig bekend over de invloed van deze interactie op de pericyten zelf. In **hoofdstuk 3** is de genexpressie van pericyten vergeleken in aan- en afwezigheid van endotheelcellen. Uit deze studie is naar voren gekomen dat interactie met endotheel differentiatie en groei van pericyten stimuleert. Tevens lieten pericyten in afwezigheid van endotheelcellen een verhoogde aanmaak van fibrotische eiwitten zien. In eerdere onderzoeken is aangetoond dat pericyten in bijvoorbeeld de nieren een belangrijke bijdrage leveren aan door schade geïnduceerde fibrose. Tot op heden is het onduidelijk of dit het gevolg is van een pathologische over-interpretatie van reparatie mechanismen, of dat endotheel dysfunctie en de daarbij horende verstoorde endotheel interactie met omliggende cellen een rol van betekenis speelt, maar onze data wijzen er in ieder geval op dat endotheel in staat is de productie van lidtekenweefsel door pericyten te onderdrukken.

Om het transsport van zuurstof en voedingsstoffen door het lichaam te kunnen faciliteren, is het vasculaire systeem afhankelijk van een goed werkend hart. Wanneer het hart niet in staat is om hierin te kunnen voorzien, spreken we van hartfalen. Hartfalen kan worden opgedeeld in falen met verminderde ejectie fractie en falen met behouden ejectie fractie. Waar verminderde ejectie fractie vaak het gevolg is van verlies aan pompkracht, bijvoorbeeld na onherstelbare schade aan de hartspier ten gevolge van een hartinfarct, is falen met behouden ejectie fractie doorgaans het gevolg van verslechterde ontspanning van het hart. Dit wordt respectievelijk systole en diastole dysfunctie genoemd. Beide vormen van hartfalen zijn geassocieerd met de aanwezigheid van meerdere comorbiditeiten, waaronder een verminderde nierfunctie, hypertensie, en obesitas. Over de jaren is er enorme vooruitgang geboekt in de behandeling van systolisch hartfalen, maar helaas is er door een tot op heden beperkt inzicht in hartfalen met een behouden ejectie fractie op dit moment nog geen succesvolle behandel methode voor deze aandoening. Bovendien is het ook nog niet geheel duidelijk hoe de verschillende comorbiditeiten bijdragen aan deze aandoening.
Om een beter inzicht te krijgen in de processen die betrokken zijn bij de ontwikkeling en progressie van diastole dysfunctie is de Zucker spontaneously hypertensive (ZSF1) rat bestudeerd. ZSF1 ratten met een mutatie in de leptine receptor ontwikkelen obesitas, gevolgd door diabetes type 2, verminderde nierfunctie en diastole dysfunctie. In **hoofdstuk 4** zijn de mircovasculaire veranderingen in het hart en de nieren van de ZSF1 ratten met de leptine receptor mutatie vergeleken met die van de ratten zonder mutatie. Wat opviel in deze dieren was dat ze diastole dysfunctie ontwikkelde, maar dat er in tegenstelling tot wat bekend is uit mensen, geen vermindering van capillaire dichtheid of toegenomen fibrose op trad in het hart. Wel ontwikkelde zich in de linker ventrikel specifieke kleine fibrotische regio's die werden gekenmerkt door snel delende en slecht georganiseerde vasculaire structuren. Binnen deze atypisch georganiseerd clusters werd tevens een verrijking aan pericyten gevonden en met de bevindingen uit **hoofdstuk 3** in het achterhoofd zijn er nieuwe studies gepland om de exacte bijdrage van de pericyten aan de fibrotische regio's verder te onderzoeken. In **hoofdstuk 5** is hetzelfde soort rat gebruik om een beter inzicht te krijgen op welke manieren verschillende comorbiditeiten bijdragen aan het ontwikkelen van hartfalen met behouden ejectie fractie. In deze studie zijn de ratten, bovenop de eerder genoemde comorbiditeiten, blootgesteld aan deoxycorticosterone en een hoog zout dieet (DZ), wat zorgde voor de ontwikkeling van ernstige hypertensie. Uit deze studie kwam naar voren dat er slechts minimale interactie was tussen de metabole factoren en DZ-geïnduceerde hypertensie. De obese ZSF1 ratten ontwikkelde de sterkste vermindering van de diastole functie en het hartminuutvolume, en slechts een minimaal additief effect werd gezien in combinatie met DZ-geïnduceerde hypertensie. Wel leidde DZ-geïnduceerde

hypertensie, zowel in aan- en afwezigheid van obesitas, tot een sterke toename in fibrose en inflammatie, en zorgde het voor mitochondriële dysfunctie en verminderde capaciteit om vetzuren te verbranden, waar de placebo-behandelde obese ZSF1 ratten juist meer gebruik leken te maken van de verbranding van vetzuren. Al met al laat deze studie zien dat de comorbiditeiten die geassocieerd zijn met diastole dysfunctie zorgen voor cruciale verschillen in remodelering van het hart, iets wat van cruciaal belang kan zijn bij het ontwikkelen en testen van toekomstige medicijnen.

Naast de eerder genoemde comorbiditeiten, zijn aan de hand van zogenaamde 'genome wide association studies' (GWAS) genetische risicofactoren gevonden die bijdragen aan de ontwikkeling van cardiovasculaire en renale aandoeningen. In deze studies wordt het DNA van een groot aantal patiënten vergeleken met dat van gezonde mensen, waarna kan worden bekeken of genetische varianten, ook wel SNPs genoemd, vaker voorkomen in een zieke populatie dan in een gezonde populatie. Deze genetische variatie ligt maar zelden in DNA coderend voor eiwitten en om die reden wordt voor functionele annotatie van de variatie voornamelijk gekeken naar de meest dichtbij gelegen genen. Helaas heeft deze benadering tot nu toe slechts ten dele gezorgd voor opheldering en klinische significantie. Epigenetische studies hebben aangetoond dat in ons DNA, naast eiwit coderende regio's, veel zogenaamde regulatie elementen liggen, zoals enhancers en repressors. Deze regulatie elementen spelen een belangrijke rol in regulatie van transcriptie. Varianten die in deze regulatie elementen liggen zouden kunnen bijdragen aan pathogenese, door verstoorde regulatie van genexpressie. Om dit verder te bestuderen voor genetische variatie geassocieerd met atherosclerose en chronische nierziekte, is respectievelijk in **hoofdstuk 6** en **hoofdstuk 7** gebruik gemaakt van 'cricular chormosome conformation capture sequencing' (4C-seq) om een beeld te krijgen van genen waarvan de expressie wordt gereguleerd door regulatie elementen die overlappen met deze variatie. In totaal zijn voor atherosclerose 326 genen gevonden die in de 3D conformatie van chromatine interactie hadden met een regulatie elementen die overlapten met atherosclerose geassocieerde genetische variatie. Op eenzelfde wijze zijn voor chronische nierziekte 304 kandidaat genen gevonden. In **hoofdstuk 7** is tevens aan de hand van 'self-transcribing active regulatory region sequencing' (STARR-seq) fysiek bewijs geleverd voor het effect dat chronische nierziekte-geassocieerde genetische variatie, liggend in een regulatie element, kan hebben op transcriptie. De beschreven pijplijn in deze studies biedt een nieuwe techniek voor het identificeren en prioriteren van kandidaat genen en vormt een aanvulling op de klassieke GWAS-interpretatie. Toekomstige studies zijn echter nodig om de implicaties van onze bevindingen te specificeren.

Curriculum vitae

Maarten Matthijs Brandt is geboren op 11 juli 1988 te Leeuwarden, Nederland. In 2007 behaalde hij zijn VWO diploma aan de Rijks Scholengemeenschap Hoeksche Waard, waarna hij begon met de studie Industrieel Ontwerpen aan de TU Delft. Gaandeweg het eerste jaar van deze studie bleken zijn interesses toch elders te liggen, waarop in 2008 werd besloten aan te vangen met de studie Biologie en Medisch Laboratoriumonderzoek aan de Hogeschool Rotterdam. In het laatste jaar van deze studie verrichtte hij onderzoek aan het Erasmus MC, binnen de groep van dr. C. Cheng, naar signaal transductie routes die ten grondslag liggen aan microvasculaire groei. In 2012 behaalde hij *cum laude* zijn Bachelor of Applied Sciences, waarna de ontwikkelde nieuwsgierigheid en interesse in de basaal medische wetenschap er geen twijfel over lieten een aangeboden promotie traject onder leiding van prof. dr. D.J. Duncker en dr. C. Cheng aan te nemen. Tijdens dit promotie traject heeft hij naast zijn onderzoek aan het Erasmus MC, ook onderzoek verricht aan het UMC Utrecht binnen de groep van prof. dr. M.C. Verhaar, en het werk beschreven in dit proefschrift is van dit traject het resultaat.

List of publications

Brandt MM, van Dijk CGM, Maringanti R, Chrifi I, Kramann R, Verhaar MC, Duncker DJ, Mokry M, Cheng C. Transcriptome analysis reveals microvascular endothelial cell-dependent pericyte differentiation.
Scientific Reports - (in press)

Brandt MM, Nguyen ITN, Krebber MM, Van de Wouw J, Mokry M, Cramer MJ, Duncker DJ, Verhaar MC, Joles JA, Cheng C. Limited synergy of obesity and hypertension, prevalent risk factors in onset and progression of HFpEF.
Journal of Cellular and Molecular Medicine – Jul 2019

Chrifi I, Louzao-Martinez L, **Brandt MM**, van Dijk CGM, Bürgisser PE, Zhu C, Kros JM, Verhaar MC, Duncker DJ, Cheng C. CMTM4 regulates angiogenesis by promoting cell surface recycling of VE-cadherin to endothelial adherens junctions.
Angiogenesis – Feb 2019

Brandt MM, van Dijk CG, Chrifi I, Kool HM, Burgisser P, Louzao-Martinez L, Pei J, Rottier RJ, Verhaar MC, Duncker DJ, Cheng C. Endothelial loss of Fzd5 stimulates PKC/Ets1-mediated transcription of Angpt2 and Flt1.
Angiogenesis – May 2018

Shariatzadeh M, **Brandt MM**, Cheng C, Ten Berge JC, Rothova A, Leenen PJM, Dik WA. Three-dimensional tubule formation assay as therapeutic screening model for ocular microvascular disorders.
Eye – May 2018

Brandt MM, Meddens CA, Louzao-Martinez L, Van Den Dungen NAM, Lansu NR, Nieuwenhuis EES, Duncker DJ, Verhaar MC, Joles JA, Mokry M, Cheng C. Chromatin conformation links distal target genes to chronic kidney disease loci.
Journal of the American Society of Nephrology – Nov 2017

Chrifi I, Hermkens D, **Brandt MM**, Van Dijk C, Burgisser PE, Haasdijk R, Pei J, Van De Kamp E, Zhu C, Blonden L, Kros JM, Duncker DJ, Duckers HJ, Cheng C. Cgnl1, an endothelial junction complex protein, regulates GTPase mediated angiogenesis.
Cardiovascular Research – Aug 2017

Octavia Y, Kararigas G, de Boer M, Chrifi I, Kietadisorn R, Swinnen M, Duimel H, Verheyen FK, **Brandt MM**, Fliegner D, Cheng C, Janssens S, Duncker DJ, Moens AL. Folic acid reduces doxorubicin-induced cardiomyopathy by modulating endothelial nitric oxide synthase.
Journal of Cellular and Molecular Medicine – Jun 2017

Chrifi I, Louzao-Martinez L, **Brandt MM**, van Dijk CGM, Burgisser P, Zhu C, Kros JM, Duncker DJ, Cheng C. CMTM3 (CKLF-Like Marvel Transmembrane Domain 3) Mediates Angiogenesis by Regulating Cell Surface Availability of VE-Cadherin in Endothelial Adherens Junctions.
Arteriosclerosis, Thrombosis, and Vascular Biology – Jun 2017

Zhu C, Mustafa D, Zheng PP, van der Weiden M, Sacchetti A, **Brandt MM**, Chrifi I, Tempel D, Leenen PJM, Duncker DJ, Cheng C, Kros JM. Activation of CECR1 in M2-like TAMs promotes paracrine stimulation-mediated glial tumor progression.
Journal of Neuro-Oncology – May 2017

Haitjema S, Meddens CA, van der Laan SW, Kofink D, Harakalova M, Tragante V, Foroughi Asl H, van Setten J, **Brandt MM**, Bis JC, O'Donnell C, Cheng C, Hoefer IE, Waltenberger J, Biessen E, Jukema JW, Doevendans PA, Nieuwenhuis EE, Erdmann J, Björkegren JL, Pasterkamp G, Asselbergs FW, den Ruijter HM, Mokry M. Additional Candidate Genes for Human Atherosclerotic Disease Identified Through Annotation Based on Chromatin Organization.
Circulation Cardiovascular Genetics – Apr 2017

Haasdijk RA, Den Dekker WK, Cheng C, Tempel D, Szulcek R, Bos FL, Hermkens DM, Chrifi I, **Brandt MM**, Van Dijk C, Xu YJ, Van De Kamp EH, Blonden LA, Van Bezu J, Sluimer JC, Biessen EA, Van Nieuw Amerongen GP, Duckers HJ. THSD1 preserves vascular integrity and protects against intraplaque haemorrhaging in ApoE-/- mice.
Cardiovascular Research – May 2016

van Dijk CG, Oosterhuis NR, Xu YJ, **Brandt MM**, Paulus WJ, van Heerebeek L, Duncker DJ, Verhaar MC, Fontoura D, Lourenço AP, Leite-Moreira AF, Falcão-Pires I, Joles JA, Cheng C. Distinct Endothelial Cell Responses in the Heart and Kidney Microvasculature Characterize the Progression of Heart Failure With Preserved Ejection Fraction in the Obese ZSF1 Rat With Cardiorenal Metabolic Syndrome.
Circulation Heart Failure – Apr 2016

Lei Z, van Mil A, **Brandt MM**, Grundmann S, Hoefer I, Smits M, El Azzouzi H, Fukao T, Cheng C, Doevendans PA, Sluijter JP. MicroRNA-132/212 family enhances arteriogenesis after hindlimb ischaemia through modulation of the Ras-MAPK pathway.
Journal of Cellular and Molecular Medicine – Aug 2015

van den Borne P, Haverslag RT, **Brandt MM**, Cheng C, Duckers HJ, Quax PH, Hoefer IE, Pasterkamp G, De Kleijn DP. Absence of chemokine (C-x-C motif) ligand 10 diminishes perfusion recovery after local arterial occlusion in mice.
Arteriosclerosis, Thrombosis, and Vascular Biology - Mar 2014

PhD training portfolio

Name PhD candidate:	Maarten M. Brandt
Erasmus MC department:	Cardiology
Research School:	COEUR
PhD period:	2012-2019
Promotor:	prof. dr. D.J.G.M. Duncker
Co-promotor:	dr. C. Cheng

Courses and Seminars	**Year**	**ECTS**
COEUR research seminar - Endothelin in the picture	2012	0.4
NHF course: Cardiac Function and Adaptation	2013	2.0
RM PhD course - Cardiovascular Regenerative Medicine	2013	0.5
NHF course: Vascular Biology	2014	2.0
COEUR course – Heart Failure Research	2014	1.5
COEUR symposium - Current Cardiac and Vascular Aging Research	2014	0.4
OIC PhD course Functional Imaging and Super Resolution	2015	2.0
Confocal Microscopy Introduction Course part 1 and 2	2015	0.3
COEUR course - Molecular Biology in Cardiovascular Research	2016	1.5
Lecture prof. G. Kararigas - Sex-specific remodeling of the heart	2017	0.1
Career Guidance Program	2017	2.0
Lecture prof. R. Kramann - Perivascular progenitor cells in disease	2017	0.1
BioBusiness Summerschool	2018	2.0

Conferences	**Year**	**ECTS**
Cardiovascular Conference (CVC) (oral - best abstract session)	2014	0.6
5th International Meeting on Angiogenesis (poster)	2014	0.9
MiVaB and DEBS annual meeting (oral - best presentation award)	2014	0.6
Cardiovascular Conference (CVC) (oral - best presentation award)	2015	0.3
Frontiers in Cardiovascular Biology (poster)	2016	0.9
American Heart Association - scientific sessions (poster)	2016	1.2
NFN scientific fall meeting (poster)	2016	0.3
Dutch-German Joint Meeting - Molecular Cardiology Working Groups (poster)	2017	0.9

NFN scientific fall meeting (oral)	2017	0.3
Frontiers in Cardiovascular Biology (poster - best presentation award)	2018	0.9
Dutch-German Joint Meeting - Molecular Cardiology Working Groups (poster - best presentation award)	2018	0.9
Dutch-German Joint Meeting - Vascular Biology (poster)	2018	0.9
Experimental Biology (poster)	2019	1.2

Teaching activities	**Year**	**ECTS**
Supervising master thesis (C.G.M van Dijk)	2013	1.1
Supervising master thesis (E. Thijssen)	2014	1.1
Supervising bachelor thesis (L. Chuttoo)	2014	1.5
Tutor (master program Regenerative Medicine and Technology - TUE)	2014	0.4
Supervising bachelor thesis (R. de Jong)	2015	1.1
Supervising bachelor thesis (C. da Luz)	2016	1.1
Supervising bachelor thesis (F. Razack)	2016	1.1
Supervising bachelor thesis (S. Zümrütçü)	2017	1.1
Supervising bachelor thesis (S. Chawki)	2018	1.1

Total ETCS: 34.3

Dankwoord

Alhoewel het fysieke schrijven van een proefschrift van tijd tot tijd een wat eenzaam karakter kent, heb ik mij altijd gesterkt gevoeld door de steun van mijn collega's, vrienden en familie. Ik zou alle mensen die daarin een bijdrage hebben gehad dan ook hartelijk willen danken.

Te beginnen met mijn promotor, prof. Dirk Duncker. Dirk, ik heb mijn tijd binnen jouw groep als een waar genoegen ervaren. Alhoewel jouw fysiologische inslag tegenover mijn interesse in basaal moleculair werk initieel slechts op bepaalde punten raakvlakken vertoonden, heb jij altijd geprobeerd deze raakvlakken uit te diepen. Jouw punctualiteit, evenals je principiële houding omtrent betrokkenheid bij een project waarvan je mede auteur bent, zijn eigenschappen waar menig collega een voorbeeld aan kan nemen. De passie en gedrevenheid waarmee jij jouw draai aan de wetenschap geeft hebben mij geïnspireerd en ik ben je daar dankbaar voor.

Caroline Cheng, een hoop moois in het leven is gebaseerd op vertrouwen. Toen jij mij in 2012 een positie aanbood om als promovendus aan de slag te gaan, realiseerde ik me dat ik daar op basis van mijn genoten opleiding eigenlijk niet voor in aanmerking kwam. Jij nam met dat vertrouwen in mij in zekere zin een risico en alleen al om die reden ben ik je zeer dankbaar. In de daaropvolgende jaren ontwikkelde ik onder jouw vleugels een zelfstandige manier van werken en het vermogen om mijn bevindingen te delen met mijn collega's en de rest van het wetenschappelijk veld. Bovendien kreeg ik van jou alle ruimte om een groot wetenschappelijk netwerk op te bouwen, en ook al sloeg de schrik me om het hart toen je me ooit "voor de grap" vertelde dat ik mijn bureau in Rotterdam kon opruimen om vanaf dat moment weer in Utrecht aan de slag te gaan, heeft de tijd waarin ik daar initieel werkzaam was een grote bijdrage geleverd aan dat netwerk. Ik durf te zeggen dat niets van dit alles van de grond was gekomen zonder jou, en het vertrouwen dat je me hebt gegeven, en ik zal je daar altijd dankbaar voor zijn.

Ook wil ik graag de leden van mijn promotie commissie, prof. Marianne Verhaar, prof. Daphne Merkus en prof. Max Kros, hartelijk danken voor de tijd die zij hebben genomen voor de beoordeling van dit proefschrift. Marianne, ik zou je daarnaast ook willen bedanken voor de mogelijkheid die je me hebt geboden om tijdens mijn promotietraject mijn werkzaamheden deels uit te voeren op jouw lab. Daphne, wij lijken elkaar gaandeweg steeds vaker tegen te komen en ik heb plezier in de gedachtewisselingen die daarmee gepaard gaan. Jouw ruime wetenschappelijk ervaring in combinatie met je toegankelijke

persoonlijkheid maken je voor mij tot een waardevolle collega, dus nogmaals, excuses voor dat akkefietje met de Alpenhoorn, ik wist niet dat je zo licht sliep.

Mijn paranimfen, Maurits en Ihsane, het is me een eer dat jullie naast mij willen staan tijdens mijn promotie en ik ben uiteraard ook dankbaar voor jullie onbaatzuchtige aanbod mij na de borrel te repatriëren naar de metropool van de randstad – Oud-Beijerland.

Ihsane, je vertelde mijn vader ooit dat je een man van me had gemaakt. Het behoeft geen verdere uitleg dat dit aan mijn kant van de tafel voor wat verbaasde blikken zorgde. Echter, wat je mijn vader probeerde te vertellen was dat ik mede door jouw enthousiaste begeleiding mijn stage, en daarmee mijn studie, succesvol had afgerond. Ik moet bekennen, je enthousiasme werkte inderdaad aanstekelijk, en niet lang na mijn afstuderen werd ik officieel je collega. Geruime tijd hebben wij vervolgens samengewerkt in de groep van Caroline, waarin jij mij gevraagd en ongevraagd bleef voorzien van advies, een luisterend oor en uiteraard koffie. Ik was op mijn beurt ook jouw steun en toeverlaat, zoals bijvoorbeeld ten tijde van je CMTM3/4-us-fiasco. Naast onze reguliere werkzaamheden hebben we samen ook veel mooie momenten meegemaakt, waaronder memorabele congressen, de borrels, onze trip naar New York en het jaarlijkse thorax zaalvoetbal toernooi – wat waren wij goed. Dit is een tijd geweest waarin ik jou leerde kennen als een echte vriend, en ik moet bekennen dat ik het oprecht jammer vond dat ik het laatste stukje van mijn promotietraject zonder je heb moeten doen, alsof ik plotseling verder moest zonder zijwieltjes. Je bent dan weliswaar niet degene die een man van me heeft gemaakt, maar de tijd die ik met je heb doorgebracht heeft mij in veel opzichten wel een completer mens gemaakt en daar ben je ik bijzonder dankbaar voor. Ik wens je het allerbeste in het vervolg van je carrière en ik hoop dat onze wegen elkaar ook daarin nog eens gaan kruisen.

Ook de collega's met wie ik kamer Ee2369 deel wil ik bedanken. Ruben, ik heb ooit het groot lexicon van nutteloze feiten gelezen. Dit was vermakelijk, ik kan het iedereen aanraden, maar jou niet. Waarom niet? Jij bent van nature een zeer vriendelijke, mobiele uitgave. Jij kent je feitjes, van racefietsen tot tuinieren. Van 's werelds snelst vallend dier, en inmiddels ook van het langzaamst promoverend exemplaar. Bedankt voor je opbouwende kritiek op mijn posters en de hulp die je mij gaf bij de interpretatie van echodata. Oana, bedankt voor de vele waardevolle tips die je mij gaandeweg toeschoof. Je bent een begenadigd wetenschapster en ik heb in de afgelopen jaren een hoop van je mogen leren. Als een ware matriarch regeerde jij over onze kamer, al bleek op een terras in Wenen dat jij jezelf niet herkende in deze rol. Dat was een wijze les. Het zal de afgelopen jaren niet altijd

makkelijk voor je zijn geweest en er zijn vast momenten waarvoor een gebaar van excuus op zijn plaats zou zijn geweest. Smakeloze grapjes en ongepaste opmerkingen, je hebt het allemaal moeten verduren, maar dan moet je maar zo denken; zo is Jens nu eenmaal en daar zullen we allemaal mee moeten leren leven. Jens, je bent een arts. Initieel moest ik daarom even aan je wennen omdat dit betekende dat, wanneer je het lab opkwam, al het glaswerk moest worden gezekerd en de pipetten moesten worden voorzien van hun "beschermhoedjes". Echter, gaandeweg realiseerde ik me dat deze – aan jouw medische achtergrond gerelateerde – klunzigheid ook impliceerde dat je wellicht over bepaalde kennis beschikte die ik zelf niet voorradig had, en wat bleek, jij was bereid deze kennis met me te delen. Ik heb me hier veelvuldig aan kunnen optrekken en daar ben ik je erg dankbaar voor. Ranga, you may consider yourself the most recent acquisition of room Ee2369. It makes you feel alive, doesn't it? You are a gifted young scientist, and I wish you all the best in your PhD journey.

Esther en Lau, men zegt wel eens; wijsheid komt met de jaren. Jullie zijn erg wijs. Dat is maar goed ook, want daar varen een hoop collega's van de 23^{e}, waaronder ik zelf, wel bij. Lau, zo vaak als ik bij jou aan je bureau heb gestaan om de map met historische protocollen van stal te halen is denk ik niet op één hand te tellen. En Esther, geen verzoek was voor jou teveel. Had je geen tijd? Dan maakte je tijd. Met jouw initiatieven voor uitjes, ijsjes en ander moois zorgde jij tevens voor cohesie tussen de collega's, een laagje cement dat de hele boel bij elkaar hield. Een lab kan niet zonder mensen zoals jullie en ik ben jullie allebei enorm dankbaar voor de tijd en energie die jullie in mij, en daarmee ook in mijn proefschrift, hebben gestoken.

Jarno, tot kort geleden had ik de fatsoenlijke gewoonte om, alvorens mij naar het volgende honk te begeven, iemand wat beter te leren kennen. Zelf noemde je dit ook wel eens principes meen ik me te herinneren. Jij, en het twijfelaartje dat we in Orlando deelden, hebben mij echter geleerd dat principes op meerdere manieren kunnen worden geïnterpreteerd. Bedankt. Martine, het schept een band dat we beide net iets langer dan gemiddeld over ons proefschrift hebben gedaan. De gesprekken die wij hierover hebben gehad hebben mij geholpen om door te zetten en ik hoop dat dit jou op eenzelfde manier verder helpt. Ook mijn overige (oud) collega's van de afdeling experimentele cardiologie – Monique, Liesbeth, Maaike, Marc, Metin, Richard, Kelly, Ilona, Zhongye, Siyu en Annemarie – wil ik van harte bedanken. Ieder van jullie heeft op zijn of haar eigen manier een substantiële bijdrage geleverd. Onder de oud collega's wil ik ook nog kort stil staan bij Dennie, Vincent en Andre. Jullie hebben een gemene deler die ik altijd erg heb kunnen

waarderen; net-over-het-randje humor. Tegelijkertijd hebben jullie alle drie een eigen idee over een postdoctorale carrière, een aspect waarover jullie met mij hebben gesproken, omdat dit destijds voor mij toekomstmuziek was waar ik maar moeilijk richting aan kon geven. Jullie blik daarop heeft mij vastigheid gegeven, waarvoor ik jullie, naast alle ongevraagde adviezen en 'afbouwende' kritiek, zeer dankbaar ben.

Christian, voor mij blijf jij altijd nummer 1. Stagiaire nummer 1, want chronologisch nummeren bleek toch eenvoudiger dan al die namen te onthouden. Desalniettemin was je wel een ontzettend goede stagiaire, en de bak met werk die je tijdens je stage hebt verzet heeft mij een vliegende start gegeven. Ik heb genoten van de – weinig aan wetenschap gerelateerde – gesprekken bij de koffieautomaat, waarbij wij genoten van ons kopje koffie, en Ihsane van zijn bakje oestrogeen met suiker. Momenteel zijn we werkzaam op verschillende instituten, maar gelukkig hebben we nog een aantal gedeelde projecten wat ervoor zorgt dat we nog regelmatig contact met elkaar hebben. Wanneer ik Christian bedank, kan ik de overige (oud) collega's uit Utrecht niet vergeten; Laura, Merle, Isabel en Jiayi, bedankt voor jullie bijdragen en het praatje bij de koffie wat ervoor zorgde dat, wanneer ik mijn gezicht na lange tijd weer in Utrecht liet zien, ik me toch altijd een beetje thuis voelde.

Jaap, ik heb je in mijn tijd bij de Nefrologie in het UMC Utrecht niet alleen leren kennen als een vriendelijke man, maar ook als een ongekend kundige man. Die kundigheid ging zo ver, dat er in den beginne momenten waren dat ik ermee kon leven als je op vakantie was wanneer ik mijn data voor de afdeling moest presenteren. Gaandeweg ben ik je kritische blik, evenals je punctualiteit, echter gaan waarderen. Sterker, ik durf te zeggen dat dit van groot belang is geweest voor mijn ontwikkeling, omdat je mij leerde op een minstens zo kritische manier over mijn bevindingen na te denken. Bedankt, en geniet van je pensioen!

Michal, I'm not really sure how our paths crossed, but somehow we ended up working together in many different projects. I've always appreciated your patience, which was necessary for me to understand fractions of the unearthly complex matter called bioinformatics. Many of the projects I've been working on over the past years couldn't have succeeded without your help, and for that I'm grateful.

De Studenten die ik na Christian heb mogen begeleiden; Eva, Lisa, Robin, Celia, Farhana, Senna en Samraa, jullie hebben veel werk verzet, en op mijn beurt heb ik ook van jullie veel kunnen leren. Bedankt voor de inzet, ik wens jullie het beste.

Jasper, ik denk dat je maar zelden zo'n onbevredigende samenwerking bent aangegaan (zowel op het financiële als op het creatieve vlak). Desondanks ben ik je erg dankbaar voor de tijd die je voor me hebt vrijgemaakt en ik ben uitermate tevreden met de cover die je voor me hebt ontworpen.

Lieve papa en mama, jullie hebben mij altijd gestimuleerd om het beste uit mezelf te halen. Toegegeven, de weg hier naartoe was bij tijd en wijle wat hobbelig, maar jullie stonden altijd achter me. Die onvoorwaardelijke steun heeft mij het vertrouwen gegeven door te zetten en hebben mij uiteindelijk gebracht waar ik nu ben. Ik kan jullie hier niet genoeg voor bedanken.

Lieve Wendy, ik zou graag met jou en de kinderen willen eindigen. Jij hebt mijn keuze om te promoveren vanaf het eerste moment gestimuleerd, ook al betekende dit dat het, met de komst van Noortje en Gijs, voor jou moeilijker werd om aan je eigen carrière te werken. De zorg voor die twee apenkoppen kwam veelal op jouw bordje, en ondanks die scheve verhouding bood je me altijd een warm en liefdevol thuis waarin ik een volwaardig deel van het gezin was en alles kon relativeren tot een wereld waarin ik gewoon papa was van twee geweldig lieve en gezonde kinderen. Dit is voor mij, en voor het voltooien van mijn proefschrift, van onschatbare waarde geweest en ik ben je daar intens dankbaar voor. Ik hou van jullie.